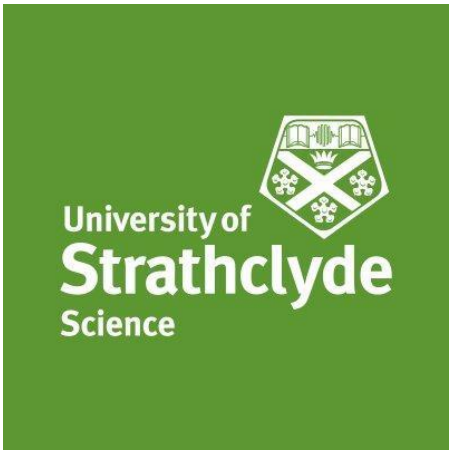

Investigating the neuro-immunomodulatory effects of 40Hz light flicker treatment in 5xFAD model of Alzheimer's Disease

A thesis presented by

Tanith A. Harte

In fulfilment of the requirements for the degree of Doctor of Philosophy

July 2023

This thesis is the result of the author's original research. It has been composed by the author and has not been previously submitted for examination which has led to the award of degree.

Signed: 

Date: 28 November 2023

Acknowledgements

My sincere thanks go to the Carnegie trust for funding this project (even granting an extension after the pandemic), and to the teams in SIPBS who helped me along the way.

I'd like to thank everyone on level 5. Margaret, thank you for allowing me to vent frustrations when experiments weren't working and for keeping a level head with your advice. Gwyn, thank you for your help with my thesis and for always encouraging me. To all my fellow students on level 5- the physics squad especially, thanks for always keeping the office lively and entertaining (yes, you Jordan and Mollie) – you always found a way to keep everyone's spirits high and were always happy to help when Fiji was having a crisis. A special thanks go to Holly(1) and Holly(2). Holly(1), thank you for always being there for celebrating the successes, laughing through our failures and participating in the ritual dances to please the PCR gods. Holly(2), thank you for livening up the lab when I went from being alone in my group to having a friend there to talk to. Thank you to Linda, Lee, Peter, and Carol for your infinite wisdom in animal husbandry and for making my mornings just that little bit brighter. Thank you to Mark Barbour for putting up with me as a lab-baby and teaching me the ways of science.

To Cassie, thanks doesn't quite cover it but thank you for always trying to talk me down, and sharing in my frustration- or booking us a holiday when that didn't work. Friday night McDonalds, wine and movie will always have a place in my heart.

I'd also like to thank my parents for their truly endless support throughout my life- thanks for always believing in me and supporting me through anything I tried to achieve- I love you. Thanks to my Ding-Dong for providing cuddles (when you deigned appropriate), entertainment and distractions whenever I tried to write. You are truly the Best Girl.

And finally, to Calum, I couldn't have gotten through this without you. For your endless belief in me even when I didn't believe in myself, for your love and your encouragement, and for tolerating me while I wrote my thesis. Thank you so much.

Abstract

AD is a chronic neurodegenerative condition affecting the aging population. Recently there has been global concern due to the rising prevalence of the disease and increasing financial burden of care. Despite the increasing prevalence of Alzheimer's Disease (AD) there are currently no non-invasive treatments available for patients, with all available therapies only targeting the symptoms of disease and not the cause. Recently, a potential new form of treatment for AD has been gaining interest due to its non-invasive properties. Several studies have found that flickering a light at a 40Hz frequency was capable of reducing the disease pathology and improve memory retention in mouse models of AD via an unknown mechanism. We sought to unveil some of the mechanisms of this potential therapy.

Using previously published methods we investigated the ability of 40Hz flickering light to reduce amyloid-β (Aβ) in the brains of 5xFAD mice- a transgenic mouse model of AD. We first used 9-month-old animals and treated for 1 hour a day for either 5 consecutive days or 15 days. In these 9-month-old animals we observed no significant changes in Aβ pathology (either plaque area or number) within the visual cortex (VC). We then changed the format of our treatment and reduced the ages of our animals to 4-5 months and revised our treatment equipment. At this reduced age we observed a significant reduction in total Aβ area alongside changes in gene expression in the VC for genes associated with the Aβ processing pathway, such as endogenous mouse APP and γ-secretase protein PSEN1. We then examined if the 40Hz light-flicker exhibited sex-dependent responses as previous studies have not examined sex-based differences. We observed that while some genes showed consistent changes between the sexes (*PSEN1* & *mAPP*) some genes exhibited significant differences between male and female 5xFAD mice (*BACE1* & *Cst7*), suggesting that the response was sex-dependent. Thus, 40Hz light flicker treatment reduced expression of Aβ in 4-5-month-old 5xFAD mice as well as inducing significant changes in gene expression within the VC.

COVID-19 Impact Statement

This PhD project was officially started in October of 2019, with the intent of investigating the effects of audio-based 40Hz sound treatment on the neuroimmunology of AD mice. Our initial plan was to use 5xFAD mice aged approximately 5-6 months old, as this is when the observed reduction in gamma oscillations occurs as well as having severe amyloid pathology and behavioural deficits. The animals were set up to begin breeding immediately in 2019, and the first few litters were ready to begin sound based treatment in late March of 2020. On the 23rd of March 2020, the government issued the stay-at-home order as a result of COVID-19. At the time I was not aware of how severe an impact this would have.

As I had missed my timepoint to treat the animals at 6 months, the thought was to treat the animals at a later timepoint when the amyloid pathology would be more severe- however, it became apparent from publications that 5xFAD animals have incremental hearing loss from approximately 5-6 months of age- meaning my animals would likely be deaf by the time the university re-opened. This meant that we, over the course of lockdown and over zoom, had to re-plan my project. Immediately before the lockdown began, we had explored the option of using a light-based therapy as previous publications showed similar effects from this. Thus, throughout the 3 months of March- July I conducted research, bought equipment, and constructed the 40Hz light circuit from home, with no guidance or support in the electrical-engineering aspect of this. Now I had the circuit and lights arranged but not in any way that could be administered to the animals.

Eventually in August of 2020 I was allowed back on-campus in an extremely limited capacity to check on animals and perform limited experiments. As time progressed the university had technically re-opened, however the limitations on duration of time, weekend closure and limited number of individuals on each floor meant that I was extremely limited in how much could actually be achieved. It was during this time I was able to set up the experimental chamber (shown in Chapter 3) and begin treatment of the animals who aged to 9 months old over the lockdown. This is to say nothing of the interruptions when a close-contact was diagnosed positive and I had to isolate for 10 days- a recurring issue in our department. The weekend interruptions were particularly intrusive as they limited our treatment method throughout to 5-day

intervals, which likely impacted the effectiveness of the treatment. Overall, COVID-19 had an extremely significant impact on the progress and flow of this PhD, as well as an impact to mental health and research output.

Communications

Alzheimer's Research UK Conference, 13-15th March 2023 Aberdeen, Scotland**-** Poster presentation – *"Post-transcriptional sex-based responses to 40Hz light flicker treatment in 5xFAD mice"*

Alzheimer's Research Scotland 2022 Conference, 17th August 2022, St.Andrews, Scotland**-** Oral presentation- *"40Hz light treatment for Alzheimer's Disease- A flicker of hope?"*

Alzheimer's Research ECR day, 4th September 2020, Online- Oral presentation, *"Developing new treatment for Alzheimer's Disease through unravelling the immunomechanisms of gamma oscillations"*

Table of Contents:

Acknowledgements ii

Abstract iii

Covid Impact statement iv

Communications v

Contents vi

List of figures & tables xi

Acronyms and abbreviations xvii

Equipment and reagents xxi

1. Chapter one: General introduction 1

1.1. Alzheimer's disease 2

1.2. Pathogenesis of Alzheimer's Disease 4

1.2.1. Amyloid β pathway 4

1.2.2. Tau protein tangles 8

1.2.3. Neuroinflammation 12

1.2.3.1. Microglial cells contribute to neuroinflammation and AD 13

1.2.3.2. Astrocytes & Oligodendrocytes contribute to neuroinflammation and AD. 18

1.2.3.3. IL-33 and its role in AD development 22

1.2.4. Biological Sex and Alzheimer's Disease 25

1.3. Mouse models of AD 28

1.4. Current therapies for AD 31

1.5. Circuitry and oscillations of the brain 33

1.5.1. Neural Oscillations 33

1.5.2. Neural Oscillations and Alzheimer's Disease 34

1.6. Use of gamma oscillatory treatment in AD 35

1.6.1. In mouse models 36

1.6.2. In humans 41

1.7. Hypothesis and Aims 42

2. Chapter Two: Materials and Methods 43
2.1. Buffers 44
2.1.1. Tris buffered saline (TBS) 44
2.1.2. Phosphate buffered saline (PBS) 44
2.1.3. Blocking buffer 44
2.1.4. 10x tris-acetic acid-EDTA buffer (TAE) 45
2.2. Mice 45
2.2.1. Genotyping- DNA extraction and Polymerase-chain reaction (PCR) 45
2.3. Tissue collection and processing 47
2.3.1. PBS perfused mice and OCT embedded tissues 47
2.3.2. Tissue homogenisation 47
2.4. Immunohistochemistry (IHC) 48
2.5. Immunofluorescence (IF) 48
2.6. Positive staining quantification 48
2.6.1. Quantifications of amyloid burden in the brain 48
2.6.2. Quantification of CD45 positive cells in the brain. 51
2.7. Enzyme-linked immune-absorbance assay (ELISA) 51
2.7.1. CNS tissue preparation 51
2.7.2. ELISA 51
2.8. Reverse-transcribed PCR 52
2.8.1. RNA Extraction 52
2.8.2. cDNA synthesis 53
2.8.3. PCR reaction 53
2.8.4. PCR analysis and controls 56
2.9. Data presentation and statistical analysis 56

3. Chapter three: 5-day and 15-day 40Hz light exposure to 9-month-old 5xFAD animals 58
3.1. Aims of Chapter 59
3.2. Results 62
3.2.1. Light Equipment Setup 62
3.2.2. Genotype confirmation of 5xFAD mice 65

3.2.3. Effect of 5-day oscillating light treatment on Aβ levels in 9-month-old mice 67
3.2.4. Effect of 5-day oscillating light treatment on CD45+ cell count in 9-month-old mice 92
3.2.5. Effect on 15-day oscillating light treatment on Aβ levels in 9-month-old mice 59
3.2.6. Effect of 15-day oscillating light treatment on CD45+ cell count in 9-month-old mice 110
3.3. Discussion 114
3.4. Limitations 116

4. Chapter four: 15-day 40Hz light exposure on 4-5-month-old 5xFAD animals 118

4.1. Aims of chapter 120
4.2. Results 120
4.2.1. Changes to treatment method 121
4.2.2. Construction of new light administration chamber 121
4.2.3. Treatment process refinements 123
4.2.4. Animals weight was unaffected by 15 days of 40Hz light treatment 124
4.2.5. Effect of 15-day light treatment on AB in 4-5m/old 126
4.2.5.1. Effect of 40Hz light flicker on soluble Aβ 1-40 and Aβ 1-42 proteins in brain of 5xFAD mice 126
4.2.5.2. Histological measurement of Aβ levels in the visual cortex 128
4.2.6. qPCR analysis of Amyloid processing pathway genes 131
4.2.7. Correlations between IL33, AD-related genes and microglia gene expression. 135
4.2.8. Effects of 15-day light treatment on CD45 expression in the visual cortex of 5xFAD mice 139
4.2.9. Effects of 15-day light treatment on expression of IL-33 and OLIG2 proteins in the brain of 4/5-month-old mice 140
4.3. Discussion 142
4.3.1. Changes in Aβ burden across brain 142
4.3.2. No changes in CD45 expression after light treatment 143
4.3.3. Changes in gene expression after 40Hz treatment 144
4.3.3.1. AD-related genes 144

4.3.3.2. Changes in microglia gene expression after treatment 146
4.3.3.3. Correlation between AD genes and IL33 mRNA expression 148
4.3.3.4. Correlations between microglia genes and IL33 149
4.3.4. Expression of IL-33 and OLIG2 proteins in the VC of 40Hz treated 5xFAD and WT mice. 150
4.3.5. Overall conclusion 151
4.3.6. Limitations 152

5. Chapter five: Sex based differences in response to 40Hz light treatment 153
5.1. Aims 154
5.2. Results 155
5.2.1. Sex-dimorphic expression of Aβ 1-40 and Aβ 1-42 in brains of 5xFAD mice 155
5.2.2. Aβ histology in visual cortex of 5xFAD mice 158
5.2.3. Effect of sex on gene expression in female and male 5xFAD mice after 40Hz treatment. 166
5.2.3.1. Relative mRNA expression between males and females in each treatment group 173
5.2.4. CD45+ inflammation in 40Hz light flicker treated female and male 5xFAD mice 183
5.2.5. Expression of IL-33 and Olig2 in the visual cortex of female and male 5xFAD and WT mice 187
5.3. Discussion 197
5.3.1. Differences in Aβ expression in the brain between sexes 197
5.3.1.1. Aβ in the whole brain 197
5.3.1.2. Aβ expression in the visual cortex of male and female 5xFAD animals treated with 40Hz-light flicker for 15 days 198
5.3.2. Sex-based differences in gene expression 199
5.3.2.1. Aβ pathway genes PSEN1, mAPP, and BACE1. 199
5.3.2.2. Expression of IL33 mRNA 201
5.3.2.3. Sexually dimorphic expression of Cst7 mRNA after 40Hz light flicker treatment 202
5.3.2.4. Expression of TMEM119 and P2YR12 mRNA 203

5.3.3. Light flicker treatment reduced CD45 expression only in male animals 203
5.3.4. Expression of IL-33 and OLIG2 protein unchanged in the VC by 40Hz light flicker treatment 204
5.3.5. Overall conclusions 205
5.4. Limitations 206

6. Chapter six: Final Discussion 208
6.1. Effect of 40Hz gamma oscillatory light treatment on Aβ pathology in 5xFAD mice 209
6.2. Post-transcriptional changes were induced by 40Hz light flicker treatment and were sex dependent. 211
6.3. Sex differences in AD, 5xFAD mice and response to 40Hz treatment 212
6.4. Limitations 213
6.5. Future work and directions 214
6.6. Final thoughts 216

7. References 217
8. Appendix A 2

List of figures and tables:

Chapter 1

Figure 1.1 Diagram of amyloid processing into pathogenic Aβ 5

Figure 1.2 Intracellular signalling induced by AβO 11

Figure 1.3 Microglia change their morphologies based on activation state 17

Figure 1.4 Maturation of oligodendrocytes under homeostatic conditions and in AD 21

Figure 1.5 Effector and producer cells of IL-33 24

Table 1.1 Summary of 4 transgenic mouse models of AD 30

Table 1.2 Summary of Tsai lab experiments methods and findings 37

Chapter 2

Figure 2.1 Diagram of murine hippocampus structure and regions 49

Table 2.1 PCR cycling for genotyping of 5xFAD mice 45

Table 2.2 Sequences and accession IDs of primers used for RT-PCR 52

Table 2.3 Cycling steps for RT-PCR gene quantification 53

Chapter 3

Figure 3.1 Workflow through treatment, breeding and harvesting of 9-month-old 5xFAD animals 58

Figure 3.2 Experimental equipment custom built for 40Hz light treatment. 61

Figure 3.3 Circuit diagram of breadboard used for 40hz light treatment. 62

Figure 3.4 PCR genotyping of 5xFAD animals 64

Figure 3.5 Representative Aβ expression in the visual cortex of treated and untreated wild-type mice after 5 days of 40Hz treatment 67

Figure 3.6 Representative Aβ expression in the visual cortex of treated and untreated 5xFAD mice after 5 days of treatment 68

Figure 3.7 Aβ measurements in the visual cortex of treated and untreated mice after 5 days of treatment 69

Figure 3.8 Representative Aβ expression in the subiculum of treated and untreated wild-type mice after 5 days of 40Hz treatment 70
Figure 3.9 Representative Aβ expression in the subiculum of treated and untreated 5xFAD mice after 5 days of 40Hz treatment 71
Figure 3.10 Aβ expression in the subiculum of treated and untreated mice after 5 days of treatment 72
Figure 3.11 Representative Aβ expression in CA1 of treated and untreated wild-type mice after 5 days of 40Hz treatment 73
Figure 3.12 Representative Aβ expression in CA1 of treated and untreated 5xFAD mice after 5 days of 40Hz treatment 74
Figure 3.13 Aβ expression in the CA1 hippocampal region of treated and untreated mice after 5 days of treatment 75
Figure 3.14 Representative Aβ expression in CA3 of treated and untreated wild-type mice after 5 days of 40Hz treatment 76
Figure 3.15 Representative Aβ expression in CA1 of treated and untreated 5xFAD mice after 5 days of 40Hz treatment 77
Figure 3.16 Aβ expression in the CA3 hippocampal region of treated and untreated mice after 5 days of treatment 78
Figure 3.17 Representative Aβ expression in CA1 of treated and untreated 5xFAD mice after 5 days of 40Hz treatment 79
Figure 3.18 Representative Aβ expression in CA1 of treated and untreated 5xFAD mice after 5 days of 40Hz treatment 80
Figure 3.19 Aβ expression in the dentate gyrus of treated and untreated mice after 5 days of treatment 81
Figure 3.20 Total Aβ plaque area across all brain regions after 5-day light treatment 83
Figure 3.21 Representative images of CD45 in the brain of WT mice after 5 days of light treatment 85
Figure 3.22 Representative images of CD45 in the brain of 5xFAD mice after 5 days of light treatment 86
Figure 3.23 Total CD45 cell counts in brain regions of 5 day treated and untreated 5xFAD and WT mice. 88
Figure 3.24 Representative Aβ expression in the visual cortex of treated and untreated female 5xFAD mice after 15 days of treatment. 90

Figure 3.25 Representative Aβ expression in the visual cortex of treated and untreated male 5xFAD mice after 15 days of treatment. 91
Figure 3.26 Aβ expression in the visual cortex of treated and untreated male and female 5xFAD mice after 15 days of treatment. 92
Figure 3.27 Representative Aβ expression in the subiculum of treated and untreated female 5xFAD mice after 15 days of treatment. 93
Figure 3.28 Representative Aβ expression in the subiculum of treated and untreated male 5xFAD mice after 15 days of treatment. 94
Figure 3.29 Aβ expression in the subiculum of treated and untreated mice after 15 days of treatment 95
Figure 3.30 Representative Aβ expression in CA1 of treated and untreated female 5xFAD mice after 15 days of treatment. 96
Figure 3.31 Representative Aβ expression in CA1 of treated and untreated male 5xFAD mice after 15 days of treatment 97
Figure 3.32 Aβ expression in CA1 of treated and untreated mice after 15 days of treatment 98
Figure 3.33 Representative Aβ expression in CA3 of treated and untreated female 5xFAD mice after 15 days of treatment. 99
Figure 3.34 Representative Aβ expression in CA3 of treated and untreated male 5xFAD mice after 15 days of treatment. 100
Figure 3.35 Aβ expression in CA3 of treated and untreated mice after 15 days of treatment 101
Figure 3.36 Representative Aβ expression in the dentate gyrus of treated and untreated female 5xFAD mice after 15 days of treatment. 102
Figure 3.37 Representative Aβ expression in the dentate gyrus of treated and untreated male 5xFAD mice after 15 days of treatment. 103
Figure 3.38 Aβ expression in the dentate gyrus of treated and untreated mice after 15 days of treatment 104
Figure 3.39 Average Aβ plaque area per region in the brains of treated and untreated 5xFAD mice after 15-day treatment 106
Figure 3.40 Representative images of CD45 in the brain of female 5xFAD mice after1 5 days of light treatment 108
Figure 3.41 Representative images of CD45 in the brain of male 5xFAD mice after1 5 days of light treatment. 109
Figure 3.42 Total CD45 cell counts for 15-day treated 9-month-old animals. 110

Table 3.1 Aβ measurements in the hippocampus and VC of 9-month-old animals treated with 40Hz light flicker for 5 days. 66
Table 3.2 CD45+ cell counts in the hippocampus and VC of 9-month-old animals treated with 40Hz light flicker for 5 days. 88
Table 3.3 Aβ measurements in the HPF and VC of 9-month-old 5xFAD animals treated with light flicker for 15 days. 105
Table 3.4 Total number of CD45+ cells in the HPF and VC of 9-month-old 5xFAD animals after 15-day 40Hz light treatment. 107

Chapter 4:

Figure 4.1 New treatment administration chamber setup. 117
Figure 4.2 Weight values for 5xFAD and WT animals over 3-week treatment period 120
Figure 4.3 Aβ 1-40 and Aβ 1-42 levels did not change across whole brain after 40Hz light treatment. 122
Figure 4.4 Effect of 40Hz treatment on Aβ burden in visual cortex. 124
Figure 4.5 Relative expression of genes mAPP, PSEN1, mBACE1 and IL33 127
Figure 4.6 Relative expression of microglia-associated genes Gpnmb, Cst7, TMEM119 and P2YR12 129
Figure 4.7 Correlations between AD-related genes and IL33 mRNA expression in untreated 5xFADs and 40hz-light treated 5xFADs and WT animals. 131
Figure 4.8 Correlations between microglia-related genes and IL33 mRNA expression in untreated 5xFADs and 40hz-light treated 5xFADs and WT animals. 133
Figure 4.9 Effect of 15-day light treatment on CD45 expression in the VC 134
Fig 4.10 Expression of IL-33+ and Olig2+ cells within the VC of 40hz light-treated and untreated animals. 136

Table 4.1 Number of plaques present in each layer of the visual cortex in 4-5month old 5xFAD animals treated with 40Hz light flicker for 15 days. 125

Table 4.2 Aβ measurements in each layer of the visual cortex in 4-5month old 5xFAD animals treated with 40Hz light flicker for 15 days 125

Chapter 5:

Figure 5.1 Aβ1-40 and Aβ1-42 expression differs by sex in 5xFAD animals 151
Figure 5.2 No significant changes across ½ brain Aβ burden in either sex 152
Figure 5.3 Effect of 40Hz light flicker on Aβ burden in primary visual cortex of 4-5-month-old female 5xFAD mice 154
Figure 5.4 Effect of 40Hz light flicker on Aβ burden in visual cortex of 4/5-month-old male 5xFAD mice 156
Figure 5.5 Effects of 40Hz light flicker treatment on the Aβ burden of each layer of the VC in female and male 5xFAD mice 157
Figure 5.6 Comparison of Aβ levels and plaque numbers between male and female 5xFAD animals in each layer of the visual cortex 159
Figure 5.7 Total levels of AB and total number of plaques in the visual cortex for male and female, 40Hz treated and untreated 5xFAD mice 160
Figure 5.8 Sex-dependent expression of AD genes PSEN1, BACE1, mAPP, IL-33 after 40Hz treatment 163
Figure 5.9 Sex-dependent expression of microglia genes Gpnmb, Cst7, P2YR12 and TMEM119 after 40Hz treatment 166
Figure 5.10 Expression of PSEN1 mRNA in males relative to females from all treatment groups 169
Figure 5.11 Expression of mAPP mRNA in males relative to females from all treatment groups 170
Figure 5.12 Expression of BACE1 mRNA in males relative to females from all treatment groups 171
Figure 5.13 Expression of IL33 mRNA in males relative to females from all treatment groups 172
Figure 5.14 Expression of Gpnmb mRNA in males relative to females from all treatment groups 174
Figure 5.15 Expression of Cst7 mRNA in males relative to females from all treatment groups 175
Figure 5.16 Expression of P2Y12 mRNA in males relative to females from all treatment groups 176
Figure 5.17 Expression of TMEM119 mRNA in males relative to females from all treatment groups 177

Figure 5.18 Representative CD45 IHC images of the visual cortex of 4-5-month-old female 5xFAD mice after 15 days 40hz light treatment. 179
Figure 5.19 Representative CD45 IHC images of the visual cortex of 4-5-month-old male 5xFAD mice after 15 days 40hz light treatment. 180
Figure 5.20 Total number of CD45+ cells in the VC of 4-5-month-old male and female 5xFADs after 15-day 40Hz light treatment 181
Figure 5.21 Representative IL-33 and Olig2 expression in the VC of treated and untreated female WT mice after 15-day 40Hz light treatment 184
Figure 5.22 Representative IL-33 and Olig2 expression in the VC of treated and untreated female 5xFAD mice after 15-day 40Hz light treatment 185
Figure 5.23 Total number of IL-33+ and Olig2+ cells in the VC of female WT and 5xFAD mice after 15-day 40Hz light treatment 186
Figure 5.24 Number of IL-33+ and Olig2+ cells in each layer of the VC of female WT and 5xFAD after 15-day 40Hz light treatment 187
Figure 5.31 Representative IL-33 and Olig2 expression in the VC of treated and untreated male WT mice after 15-day 40Hz light treatment 188
Figure 5.31 Representative IL-33 and Olig2 expression in the VC of treated and untreated male 5xFAD mice after 15-day 40Hz light treatment 189
Figure 5.23 Total number of IL-33+ and Olig2+ cells in the VC of male WT and 5xFAD mice after 15-day 40Hz light treatment 190
Figure 5.24 Number of IL-33+ and Olig2+ cells in each layer of the VC of male WT and 5xFAD after 15-day 40Hz light treatment 191

Table 5.1 Aβ measurements in each layer of the visual cortex in 4-5month old male and female 5xFAD animals treated with 40Hz light flicker for 15 days. 155
Table 5.2 Plaque counts in each layer of the visual cortex in 4-5month old male and female 5xFAD animals treated with 40Hz light flicker for 15 days 155

Acronyms and abbreviations:

Chapter 1- Introduction	
AD	Alzheimer's Disease
CNS	Central nervous system
EOAD	Early onset Alzheimer's Disease
LOAD	Late onset Alzheimer's Disease
Aβ	Amyloid-β
APP	Amyloid precursor protein
BBB	Blood- brain barrier
ADAM10	A disintegrin and metalloprotease domain-containing protein 10
AICD	APP Intracellular Domain
BACE1	Beta-secretase 1
sAPPβ	Soluble βAPP
CTFβ	C-terminal β fragments
PSEN1	Presenillin-1
AβO	Aβ oligomers
MAPT	Microtubule-associated protein tau
PHF	Paired helical fragments
NFT	Neurofibrillary tangles
PRPc	Cellular prion protein
PSD	Post-synaptic density
mGluR5	Metabotropic glutamate receptor 5
eEF2	Eukaryotic elongation factor 2 kinase

Pyk2	Protein tyrosine kinase 2
NMDA	N-methyl-d-aspartate receptor
ROS	Reactive oxygen species
DAM	Disease associated microglia
P2yr12	Purinergic receptor 12
TMEM119	Trans-membrane protein 119
Cst7	Cyastatin 7
Iba1	Ionised calcium-binding adaptor molecule 1
TREM2	Triggering receptor expressed on myeloid cells 2
LDL	Low-density lipoprotein
APoE	Apolipoprotein E
GFAP	Glial fibrillary acidic protein
DAA	Disease associated astrocytes
OPC	Oligodendrocyte precursor cell
DAO	Disease associated oligodendrocytes
MBP	Myelin basic protein
MOG	Myelin oligodendrocyte protein
GM-CSF	Granulocyte macrophage colony stimulating factor
sST2	Soluble ST2
SLE	Systemic lupus erythematosus
MS	Multiple sclerosis
RA	Rheumatoid arthritis
HRT	Hormone replacement therapy

5xFAD	5x familial Alzheimer's Disease (mouse model expressing 5 mutations)
Thy-1	Thy-1 cell surface antigen
AC	Auditory cortex
mPFC	Medial prefrontal cortex
SCN	Suprachiasmatic nucleus

Chapter 2- Methods	
TBS	Tris-buffered saline
NaCl	Sodium chloride
DI.H2O	Deionised water
TBST	Tris-buffered saline tween
PBS	Phosphate buffered saline
BB	Blocking buffer
BSA	Bovine serum albumin
TAE	Tris -acetic acid – EDTA buffer
WT	Wild-type animal
BPU	Biological procedures unit.
PCR	Polymerase chain reaction
IHC	Immunohistochemistry
RT	Room temperature
HRP	Horseradish peroxidase
IF	Immunofluorescence
SUB	Subiculum

ROIs	Regions of interest
ELISA	Enzyme-Linked Immuno-Absorbance assay
SUB	Subiculum (brain region)

Chapter 3- 5-day and 15-day 40Hz light exposure to 9-month-old 5xFAD animals	
LED	Light emitting diode
WT-UT	Untreated (control) wild-type mice
WT-T	40Hz-light flicker treated wild-type mice
FAD-UT	Untreated (control) 5xFAD mice
FAD-T	40Hz-light flicker treated 5xFAD mice

Equipment and reagents

Reagents and kits		
Reagent	**Supplier**	**Product code**
Tris-hydrochloride	Sigma Aldrich	1185-52-1
Sodium chloride	Fisher Scientific UK	10428420
Sodium hydroxide	Fisher Scientific	10488790
Hydrochloric acid	Sigma Aldrich	258148
Potassium phosphate monobasic	Sigma aldrich	P5655
Potassium chloride	Sigma Aldrich	P9333
Bovine Serum albumin	Sigma Aldrich	A4503
ImmEdge hydrophobic pen	Vector Laboratories	H4000
Tween 20	VWR	900564-5
Glacial acetic acid	Fisher Scientific	64-19-7
0.5M EDTA	Thermofisher Scientific	AM9261
PHIRE Tissue Direct Kit	Thermofisher Scientific	F-170
Optimal cutting temperature (OCT) compound	Leica	14020108926
AEBSF protease inhibitor	Thermofisher Scientific	78440
Vectamount aqueous mounting medium	Vector Laboratories	H-5501-60
AMEC Red substrate	Vector Laboratories	SK4285
Horseradish peroxidase	Thermofisher Scientific	N504

Haematoxylin	Sigma Alrich	GHS232
Vectashield with DAPI	Vector Laboratories	H-1500
Guanidine hydrochloride	Sigma Aldrich	G3272
RNALater	Thermofisher Scientific	AM7024
Trizol	Thermofisher Scientific	15596026
Propranolol	Thermofisher Scientific	04098.K2
Glycogen	Thermofisher scientific	R0561
Sodium acetate	Thermofisher Scientific	R1181
Quantitect reverse transcription kit	Qiagen	205311
PowerTrack SYBR Green master mix	Thermofisher Scientific	A46109
Mouse Aβ 1-40 ELISA kit	Thermofisher Scientific	KMB3481
Mouse Aβ 1-42 ELISA kit	Thermofisher Scientific	KMB3441
Tween 20	VWR	900564-5
Chloroform	Thermofisher Scientific	J67241.K2
Acetone	VWR	26066.321
Ethanol	Fisher	64-17-5
Antibodies		
Target	**Supplier**	**Product code**
Rabbit anti-mouse Aβ mAb	Cell Signalling Technology	D54D2
Rabbit anti-mouse CD45 mAb	Cell Signalling Technology	D3F8Q

Goat anti-mouse IL-33 pAb	Thermofisher Scientific	PA5-47007
Rabbit anti-mouse Olig2 pAb	Merck Millipore	AB9616
Donkey anti-goat 488 2ndary Ab	Invitrogen	A11055
Donkey anti-rabbit 488 2ndary Ab	Invitrogen	A21206
Goat anti-rabbit 555 2ndary Ab	Invitrogen	A32732
Equipment		
Name	**Supplier**	**Software / version**
Kodak BioMax MBP3000 power supply	Kodak	N/A
INGenius LHR Gel documentation	Syngene	Genetools
Tissueruptor 230v	Qiagen	N/A
Herause Fresco 21 Microcentrifuge	Thermofisher scientific	N/A
Basic IKA Labortechnik Shaker	IKA	N/A
Eclipse 501 Microscope	Nikon	NIS Elements F3.2
Biotek Epoch microplate spectrophotometer	Agilent Technologies	Gen5
NanoDrop2000c Spectrophotometer	Thermofisher Scientific	NanoDrop software v1.6
StepOne Real-Time PCR system	Thermofisher Scientific	StepOne software v2.3
Multifuge 3S-R	Kendro laboratory products	N/A

Optima MAX-XP Ultracentrifuge	Beckman Coulter	N/A
40Hz Light Flicker Equipment		
White LED Lights	Wholesale LED Lights	60 x 5050 SMD, 14.4W, 1020 Lumen
Solderless flexible breadboard jumper-wires	Elegoo	Amazon
Arduino UNO Rev3	Arduino	A000066
Electrical insulation tape	Amazon	Amazon
MOSFET N-CH 60V 2.5A	Digikey	IRLD024PBF
25Ohm Resistors	Digikey	25J25RE
Battery Holder AA 8-cell	Digikey	BH48AAW
Capacitors 47Uf 16V	Digikey	25J25RE
Breadboard 6.50 x 2.14”	Digkey	TW-E40-1020
Eventek DC Variable Powersupply (0-30V, 0-10A)	Eventek	Amazon

Chapter 1

General Introduction

1. Introduction

1.1 Alzheimer's disease

Alzheimer's Disease (AD) is a chronic neurodegenerative disease generally associated with late life-stages and is the leading cause of dementia. In recent years it has become a major health concern worldwide due to aging populations and a lack of clear prevention methods. Historically, AD has plagued mankind since before the ancient Egyptians (Yang *et al.,* 2016) and yet despite centuries of research efforts expanding our understanding of the pathology of the disease, it continues to affect the aging population well into the 21st century. As the disease pathogenesis is not yet fully understood, there is currently no effective treatment available for this disease.

AD is characterised by development of extracellular amyloid plaques, chronic inflammation, protein tangles and eventual irreparable damage to brain tissues within the central nervous system (CNS). These pathologies result in early symptoms such as memory loss, mood, and personality changes, increases in anxiety, and depression, which give indication to the nature of the underlying disease (Bature *et al.,* 2017). As the disease progresses symptoms such as memory loss worsen and neurological symptoms such as psychosis, difficulty with language and numeracy, restlessness and agitation increase, and attention span shortens. In the late stages, AD symptoms reach peak severity with loss of communication, difficulty swallowing, seizures, and eventual death (Mckhann *et al.,* 2011).

AD is split into 2 "types" based on the age of disease onset. The first is early onset associated with those aged 65 or under (EOAD) and is linked to hereditary genetic mutations on genes for amyloid precursor protein (APP) and proteins involved in the γ-secretase protein- presenilin 1and 2 (PSEN1 / 2) (Ayodele *et al.,* 2021) leading to its other name of "familial" AD. EOAD is an aggressive form of the AD resulting in more rapid pathology development, a high mortality rate and larger social impact due to the young age of the onset (Mendez, 2017). The second and most prevalent type is known as late onset AD which is associated with patients aged 65 and over (LOAD). Despite EOAD being termed familial AD, EOAD also has a strong genetic element with an estimated hereditability of 60-80% (Gatz *et al.,* 2006). Both types can be further divided into subcategories termed "mendelian EOAD/LOAD" which are cases where there is a family history of disease (i.e an inheritable mutation) and non-mendelian EOAD/LOAD where there is no family history and the genetic mutation is spontaneous. In the UK AD is further categorised by the severity of symptoms based

on results from cognitive tests such as the Mini Mental State Exam (MMSE), a set of 30 questions designed to test cognitive impairment. Mild AD is scored at 21-16, moderate AD at 10-20 and <10 as severe AD (National Institute for Health and Care Excellence, 2018).

While many genetic risk factors for AD have been identified, there has not been a single identified root cause of AD. Instead, it is thought to be a multifactorial disease. There is evidence of changes in the microbiome influencing the development of AD due to the intimate link between gut health and brain health via the gut-brain-axis (Varesi *et al.,* 2022). Similarly, there is evidence for the oral microbiome contributing to AD pathogenesis (Kamer *et al.,* 2009). Environmental factors such as air pollution (such as nitrogen oxides and ozone (Killin *et al.,* 2016) and nutritional factors such as decreased Vitamin D and malnutrition (Bianchi, Herrera and Laura, 2021) also seem to play a role in AD. The disease is therefore highly complex with many risk factors and contributing pathologies, making it very difficult to identify a single instigating factor to facilitate treatment.

The global financial burden of AD was estimated at approximately $1.313 trillion USD (Wimo *et al.,* 2023), with approximately 55.2 million people living with AD worldwide with an increase of 4.6 million new cases per year. The prevalence increases significantly in populations aged 65 years or older due to the increased frequency of LOAD. This results in a significant financial burden worldwide due to the cost of palliative care for patients and long-term pharmacological application through the duration of the disease. AD also significantly affects the families of those afflicted (Seidel and Thyrian, 2019) causing increased financial stress due to cost of care, psychological stress, and depression from the burden of care and loss of a family member (Papastavrou *et al.,* 2007).

1.2 Pathogenesis of AD

AD is a chronic, complex disease involving multiple pathologies and associated risk factors, from microbiota and lifestyle through to genetic family history. However, from extensive research into the disease, 3 major hallmarks of pathology applicable to AD emerged. These are the build-up of toxic amyloid fragments, the development of neurofibrillary tangles and increased inflammation within the brain termed neuroinflammation (D. J. DiSabato et.al , 2016).

1.2.1 Amyloid-β pathway

One of the oldest – and still current- hypotheses for the pathogenesis of AD is the build-up of Amyloid-β (Aβ) producing plaques in the brain (Glenner and Wong, 1984). This hypothesis states that once plaques develop, they promote neuroinflammation via stimulation of immune cells and interrupt communication between neurons at the synapses, eventually leading to loss of neurons.

Aβ is formed by the abnormal processing of APP, a protein expressed in high levels in neurons as an integral membrane protein which is associated with neural plasticity, signal transduction and cell growth (Turner *et al.,* 2003). It has also been linked to maintenance of vasculature in animal models, suggesting it may play a key role in maintaining the blood brain barrier (BBB) (D'uscio and Katusic, 2019). In AD, mutations in genes associated with processing of APP result in APP being abnormally cleaved resulting in amyloid molecules of varying lengths and varying pathogenic potential (Selkoe *et al.,* 2016) (Fig 1.1), eventually leading to fibrillation and accumulation of Aβ plaques. Of these varying lengths of Aβ, the most extensively studied have been fibril lengths Aβ1-40 and the less soluble and more neurotoxic Aβ1-42 (Kuperstein *et al.,* 2010; Qiu *et al.,* 2015).

APP is cleaved by 3 different enzymes in the 2 major amyloid pathways. In the non-amyloidogenic pathway it is first cleaved by α-secretase (e.g., A disintegrin and metalloprotease domain-containing protein 10 (ADAM10)), resulting in soluble APPα and C-terminal 83 (C83) fragments. The C83 fragment is then cleaved a second time by γ-secretase to produce APP intracellular domain (AICD) and P3. After cleavage, AICD is release into the cytoplasm where it functions as a transcription factor (Shu *et al.,* 2015).

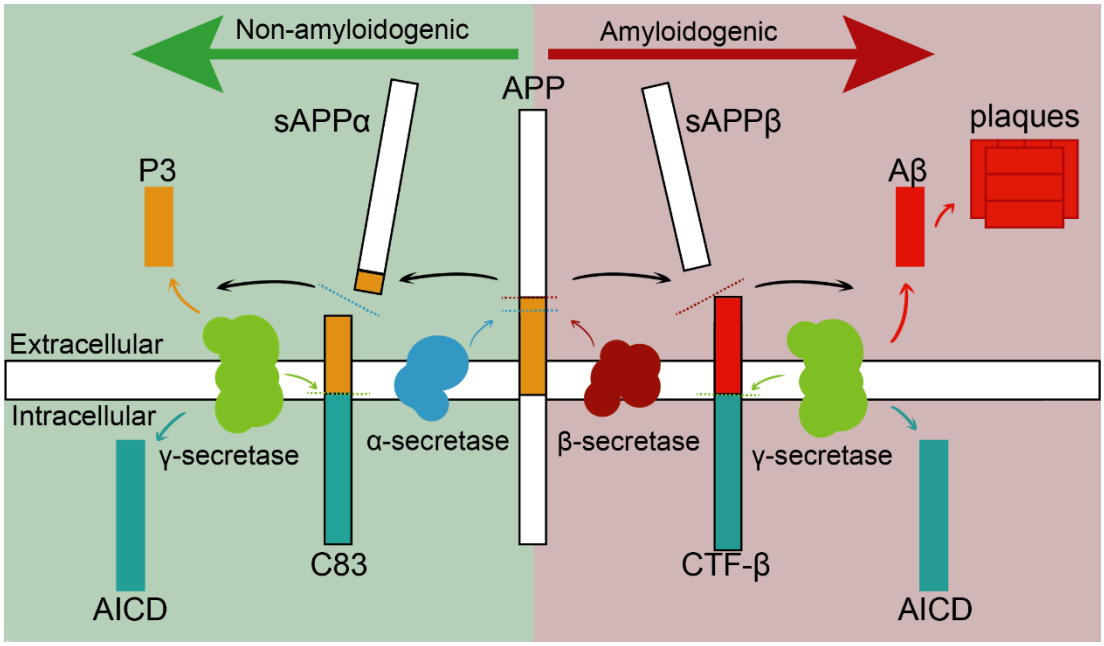

Figure 1.1- Simplified diagram of amyloid cleavage into pathogenic Aβ: *The amyloidogenic pathway associated with AD vs the non-amyloidogenic pathway associated with non-pathogenicity.* ***Non Amyloidogenic-*** *APP is first cleaved by α-secretase to produce sAPPα and C-terminal 83 (C83). C83 is then cleaved by γ-secretase in the second instance to produce extracellular P3 (function unknown) and the intracellular signalling molecule AICD.* ***Amyloidogenic****- APP) is cleaved by β-secretase to produce sAPPβ and CTF-β, then cleaved a second time by γ-secretase to produce APP intracellular domain (AICD) and neurotoxic Aβ. Aβ can then oligomerise and aggregate to form plaques.*

In the amyloidogenic pathway the APP is instead first cleaved by β-secretase (Beta-secretase 1 (BACE1) which cleaves at a different location on the full-length APP molecule, resulting in soluble βAPP (sAPPβ) fragments and C-terminal β fragment C99 (CTFβ). BACE1 is found at significantly higher levels in human AD brain extracts (Vassar *et al.,* 1999), linking excess of this cleavage protein to the amyloidogenic pathways of AD. The cleavage of the C99 fragment is conducted by γ-secretase but due to the original mis-cleave, the resulting molecules are AICD and neurotoxic Aβ, with the most frequent length being Aβ1-40 and the most pathogenic being Aβ1-42, due to its insolubility and higher rate of aggregation (Turner *et al.,* 2003).

The γ-secretase protease is a complex of 4 individual proteins; PSEN1, nicastrin, anterior pharynx-defective 1 and presenilin enhancer 2. This complex has a wide number of substrates in normal function, however gene mutations resulting in defective subunit proteins in this complex have been linked to AD progression due to alterations in its function (Petit et al., 2022). Mutations in the APP processing pathway (such as the most frequent mutation- valine-isoleucine substitution mutation at protein position 717 (V717I)) are therefore closely linked to development of neurodegenerative diseases such as AD. Presenilins are transmembrane proteins which comprise the catalytic subunits of the gamma-secretase enzyme complex (Strooper, Iwatsubo and Wolfe, 2012). Mutations on presenilin genes *PSEN1* and *PSEN2* are also strongly associated with AD as these mutations affects Aβ production by altering the γ-secretase enzymes responsible for cleaving APP, resulting in increased Aβ production (Mayeux and Stern, 2012). Indeed, recent hypotheses regarding the role of PSEN1 suggest that AD is associated with a loss of PSEN function rather than it playing a direct pathological role (Shen and Kelleher III, 2006). This hypothesis resulted from experiments in PSEN1 knock-out models of AD which develop progressive neurodegeneration similar to human AD, and that this pathology occurs even without the presence of Aβ in humans (Dermaut *et al.,* 2004). Mutations on *PSEN1* and *PSEN2* (such as the substitution mutation of methionine at protein 146 with leucine) are among the rarest forms of AD, resulting in EOAD- often termed “familial AD” due to its strong hereditary genetic nature (Alzforum, 2023b).

Once Aβ is formed, it then begins to aggregate into large structures around a plaque “seed”- the dense core at the centre of a plaque aggregation. These structures can

be highly organised as fibrils or disordered as oligomers. These exhibit differences in their toxicity and pathology- oligomers tend to be more neurotoxic due to their smaller size, allowing them to easily diffuse into tight tissue junctions (Verma, Vats and Taneja, 2015) .Thus these Aβ oligomers (AβO) are more closely correlated with disease severity (Lue *et al.,* 1999) prior to the development of insoluble plaques (Lewczuk *et al.,* 2010). Studies have shown that AβO is directly toxic to neurons and follows similar patterns of spread through the brain to the insoluble fibrils (Kim et al., 2003). Further research into these unveiled properties similar to prions, and that AβO appear to be capable of interacting with cell membranes and either spontaneously forming cation pores or facilitating ion entry into the cells permitting intracellular flux of Ca^{2+} and other ions which leads to neuronal death (Kawahara *et al.,* 2000; Kayed *et al.,* 2004; Demuro *et al.,* 2005).

Despite the evidence showing its toxicity, more recent studies have begun to suggest a physiological role for Aβ in homeostasis. In mouse models that do not produce APP, the addition of Aβ was sufficient to rescue homeostatic synaptic plasticity (Galanis *et al.,* 2021). Similar studies have shown in-vivo that endogenous Aβ was required for the induction of brainwaves associated with memory formation (Puzzo *et al.,* 2011). It could therefore be suggested that AD is associated with an imbalance of Aβ production resulting in excessive, neurotoxic levels of Aβ.

Aβ can exist in the brain in many different forms and levels of solubility, and its deposition is suggested to begin well before the onset of AD symptoms (Benzinger *et al.,* 2013). However, there has been a great deal of controversy surrounding the amyloid hypothesis, particularly in recent years (Frisoni *et al.,* 2022). Studies have shown that Aβ deposition occurs in elderly adults who do not show symptoms of cognitive impairment associated with AD (Aizenstein *et al.,* 2008; Mathis *et al.,* 2013)that it is not necessarily sufficient to cause disease alone. Instead, more recent hypotheses suggest that it is only one factor, with other factors such as tau tangles being necessary for development of disease, further suggesting that effective future treatments must be able to target multiple aspects of pathology.

1.2.2 Tau protein tangles

Tau proteins are phosphoproteins found mainly in neurons in the CNS, with the key role of stabilising microtubules of axonal cells cytoskeleton. The gene encoding for tau proteins is microtubule-associated protein tau (*MAPT*) located in chromosome 17 and it encodes for 6 isoforms of the protein identified by varying binding domains (Schraen- Maschke *et al.,* 2008).

Tau plays an important physiological role. It is abundant in the CNS, particularly within neurons in the axonal compartment where it can then be released extracellularly. While there is strong evidence of its role as a microtubule binding protein, its functions are highly dynamic and therefore complex (Kellogg *et al.,* 2018). In a healthy CNS, tau binds to microtubules to stabilise them and regulate their assembly, though the precise mechanisms of this are poorly understood (Barbier *et al.,* 2019). In animal models tau has been shown to be required for maturation of neurons (Ghoshal, Binder and Vitek, 2001) emphasising the key physiological role tau plays in the development of the CNS. However, evidence suggests that phosphorylation of tau reduces its functional capabilities to stabilise microtubules (Neddens *et al.,* 2018).

In AD these tau proteins become hyperphosphorylated via associated Aβ pathology, resulting in aggregation into paired helical fragments (PHF) which then accumulate into intracellular neurofibrillary tangles (NFTs) which studies suggest are responsible for the neurodegeneration observed in AD (Lee *et al.,* 2005). Tau is suggested to be one of the key aspects of AD pathology resulting in neuronal damage and death. Studies have proven this, as AD symptoms are seen only in the presence of NFTs- not simply Aβ plaques (Takashima *et al.,* 1993) and that tau has a stronger correlation with cognitive decline in human patients than any other AD biomarker (Huber *et al.,* 2018). These NFTs have been shown to inhibit the formation of microtubules and can lead to cell degradation (Del C. Alonso *et al.,* 2001). Overexpression of these proteins also alters cell structure and contents, with clustering of mitochondria resulting decreases in growth rate and ATP synthesis (Ebneth *et al.,* 1998). Tau pathology involves intracellular enzymes and is strongly associated with Aβ oligomers development, though not with other forms of Aβ (Götz *et al.,* 2001; Lewis *et al.,* 2001; Larson *et al.,* 2012; Li *et al.,* 2016).

The MAPT gene encoding for tau proteins has two halotypes- H1 and H2. H1 is strongly associated with development of many neurogenerative disorders, including AD (Schraen- Maschke *et al.,* 2008; Allen *et al.,* 2014). The regular homeostatic function of tau is involved in axonal transport, neurogenesis, and neuroplasticity, therefore mutations in *MAPT* lead to instability of microtubules, resulting in protein aggregation and neurotoxicity. Mutations in the genes encoding for MAPT lead to changes in protein structure resulting in reduced stability, altered binding properties and dysfunction of the protein (Strang, Golde and Giasson, 2019; Alzforum, 2023a). This in turn leads to increased susceptibility to neurodegenerative disorders due to the decreased stability which, when combined with Aβ and neuroinflammation, leads to excess phosphorylation of tau.

One current hypothesis supported by studies suggests that AβO interact with the cellular prion protein (PrP^c) which is found on the cell membrane at the post synaptic density (PSD) (Larson *et al.,* 2012). This induces either a conformational change or internal reaction of PrP^c which induces intracellular metabotropic glutamate receptor 5 (mGluR5) to phosphorylate several intracellular targets including Fyn (Larson *et al.,* 2012), eukaryotic elongation factor 2 kinase (eEF2-kinase) and protein tyrosine kinase 2 (Pyk2) (Haas *et al.,* 2016; Salazar *et al.,* 2019)

Fyn is a tyrosine-protein kinase (Nygaard, 2017) found intracellularly and has been strongly associated in AD pathology. Fyn phosphorylates tau thus contributing to the hyperphosphorylation leading to NFTs, as well as activating N-methyl-d-aspartate (NMDA) receptor subunit “NR2B” (Paoletti and Neyton, 2007; Trepanier, Jackson and MacDonald, 2012). This activation results in an increase in Ca^{2+} transport into neuronal cell bodies and thus destabilises cellular membranes resulting in cell damage and death (Demuro *et al.,* 2005; Zempel *et al.,* 2010; Ghosal *et al.,* 2016). It has also been shown that tau can activate the NR2B subunit through a Fyn-independent pathway, though the specifics of this mechanism have yet to be explained (Miyamoto *et al.,* 2017; Goyena, 2019).

Pyk2 is phosphorylated by Fyn and has been shown to then also phosphorylate tau (Li and Götz, 2018) thus also contributing to hyperphosphorylation. While its downstream function has not yet been determined, eEF2-kinase is also phosphorylated by AβO binding to PrP^c which then further activates eEF2. Through

this complex intracellular pathway, AβO induces the hyperphosphorylation of tau, drawing the molecule away from microtubules and into production of NFTs (Fig 1.2) (Ebneth *et al.*, 1998; Roberson *et al.*, 2011; Saha and Sen, 2019).

The initial seeding of tau within the CNS and how it spreads is poorly understood, and it is hypothesised that it is associated with inflammation- though there is a “chicken or egg” problem regarding which is the instigator of the pathology.

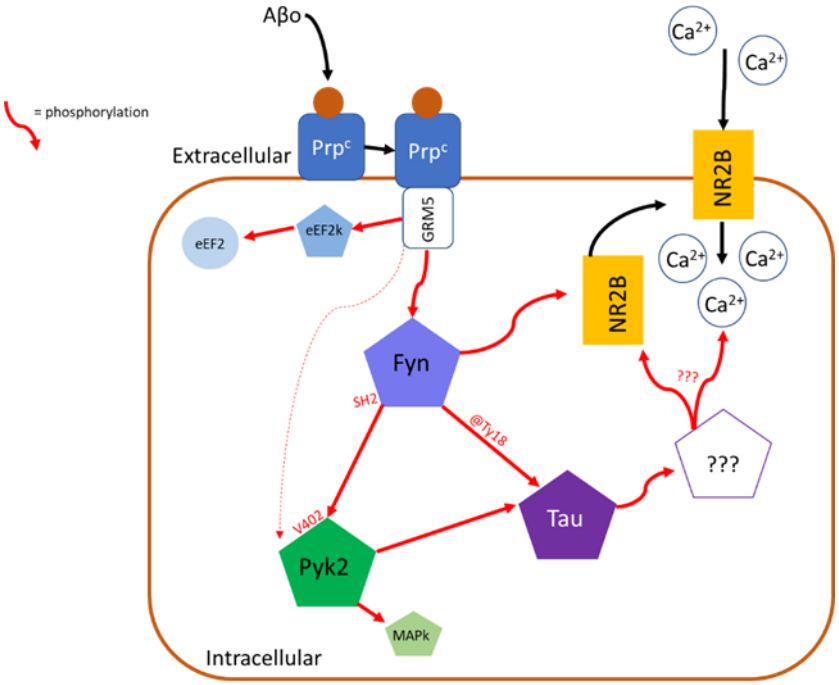

Figure 1.2- Intracellular signalling of Fyn-kinase induced by AβO resulting in phosphorylation of Tau: *AβO binds to PRP^c, triggering phosphorylation of intracellular GRM5. GRM5 phosphorylates Fyn, which then phosphorylates Tau at residue Ty18, resulting in pTau. Fyn also phosphorylates Pyk2 which further phosphorylates Tau as well as MAPkinases. Fyn activates the NR2B NMDA subunit resulting in Ca^{2+} ion influx. Tau can also induce Ca^{2+} influx through an unidentified mechanism independent from Fyn.*

1.2.3 Neuroinflammation

Neuroinflammation describes an inflammatory response within the CNS mediated by resident immune cells- usually glial cells (D. DiSabato, Quan and Godbout, 2016) such as microglia and astrocytes and infiltrating peripheral immune cells in diseases such as AD where the BBB is disrupted. These cells produce inflammatory proteins and mediators such as pro-inflammatory cytokines (e.g., IL-1β, IL-6 and TNF-α) and reactive oxygen species (ROS) in response to tissue damage caused by stressors or foreign entities such as bacteria- or in AD, Aβ. In contrast, some of these cells also play a regulatory role by producing anti-inflammatory cytokines (e.g IL-10, TGF-β) (Rubio-Perez and Morillas-Ruiz, 2012). These signalling molecules are produced to alarm the surrounding cells to respond to the stressor and thus are essential to protecting the CNS. However, in AD the constant presence of Aβ and tau promotes a continuous inflammatory immune response i.e a chronic state of inflammation (Heneka *et al.,* 2018), resulting in damage to the surrounding cells. This chronic inflammation has also been suggested to alter the function of microglia (Sobue *et al.,* 2021), oligodendrocytes (Kenigsbuch *et al.,* 2022) and astrocytes (Di Benedetto *et al.,* 2022) and is suggested to play a key role in the pathogenesis of AD.

The BBB plays an essential role in segregating the brain from the peripheral immune system whose pro-inflammatory responses and cytotoxic cells could be harmful to the delicate cells within the CNS. In neurodegenerative diseases such as AD there is disruption to the BBB resulting in transport of neurotoxic blood-products and inflammatory peripheral immune cells into the CNS which contribute to the development of neuroinflammation. (Mietelska-Porowska and Wojda, 2017; Montagne, Zhao and Zlokovic, 2017)

However, neuroinflammation is a double-edged sword. While excessive inflammation is damaging to delicate neurons, it is essential for the activation of immune cells to promote clearance of debris and pathogenic materials. Without the pro-inflammatory stimulation from the neuroimmune system there would be no maintenance of neurons and no clearance of invading pathogens (Klein, Garber and Howard, 2017). It could therefore be suggested that AD is associated with an imbalance in the delicate system of regulation and inflammation within the CNS.

1.2.3.1 Microglial cells contribute to neuroinflammation and AD

Microglial cells are macrophages native to the immune-privileged CNS. These cells are distinct from peripheral macrophages by phenotype and native properties due to the unique cellular surroundings encountered in the CNS (Cameron and Landreth, 2011), as well as the fact that these macrophages originate from the yolk-sac (Cuadros *et al.,* 2022). Microglia play an essential role in maintenance of the brain through their role in synaptic pruning, (Sobue *et al.,* 2021) guiding development of neural circuits (Squarzoni, Thion and Garel, 2015) and phagocytosis of apoptotic cell debris (Márquez-Ropero et al., 2020). They are responsible for immune surveillance and mounting a cytotoxic response to pathogens as well as tissue regeneration and clearance of debris (Spangenberg and Green, 2017). Microglia are therefore essential for homeostatic function of the brain; however, under certain conditions they can become highly damaging to neurons and other cells within the CNS via their role in inflammation.

Their homeostatic function can be seen in early AD stages when plaques are small, microglial cells take on a protective role in clearing plaques and removing build-up of fibrils (Condello et al., 2015); however this is limited to small plaques and similar effects are not observed in the larger insoluble plaques associated with late-stage disease. Once Aβ and tau deposition begins, microglia enter an activated state by upregulating genes for inflammatory cytokines such as IL-1β and IL-6 as well as genes associated with phagocytosis (Rogers and Lue, 2001; Atagi *et al.,* 2015; L. Zhong *et al.,* 2017).

As AD develops and pathology accumulates, microglial cells enter a state of chronic activation, resulting in an increased inflammatory immune response (Hanisch, 2002; Cameron and Landreth, 2011; Spangenberg and Green, 2017) (Fig 1.3) which leads to impaired phagocytic ability, increased inflammation, and damage to neurons. These chronically activated microglia undergo a change in phenotype and function to become what are known as disease-associated microglia (DAM). These cells display a ramified phenotype as well as a distinct gene profile (Sobue *et al.,* 2021) (Fig 1.3), through reduction in the expression of microglia specific markers such as TMEM119 (trans-membrane protein 119) and chemotaxis marker P2YR12 (Purinergic receptor P2Y12), and an upregulation of pro-inflammatory markers such as CD45 (lymphocyte common antigen), Cst7 (Cystatin F), Iba1 (ionised calcium-binding adaptor molecule

1) and TREM2 (Triggering receptor expressed on myeloid cells 2) (L. Zhong *et al.,* 2017; Bundy *et al.,* 2019). The specific function of TMEM119 has yet to be determined, but currently it is used as an identifying marker for subsets of microglia as it is not expressed by infiltrating myeloid cells from the periphery. Similarly, P2YR12 is a purinergic receptor expressed by subsets of microglia and is used as a chemotaxic receptor for adenosine diphosphate (ADP) allowing microglia to migrate to areas of cellular damage or distress. These two markers are generally expressed by homeostatic microglia but are found to be decreased or lost entirely in AD (Kenkhuis *et al.,* 2022). In contrast, CD45 is a marker widely expressed on all immune cells, including microglia, and is used as an antigen-signalling molecule which can modulate immune cell activation (Tan *et al.,* 2000) and is suggested to be upregulated in AD in response to the proinflammatory environment (Hopperton *et al.,* 2018). Iba1 is widely expressed by both homeostatic and activated microglia but has been shown to be increased during neuroinflammation and was found in high levels the grey-matter of AD patients (Kenkhuis *et al.,* 2022). Finally, Cst7 encodes for the protein cystatin F which is found at highest concentrations within lyso/endosomal compartments and is associated with a pro-inflammatory phagocytic response (Sala Frigerio *et al.,* 2019).

In order to reach the Aβ plaques, microglia must migrate towards the site of damage. To achieve this, they respond to Aβ via chemotaxis in a TREM2 or purinergic receptor-dependent manner (Mazaheri *et al.,* 2017) after plaques are opsonised by the complement system. After exposure they also enter an activated state by upregulating genes for inflammatory responses and phagocytosis (Rogers and Lue, 2001; Atagi *et al.,* 2015). Other molecules have also been suggested to opsonise insoluble Aβ plaques, such as low-density lipoproteins (LDL) and Apolipoprotein E (ApoE). TREM2 has been shown to interact directly with ApoE (Yeh *et al.,* 2016) after ApoE localises with Aβ plaques, promoting the phagocytosis of Aβ fibrils and plaques. LDLs also opsonised the Aβ, as well as speeding their breakdown within the microglia (Yeh *et al.,* 2016) explaining why ApoE genes are closely linked to AD. TREM2 has also been implicated in the pathogenesis of AD, particularly via the interactions between microglial cells and Tau. TREM2 deficient microglia exhibit reduced phagocytosis of apoptotic neurons, cellular debris and, essentially, Aβ (Takahashi, Rochford and Neumann, 2005) suggesting TREM2 is essential for microglia function in development AD. Mutations in the genes encoding for TREM2 (such as the substitution mutation resulting in the replacement of arginine with histidine at protein site 62- the R62H

mutation (Alzforum, 2018)) have also been associated with AD due to their resulting reduction in microglial phagocytotic ability, as changes in the structure of TREM2 affect its function and efficacy resulting in defective or limited activation of immune cells- particularly microglial cells- and thus links mutations in the genes encoding for cells of the neuroimmune system the pathology of AD (Jay *et al.,* 2015; Wang *et al.,* 2015). Studies using gene-deficient mice showed that removing or inhibiting microglia resulted in decreased Tau pathology and limited its spread throughout the brain (Asai et al., 2015; Leyns et al., 2017). This suggests that microglia participate, via phago- and exocytosis, in spreading the pTau proteins through regions of the brain that are not connected via synapses, allowing for seeding events in new neurons (Asai et al., 2015).

ApoE is the major lipid transporter within the CNS, facilitating the distribution of lipids to cells throughout the body as well has playing a role in intracellular signalling (Huang and Mahley, 2014). APoE has multiple isoforms resulting from mutations on its encoding gene, with only some being associated with increased risk of AD, the most significant of which is heterozygous expression of APOE ε4 (ApoE4) (Fernandez *et al.,* 2019). As ApoE is the major lipid transporter within the CNS, alterations in this gene lead to widespread consequences. The presence of the ApoE4 mutation leads to earlier deposition of Aβ and influences production of oligomeric Aβ (Kim et al., 2003). This gene is also directly linked to inflammation through its association with astrocytes and microglia (Fernandez *et al.,* 2019). In microglia, the ApoE4 isoform is associated with less effective clearance of debris and a less activated cell phenotype when compared to other isoforms (Wang *et al.,* 2022). Similar to its effects on Aβ formation and deposition, ApoE4 also exerts its pathogenic effects via Tau. Patients with ApoE4 exhibit significantly more tau pathology and memory impairment (Weigand *et al.,* 2021) While ApoE4 expression varies between ethnicity, it is estimated 25% of the Caucasian population carries at least one allele, making it a highly prevalent genetic predisposition to AD (Gharbi-Meliani *et al.,* 2021). Interestingly, African-Americans and Hispanic populations show lower susceptibility to ApoE4 mutations despite a similar prevalence, suggesting an as-yet unidentified racially-associated protective factor (Beydoun *et al.,* 2021).

DAMs also expressed reduced CD45- a receptor-linked tyrosine phosphatase widely expressed on all leucocytes and associated with activation of T-cells in the peripheral

immune system (Courtney *et al.,* 2019a)Within the CNS microglia usually express low-intermediate levels of CD45 relative to their peripheral counterparts and this has historically been used to identify these cell types alongside CD11b. However, CD45 expression is low relative only to peripheral macrophages and changes based on the inflammatory profile of the brain (Rangaraju *et al.,* 2018; Courtney *et al.,* 2019a).

Microglial cells also appear to have a key interaction with the adaptive immune system. One study using RAG-5xFAD mice compared to 5xFAD mice found that RAG-mice (those with no adaptive immune cells) exhibited defective microglial activation. The authors identified pre-immune IgG that specifically interacted with the microglial cells to upregulate their phagocytic abilities, rather than interacting with Aβ directly to opsonise it (Marsh *et al.,* 2016). This activation occurred via the Fc receptor on the microglia cells, which have been shown to be resistant to chronic inflammation (Koenigsknecht-Talboo and Landreth, 2005). This contrasts with other receptors associated with phagocytosis. Microglial cells exhibited impaired phagocytosis of insoluble Aβ after exposure to chronic inflammatory immune responses. This study also suggested that temporary exposure to anti-inflammatory cytokines such as IL-10 ameliorated this effect (Koenigsknecht-Talboo and Landreth, 2005).

Overall, the role of microglial cells appears to be protective in the early stages of AD but as disease progresses and chronic activation sets in, these cells become more harmful via their transport of tau, production of inflammatory cytokines and inability to clear plaques. They therefore are a key element of neuroinflammation involved in AD pathology.

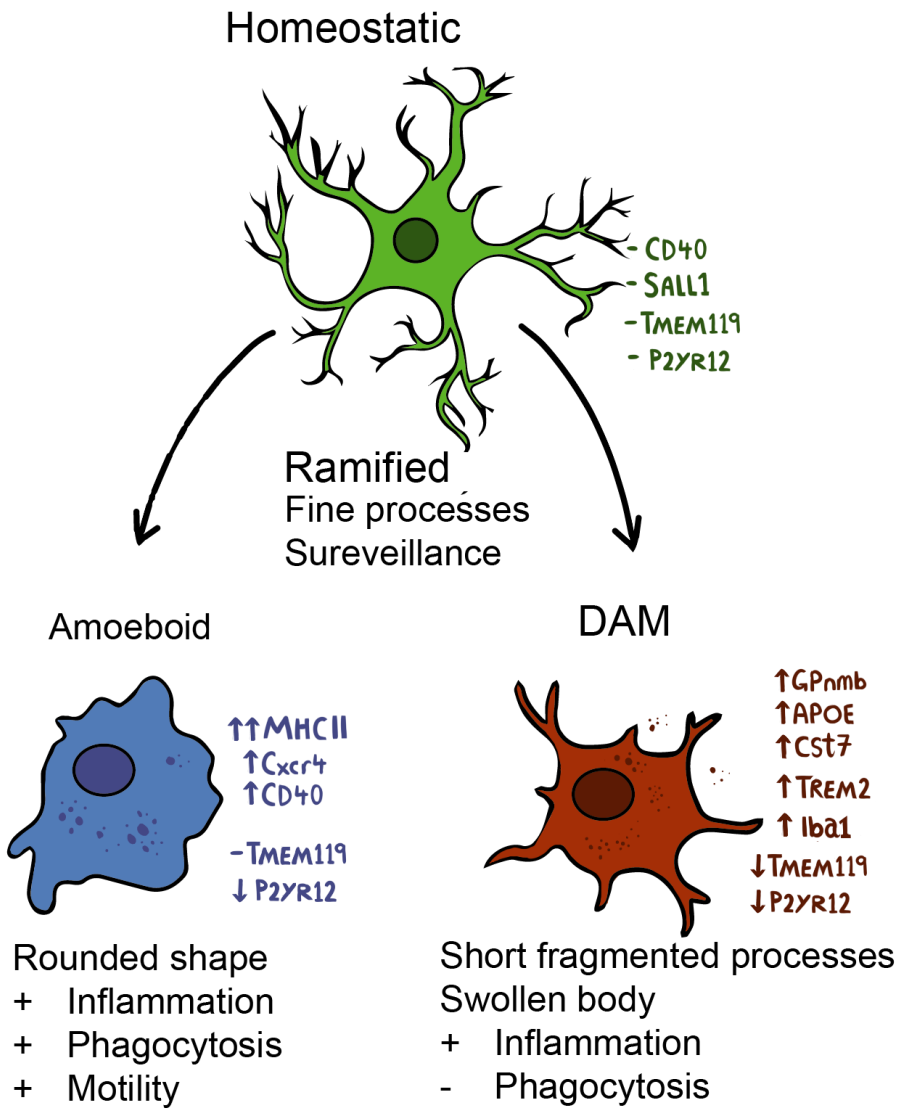

Figure 1.3- Microglia change their morphologies based on activation state. *Homeostatic (or ramified) microglia display long, fine processes which stretch out around surrounding cells to monitor for pathogens or alarmins, expressing microglia-specific markers TMEM119 and P2YR12 as well as macrophage marker CD40 and intracellular transcription factor SALL1. Once stimulated by cytokines or alarmins the homeostatic microglia can then become activated and enter an amoeboid with very few/no processes to allow for high motility and a focus on phagocytosis, upregulating MHII and CD40 and chemokine Cxcr4. In AD, inflammation is chronic and microglia eventually adapt a distinct DAM morphology alongside a profile of increased inflammation and reduced phagocytotic ability. DAMs display increased expression of Cst7, TREM2, Gpnmb, Iba1 and ApoE, and decreased expression of TMEM119 and P2YR12.*

1.2.3.2 Astrocytes and oligodendrocytes contribute to neuroinflammation and AD

Astrocytes are another group of glial cells found in the CNS, known for their characteristic star-shape. These cells bridge the gap between neurons and immune cells through their release of excitatory (such as glutamate) and inhibitory (such as GABA) neurotransmitters as well as stimulatory (such as IL-6) -and inhibitory (such as TGF-B) cytokines (Sofroniew and Vinters, 2010; Giovannoni and Quintana, 2020)They are capable of responding to pathogenic or harmful stimuli by entering a state termed "reactive astrogliosis" (Sofroniew and Vinters, 2010), as well as producing neurotransmitters and their precursors to aid neurons in communication (Talantova *et al.,* 2013; Jo *et al.,* 2014).

Astrocytes are also capable of producing cytokines both inflammatory-such as IL-6 (Oh *et al.,* 2010)- anti-inflammatory- such as TGF-β (Sofroniew, 2015)- and cytokines to stimulate microglia- such as GM-CSF. These cytokines affect microglial activity, as well as influencing neuron survival and proliferation suggesting cross-talk between these glial cells. Astrocytes also have a critical role to play in maintaining the BBB via their role in supporting endothelial junctions (Correale and Gaitán, 2019). Astrocytes interact with neurons via neurotransmitters glutamate and GABA which have both been shown to affect the behaviour and morphology of microglial cells (Fontainhas *et al.,* 2011; Lee, Schwab and Mcgeer, 2011). Astrocytes similarly regulate neuronal levels of glutamate via glutamine synthetase- expression of which is altered in AD (Schousboe, 2019), leading to increased glutamate availability and excitotoxicity (Butterfield and Pocernich, 2003; Olabarria *et al.,* 2011).

Reactive astrogliosis is measured by increased expression of glial fibrillary acidic protein (GFAP) and S100β, which are characteristic markers of severe AD and associated neurodegeneration (Mrak, Sheng and Griffin, 1996). Studies have suggested astrocytes play a key role in pathogenesis of AD due to interruptions in their homeostatic role in maintaining synaptic plasticity and interacting with the immune system through mediators such as neurotransmitters and cytokines. There is also evidence that astrocytes are capable of engulfing AβO via phagocytosis, however the fibrils instead remain within the astrocytes affecting their function (Söllvander *et al.,* 2016). With this chronically activated state, astrocytes upregulate

GFAP and expression of genes for inflammation, differentiation and complement cascade to become “disease associated astrocytes” (DAA) (Habib *et al.,* 2020). Critically, astrocytes are essential for the maintenance and support of oligodendrocytes (Tognatta *et al.,* 2020), and this change in reactive profile may limit the supportive capacity of the astrocytes leading to increases in AD pathology.

Oligodendrocytes are another type of glia that are highly prevalent in the white matter of the CNS. Their homeostatic function is primarily to produce the myelin sheaths which insulate neuronal axons, facilitating the electrical conduction of action potentials. They also play a regulatory role to neurons by producing neurotrophic and inhibitory factors (Nasrabady *et al.,* 2018). Oligodendrocytes begin with neural stem cells which then differentiate into oligodendrocyte precursor cells (OPCs) (Fig 1.4). These are young glial cells capable of interacting with other neuroimmune glial cells via production of cytokines (such as IL-1β and IL-33) and chemokines (such as CCL2), as well as major histocompatibility complex 1 and 2 (Boccazzi *et al.,* 2021). OPCs also express key oligodendrocyte transcription factors such as Olig1, Olig2 and Sox10 (Liu *et al.,* 2007) which they continue to express as they mature into premyelinating, and then myelinating oligodendrocyte cells. It is through OPCs that the CNS is capable of replenishing oligodendrocytes in response to damage or stress, making these the most proliferative cells in the brain. However, OPCs and oligodendrocytes are highly sensitive to stress due to their large energy demands and are therefore vulnerable to oxidative stress associated with inflammation (Nasrabady *et al.,* 2018).

In AD, white matter loss occurs early and thus disruption of myelin production occurs resulting in loss of signal along neuronal axons (Dong *et al.,* 2018). This loss of myelinating cells may be associated with Aβ deposition, as studies have shown Aβ is toxic to oligodendrocytes (Xu *et al.,* 2001; X. Zhong *et al.,* 2017). Similarly, tau has been associated with demyelination of white matter in human patients (McAleese *et al.,* 2015) however it is unclear if this is direct damage or if increases in tau result in increased inflammation which is harmful to oligodendrocytes. Mature myelinating oligodendrocytes, much like other glia, enter a disease associated state (DAO) in AD. DAO express upregulation in genes associated with immune signalling (e.g. IL-33) and complement cascade similar to other glia. However, unlike other glia this state occurs much later in disease and is not induced by Aβ, instead it is hypothesised

DAOs are a result of surrounding inflammation and accumulation of cell damage (Kenigsbuch *et al.,* 2022).

Astrocytes and oligodendrocytes are essential for the homeostatic function of the brain, and alterations to their function- particularly in the direction of upregulated inflammatory genes and cytokine expression- is indicative of chronic diseases such as AD. However, it remains unclear if this is simply a downstream response to the chronic cellular damage or if this is a key aspect of pathology.

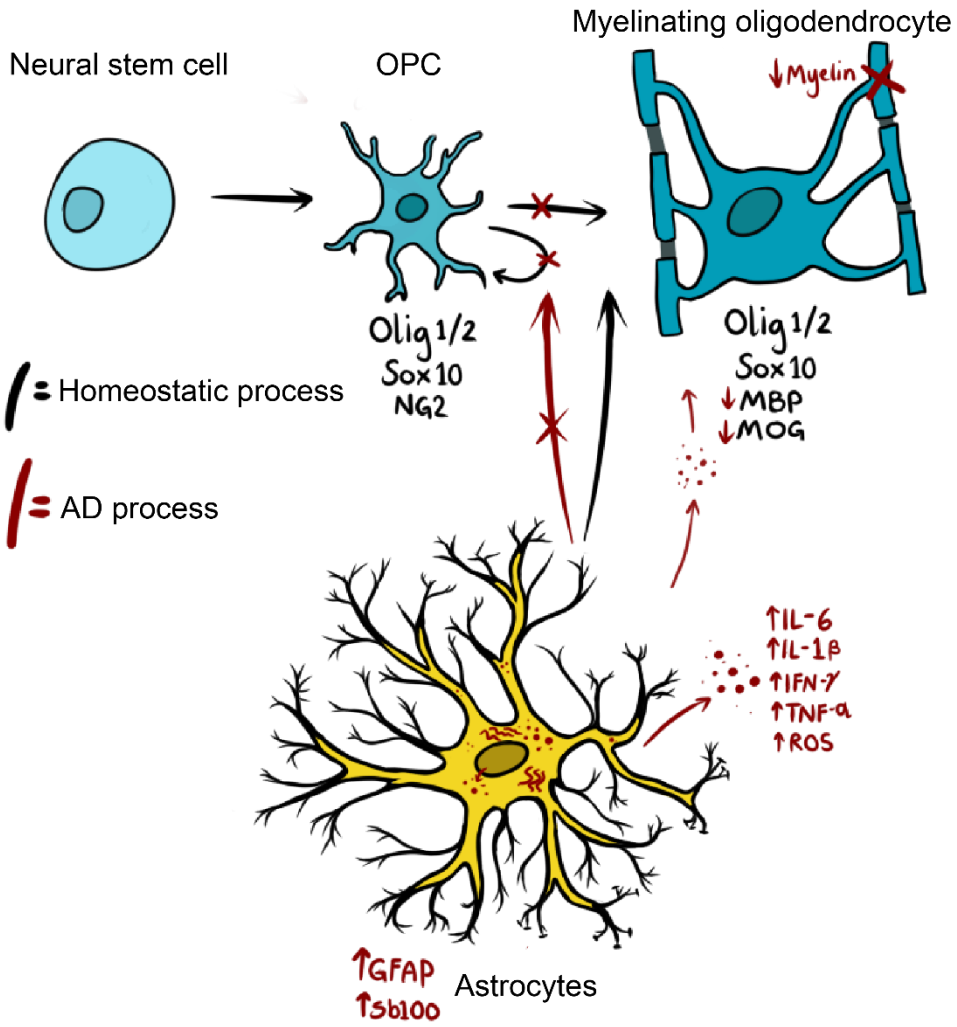

Figure 1.4- Maturation of oligodendrocytes under homeostatic conditions and in AD. *Oligodendrocytes originate from neural stem cells which differentiate into oligodendrocyte precursor cells, which express Olig1, Olig2, Sox10 and at this stage NG2. Upon signals from astrocytes and after migrating to a site of myelin damage they then mature into myelinating oligodendrocytes. Myelinating oligodendrocytes express Olig1/2 transcription factors as well as sox10 but also express myelin basic protein (MBP) and myelin oligodendrocyte protein (MOG). At this stage the oligodendrocytes wrap the axon of neurons to insulate the electrical signals transmitted. In AD, astrocytes upregulate inflammatory markers such as Sb100 and GFAP and increase production of proinflammatory cytokines and ROS, likely in response to deposition of neurotoxic Aβ and tau. This affects the maturation of OPCs, as well as damaging myelinating oligodendrocytes resulting in loss of myelin throughout the brain of AD patients.*

1.2.3.3 IL-33 and its role in AD development

Cytokines are signalling proteins used by cells to communicate with each other and regulate inflammation, usually produced by tissue and immune cells to stimulate surrounding cells. Within the CNS the main producers of cytokines are glial cells which use cytokines as a means of stimulating immune response to threats, as well as playing a role in neuromodulation via influencing synaptic plasticity (Vezzani and Viviani, 2015). Generally, cytokines can be pro-inflammatory (e.g., IL-6, TNF-α) or anti-inflammatory (e.g., TGF-β, IL-10) depending on the cells, tissue environment and disease status. However, some cytokines are pleiotropic in their function, promoting both inflammatory and anti-inflammatory effects depending on the disease or model being researched. One such example is IL-33.

IL-33 is an alarmin in the IL-1 cytokine family first described in 2005 (Schmitz *et al.,* 2005). It is widely expressed across the body by epithelial, endothelial, and immune cells which operates as both an extracellular cytokine and a nuclear transcription regulator (Choi *et al.,* 2012). The extra-cellular target of IL-33 is its specific receptor ST2, though the decoy receptor named soluble ST2 (sST2) can also interact with it as a means of limiting its activity and influence. In this way an axis is maintained between ST2/IL-33. This axis has been found to be unbalanced in diseases such as fibrosis (Kotsiou, Gourgoulianis and Zarogiannis, 2018), heart failure (Aimo *et al.,* 2019) and autoimmune diseases (Miller, 2011). Within the CNS IL-33 is expressed in the nucleus of -and released extracellularly by- grey-matter astrocytes (Gadani *et al.,* 2015) and oligodendrocytes (Vainchtein *et al.,* 2018; Neurochemistry, 2019). Within the CNS ST2 is expressed primarily by microglia (Y. Yang et al., 2017) and astrocytes (Jiao *et al.,* 2020) suggesting these are the primary effector cells responding to the alarmin or stimulatory signal (Fig 1.5).

IL-33 has a pleiotropic role, exhibiting both inflammatory and regulatory effects within the CNS (Zharichenko, 2020) depending on a variety of factors many of which are poorly understood. In microglia, IL-33 has been shown to stimulate a shift towards a less inflammatory "M2" phenotype (Gadani *et al.,* 2015) in stroke models but has also shown to mediate inflammatory IL-6 microglial responses (Cao, Liao, Lu, Yao, Wu, Zhu, Shi and Wen, 2018). IL-33 produced by astrocytes has also been shown to promote synapse engulfment by microglia, suggesting its complex role in synapse homeostasis and maintenance (Vainchtein *et al.,* 2018). IL-33 is essential for the

development and maturation of oligodendrocytes as well as integrity of the myelin sheath (Hsin-Yu Sung *et al.*, 2019).

Recent evidence suggests that IL-33 plays an important role in the development of AD. In human patients, expression of IL-33 protein by astrocytes and its receptor ST2 by microglia was increased in the brains of AD patients compared to healthy controls (Zhi *et al.*, 2014), particularly in cells surrounding Aβ plaques. In contrast, other studies have reported decreased levels of mRNA encoding for IL-33 in brain tissue and circulating serum levels (Saresella, Marventano, Piancone, Rosa, *et al.*, 2020). Indeed, mutations in IL-33 genes such as the rs1157505 single-nucleotide polymorphisms have been suggested to be a risk factor for development of LOAD (Chapuis *et al.*, 2009; X. Zhong *et al.*, 2017). There is also conflicting evidence for IL-33s role in AD development in mouse models. An APP/PS1 model of AD suggested that IL-33 was protective in AD-pathology by reducing expression of sAβ (Amy K Y Fu *et al.*, 2016) by increasing expression of endopeptidases and shifting microglia towards an alternative (M2) phenotype measured by upregulation of anti-inflammatory genes *Arg1* and *Fizz1.* Meanwhile other studies have found that IL-33 is necessary to promote production of pro-inflammatory cytokines (Cao, Liao, Lu, Yao, Wu, Zhu, Shi, Wen, *et al.*, 2018) and NO (Kempuraj *et al.*, 2013) which are shown to be contributors to neuroinflammation and therefore associated with AD pathology.

The number of conflicting reports of the pro/anti-inflammatory role of IL-33 and its role in autoimmunity - and specifically in AD - mean there is still much to be understood around this cytokine and its role in neurogenerative diseases.

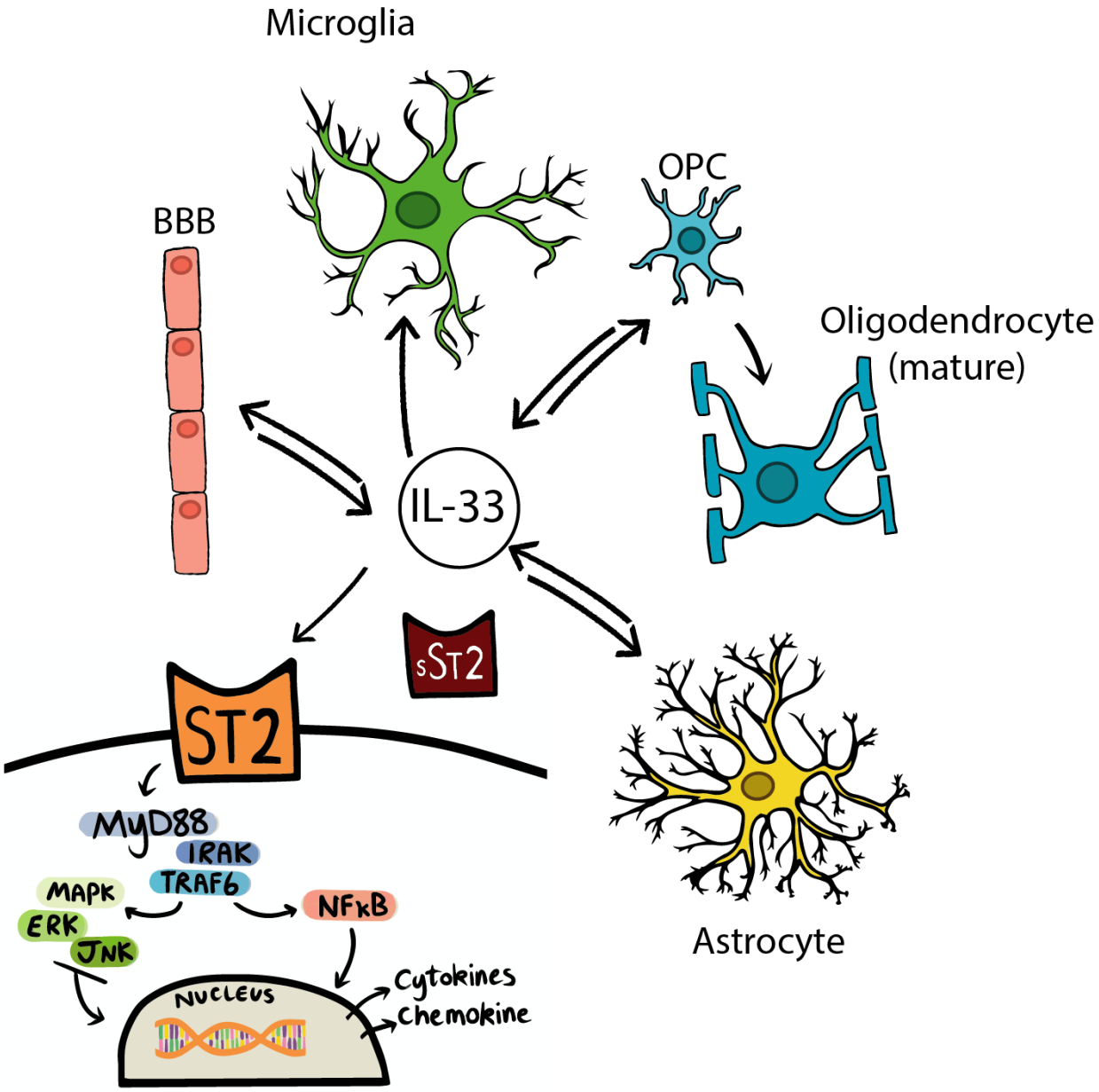

Fig 1.5- Effector and producer cells of IL-33. *IL-33 protein is produced by grey-matter astrocytes, oligodendrocytes, and epithelial cells of the BBB as both an alarmin and an effector cytokine. Its effector cells are, similarly, astrocytes, oligodendrocytes, and microglial cells. IL-33 interacts with ST2 expressed on the cell membrane of its effector cells. After binding it induces intra-cellular signalling cascades of the MAPK/JNK and NFκB pathways, eventually resulting in transcription of cytokines and chemokines. Through these pathways it mediates neuromodulatory and neuroinflammatory effects within the CNS. The function of IL-33 is regulated by extracellular production of sST2 which acts as a decoy, binding extracellular IL-33 to limit its effects.*

1.2.4 Biological sex and AD

Men and women are different. While this statement may seem obvious, it is important to understand that these differences have far-reaching consequences in brain circuitry (Rurak *et al.,* 2022), immune function (Osborne, Turano and Schwarz, 2018) and susceptibility to disease. This is particularly true for autoimmune diseases, with women being 4 times more likely to develop systemic lupus erythematosus (SLE) and Grave's disease and twice as likely to develop multiple sclerosis (MS) and rheumatoid arthritis (RA) (Ji, Sundquist and Sundquist, 2016). This increased susceptibility to autoimmune diseases is hypothesised to come from the more readily-inflammatory female immune system (Beagley and Gockel, 2003; Klein and Flanagan, 2016; Osborne, Turano and Schwarz, 2018; Murtaj *et al.,* 2019). However, the susceptibility to other diseases such as inflammatory bowel disease (Rustgi, Kayal and Shah, 2020) changes across lifespan, with males and females exhibiting different incidence rates at different ages. Given that expression of sex hormones changes across the human lifespan in both sexes (Nugent *et al.,* 2012) this likely points towards hormones as a strong factor in influencing the development of autoimmune disease.

While there has been much research into the general pathology of AD, there has been relatively little research into the effects of biological sex and associated hormonal differences on the pathology of AD. Dementia is the leading cause of death amongst women in the UK, with women making up 61% of diagnosed dementia cases in the UK in 2015 (Alzheimer's Research UK, 2015) and women having a 20% lifetime risk of developing AD compared to 10% in men ('2022 Alzheimer's disease facts and figures', 2022). Women are also more susceptible to the ApoE4 mutation than men (Neu *et al.,* 2017; Anstey *et al.,* 2021). So why are women more likely to get AD, and how does their pathology differ from men?

Some publications argue the reason for the disparity in numbers is simply the extended lifespan of women as women live longer with a life expectancy of 80.8 compared to 76.6 in men within Scotland ('Life Expectancy in Scotland 2019-2021', 2022) and therefore live long enough to get dementia (Chêne *et al.,* 2015). While there is no doubt this is a factor to be considered, viewing this as the sole reason is short-sighted at best. Evidence suggests there are many factors associated with sex at play such as the innate differences in hormone signalling which can directly influence brain

development and immune function, thus affecting neuroinflammation in the CNS and the pathogenesis of AD (Duffy *et al.,* 2011; Osborne, Turano and Schwarz, 2018).

One of the key differences between males and females is the production of sex hormones. The classical view is that males produce significantly higher levels of androgens (e.g., testosterone) while females produce more estrogen (e.g., progesterone, estradiol). More modern views appreciate that while these observations remain true, there is instead a delicate balance of these two sex hormones in both sexes (Hammes and Levin, 2019). Regardless of sex, the difference in expression of these signalling hormones begins very early in neural development and directly affect the development of the brain (Fish *et al.,* 2020). As humans age our bodies express varying levels of these hormones, with peaks during puberty followed by a steady decline throughout aging in both sexes (Horstman *et al.,* 2012). One key difference however is that while men experience a gradual decline in testosterone production across their lifespan, in mid-late life stages women experience menopause which is induced by a sharp decrease in production of estrogen and progesterone as a result of loss of ovarian function (Greendale, Lee and Arriola, 1999). Changes in hormone expression have been linked to development of AD in both sexes, but this difference in expression in mid-late life may explain part of the sex-difference in AD cases (Fisher, Bennett and Dong, 2018; Cui *et al.,* 2022).

Studies have shown that women are considerably more likely to develop AD post-menopause, and that this risk was reduced by hormone replacement therapy (HRT) of progesterone and estrogen (Zhou *et al.,* 2020). Estrogens are well known to have intense effects on immune cells, particularly microglial cells (Loiola *et al.,* 2019) as well as directly influencing expression of neurotransmitters (Adams *et al.,* 2004; Belelli *et al.,* 2006). Similarly, as men age, they experience reduction in testosterone production (Harman *et al.,* 2001) and this reduction in testosterone has been linked to higher incidence of AD (Marriott *et al.,* 2022). Hormone replacement therapy of testosterone has been shown, in some studies, to reduce AD symptoms and pathology in men (Marriott *et al.,* 2022). It is, however, worth noting that testosterone is converted into estrogen by aromatases in the brain (Azcoitia, Mendez and Garcia-Segura, 2021) and so this protective effect may be due to testosterone converted to estrogen rather than directly by testosterone itself.

Sex hormones have also been shown to impact the immune system. Female immune systems have a tendency towards more reactivity due to the influence of estrogen in both the peripheral immune system (Beagley and Gockel, 2003) and within the CNS (Murtaj *et al.,* 2019). Given the important role of neuroinflammation in AD development, it is perhaps unsurprising that women experience higher rates of disease. There are also other protein differences between men and women.

In both sexes it therefore appears that the dysregulation of sex hormones leads to pathology associated with AD. However, research to understand the impact of sex on AD development and even neuroscience as whole remains a relatively new field of research. Despite the evidence of key differences between the sexes, the overwhelming majority of research across many diseases is conducted using male animals alone. Many suggest this lack of inclusion is due to complications of hormonal cycles- a perception which has been proven false as males exhibit as much variability in females (Prendergast, Onishi and Zucker, 2014), additional complexity in analysis and additional cost. Perhaps more unhelpfully, many publications neglect to mention the sex of the animals used at all (Beery and Zucker, 2011) and often those that do include both sexes fail to include comparison between the two. Furthermore, the majority of cell-lines available for purchase for in-vitro experiments do not state the sex of the source animal (Park *et al.,* 2015). This lack of consideration for sex in in-vivo and in-vitro research has serious consequences when drugs or treatments reach clinical trials, with women often experiencing higher rates of, or more serious adverse events (Harkin *et al.,* 2001; Raz and Miller, 2013). The lack of inclusion of sex as a factor in both experiments and reporting of results is therefore detrimental to women, and further steps should be taken by researchers as a whole to include both sexes- or at the very least standardise inclusion of the information of their cell-lines or animals used.

These publications and findings emphasise the key role of sex in determining AD pathology and outcomes, as well as highlighting a gap in the current research. By identifying how men and women respond differently to treatments and immune-challenge we can better understand how to tailor treatments to combat disease.

1.3 Mouse models of AD

Animal models of disease are key tools in biomedical research allowing insight into complex mechanisms and interplay between organs and cells, from autoimmune diseases to infectious diseases. They have been essential for understanding pathologies and for developing treatments for humans. Given the incredible complexity of the brain and the neuroimmune interaction, there are currently no means to replicate the complex AD pathology without the use of animal models of the disease. Use of AD models also allows us to naturally investigate the effects of sex on development of pathology. Over the decades of research into AD pathology multiple murine models have been developed which emulate different aspects of the disease via mutations and additions of human genes, and thus allow in-depth research into the pathogenesis of AD and development of potential drugs and targets.

Mouse models of AD can be created by inducing transgenic expression of an AD-associated human gene insert. This is achieved by introduction of a synthetic cDNA controlled by a native promoter, resulting in artificial expression of the transgenic gene (Elder, Gama Sosa and De Gasperi, 2010). This typically involves excessive expression of a single gene variant- because of this, these models can be inaccurate as the genes are expressed at a level not synonymous with human expression. The animals are still able to express their own, native version of these proteins which can interfere with the transgenic proteins (Yokoyama *et al.,* 2022). The APP gene responsible for coding the β-secretase is an ideal choice as this increases the overall Aβ burden in the mice and its mutation is termed the Swedish mutation (Swe). Mutations at other locations on the APP gene result in a shift in the ratio of $A\beta_{40:42}$ with higher aggregation of Aβ due to longer peptide chains thus resulting in increased pathology (Sasaguri *et al.,* 2017). There are 3 frequently used mutations of this kind named London (Lon), Florida (Flo) and Iberian (Ibe) (Wisniewski and Sigurdsson, 2010; Jankowsky and Zheng, 2017). The second mutation target is *PSEN1* gene which alters the processing by γ-secretase resulting in longer and thus more pathogenic Aβ chains. Finally, some models focus specifically on the phosphorylated tau aspect of disease by introducing mutations in MAPT. Different models with specific mutations exhibit unique pathologies and immune interactions allowing for study of a single gene mutation and its effects, to the effects of multiple mutations. Examples of such models are the 5xFAD model which is named for its 5 key mutations- 3 on *APP* (Swe, Lon, Flo) and 2 on *PSEN1* (M146L, L286V) resulting in a model that focuses

on rapid amyloid plaque development. These mice develop pathology as early as 2 months of age and so allow for a quick turn-around in experiments and high focus on the amyloid pathology of AD. The key drawback to this model, however, is the absence of any clear tau pathology. These mice also exhibit cerebral amyloid angiopathy and abnormalities in myelin (Chu *et al.,* 2017). Another frequently used transgenic AD mouse model is the APP/PS1 model. These mice have a single *APP* mutation (Swe) and *PSEN*1 mutation (L166P) and are similarly rapid to develop symptoms beginning at 3-4 months but also exhibit phosphorylation of tau allowing the study of multiple aspects of AD pathogenesis (Radde *et al.,* 2006).

Mouse models can also be created by "knocking-in" a gene- in this method the native expression of the gene is fully preserved but the resulting protein is modified to contain a mutation. One example of a knock-in model is 3xTg mice which express 3 mutations on 3 genes: transgenic *APP* (Swe), *PSEN1* (M146V) and Tau mutation P301L. This model therefore develops Aβ plaques at 6 months of age and NFTs starting at 12 months, allowing study into both aspects of AD hallmark pathologies (Oddo et al*.,* 2003).

Interestingly, all three models described here and summarised in Table 1.1 exhibit a sex-based disparity in disease severity, with females exhibiting significantly more pathology earlier than males (Jiao *et al.,* 2016; Sadleir, Popovic and Vassar, 2018; Bundy *et al.,* 2019; Dennison *et al.,* 2021). These models are among the most commonly used to study AD pathologies, and all of these express their genetic modifications under the control of the Thy1 promoter located on chromosome 9. Thy-1 is an immunoglobin superfamily member expressed by neurons in the nervous system as well as both immune cells of the peripheral immune system and cells across the body. Its promoter has been suggested to contain an estrogen responsive element (Sadleir *et al.,* 2015) which may explain why females of these mouse models tend towards more severe pathology than males. However, the differences may also be due to innate differences in inflammation and gene expression between the sexes, making their inclusion in sex-balanced studies all the more relevant to human AD.

Table 1.1 Summary of 3 transgenic mouse models of AD.

AD mouse model	5xFAD	APP/PS1	3xTg
Model type	Transgenic	Transgenic	Transgenic + KI
Mutations	3xAPP (Swe, Lo, Flo)	1x APP (Swe)	1xAPP (Swe)
	2X PSEN1 (M146L, L286V)	1x PSEN1 (L166P)	1x PSEN1 (M146V)
			1x Tau (P301L) **(KI)**
Promoter	Thy1.2	Thy1.2	Thy1.2
Pathology	Aβ	Aβ + some tau (No fibrils)	Aβ + Tau
Onset	2 months	3-4 months	6 months
Sex differences?	**Y**	**Y**	**Y**
Citation	(Oblak *et al.,* 2021; Sil *et al.,* 2022)	(Yokoyama *et al.,* 2022)	(Sasaguri *et al.,* 2017; Yokoyama *et al.,* 2022)

KI: Mouse model "Knock-In".

Animal models have been the key tool in advancing our understanding of diseases and are ideally suited to study the complex pathologies of AD. However, there are major drawbacks to animal models that must be considered. Aside from ethical and financial considerations, there are many differences between human AD and murine models. While having mice develop symptoms early allows for rapid research, it does not mimic human disease which gradually develops with age. Furthermore, the rapid development of CNS pathology in murine models is often induced via overexpression of non-murine genes which is not observed in human AD patients and therefore creates numerous other pathologies not associated with AD, thus the models are not closely representative of human conditions. For example, natural murine tau proteins vary significantly in their properties and are not able to develop NFTs, which is a key hallmark of human AD, so mutations must be introduced to allow development of human tau proteins. This therefore limits the similarity between the model and human AD (Ecol, 2017).

Despite these differences and considerations, animal models allow us to provide key insights into the pathology and development of AD and other diseases of the CNS. There is currently no alternative way for us to model the vast complexity and intricacy of the brain and its interaction with the immune system, and therefore animal models remain a staple in research.

1.4 Current Therapies for AD

To date there is no known cure for AD due to its complexity and the fact that pathology begins to occur long before detectable symptoms. Within the UK, the National Institute for Health and Care Excellence (NICE) advises that patients diagnosed with AD are encouraged to participate in group cognitive stimulation and reminiscence therapy and remain physically active to mitigate further neurodegeneration. NICE also advises on pharmacological interventions which may be used to treat or reduce symptoms associated with disease, but these are not for long-term use and instead only a temporary measure (National Institute for Health and Care Excellence, 2018). Currently there are only two classes of drug available on market which are targeted at treating the disease symptoms and/or delaying development of AD for patients. These two classes target excitatory neurotransmitters and modulate their levels within the CNS.

Acetylcholine is a neurotransmitter associated with memory recall and is released from the synaptic cleft between neurons then hydrolysed by cholinesterase at the recipient nerve. AD is associated with a marked decrease in acetylcholine and so one method of treating AD symptoms targets the cholinesterase enzymes. By inhibiting the degradation of acetylcholine, the neurotransmitter can accumulate in the synapses thus reducing the symptoms of AD. This class of drugs is termed “cholinesterase inhibitors” and is used to treat mild to moderate cases of AD (Kumar *et al.,* 2018). However, acetylcholine and its receptors are ubiquitously expressed throughout the body in muscular tissue (Evans *et al.,* 1987) cardiovascular tissue (Roy *et al.,* 2013) and the gut epithelium (Keely, 2011) thus cholinesterase inhibitors and their resulting build-up of acetylcholine can induce serious side effects and are therefore only prescribed in short-term doses.

AD is also associated with excessive build-up of another excitatory neurotransmitter, glutamate. Memantine is a drug that blocks the NMDA receptor- a glutamate receptor

(Danysz and Parsons, 2012). By competitively blocking this receptor the accumulation of glutamate is prevented thus reducing neuronal levels of glutamate and preventing toxicity to cells. NMDA antagonists are used to treat moderate to severe cases of AD and are often prescribed alongside cholinesterase inhibitors.

While no other treatments are commercially available, a variety of clinical trials are ongoing aimed at targeting novel molecules such as γ-secretases (Rynearson *et al.,* 2021) and tau-associated proteins (Ji and Sigurdsson, 2021). While these molecules are associated with AD development, targeting them directly has widespread consequences due to their involvement in normal metabolism, meaning they are not ideal targets. There have been countless attempts at developing an antibody against the abnormal proteins associated with AD, however until recently these have all failed clinical trials due to lack of efficacy or toxicity to participants (Mullard, 2019; Imbimbo et al., 2023).

Recently there have been promising results from some phase 3 clinical trials of antibody-based therapies for AD. Lecanemab (Trial ID: NCT03887455) and Donanemab (Trial ID: NCT04437511) both target Aβ, the hallmark pathology of AD, binding to the plaques to mark them for destruction by native immune cells (U.S. Food and Drug Administration, 2023).Lecanemab functions by targeting the protofibrils Aβ and thus almost completely removes Aβ plaques as well as preventing further deposition and limiting cognitive decline. Donanemab functions similarly, with neither antibody affecting the overall pTau presence in the brain (Shi *et al.,* 2022). However, trials of both drugs come with the risk of brain haemorrhages at a rate of 10-15% for donanemab and 12.6% for lecanumab (Piller, 2022; Rashad *et al.,* 2022; van Dyck *et al.,* 2023) and despite the almost-total removal of Aβ by Lecanemab patient outcomes were not significantly improved (i.e disease ultimately continued to progress). It is also worth noting that several antibodies such as solanezumab and bapineuzumab made it to phase 3 clinical trials before being deemed unsafe or ineffective. This emphasises the need for less invasive therapies to combat the disease. These treatments also do not target any of the other associated pathologies and are only applicable after development of symptoms.

There is therefore a need for a non-invasive, low risk therapy that is easy to administrate and provides measurable decreases in disease pathology and

symptoms. One potential therapy that appears to offer all this is the treatment of gamma oscillations in the CNS.

1.5 Circuitry and oscillations of the brain.

The CNS and specifically the brain- is immensely complex, with a massive variety of neural cells, connections, pathways, and an intricate relationship with both the peripheral and CNS immune system. This brief review will cover the circuitry relevant to the project.

1.5.1 Neural oscillations

Neural oscillations- often referred to as brainwaves- are small electrical impulses produced by neurons in the brain in a rhythmic pattern either in individual cells (via oscillations in membrane potential) or between neurons via action potentials to facilitate synchronisation. These coordinated waves occur widely across brain regions and are considered by some to be essential to operation of the human brain- from memory consolidation and problem solving to sleep and rest (Ward, 2003). The oscillations can be grouped based on their frequency, with each group currently thought to be associated with a different type of brain function. The slowest of these waves are Delta waves which oscillate <4Hz range, are most highly expressed in the sleeping brain and therefore thought to be essential for the rest and revitalisation of the brain. Theta waves oscillate in the 4-7Hz range and are among the most regular waves in the mammalian brain- particularly in the HPF- as they occur in both the waking and sleeping state. Alpha waves oscillating in the 8-13Hz range are associated only with the waking state and are thought to be the only suppressive oscillation. Beta waves oscillate from 12.5-30Hz and are frequently further split into three groups: Low beta or Beta 1 waves (12.5-15Hz), Mid Beta or Beta 2 waves (15-20Hz) and High Beta or Beta 3 waves (18-30Hz). Finally, the fastest waves are Gamma waves which occur from 30-90Hz. These waves are at their most frequent during attention and stimulatory environments, leading to their hypothesised association with cognitive function. However, the function of these rhythms is hypothetical at our current stage of research and largely remain a mystery (Bear, Connors and Paradiso, 2016).

Given the nature of these oscillations and their hypothesised association with cognitive function, research has been conducted into their role in psychological

conditions such as epilepsy, depression, and AD, where altered oscillatory patterns- either increased or decreased- have been observed (Herrmann and Demiralp, 2005; Nakazono *et al.,* 2017; Fitzgerald and Watson, 2018; Byron, Semenova and Sakata, 2021). This suggests an underlying pathology associated with these oscillations which may be symptomatic or causative of the disease, although which is yet to be revealed (Ward, 2003). Of interest in relation to AD due to their association with consciousness and memory formation (van Vugt *et al.,* 2010) are Gamma waves.

Although these waves are naturally altered in patients suffering from diseases such as AD, schizophrenia, and depression, it has been shown that these waves can be induced through non-invasive methods of stimulation. These can be induced via somatostimulation- by vibration at mechanosensors in the hands (Jamali and Ross, 2014), visually- through light flickering at 40hz (Singer *et al.,* 2018) or through auditory receptors- either monoaurally (where 2 signals are overlapped before being heard) or binaurally (where a different frequency is played in each ear and the brain generates a third tone of the difference between the two; eg 120hz in the left ear and 160hz in the right results in a 40hz difference). The stimulation of these gamma waves offers a potential non-invasive mechanism to reduce disease symptoms. However, the results of these oscillation-based treatments are usually short lived and require continuous treatment. There is no data yet available to determine if long-term application of these treatments can stimulate the neurons to regain their ability to produce these waves independently of the external stimulation.(Cimenser *et al.,* 2021)

1.5.2 Neural oscillations and AD

While gamma waves are altered in many neuropsychiatric diseases, such as schizophrenia and depression (Herrmann and Demiralp, 2005), studies in AD have suggested that they are decreased in AD patients- sometimes decades before pathological symptoms (such as tau and Aβ) develop (Ribary *et al.,* 1991). This decrease is similarly displayed in animal models of AD (Klein *et al.,* 2016) suggesting altered gamma wave oscillation is associated with the development of disease pathology induced by the genetic mutations introduced to the model.

There have been many studies into the state of gamma waves in human AD patients with inconclusive results. Some studies in AD patients have revealed that AD is associated with lower gamma oscillatory activity in the frontal lobe correlating with

synaptic dysfunction occurring long before the pathological progression to neuronal cell death (Casula *et al.,* 2022), as well as reduced synchronisation (Koenig *et al.,* 2005) and delays in responses (Başar *et al.,* 2016). It is suggested that this change occurs prior to deposition of tau and Aβ (Klein *et al.,* 2016). In contrast, other studies report increased gamma oscillatory activity in AD patients versus age-matched controls (van Deursen *et al.,* 2011). Regardless of whether the oscillations are increased or decreased, the alterations appear to be associated to the pathology of aging and development of AD.

While the changes in gamma oscillations are detectable decades before the onset of disease it has not yet been determined if this is a symptom or an initiating factor. It is possible the changes in gamma oscillations are induced by the deposition of AβO, which also begins long before symptoms develop as a result of neuron damage and the blocking of interaction between neurons by Aβ. Some studies suggest the alteration in gamma oscillatory patterns is linked to neuroinflammation and oxidative stress (Ta *et al.,* 2019) which was further verified using a chronic-inflammation animal model expressing enhanced NF-κB activity which showed anti-inflammatory treatment helped to restore gamma oscillations (Fielder *et al.,* 2020). Given the hypothesised role of gamma oscillations in the cerebral cortex as the key network for accurate information flow and cellular communication in attention, cognition, and memory, it is likely that the interruption or alteration of this system contributes to the development of AD.

A novel area of research has recently emerged, combining the study of neural oscillations with the study of AD, resulting in discoveries regarding the gamma wave frequency; specifically, at 40hz. Research into this area is relatively new and thus the mechanisms of the improved symptoms observed after application of gamma oscillation treatment have not yet been determined.

1.6 Use of gamma oscillatory treatment in AD

As gamma oscillation changes are observed long before measurable pathology of AD, it may provide a key opportunity for treatment before extensive pathology and resulting cell damage can occur. The methods of administration are also non-invasive, such as flickering a light and listening to a sound therefore and can be performed at home without distress to the patient. There has therefore been significant interest in

the use of 40Hz therapies to reduce AD symptoms (Iaccarino, Annabelle C. Singer, *et al.*, 2016; Singer *et al.*, 2018; Adaikkan *et al.*, 2019; Martorell *et al.*, 2019).

1.6.1 40Hz gamma oscillations in mouse models of AD

In 2016 a paper published by Iaccarino et.al stated surprising findings of effective application of gamma oscillatory treatment for AD. By utilising a light flickering at 40Hz frequency the authors were able to reduce AD pathology across several animal models of the disease (Iaccarino, Annabelle C. Singer, *et al.*, 2016) . This group went on to publish 2 further papers and a protocol for their methods (Singer *et al.*, 2018; Adaikkan *et al.*, 2019; Martorell *et al.*, 2019). Findings from these papers are briefly summarized in Table 1.2.

The first paper published in 2016 (Iaccarino et al., 2016) used 5xFAD Pv-Cre mice, 5xFAD, APP/PS1 and Tau P301S models of AD. After administering 20Hz, 40Hz, 80Hz and random flickering light for 1 hour a day over 7 days, they found that only the 40Hz flicker reduced Aβ pathology and reduced tau phosphorylation in the VC. They attributed this change to a shift in microglial activation state, as they observed changes in cell morphology (measured by Iba1 labelling of reduced process length) and changes in the expression of microglia phagocytic genes without a change in inflammation (measured by IL-6 and IL-1β gene expression). The study states male mice were used for certain experiments but is overall unclear about the sex of the animals.

The second study published in 2019 (Martorell *et al.*, 2019) examined the application of both 40Hz oscillating sound and a combination of 40Hz light and sound, both administered for 1 hour a day over 7 days. They used mice aged 6 or 9 months of age, though sex of the animals was not mentioned. Here they observed the audio-only treatment reduced Aβ burden within both the auditory cortex (AC) and CA1 in APP/PS1 and 5xFAD, and in the same regions they found reduced tau phosphorylation in P301S mice. By combining the treatments, they found the effect of reduced pathology extended further than either treatment alone, reaching the VC, AC, CA1 and medial-prefrontal cortex (mPFC) measured by reduced Aβ and altered gene expression. In addition, they observed behavioural improvements in the memory of the animals after treatment compared to untreated controls with improved scores in Morris-water-maze and novel object behavioural tests. Their overall conclusion was

that the 40Hz treatment stimulated microglia to clear Aβ and increased amyloid trans-vascular transport, though did not specify a mechanism.

The third and final study by this group was published in 2019 (Adaikkan *et al.,* 2019), using 8-month-old male P301S mice to determine the effect of extended treatment duration. They used 40Hz light flicker for 1 hour a day over 22 days and observed reduced tau phosphorylation in the VC. In addition, they reported reduced neuronal & synapse loss in the PFC and CA1, suggesting the extended treatment duration was more capable of reaching brain additional brain regions than the shorter, 7-day treatment. The authors stated that the precise mechanisms of changes in microglia induced by the treatment remained elusive.

Table 1.2 – Summary of Tsai-group 40Hz gamma oscillatory treatment for AD using animal models

*Behavioural changes measured by novel object location, Morris water maze, novel object recognition tests, and therefore do not have a specific associated region for changes.

Treatment	Model	Sex	Age	Brain region	Reduced disease phenotype	Reference
40Hz light (1hr / 7days)	5xFAD, 5xFAD-Pv-Cre, APP/PS1	Male?	3 months & 6 months	VC	Reduced Aβ	(Iaccarino, Annabelle C. Singer, *et al.*, 2016)
	Tau P301S	Male	6 months	VC	Reduced tau phosphorylation	
40hz sound (1hr / 7days)	5xFAD, APP/PS1	Male	6 months & 9 months.	AC and CA1	Reduced Aβ	(Martorell *et al.*, 2019)
	5xFAD	?	6 months	N/A*	Improved memory performance	
	Tau P301S	?		AC and CA1	Reduced tau phosphorylation	
Combined 40Hz light and sound	5xFAD	?	6 months	AC, VC, CA1 & mPFC	Reduced Aβ,	
40Hz light (1hr / 22 days)	P301S	Male	8 months	VC	Reduced tau phosphorylation	(Adaikkan *et al.*, 2019)
					DNA damage markers	
				VC, PFC, CA1	Reduced neuronal &/ synapse loss.	
				N/A*	Improved memory performance	
40Hz light (1hr / 42 days)	CK-p25	**Female**-histology **Male**-RNA-seq, behaviour & western-blotting	?	VC, PFC, CA1 and somatosensory cortex	Neuronal Loss	(Adaikkan *et al.*, 2019)
				VC	Neuroinflammation	
				VC	DNA damage marker	

These publications stimulated a new vigour into study of 40Hz gamma entrainment as a treatment for AD, resulting in other publications into the field of gamma entrainment.

In 2020, a study using 12-month old male 3xTG mice found that combining the 40Hz light flicker with physical exercise reduced Aβ in the VC further than 40Hz light flicker or exercise alone. They treated the animals for 6 days a week for 12 weeks, with 50 minutes of exercise and/or light flicker each day. From the combined treatment they found reduced Aβ pathology, decreased apoptosis and increased neurogenesis in the hippocampus and improved cognitive functions (Park *et al.,* 2020). The authors stated that the light flicker induced "various positive cellular effects" but did not allude to a suspected mechanism for the changes.

Another study published in 2020 examined the effects of the 40Hz light in treating circadian rhythm disorder in aged female APP/PS1 mice as the circadian clock is dysregulated in human patients resulting in significant interruptions to sleep leading to exacerbation of AD symptoms (Saeed and Abbott, 2017). By administering the light flicker treatment 1 hour per day for 30 days, the animals returned their sleep cycles to a state comparable with control mice, whilst also showing significantly reduced Aβ and tau. This effect was induced by restoration of circadian rhythm associated genes *Bmal1*, *Clock* and *Per2* within the suprachiasmatic nucleus (SCN, the "central clock" of the brain)- though precisely how these changes were induced remains unclear (Yao *et al.,* 2020). This study is of particular interest given that it is the first published in the area that utilised female mice- however, it was still an unbalanced study in that they did not use any males for comparison.

The findings from the above studies strongly suggest that 40Hz light flicker treatment has potential to be a non-invasive treatment for AD. However, these studies lack one very important criterion; sex-balance in the animals used. While one study used females, none of these studies examined the differences in sexes in response to 40Hz gamma entrainment treatment. That was one of the aims of this study, however in 2023, a large study by Soula et.al used both sexes (Soula *et al.,* 2023).

This study first examined the effect of 1 hour of 40Hz light on 2 models of AD- the APP/PS1 model and the 5xFAD model. Through several experiments they used 6 cohorts of animals. The first 5 cohorts received 1hr of 40Hz light flicker (or control- either no light or continuous light) and measured treatment effectiveness using IHC. The first of these cohorts was 12-month-old, sex-balanced APP/PS1 mice, and they found no significant changes in Aβ burden in any brain region measured by histology after 40Hz treatment. The second cohort used 5-month-old male APP/PS1 mice, and in this group they observed a decrease in overall Aβ burden in the 40Hz treated group, though the authors attribute this change to the high variability of plaques across hemispheres and between the posterior and anterior variability within regions. The third cohort repeated the second, using 5-month-old male APP/PS1 mice and observed no significant difference in Aβ burden between treated and untreated groups. The fourth cohort used sex-balanced 4-month-old 5xFAD mice and they found no significant differences in Aβ burden after 40Hz light flicker treatment. The fifth cohort used 7-month-old APP/PS1 male animals and observed no difference in Aβ burden after 40Hz light treatment. The final cohort used sex-balanced 5xFAD mice treated with 40Hz light flicker for 7 days and measured Aβ using both histology and ELISA. In this group they observed no significant changes in Aβ pathology using IHC, however in the ELISA measurement they observed a significant decrease in Aβ 1-42 in the VC of 40Hz treated male animals. They then determined if the 40Hz light was indeed stimulating the 40Hz gamma oscillations in the brain and found that while V1 neurons were stimulated, the effect did not reach to the HPF, and that the 40Hz light flicker was insufficient to stimulate native gamma oscillations in the VC or HPF. The authors finally concluded that the 40Hz light entrainment was not an effective treatment for stimulating microglia and clearance of Aβ plaques, stating that the animals were stressed by the lights (measured by avoidance behaviour and cholinergic activity in the brain).

The contrast in results suggests that entrainment of gamma oscillations within the CNS by flickering light or sound is complex, and there remains much to be understood surrounding how - and if - it can stimulate reduction of Aβ, and whether there is a sex bias in response.

1.6.2 40Hz gamma oscillations in human AD patients

Despite our lack of understanding surrounding the mechanisms of the 40Hz treatment, studies into 40Hz gamma entrainment in human AD patients has already begun in small early clinical trials.

Results from a small feasibility study using 10 patients in 2021 found improved connectivity within the brain, and evidence of changes in immune factor expression after 40Hz sound and 40Hz light flicker treatment. This study was primarily to investigate safety of the treatment- though it is of note that female patients appeared to be less responsive to the treatment (He *et al.,* 2021). Another small study using 22 patients with mild-moderate AD found that 40Hz light flicker treatment improved sleep patterns (Cimenser *et al.,* 2021) in patients, alongside improved functional abilities. Additional studies in human trials have so far shown increased cerebral blood flow (Pastor *et al.,* 2002). One group sought to optimise the entrainment by experimenting with different light wavelengths (red, white, green, and blue) and found that white light flickering at 34-38Hz was most effective at entraining gamma waves in healthy human patients.

There are currently also 3 ongoing clinical trials investigating 40Hz gamma oscillatory treatment listed as active on clinicalTrials.gov. The first (trial ID: NCT05776641) being conducted in Massachusetts, USA by the Massachusetts Institute of Technology (MIT) intends to use 40Hz light and sound in cognitively healthy -but at risk of AD- patients to determine if the treatment can prevent development of dementia. The second (trial ID: NCT05655195) also being conducted in Massachusetts USA by MIT intends to administer daily 40Hz light and sound-based treatment to AD patients for 6 months to investigate the effects of chronic treatment. The third trial (trial ID: NCT03657745) is being conducted by a private company, Alzheimer's Light LLC to measure the effectiveness of an iPad app at administering the 40Hz light flicker treatment on patients suffering from AD.

There remains much to be understood surrounding the effectiveness and the mechanisms of the treatment, however. Carriers of different mutations in different animal models may respond differently, as may different ethnic populations (given the genetic background of these populations). Between the animal and human studies

briefly reviewed here, there also appears to be an as-yet un-investigated sex-based bias in the response to 40Hz gamma entrainment therapies.

1.7 Hypothesis and aims.

The overall hypothesis of this project is that the 40Hz gamma oscillatory treatment changes the levels of amyloid deposition in the CNS possible through modulating genes and proteins associated with the APP processing pathway, and that these will be differentially modulated depending on biological sex.

The specific aims of this project are:

1. To develop a 40Hz equipment setup capable of administering 40Hz light flicker treatment to a mouse model of AD.

2. To investigate the effect of 40Hz light flicker treatment on the deposition of amyloid in CNS tissues

3. To understand the effects of 40Hz light flicker treatment on the expression of genes associated with neuroinflammation and those associated with Aβ generation.

4. To determine if the response of 5xFAD mice to 40Hz light flicker treatment is sex-dependent.

Chapter 2

Materials and methods

2. Materials and Methods

2.1 Buffers

2.1.1. Tris buffered saline (TBS)

10x TBS was prepared by adding 24g tris base and 88g sodium chloride (NaCl) to 900ml de-ionised water (DI.H_2O) on stirrer at room temperature (RT). Once dissolved, solution pH was adjusted to 7.6 using hydrochloric acid / sodium hydroxide. Once pH was reached, final volume adjusted to 1L. 10x TBS stored at RT for several months and diluted to 1x TBS in DI.H_2O where required. 1x Tris buffered saline tween (TBST) was prepared by combining 1ml of Tween-20 with 1L of TBS.

2.1.2. Phosphate buffered saline (PBS)

10x PBS was prepared by adding 80g NaCl, 2g potassium chloride (KCl), 2.4g potassium phosphate monobasic (KH2PO4), 14.4g disodium phosphate heptahydrate (Na2HPO4 · 7H2O) to 900ml DI.H_2O. pH was then adjusted to 7.4, and the final volume adjusted to 1L using DI.H_2O. The buffer was further diluted in DI.H_2O to prepare 1x PBS, which will be used in experiments.

2.1.3. Blocking buffer (BB)

To prevent nonspecific binding of primary antibodies, some primary antibodies required serum from the host animal in the BB to improve blocking capabilities and reduce non-specific staining.

Non-serum BB: 0.2g bovine serum albumin (BSA) was added and dissolved in 10ml TBST solution. 25-50µl of Triton x-100 was added and mixed thoroughly.

Serum BB: 0.2g BSA was added to 8ml TBST until dissolved. A further 2ml of sera from host animal species of the primary antibody was added to the solution before adding 25-50µl of tritonx-100. The solution was mixed thoroughly.

All BB was stored in a fridge for a maximum of 5 days.

2.1.4. 10x Tris-Acetic acid-EDTA buffer (TAE)

48.4g Tris base was dissolved in 750ml DI.H_2O while on mixer at RT. 11.42ml glacial acetic acid (CH_3COOH) was added, followed by 20ml of 0.5M pH8.0 EDTA solution. Solution was confirmed to be pH 8.5. 10x solution stored for 2 weeks at 5°C and where required diluted to 1x solution.

2.2 Mice

Homozygous 5xFAD mice on a C57BL/6 background were purchased from Jackson laboratories (Stock No: 006554) and backcrossed to Wild Type (WT) C57BL/6 mice supplied by University of Strathclyde biological procedures unit (BPU) for 10 generations resulting in a mixed litter of homozygous WT and heterozygous 5xFAD offspring. Ear clippings were taken using an ear-punch for genotyping, and samples were flash frozen on dry ice and stored at -80°C where not used immediately.

All mice were maintained in the BPU at the University of Strathclyde on a 12-hour day / 12-hour night cycle. When not undergoing experiments, all animals had ad-libitum access to food, water, and enrichment.

Mice were separated by gender and genotype, then blind assigned to treatment and control groups. All animal experiments were performed in the BPU at Strathclyde university under the guidelines of the UK Animals (Scientific Procedures) Act 1986 and were conducted under project licence PP0688944 with local ethical approval and granted by the UK Home Office.

Throughout experimental treatment animals were closely observed for signs of sterotypy or signs of stress which may affect the animals wellbeing and the outcomes of experiments. Behavioural observations from each treatment session were recorded. Animals from one experimental section were also weighed daily to determine changes in weight which may be indicative of stress.

2.2.1. Genotyping - DNA extraction and polymerase-chain reaction (PCR)

PCR was used to genotype litters of mice to identify heterozygous 5xFAD mice from WT mice. DNA was extracted from ear clippings using a PHIRE Tissue Direct PCR Kit. Tissue was placed into PCR tubes and 20µl of dilution buffer added, followed by adding 0.5µl of DNA release buffer. Samples were vortexed, briefly centrifuged and then left to incubate at RT for 3 minutes. They were then incubated in a heat-block at 98°C to lyse cells. Following that the samples were vortexed and the lysate was extracted and placed into a fresh, sterile PCR tube.

For each sample, 1µl of each primer, 10µl of PCR-master mix solution and 1µl of DNA were topped with DI.H2O to make 20µl final volume of the mixture. Samples were then briefly vortexed. PCR primers (FWD: ACC CCC ATG TCA GAG TTC CT; Mutant Rev: CGG GCC TCT TCG CTA TTA C; WT Rev: TAT ACA ACC TTG GGG GAT GG)

and cycling conditions (Table 2.1) were recommended by Jackson laboratories (Protocol 31769, v1.0), the times were recommended by PHIRE Tissue Direct kit.

Table 2.1- PCR cycling conditions used for genotyping 5xFAD mice.

PCR conditions			
STEP	**TIME**	**TEMP (°C)**	**NOTE**
1	5m	94	Denaturing
2	5s	94	
3	5s	65	-0.5°C per cycle decrease
4	20s	68	
5	-	-	Repeat steps 2-4 for 10 cycles (touchdown)
6	5s	94	
7	5s	60	
8	20s	72	
9	-	-	Repeat steps 6-8 for 28 cycles
10	1m	72	
11	-	10	Hold

m: minutes; s: seconds.

2% agarose gel was prepared by combining 0.2g agarose with 10ml TBST and 2µl ethidium bromide, then microwaving solution on high heat. Gel was then allowed 15 minutes to set in the gel tank. After gel had set, TAE buffer (with 2µl ethidium bromide) was added to the gel tank to cover the gel and all wells. 15µl of each PCR reaction was loaded into each well alongside a DNA-ladder. Gels were then run for 60 minutes at 50Hz. After electrophoresis, bands were visualised and findings recorded.

2.3 Tissue collection & processing

After final day of treatment, mice were sacrificed using CO_2 at <20% flow rate, and death was confirmed prior to dissection. If blood was collected, the right atria was severed using scissors, and blood collected from the chest cavity using a syringe. Animals were then perfused transcardially with ice-cold PBS (pH 7.4) until flow was clear of blood. Blood was allowed to coagulate and serum removed. Animal was decapitated, and an incision cut using small scissors along the sagittal suture of the

skull starting at the base of the spinal cord. Skull cap was then peeled off using forceps and brain- including cerebellum but excluding olfactory bulb- extracted from skull using forceps. Spinal cord was harvested by removing all peripheral tissue from the spine, then using a 12G needle inserted into the lumbar spinal cord opening and PBS (pH 7.4) to flush the cord out by pressure.

1.3.1 PBS perfused mice and OCT embedded tissues

Once tissue was extracted, they were then submerged in optimal cutting temperature compound (OCT) and then snap-frozen on dry ice. Tissues were stored at -20°C until sectioning. Fresh frozen tissue was sectioned using a Shandon cryostat to 10μm thick unless stated otherwise and placed onto frosted glass slides. Sections were then allowed to dry overnight at RT, before slides were individually wrapped in foil and stored at -20°C for up to 1 year.

1.3.2 Tissue homogenisation

Mice were perfused with PBS and tissues were collected and placed into a bijou containing 1ml of PBS (pH7.4) with a cocktail of protease and phosphatase inhibitors (Thermo Scientific, Cat no:78440) both at 10μl/ml and stored on ice. The volume of buffer for each tissue was standardised according to the tissue weight. For brain tissue this was at 0.001g = 1μl, and for spleen at 0.001g=4μl. Tissue was then homogenised for 30 seconds on ice using Qiagen Tissueruptor 230v at 10,000 RPM using Tissueruptor transparent disposable probes until all visible solids were disappeared. Tissue was then frozen at -20°C to facilitate final lysing of cells via a freeze-thaw cycle. After defrosting tissue homogenates were spun on a centrifuge (Heraues Fresco 21 Microcentrifuge) at 8000 RPM for 15 minutes, then lysates were removed and stored at -20°C until use for ELISA.

1.4 Immunohistochemistry (IHC)

Slides were taken out of freezer and defrosted at RT for 20 minutes, then fixed in ice cold 75% acetone: 25% ethanol solution for 10 minutes. Slides were then air dried at RT for 10 minutes. Wax outlines were applied around tissue. Tissue was then rehydrated for 25 minutes in 1x TBS, followed by 1 hour incubation with BB at RT. Sections were then added with primary antibody diluted in BB and slides were incubated overnight in a humidity chamber at 5°C.

On the following day, slides were brought back to RT and then washed 3 times in 1x TBST for 5 minutes per wash on a shaker. After washing, secondary antibody diluted in BB was applied to tissues on slides and incubated for a further 1 hour at RT. Slides were then washed 3 times again in TBST. Horseradish peroxidase (HRP) (diluted 1:500) was applied for 45 minutes at RT, then slides washed for another 3 times. Finally, impact AMEC Red substrate was added until a colour change observed. Slides were then briefly dipped in DI.H_2O to stop the reaction, then dipped in haematoxylin for 1 minute. Slides were then washed in a well under running water until clear. Finally, coverslips were mounted using Vectamount aqueous mounting medium. Slides from IHC were observed under a Nikon Eclipse 501 Microscope, and stored in slide-boxes at RT.

1.5 Immunofluorescence (IF)

As described in IHC staining, tissue sections were defrosted, fixed, and treated with BB. Following that, sections were incubated with primary antibody overnight at 5°C.

On the following day slides were brought back to RT and then thoroughly washed in TBST. Tissue sections were then incubated with flurophore conjugated secondary antibody for 1 hour at RT in dark conditions to prevent photobleaching. Slides were then washed 3 times again in TBST. Finally, Vectashield with DAPI (Vector Laboratories) was added before covering with coverslides. Slides were allowed 15 minutes to set at RT before being stored at 5°C until imaging.

1.6 Positive staining quantification

1.6.1 Quantification of levels of amyloid burden in the brain

To ensure the treatment was inducing the oscillations and having the desired impact, the measure of amyloid burden was used as previous studies have confirmed that 40Hz oscillations reduces the level of amyloid in the brain (Iaccarino et al., 2016).

Amyloid staining was performed using Amyloid-β antibody to measure total amyloid burden. Staining was evaluated and images were taken using a Nikon Eclipse e600 epifluorescence upright microscope and WinFluor software. Images were taken from appropriate channels for DAPI and β-amyloid-FITC at 20x objective and saved in .tiff format for analysis in ImageJ software.

In Chapters 2 and 3, 20x images were taken of the DG, CA3, CA1, Subiculum (SUB) and VC regions of mouse brain sections. These images were then opened using image J, and a threshold was set to convert the image to stark black and white. The same threshold was set for all images between samples to reduce variability. The "analyze particles" function was then used to measure the volume of amyloid in the region by size, with a minimum particle size of 3μm set to remove noise and ensure only large plaques were counted. Plaques on the edges of all images were not counted. For each mouse, 3 replicates of connective sections from the same area per region were imaged and quantified, and an average amyloid burden of the three images was used for statistical analysis.

In Chapters 4 and 5, Qupath histological analysis software was used to quantify the Aβ burden due to its efficiency and ease of use. Immunofluorescent images were taken and merged using ImageJ "merge channels" function. Images were then moved into Qupath. We used the "cell density" function to identify different cortical layers and set regions of interest (ROIs), then we used a threshold based on several images which remained the same through analysis of all images to measure Aβ burden. The total area was quantified and measured by the area of the ROI to give a percentage of the ROI that was positive for Aβ.

We measured the total plaque area (mm^2) per region by imaging representative comparable regions in treated and untreated mice. We quantified staining in the visual cortex (VIS), as this was the region most affected by the visual 40Hz stimulation shown in other studies (Iaccarino, Annabelle C. Singer, *et al.,* 2016) , and the SUB region (Fig 3.3) as this is the most affected region in AD (Ishizuka, Weber and Amaral, 1990) and the CA1, CA3 and DG regions across all cell layers.

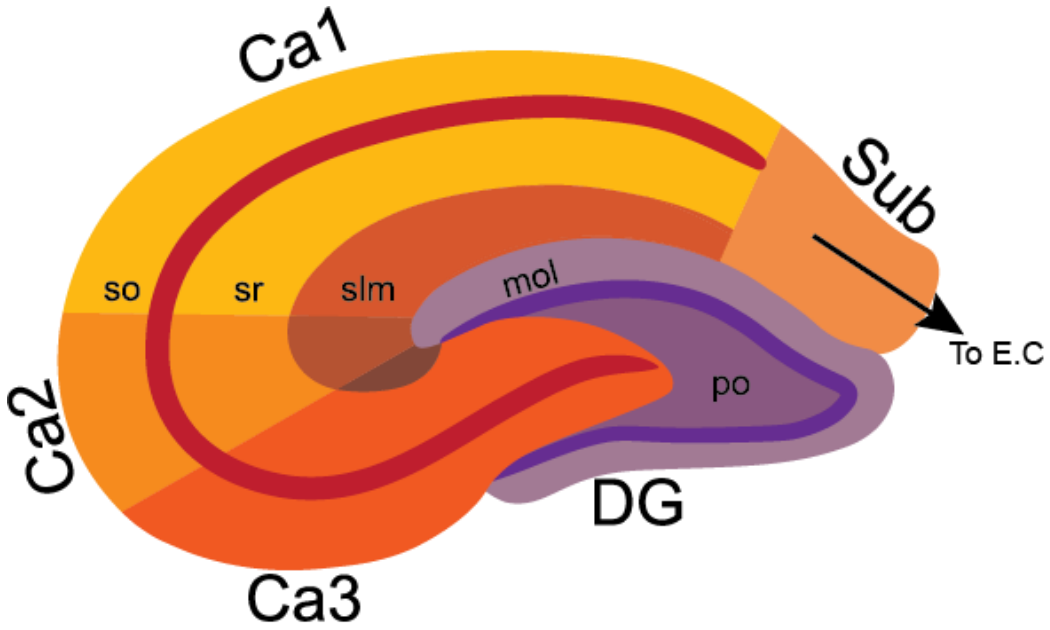

Figure 2.1- Diagram of murine hippocampus structure and regions. *The Dentate Gyrus (DG) is composed mainly of granular cells in 3 layers- the molecular (mol, light purple), granular (darkest purple) and polymorphic layer (middle purple). The cornu ammonis (CA) region is split into 3 main subjections- CA1, CA2 and CA3. Each of these layers is composed of 4 sub-layers. The stratum-oriens (so) is the "outer most" layer of cells. The stratum-radiatum (sr) contains the schaffer lateral cells which connect CA3 to CA1. The stratum- lacunosum-moleculare (slm) layer. CA1 connects to the subiculum (SUB) which then leads onto the enthorinal cortex (E.C) and Visual cortex (VC). We analysed Aβ burden across all 3 cell layers in our images.*

1.6.2 Quantification of CD45 positive cells in the brain

After IHC staining, images were taken using Nikon Eclipse 501 Microscope and NIS-elements F3.2 software. Representative images of the DG, CA3, CA1, SUB and VIS regions of the brain were taken at 10x and 20x, with quantification being conducted on 10x images. Cells positive with CD45 staining were then manually counted using ImageJ or Qupath software. 3 evenly distributed areas for each region for all samples were quantified and an average taken.

1.7 Enzyme-Linked Immuno-Absorbance Assay (ELISA)

1.7.1 CNS tissue preparation

Tissue was snap frozen and stored at -80°C until used. Tissue was then weighed, and 8x volume of ice-cold 5M Guanidine hydrochloride solution was added. Tissue was then homogenised for 30 seconds on ice using Qiagen Tissueruptor 230v at 10,000 RPM using Tissueruptor transparent disposable probes until all visible solids were disappeared, and then placed on a shaker at RT for 3 hours. After 3 hours, the samples were diluted 5x with PBS (pH 7.4) containing AEBSF protease inhibitor at 10µl/ml. Samples were then centrifuged at 16,000G for 20 minutes at 4°C. The supernatant was extracted and snap-frozen to store at -80°C until used.

1.7.2 ELISA

ELISAs were used to quantify levels of amyloid-β and cytokines in the supernatants of homogenised mouse tissues. High binding affinity ELISA plates were coated in 50µl per well of capture antibody diluted in coating buffer (PBS) according to the manufacturers protocol. Plates were sealed carefully and left to incubate overnight at 5°C. On the following day, wells were aspirated and washed 3 times with PBST. Wells were then blocked with 100µl assay diluent (PBS + 10% fetal bovine serum) and incubated at RT for 1 hour. Known concentration of cytokines were prepared and used as standards according to manufacturer protocol and added to wells in the plate, together with testing samples. Plate was then incubated at RT for 2 hours, followed by washing with PBST. Then 50µl of detection antibody diluted in assay diluent was added to each well and plate was incubated for 1 hour at RT. Plates were then washed 3 times with PBST and 50µl of Avidin-Horseradish peroxidase (HRP) diluted according to manufacturer protocol was added to each well and incubated at RT for 1 hour. Plate was washed 3 times with PBST. Finally, 100ul of 1x 3,3′,5,5′-Tetramethylbenzidine solution was added to each well and allowed to incubate at RT

until a visible colour developed. Finally, 50µl of stop solution (1M sulfuric acid) was added. Plates were then read using a microplate spectrophotometer at 450nm. Sample concentrations were then calculated from the standard curve formula.

1.8 Reverse-transcribed PCR

2.8.1 RNA extraction

The primary VC was macrodissected from left hemisphere of the brain, and snap frozen in RNAlater (Thermofisher: AM720) then stored at -80°C for up to 1 year. The remaining hemisphere minus the visual region was also snap frozen in RNAlater and stored. RNA was extracted from tissue using Trizol and a handheld homogeniser. Samples were incubated in Trizol reagent for 10 minutes post-homogenisation, then chloroform added, and another 5-minute incubation performed on ice. Samples were centrifuged at 12000G for 15 minutes at 4°C to phase-separate protein, DNA and RNA.

The RNA lysate supernatant was removed to another bijou, and a solution of ice-cold propran-2-ol, glycogen (0.05µg/µl) and sodium acetate (300mM final concentration) added to precipitate the RNA lysate. Samples were incubated for 1 hour on ice before being centrifuged for 10 minutes at 12000G at 4°C. Supernatant was discarded and pellet resuspended in ice-cold 75% ethanol then vortexed thoroughly as a wash step, repeated 3 times. Samples were then centrifuged at 7500G for 5 minutes, and ethanol supernatant discarded. Samples were allowed to air-dry in the fume hood for 5-10 minutes to evaporate any remaining ethanol. Samples were then resuspended in RNAse-free water (volume depending on sample type; ½ brain suspended in 40µl and VIS region suspended in 10µl) and incubated in a heatblock at 60°C for 10-50 minutes to aid solubilisation. Determination of RNA concentration of samples was conducted using a Thermo-scientific NanoDrop2000c Spectrophotometer. A260/280 and A230/260 values were also recorded to ensure consistent purity of samples, and any samples beneath the 1.7 threshold were re-extracted. After RNA extraction, samples were snap frozen on dry ice and stored at -80°C for a maximum of 2 weeks until cDNA preparation.

2.8.2 cDNA synthesis

cDNA conversion was performed using the Quiagen Quantitect Reverse Transcription kit (Qiagen, Cat: 205311) according to manufacturer's protocol. This kit includes a genomic-DNA wipeout step to reduce contamination by genomic DNA in RNA samples. 1µg of RNA was reverse transcribed per 20µl reaction. Samples were then diluted to 10ng/ul using RNA-free H_2O.

2.8.3 PCR reaction

The qPCR reaction was performed using 96 well-plate and PowerTrack SYBR Green Master Mix (Thermofisher: Cat: A46109). All reagents were defrosted on ice prior to experiment.

A mastermix was created and then pipetted into each well used for the assay-quantities varied depending on number of wells. Each well contained: 5µl of master-mix, 0.5µl of forward primer and 0.5µl of reverse primers (from a 10uM stock) 0.25µl of yellow sample buffer (supplied with kit), 2.75µl of RNA/DNA-free water and 1µl of 10ng/µl cDNA. Each well therefore contained: 1ng/µl cDNA and 500nM Fwd/Rev primers and water to bring total volume to 10µl. RT-PCR steps were performed as per manufacturer instructions, and dissociation step performed to analyse the melt-curves and ensure single products were being generated (Table 2.2).

Table 2.2 Cycling Steps for RT-PCR Gene quantification

Steps for RT-PCR were used as per manufacturer recommendations. *60°C or 65°C were used where specified depending on the optimised conditions for the primer.

STEP	TIME	TEMP (°C)	NOTE
1	2m	95	Enzyme activation
2	5s	95	Denature
3	5s	60*	Anneal/extend
4	-	-	Repeat steps 2-3 for 40 cycles
Melt-curve analysis / dissociation steps			
1	1.99°C / second		15 seconds
7	1.77°c / second		1 minute
9	0.075°C / second		Dissociation

Table 2.3- Sequences and accession IDs of primers used for qPCR

Primer Target	Primer Fwd'	Primer Rev'	Product size (bp)	Tm used	Accession ID
IL33	CTA CTG CAT GAG ACT CCG TTC TG	AGA ATC CCG TGG ATA GGC AGA G	136	60°C	NM_001360725.1
mAPP	TCC GTG TGA TCT ACG AGC GCA T	GCC AAG ACA TCG TCG GAG TAG T	133	60°C	NM_001198826.1
PSEN1	GAG ACT GGA ACA CAA CCA TAG CC	AGA ACA CGA GCC CGA AGG TGA T	132	60°C	NM_001362271.1
BACE1	GGG CAG TAG TAA CTT TGC AGT	GAG GTC TCG ATA TGT GCT GGA	91	60°C	NM_001410457.1
TMEM119	GTG TCT AAC AGG CCC CAG AA	AGC CAC GTG GTA TCA AGG AG	110	65°C	NM_146162.3
P2YR12	CAA GGG GTG GCA TCT ACC TG	AGC CTT GAG TGT TTC TGT AGG G	148	65°C	NM_027571.4
Gpnmb	AGA AAT GGA GCT TTG TCT ACG TC	CTT CGA GAT GGG AAT GTA TGC C	170	60°C	NM_053110.4
Cst7	ACC AAT AAC CCA GGA GTG CTT A	TGA CCC AGA CTT CAG AGT AGC A	262	60°C	NM_009977.3

2.8.4 PCR analysis and controls

In Chapters 4 and 5, RT-PCR data used 3-well replicates per animal with GAPDH as a reference gene. GAPDH CT values were averaged, and gene values normalised to that average using the ΔΔCt method (Livak and Schmittgen, 2001). Each data set used CT values from a minimum of 3 animals. An average was taken from 3 reps per animal, and the average plotted in all graphs. In Chapter 5, male CT values were normalised to their respect female group CT instead of WT-UT controls.

All extracted RNA was checked for contamination by running a standard PCR with GAPDH primers. Any samples that amplified with a Ct value above 35 were discarded. This value was reached based on optimisation experiments to remove amplification of non-specific amplification of background nucleic acids or degradation of fluorophores (Caraguel *et al.,* 2011).

1.9 Data presentation and statistical analysis

For IHC results, representative images were selected from one replicate of one mouse showing results closest to the average outcome from 3 replicates. Images were processed using image J analysis software. For CD45, Aβ and IL-33 +Olig2 stained images a minimum of 3 replicates were imaged for each animal, and a minimum of 3 animals used per group. CD45 data was manually counted by experimenter using Image J cell-counter application. Aβ data was assessed by setting a threshold based on several images and counting particle size using Image J (Schneider, Rasband and Eliceiri, 2012) or Qupath v.0.3.2 software where specified (Bankhead et al., 2017). Once a threshold was decided for Aβ and IL-33/Olig2 analysis, the threshold was not changed between images to prevent bias.

Data was assessed for normality using Graphpad Prism 9.0. As n numbers were too small to use the D'agostino and Pearson normality test for several experiments ($n<5$) and due to high variation in groups (e.g, WT-UT Aβ values were close to 0 μm^2 compared to FAD-UT Aβ values of 50+ μm^2). The Shapiro-Wilk or Kruskal-Wallis test was used instead where stated.

When comparing Aβ burden values from histology tests between sex-combined data (Chapters 3 and 4, the 4 groups being WT-UT, WT-T, FAD-UT, and FAD-T where UT= untreated control and T= 40Hz light treated), a two-way ANOVA was used to assess differences between 2 independent variables (genotype and treatment group)

against the dependent variable (Aβ burden). Two-Way ANOVA was selected to compare 3 hypotheses- That genotype was a factor affecting Aβ burden, treatment group was a factor affecting Aβ burden, and that there was an interaction between treatment group and genotype, where the null hypothesis (H0) states that there is no significant difference (i.e. the means of groups were equal) or the alternative hypothesis (H1) that there is a difference in the means, so one of these variables is a factor affecting Aβ burden. However, each two-way ANOVA used Tukey's multiple comparisons to compare WT-UT with WT-T and FAD-UT, and FAD-UT with FAD-T to determine differences between untreated 5xFADs and WT animals, and differences between Aβ burden in 5xFADs after treatment. All ANOVAs used Tukey's correction and 3 degrees of freedom (between columns) where specified to identify the specific groups between which differences existed and identify the specific P-value of the difference.

Where there were 3 variables to be analysed (e.g., Sex, Genotype, Treatment or Sex, treatment, and cortical layer) a 3-way ANOVA was performed to assess interactions between the 3 variables. Tukey's multiple comparisons test was also performed to determine where significant differences were specifically occurring.

For RT-PCR results (Chapters 4 and 5) a one-way ANOVA was similarly used to compare the 4 groups (WT-T/UT, FAD-T/UT) as results had already been normalised to WT-UT group. In comparisons between male and female expression of genes within genotype and group (e.g., male WT-UT compared to female WT-UT values), an unpaired t-test was used to compare the means of the two independent groups (male compared to female, where sex is the only independent variable).

Statistical tests, P values, degrees of freedom (Df) and sample sizes are specified in figure legends for all data, and data= mean +/- S.E.M. A 95% confidence interval was used, meaning P*<0.05, P**<0.01, P***<0.001, where P<0.05 considered statistically significant. F values are reported as F (DF*numerator*, DF*denominator*) = F-value.

Chapter 3

5-day and 15-day 40Hz light exposure to 9-month-old 5xFAD animals

3. 5-day and 15-day 40Hz light exposure to 9-month-old 5xFAD animals

This study uses 5xFAD mice on a C57BL/6 background to investigate the immune response to 40Hz light-flicker mediated induction of gamma oscillations in the brain. Heterozygous 5xFAD mice rapidly develop Aβ plaques and synaptic deficits beginning from 2 months of age (Oakley *et al.,* 2006; Richard *et al.,* 2015) which rapidly increase in size and number as animals age. Previous studies have shown that administering light flicker treatment to 4-6-month-old 5xFAD mice reduced amyloid pathology and activated microglial immune responses (Iaccarino, Anabelle C. Singer, *et al.,* 2016; Singer *et al.,* 2018; Garza *et al.,* 2020). To begin, we sought to replicate these effects before we began looking into other immunological mechanisms of the treatment. The initial plan was to use mice at 4 and 6 months to determine if there was a difference in age at which treatment was administered. However, due to the urgent and swift COVID-19 lockdown beginning in March 2020 this timepoint became unfeasible as the University of Strathclyde shut down all access and the mice aged past both timepoints. By the time access was restored, the mice had aged to 9 months. To prevent needless loss of animals, we planned to use these mice at this late stage, which we hypothesised would more closely represent the human disease, where pathology is not detected until later life-stages and is therefore already severe. The use of 40Hz light flicker had not been previously studied in late stage of disease in 5xFADs had also, therefore this offered the opportunity to provide potential insight into the treatment's efficacy at late-stage disease where symptoms were severe, and thus further inform effectiveness of diagnosed AD patients.

Mice were treated with 5 days of consecutive treatment or 3 weeks of 5 days of treatment (Monday – Friday), then the effect of the treatment was measured by analysing the amyloid burden and neuroinflammation within the brain (Fig 3.1). For each target molecule we imaged the VC primarily as this was shown to be the only region affected by visual stimulus. We also imaged the subiculum, CA1, CA3 and DG as these are closely associated with AD pathology progression, and we wished to determine if there were even minor changes in these regions. Mice were treated for 5 consecutive days or 15 days (3 sets of 5 consecutive days excluding weekends due to COVID restrictions) where specified throughout this chapter.

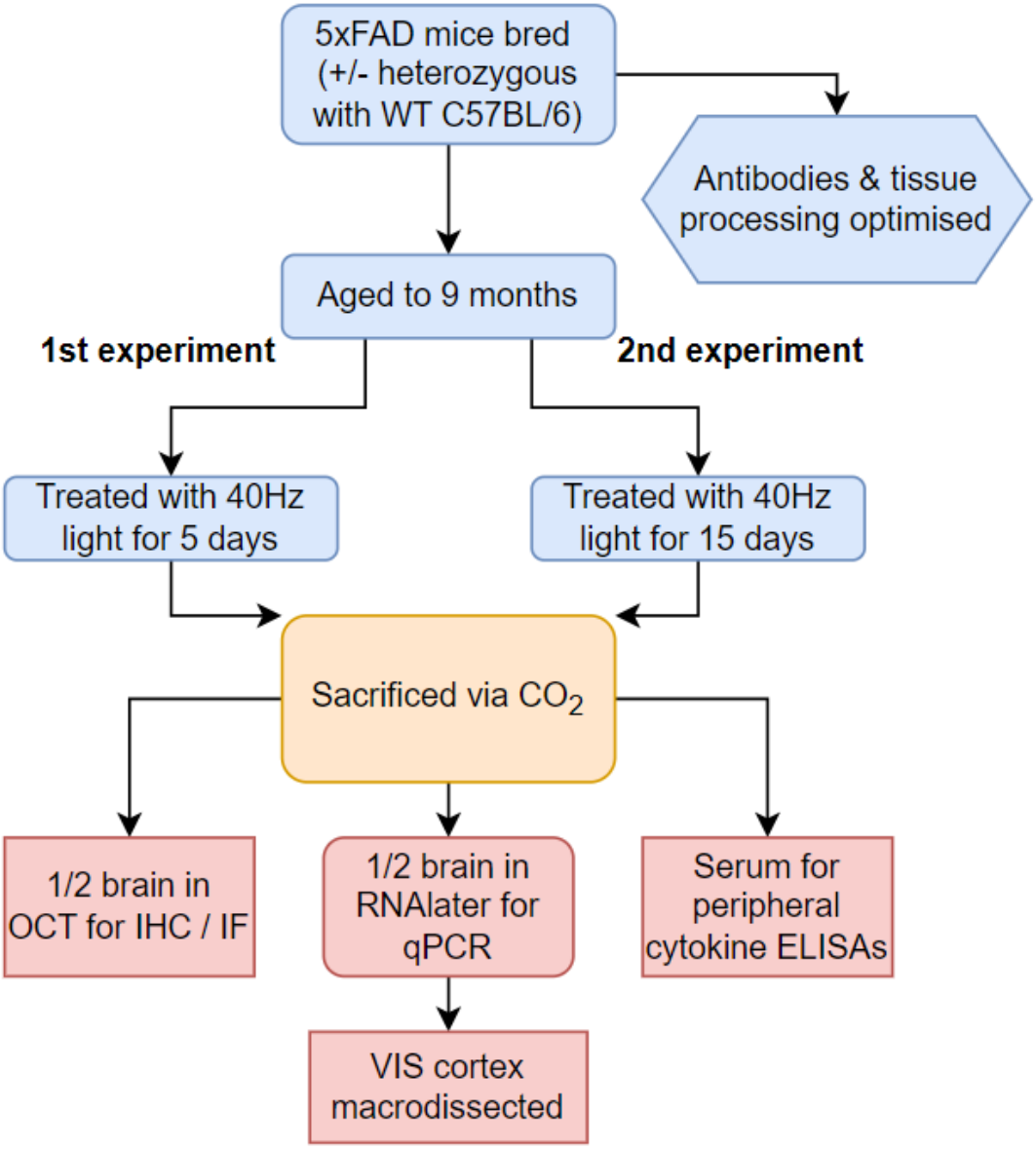

Figure 3.1- Workflow through treatment, breeding and harvesting of 9-month-old 5xFAD animals.

Flow diagram shows the work process from breeding heterozygous 5xFAD mice with WT-C57BL/6 supplied by University of Strathclyde BPU. While animals were aged to 9 months old, antibodies were researched, purchased, and optimised. Different methods of fixation and tissue processing methods were also investigated. Once animals reached 9 months old, they were treated with 40Hz light flicker for 5 days or 15 days where specified. Animals were then sacrificed via CO_2 and tissues harvested and dissected where specified.

3.1 Aims of Chapter

1. The first objective in this chapter was to construct the circuit required to administer the 40Hz light flicker, alongside constructing the administration chamber.

2. To generate and validate the 5xFAD mouse model of AD for our purposes, including genotyping methods to identify heterozygous animals from WT littermates.

3. To measure the effects of administration of 5 days of 40Hz light flicker on Aβ burden and neuroinflammation in 9-month-old 5xFAD animals. This was to be measured by expression of Aβ in the hippocampus and visual cortex.

4. To determine the effects of administration of 15 days of 40Hz light flicker on 9-month-old 5xFAD animals, with the same measurements and outcomes as the third aim. The main aim being to see if this extended treatment time had additional impact compared to the 5-day treatment.

3.2 Results

At 9 months of age, 5xFAD animals exhibit severe amyloid accumulation. We used a pan-amyloid-β staining as a measure of the treatments effectiveness before investigating the treatments effects on markers which had not yet been studied after this treatment, such as CD45.

3.2.1 40Hz light flicker treatment setup

To facilitate light flicker, equipment was purchased, and custom built for this purpose (Figure 3.1). A strip of light-emitting diodes (LEDs) in the white spectrum (natural white, 4000K, 390-700nm at 1090 lumens/meter) was programmed to turn on for 50% of each duty cycle to provide a clear flickering stimulus. Lights set to flicker at 40Hz (25ms period) with lights on for 12.5ms and off for 12.5ms. This was achieved using a previously published Arduino code (Appendix A)

To generate the 40Hz flicker the LEDs were assembled to a circuit-board managed by an Arduino system (Figure 3.2). Flicker at 40Hz was confirmed using an oscilloscope, and sufficient light output (approx. 1000 lux) confirmed using a lux meter.

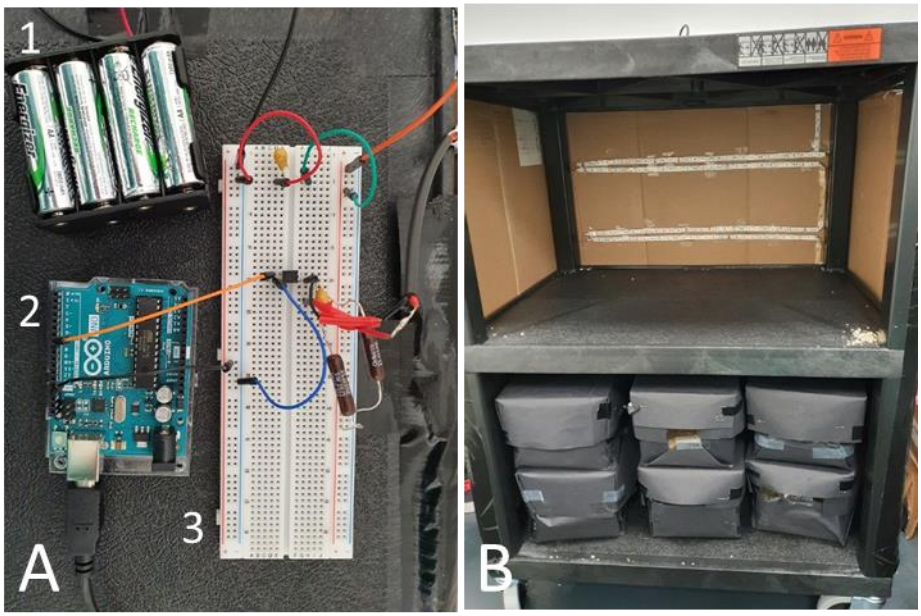

Figure 3.2 - Experimental equipment custom built for 40Hz light treatment. ***A****: Arduino system (A2) and LED lights were connected to the breadboard (A3) and rechargeable battery pack power source (A1). Arduino is connected to a PC (not shown) as a power source via USB.* ***B****: Cage setup and spacing of LED lights used for duration of 40Hz light administration. Cages are clear plastic with a wire lid, wrapped on 5 sides with black paper. The exposed side faces the LED lights. Cages measure 33cm long, 12cm wide and 13cm deep, with the shortest side facing the light.*

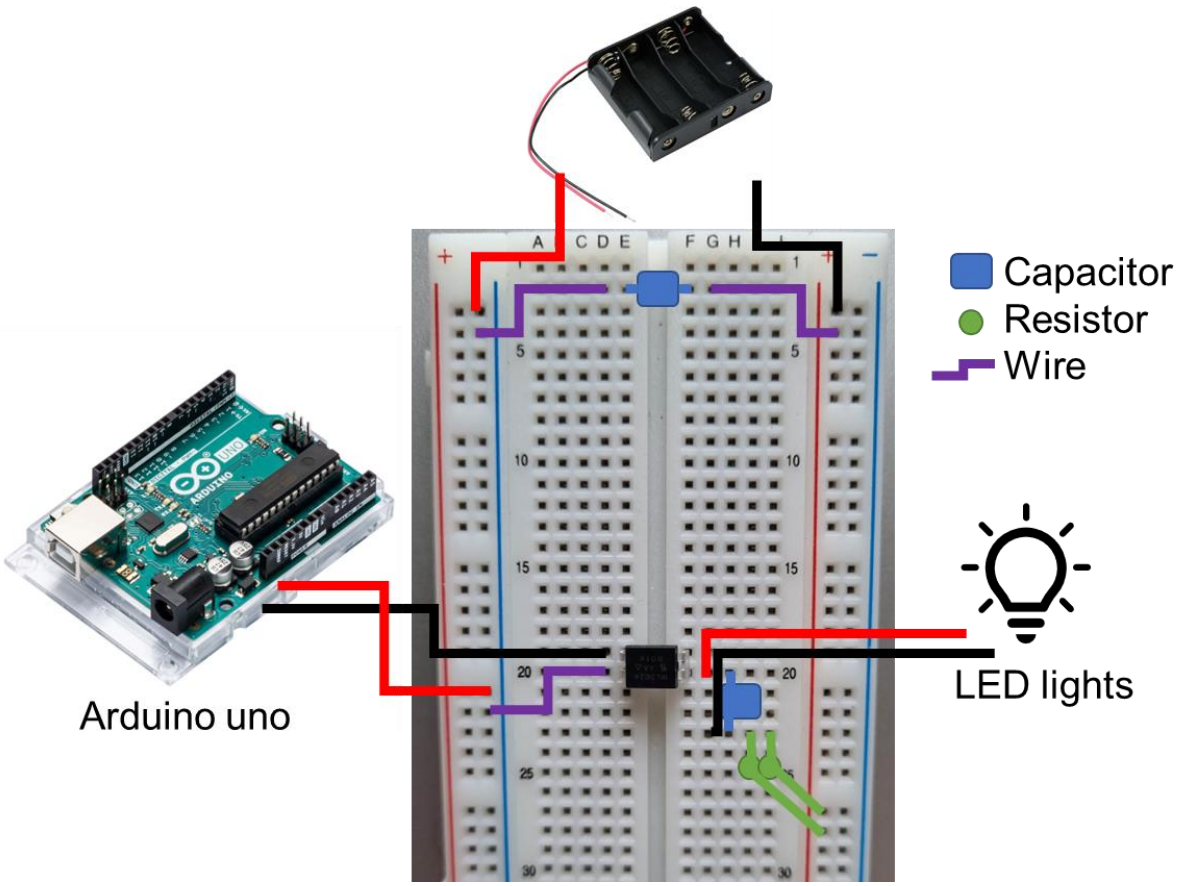

Figure 3.3- Circuit diagram of breadboard used for 40hz light treatment.

The circuit from the original published protocol had to be adapted as the original did not power the lights. Circuit diagram shows 47µF/50v capacitors (blue), 5W/25Ohm resistors (green) and wires (purple) used. Arduino (left), power source (top) and LED light output (right) each have positive current (black) and ground (red) wires. The power source used rechargeable AA batteries. The Arduino system was connected to, and powered by, a laptop which was used to apply the 40Hz flicker code.

Prior to experiment, animals were placed into individual clear plastic cages of identical size to their “home” cage wrapped in black paper on 5 sides. This prevents animals from seeing other animals and the experimenter and allows the LED lights to be the only source of light into the cage. Cages had sawdust bedding but no food or water available for the duration to prevent gamma stimulation from enrichment rather than from the lights. Animals were allowed 1 hour in the dark to habituate to environment before LED lights were activated for the treatment group. Light flicker treatment was administered for 1 hour then animals returned to original holding cages. Mice in the control group remained in dark conditions for the entire habituation and treatment duration.

3.2.2 Genotype confirmation of 5xFAD mice

Once weaned (approximately 6 weeks old) animals were ear-tagged for identification and the tissue was used for genotyping as per section 2.1. The PCR identifies 2 genes: a human transgene-insert at 129bp, and a native mouse gene at 216bp. Thus, homozygous WT mice exhibit one band at 216bp, homozygous 5xFAD mice exhibit one band at 129bp and heterozygous 5xFAD mice exhibit 2 bands; one at 216bp and one at 129bp (see Fig 3.4). We aimed to used heterozygous mice through this experiment, and thus each litter was genotyped after weaning. The results of our in-house testing were confirmed by TransnetYX, an external genotyping service. While the rapid Aβ deposition of mice homozygous for the transgene insert proved appealing, we opted to use heterozygous mice in this study due to the high mortality rate observed in pups of these animals within our facility, combined with the lack of available published data for homozygous animals.

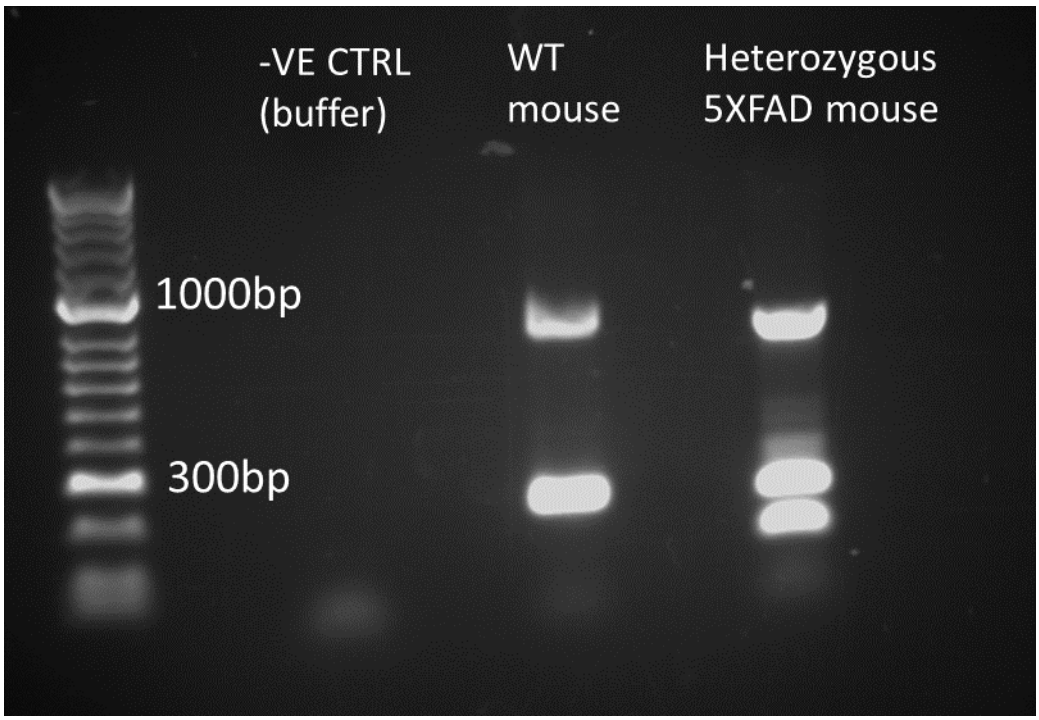

Figure 3.4 – PCR genotyping of 5xFAD animals

Example of PCR results identifying heterozygous 5xFAD mouse (two bands at 216bp and 129bp) from homozygous WT C57BL/6 mouse (single band at 216bp). A 5KB DNA ladder is shown at the left with indicated positions of the 1000 and 300 bp bands. The top band at 1000bp is included in the kit used for the reaction and indicates the presence of DNA. The single band displayed at approximately 300bp on the WT mouse is the 216bp endogenous mouse gene. The heterozygous 5xFAD mouse also displays this, as well as a second band at 129bp.

3.2.3 Effect of 5-day oscillating light treatment on Aβ burden in the brain of 9-month-old mice

Our initial experiments used 5 days of 1 hour stimulation with light treatment on female mice aged 9 months. While other labs have not conducted 5-day studies, this treatment length was selected based on limited access to the University upon our return in the summer of 2020 after the COVID-19 lockdown. All data for the 5-day treatment are from 4 female mice per treatment group.

Immunofluorescence staining was quantified using an anti-Aβ antibody specific to all fragment lengths of amyloid, as our interest was not in specific sizes of Aβ but the overall amyloid burden of the brain. Only plaques greater than 3μm^2 in area were measured. Our primary focus was the VIS region, as the Tsai group has shown that this is the area most affected by the 40Hz light treatment. For statistical analysis the WT and 5xFAD groups were compared using Two-Way ANOVA, then used Tukey's multiple comparisons test to examine the differences between specific groups. As the 5xFAD model is well documented for its rapid Aβ deposition compared to WT-UT (Oakley *et al.,* 2006) we have not reported significant differences between these two, instead we focused on the difference between treatment groups.

After performing IF stains of the visual cortex of untreated mice we found our 5xFAD animals (5xFAD-UT, Fig 3.6) did show the anticipated heavy amyloid burden (>80μm^2 on average per image) when compared to the untreated WT animals (WT-UT, Fig 3.5) which consistently showed 0 amyloid plaques of 3μm or larger. However, the untreated 5xFAD and treated 5xFAD animals showed no significant difference in the Aβ burden in the VC (120.1 ±39.6μm^2 vs 96.4 ±65 μm^2 respectively, Table 3.1). Upon further investigation by examining the data from individual animals, it appeared one of the treated mice showed significantly higher amyloid burden (>150 μm^2, Fig 3.7B), however there was no justification to remove this animal from the data.

Imaging of the SUB region showed significantly higher values of amyloid burden as compared to other regions in the 5xFAD animals (Fig 3.8, 3.9, Table 3.1). Again, no statistical significance was found between treated and untreated 5xFAD animals (Fig 3.10 A)- however, detailed inspection of the data revealed two apparent groups with 2 mice in the treated group low-trending results (approx. 50 μm^2), and 2 showing high-trending (approx. 200 μm^2) (Fig 3.10 B)

Analysis of the levels of A® in CA1 (Figs 3.11,12,13), CA3 (Figs 3.14,15,116) and DG (Figs 15,16,17) regions of 5xFAD animals showed high levels of A® which was unaffected by treatment, with no statistically significant difference between the untreated and 40Hz treated groups (Table 3.1). All WT animals consistently showed 0 positive A® staining. Analysis of individual mouse data showed mouse 1 of the treated group was an outlier consistently showing high levels of Aβ while mouse 3 and 4 of the treated group showed consistently lower level of A®.

Table 3.1- Aβ measurements in the hippocampus and VC of 9-month-old animals treated with 40Hz light flicker for 5 days.

Images of brain sections immunostained for Aβ were quantified using ImageJ software, measuring plaques of 3µm^2 or greater. 3 sections were imaged per animal then averaged. Data here shows the average of all animals in each group (n=4). All units shown are in µm^2 ± S.E.M

All units in µm^2		Brain region				
		VC	**SUB**	**CA1**	**CA3**	**DG**
Untreated	**Wild-type**	0	0	0	0	0
	5xFAD	96.42 ±65	130 ±21.4	58.45 ±14.5	54 ±30.9	78 ±43.7
40Hz light treated	**Wild-type**	0	0	0	0	0
	5xFAD	120.1 ±39.6	123 ±89.5	40 ±25.8	57 ±32.5	77 ± 52.3

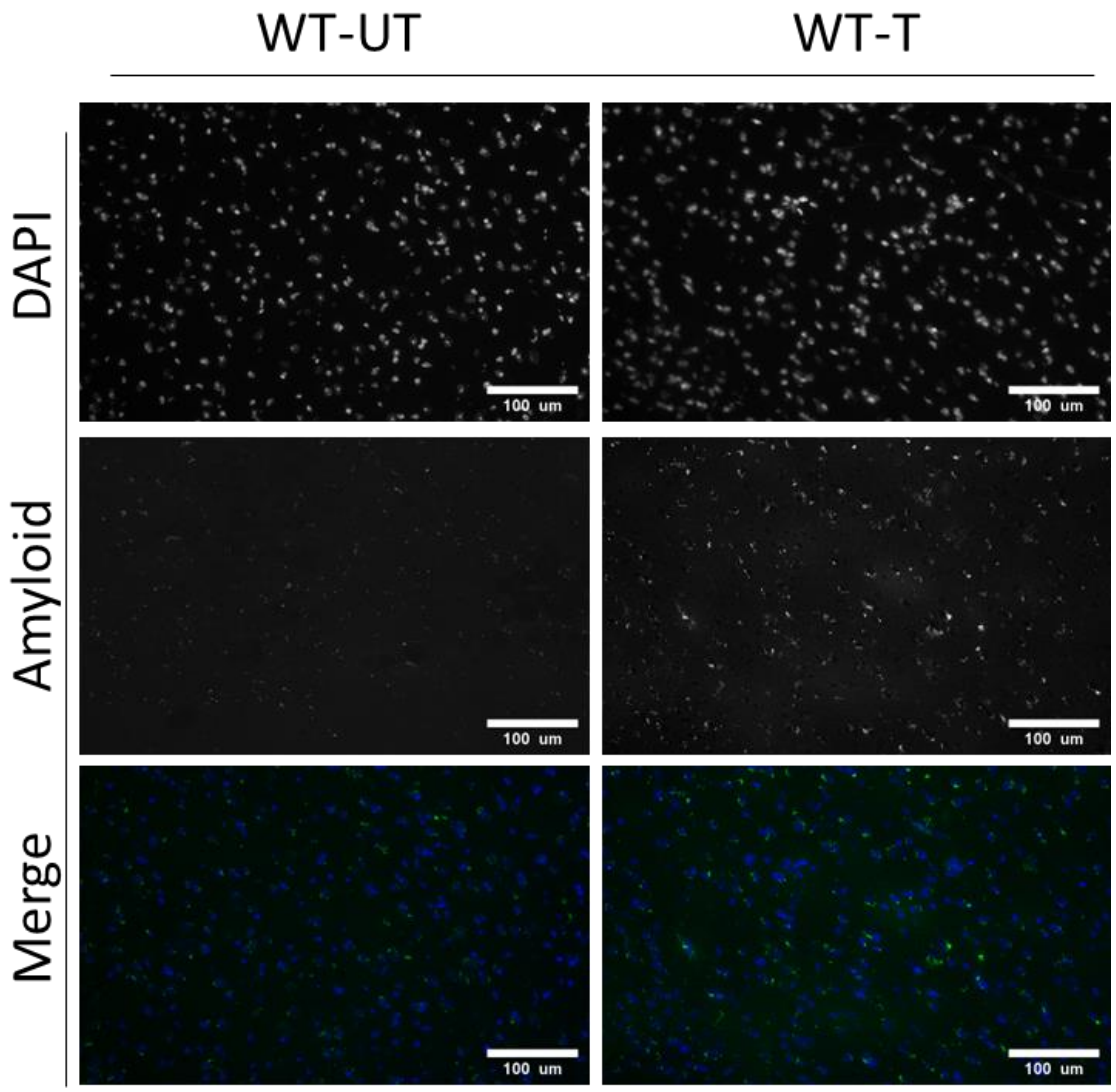

Figure 3.5- Representative Aβ expression in the visual cortex of treated and untreated wild-type mice after 5 days of 40Hz treatment. *9-month-old wild-type female animals were exposed to 1 hour of 40Hz light flicker (WT-T) or 1 hour of darkness (WT-UT) for 5 consecutive days, then animals were sacrificed, and brains were removed. Sagittal sections of brain tissues at 10µm were immunofluorescence stained using a pan-amyloid antibody. All images were taken at 20x objective of the visual cortex. Representative images for DAPI staining (top row), Aβ staining (mid row) and the merged images showing Aβ in green and DAPI in blue (bottom row). Scale bar shows 100µm*

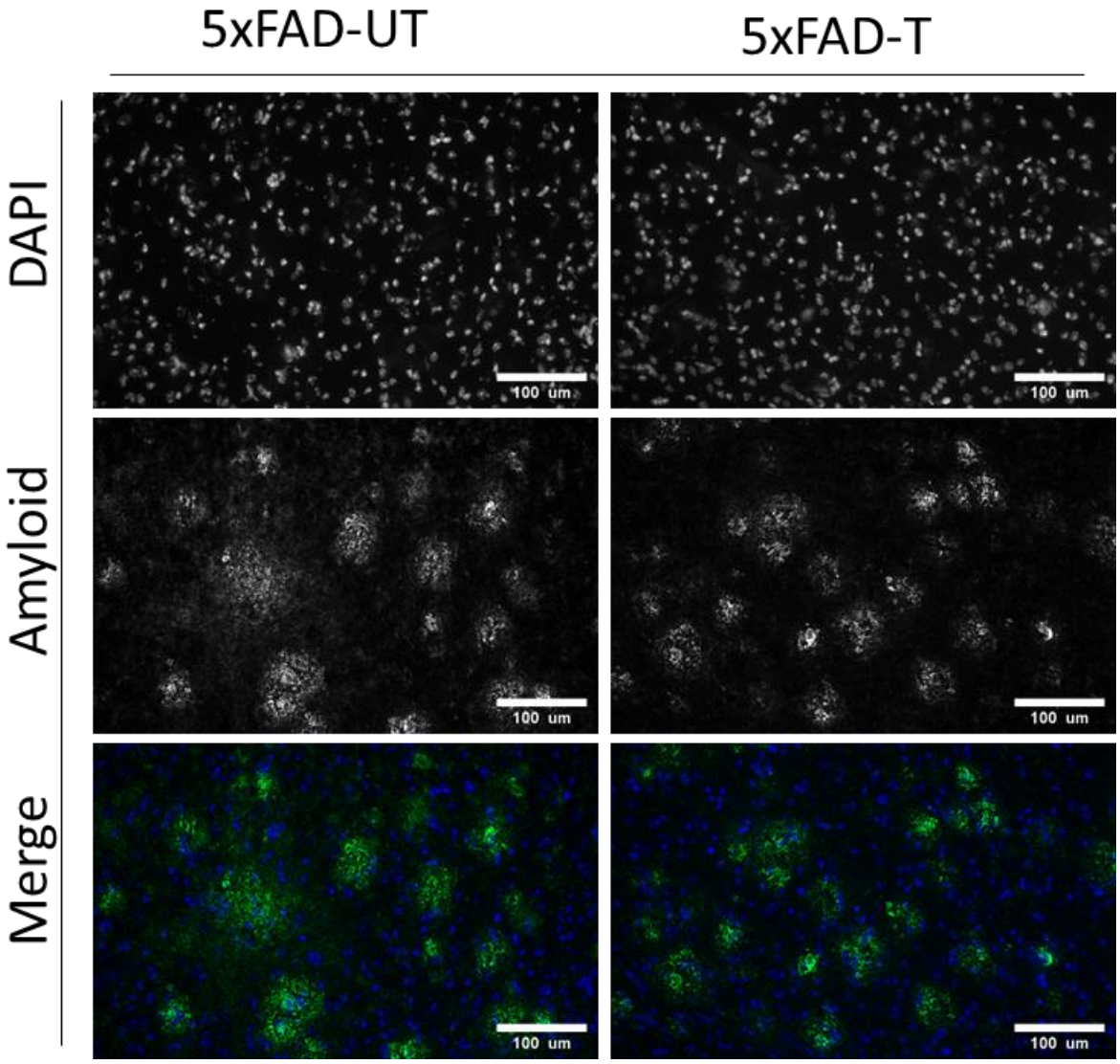

Figure 3.6- Representative Aβ expression in the visual cortex of treated and untreated 5xFAD mice after 5 days of treatment. *9-month-old 5xFAD female animals were exposed to 1 hour of 40Hz light flicker (5xFAD-T) or 1 hour of darkness (5xFAD-UT) for 5 consecutive days, then animals were sacrificed, and brains were removed. Sagittal sections of brain tissues at 10µm were immunofluorescence stained using a pan-amyloid antibody. All images were taken at 20x objective of the visual cortex. Representative images for DAPI staining (top row), Aβ staining (mid row) and the merged images showing Aβ in green and DAPI in blue (bottom row). Scale bar shows 100µm.*

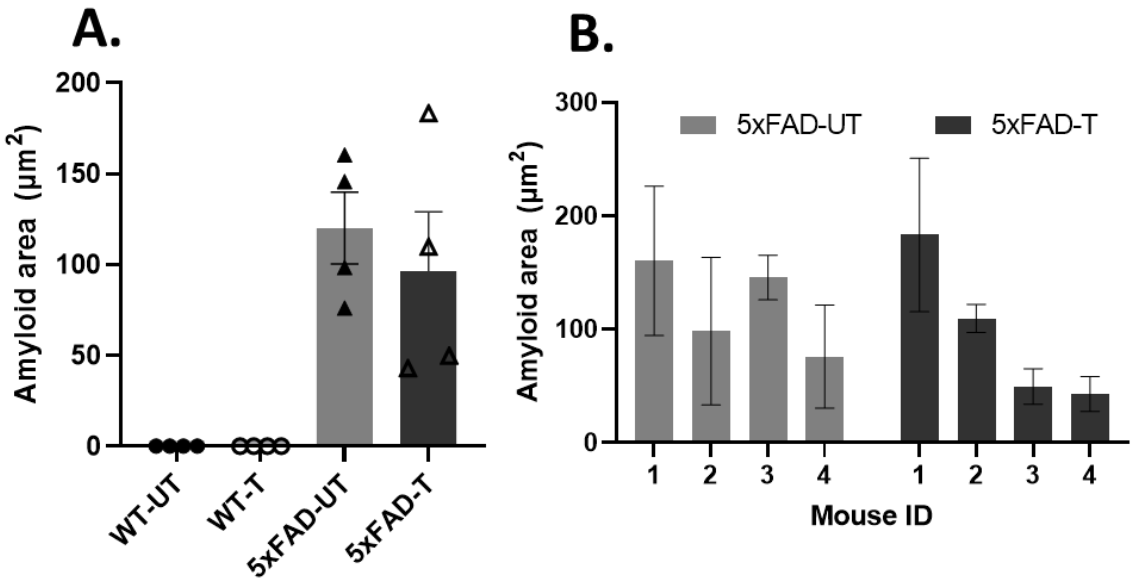

Figure 3.7- Aβ measurements in the visual cortex of treated and untreated mice after 5 days of treatment. *9-month-old WT and 5xFAD female animals were exposed to 1 hour of 40Hz light flicker (5xFAD-T & WT-T) or 1 hour of darkness (5xFAD-UT & WT UT) for 5 consecutive days, then animals were sacrificed, and brains were removed. Sagittal sections of brain tissues at 10µm were immunofluorescence stained using a pan-amyloid antibody.* ***A:*** *Average Aβ burden in the visual cortex of 4 mice in each group (±S.E.M.) Each point represents 1 animal.* ***B:*** *Average amyloid in μm^2 of 3 representative regions for each individual animal in untreated or treated 5xFAD mice (±S.E.M.) n=4 female mice per group. Two-way ANOVA with Tukey's multiple comparisons performed; no statistical significance found between treated and untreated groups. Genotype: F (1,32) = 34.57, P=0.6, Treatment: F (1,32) = 0.414, P=0.53.*

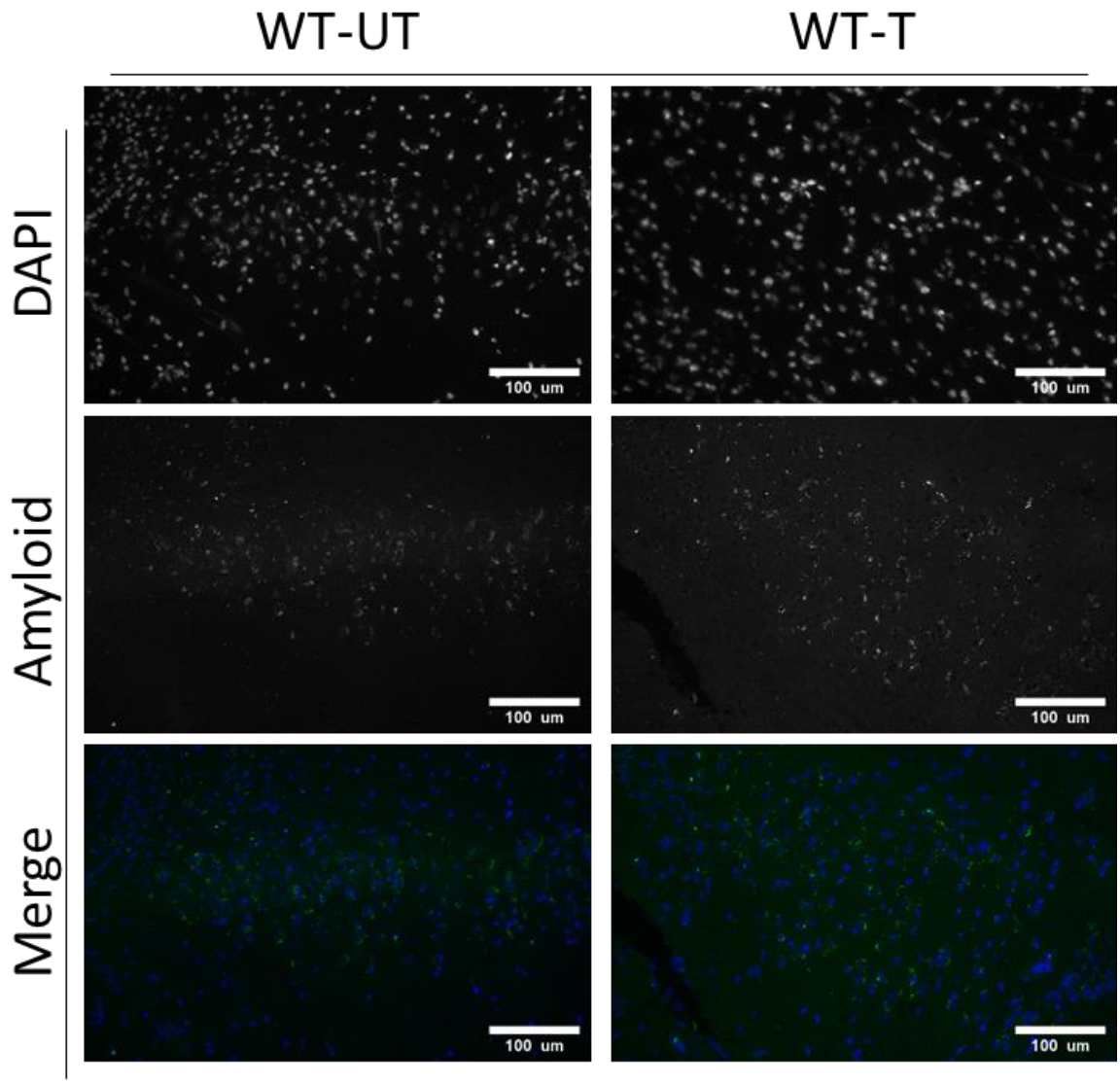

Figure 3.8- Representative Aβ expression in the subiculum of treated and untreated wild-type mice after 5 days of 40Hz treatment. *9-month-old wild-type female animals were exposed to 1 hour of 40Hz light flicker (WT-T) or 1 hour of darkness (WT-UT) for 5 consecutive days, then animals were sacrificed, and brains were removed. Sagittal sections at 10μm were immunofluorescence stained using a pan-amyloid antibody. All images were taken at 20x objective of the subiculum. Representative images for DAPI staining (top row), Aβ staining (mid row) and the merged images showing Aβ in green and DAPI in blue (bottom row). Scale bar shows 100μm.*

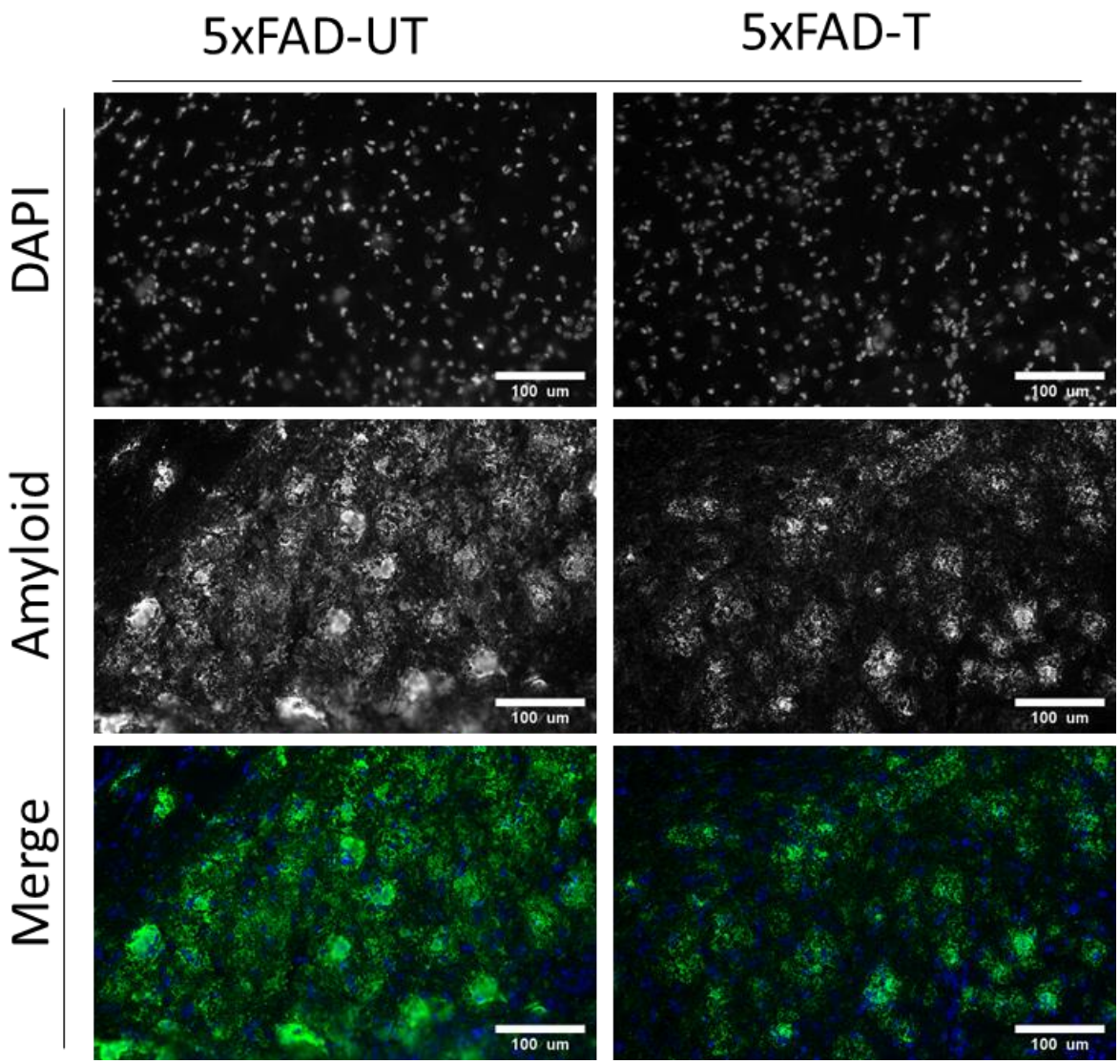

Figure 3.9- Representative Aβ expression in the subiculum of treated and untreated 5xFAD mice after 5 days of 40Hz treatment. *9-month-old 5xFAD female animals were exposed to 1 hour of 40Hz light flicker (5xFAD-T) or 1 hour of darkness (5xFAD-UT) for 5 consecutive days, then animals were sacrificed, and brains were removed. Sagittal sections at 10µm were immunofluorescence stained using a pan-amyloid antibody. All images were taken at 20x objective of the subiculum. Representative images for DAPI staining (top row), Aβ staining (mid row) and the merged images showing Aβ in green and DAPI in blue (bottom row). Scale bar shows 100µm.*

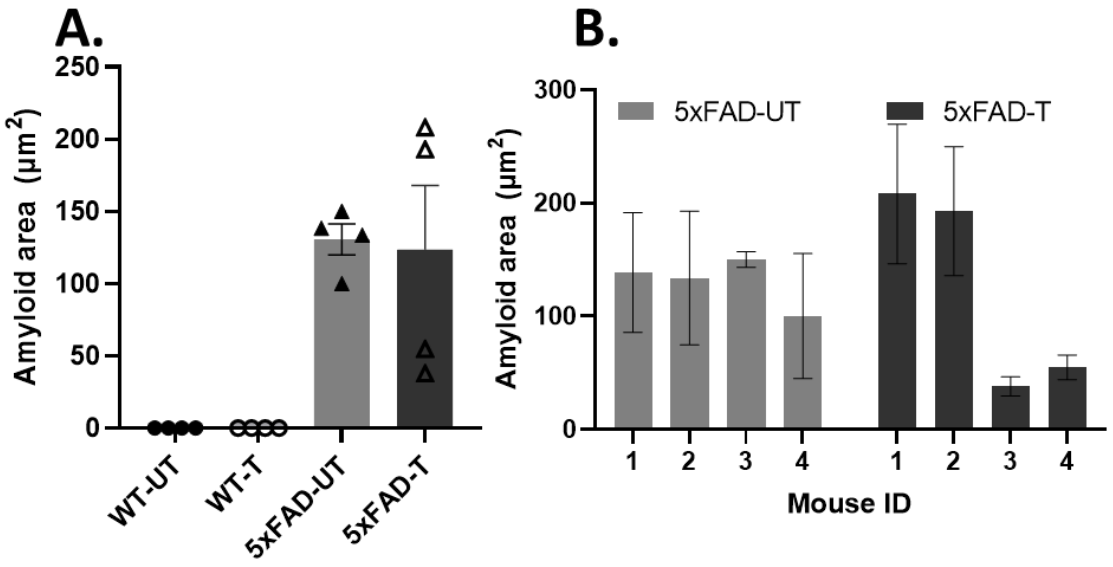

Figure 3.10- Aβ expression in the subiculum of treated and untreated mice after 5 days of treatment. *9-month-old WT and 5xFAD female animals were exposed to 1 hour of 40Hz light flicker (5xFAD-T & WT-T) or 1 hour of darkness (5xFAD-UT & WT-UT) for 5 consecutive days, then animals were sacrificed, and brains were removed. Sagittal sections at 10µm were immunofluorescence stained using a pan-amyloid antibody.* ***A:*** *Average Aβ burden in the subiculum of 4 mice per group (± S.E.M.) Each point represents 1 animal.* ***B:*** *Average amyloid in µm² of 3 reps for each individual animal per group (±S.E.M.) n=4 female mice per group. Two-Way ANOVA with Tukey's multiple comparisons performed; no statistical significance found between treated and untreated groups. Genotype- F (1,32) = 30.89, P=0.0001. Treatment- F (1,32) =0.025, P=0.88.*

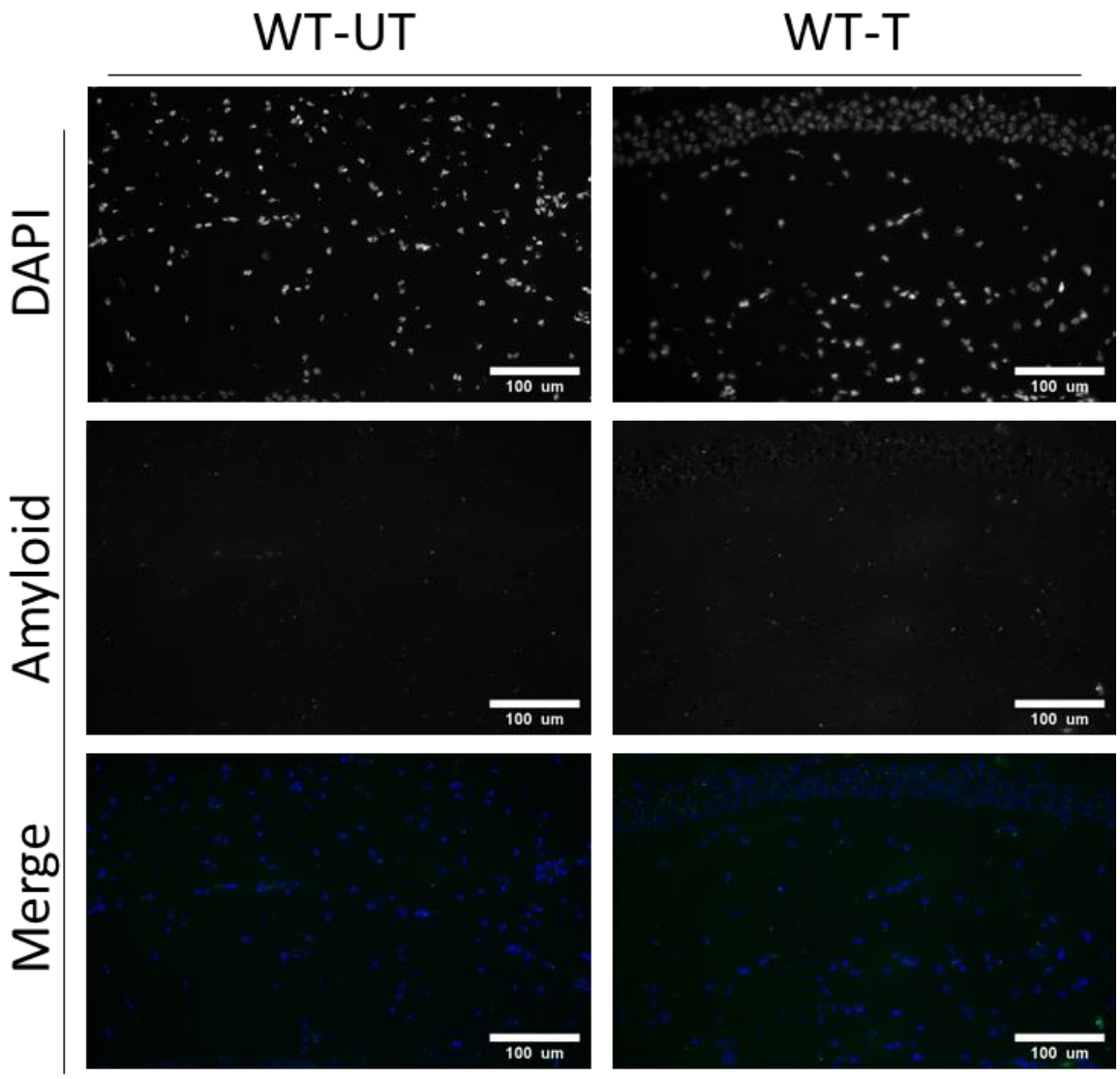

Figure 3.11- Representative Aβ expression in CA1 of treated and untreated wild-type mice after 5 days of 40Hz treatment *9-month-old wild-type female animals were exposed to 1 hour of 40Hz light flicker (WT-T) or 1 hour of darkness (WT-UT) for 5 consecutive days, then animals were sacrificed, and brains were removed. Sagittal sections at 10μm were immunofluorescence stained using a pan-amyloid antibody. All images were taken at 20x objective of CA1. Representative images for DAPI staining (top row), Aβ staining (mid row) and the merged images showing Aβ in green and DAPI in blue (bottom row). Scale bar shows 100μm.*

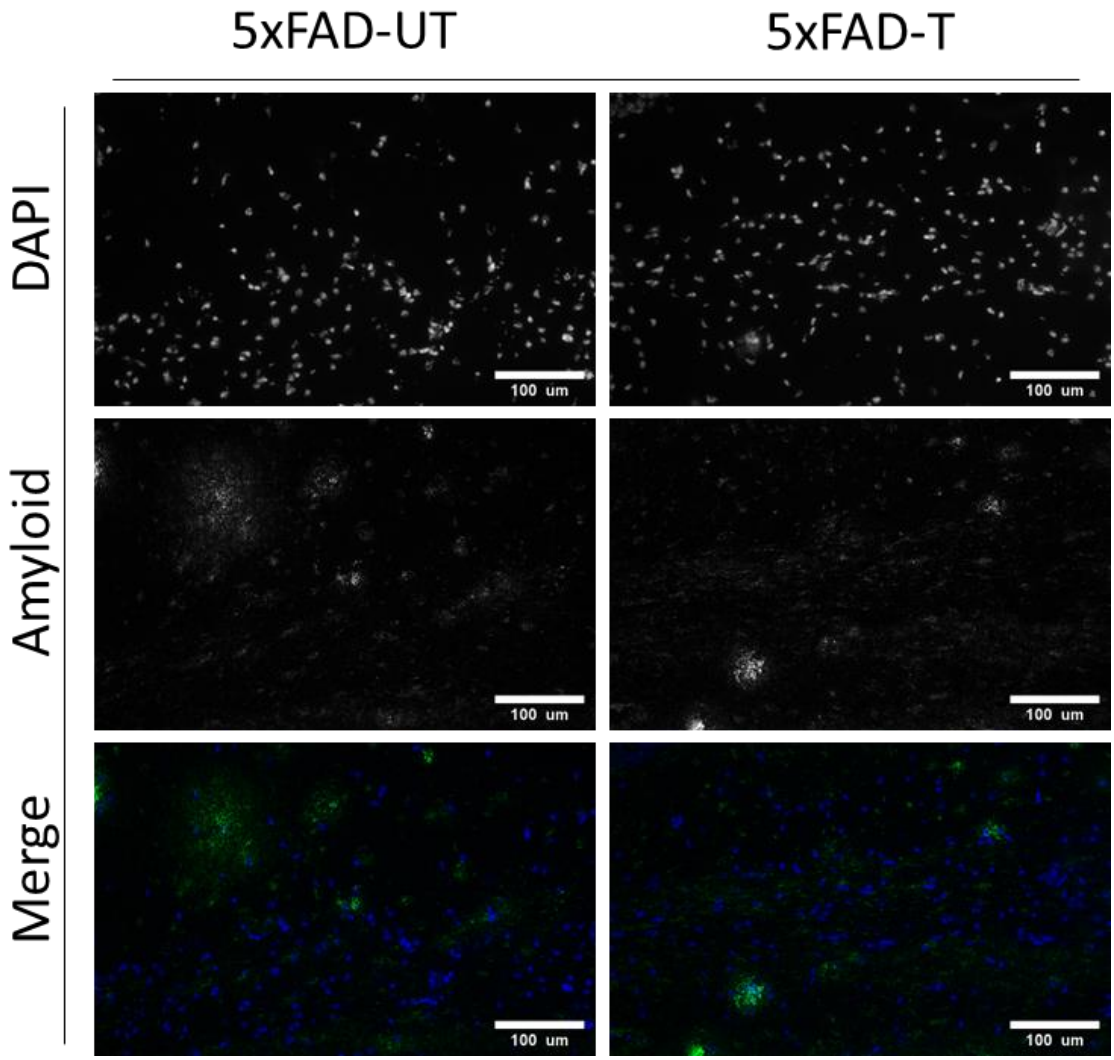

Figure 3.12- Representative Aβ expression in CA1 of treated and untreated 5xFAD mice after 5 days of 40Hz treatment *9-month-old 5xFAD female animals were exposed to 1 hour of 40Hz light flicker (5xFAD-T) or 1 hour of darkness (5xFAD-UT) for 5 consecutive days, then animals were sacrificed, and brains were removed. Sagittal sections at 10μm were immunofluorescence stained using a pan-amyloid antibody. All images were taken at 20x objective of CA1. Representative images for DAPI staining (top row), Aβ staining (mid row) and the merged images showing Aβ in green and DAPI in blue (bottom row). Scale bar shows 100μm.*

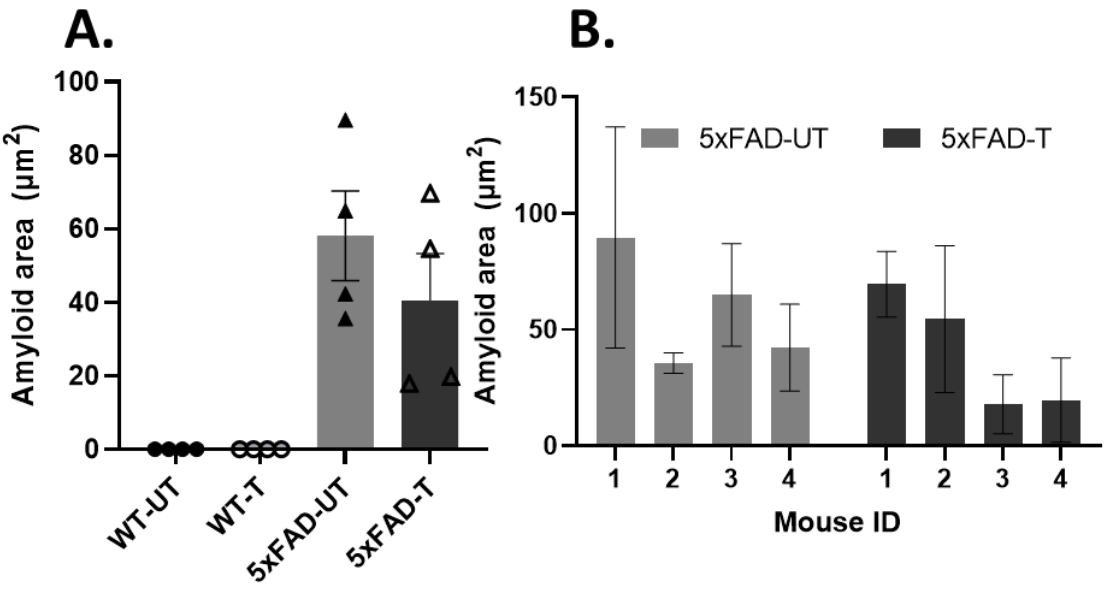

Figure 3.13- Aβ expression in the CA1 hippocampal region of treated and untreated mice after 5 days of treatment. *9-month-old WT and 5xFAD female animals were exposed to 1hr of 40Hz light flicker (5xFAD-T & WT- T) or 1hr of darkness (5xFAD- UT & WT-UT) for 5 consecutive days, then animals were sacrificed, and brains were removed. Sagittal sections at 10µm were immunofluorescence stained using a pan-amyloid antibody. All images were taken at 20x objective of the CA1 region of the hippocampus.* ***A:*** *Average Aβ burden in the CA1 region of the hippocampus of 4 mice per group (±S.E.M.) Each point represents 1 animal.* ***B:*** *Average amyloid in µm² of 3 reps for each individual animal per group (±S.E.M.) n=4 female mice per group. Two-Way ANOVA with Tukey's multiple comparisons performed; no statistical significance found between treated and untreated groups. Genotype: F (1,32) = 30.76, P=0.0001, Treatment: F (1,32) =1.124, P=0.31.*

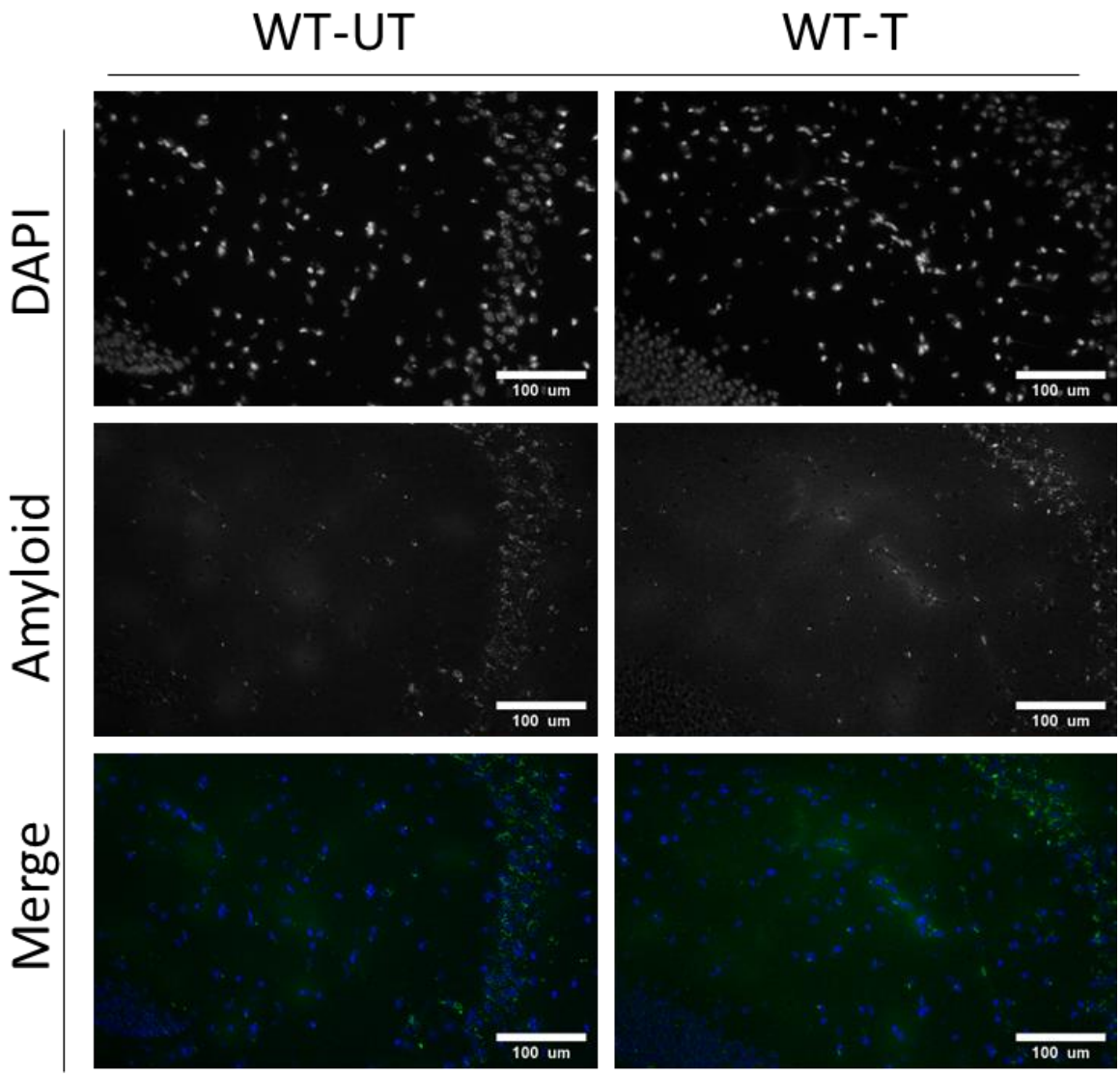

Figure 3.14- Representative Aβ expression in CA3 of treated and untreated wild-type mice after 5 days of 40Hz treatment *9-month-old wild-type female animals were exposed to 1 hour of 40Hz light flicker (WT-T) or 1 hour of darkness (WT-UT) for 5 consecutive days, then animals were sacrificed, and brains were removed. Sagittal sections at 10μm were immunofluorescence stained using a pan-amyloid antibody. All images were taken at 20x objective of CA3. Representative images for DAPI staining (top row), Aβ staining (mid row) and the merged images showing Aβ in green and DAPI in blue (bottom row). Scale bar shows 100μm.*

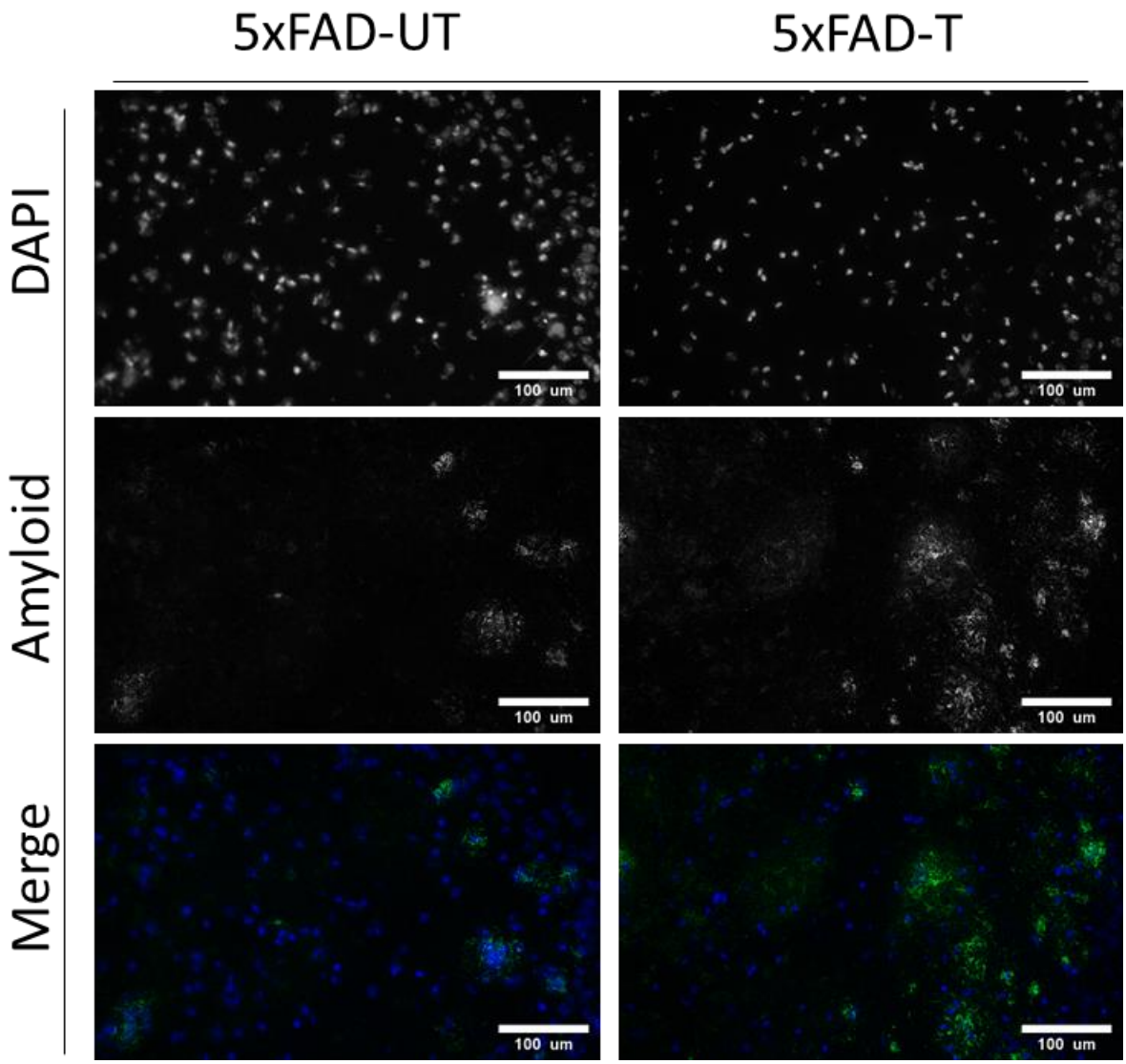

Figure 3.15- Representative Aβ expression in CA3 of treated and untreated 5xFAD mice after 5 days of 40Hz treatment. *9-month-old 5xFAD female animals were exposed to 1 hour of 40Hz light flicker (5xFAD-T) or 1 hour of darkness (5xFAD-UT) for 5 consecutive days, then animals were sacrificed, and brains were removed. Sagittal sections at 10µm were immunofluorescence stained using a pan-amyloid antibody. All images were taken at 20x objective of CA3. Representative images for DAPI staining (top row), Aβ staining (mid row) and the merged images showing Aβ in green and DAPI in blue (bottom row). Scale bar shows 100µm.*

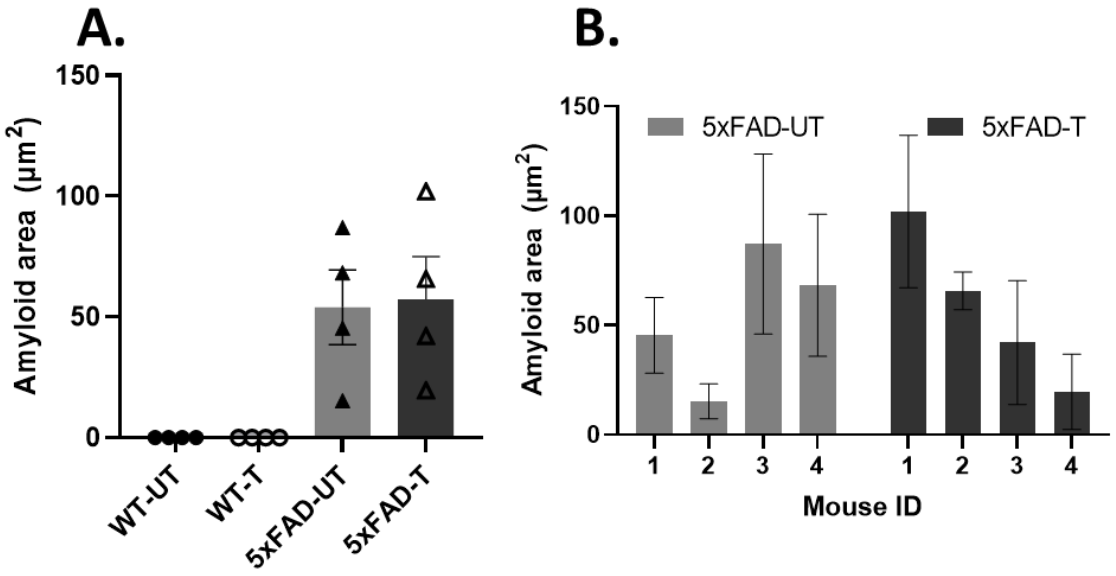

Figure 3.16- Aβ expression in the CA3 hippocampal region of treated and untreated mice after 5 days of treatment. *9-month-old WT and 5xFAD female animals were exposed to 1hr of 40Hz light flicker (5xFAD-T & WT-T) or 1hr of darkness (5xFAD-UT & WT-UT) for 5 consecutive days, then animals were sacrificed, and brains were removed. Sagittal sections at 10µm were immunofluorescence stained using a pan-amyloid antibody.* ***A:*** *Average Aβ burden in the CA3 region of the hippocampus of 4 mice per group (± S.E.M.) Each point represents 1 animal.* ***B:*** *Average amyloid in µm² of 3 reps for each individual animal per group (±S.E.M.) n=4 female mice per group. One-Way ANOVA performed; no statistical significance found. Two-Way ANOVA with Tukey's multiple comparisons performed; no statistical significance found between treated and untreated groups. Genotype- F (1,32) =25.35, P=0.0003, Treatment: F (1,32) =0.02, P=0.88.*

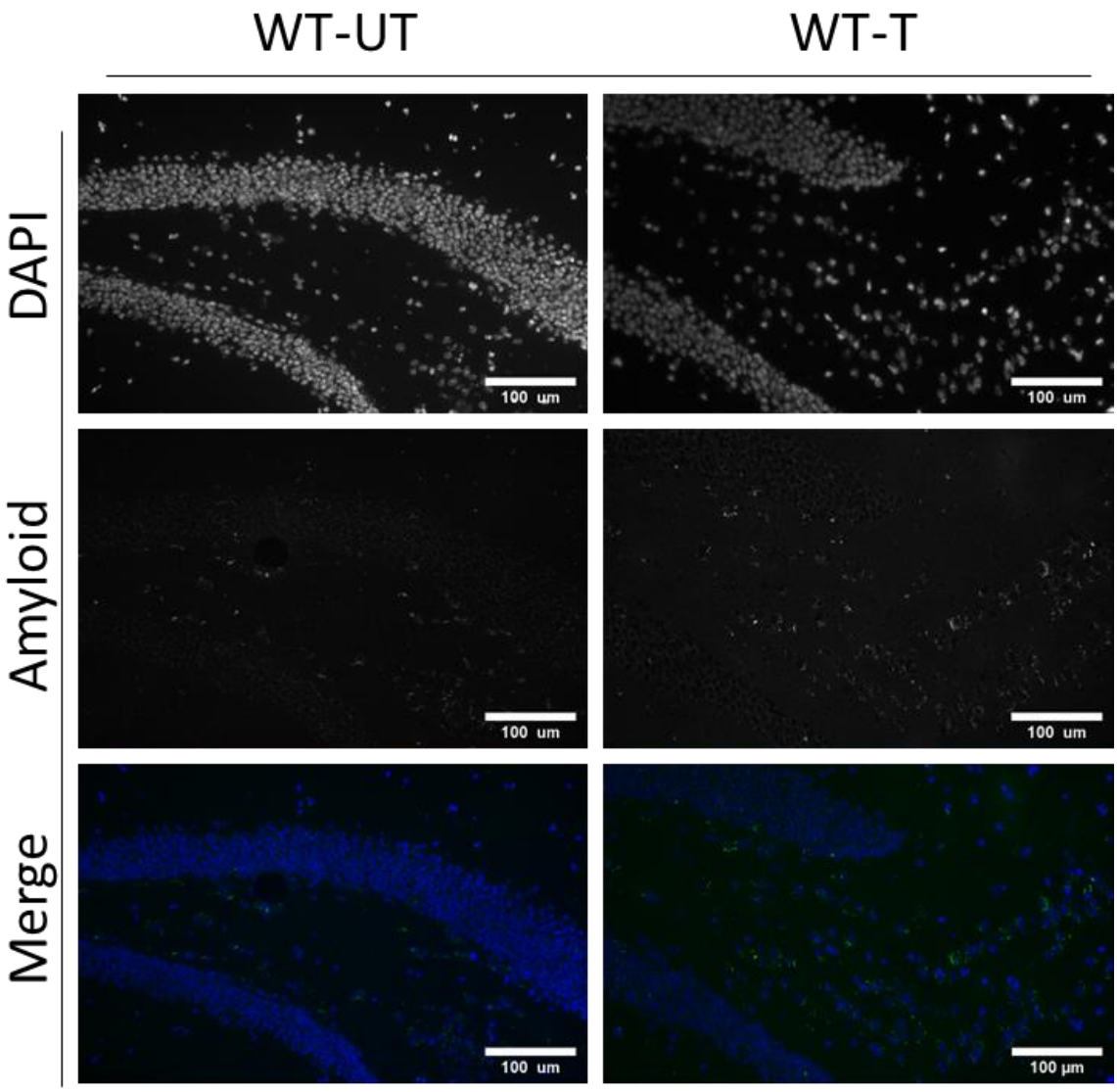

Figure 3.17- Representative Aβ expression in DG of treated and untreated wild-type mice after 5 days of 40Hz treatment. *9-month-old WT female animals were exposed to 1 hour of 40Hz light flicker (WT-T) or 1 hour of darkness (WT-UT) for 5 consecutive days, then animals were sacrificed, and brains were removed. Sagittal sections at 10µm were immunofluorescence stained using a pan-amyloid antibody. All images were taken at 20x objective of the DG. Representative images for DAPI staining (top row), Aβ staining (mid row) and the merged images showing Aβ in green and DAPI in blue (bottom row). Scale bar shows 100µm*

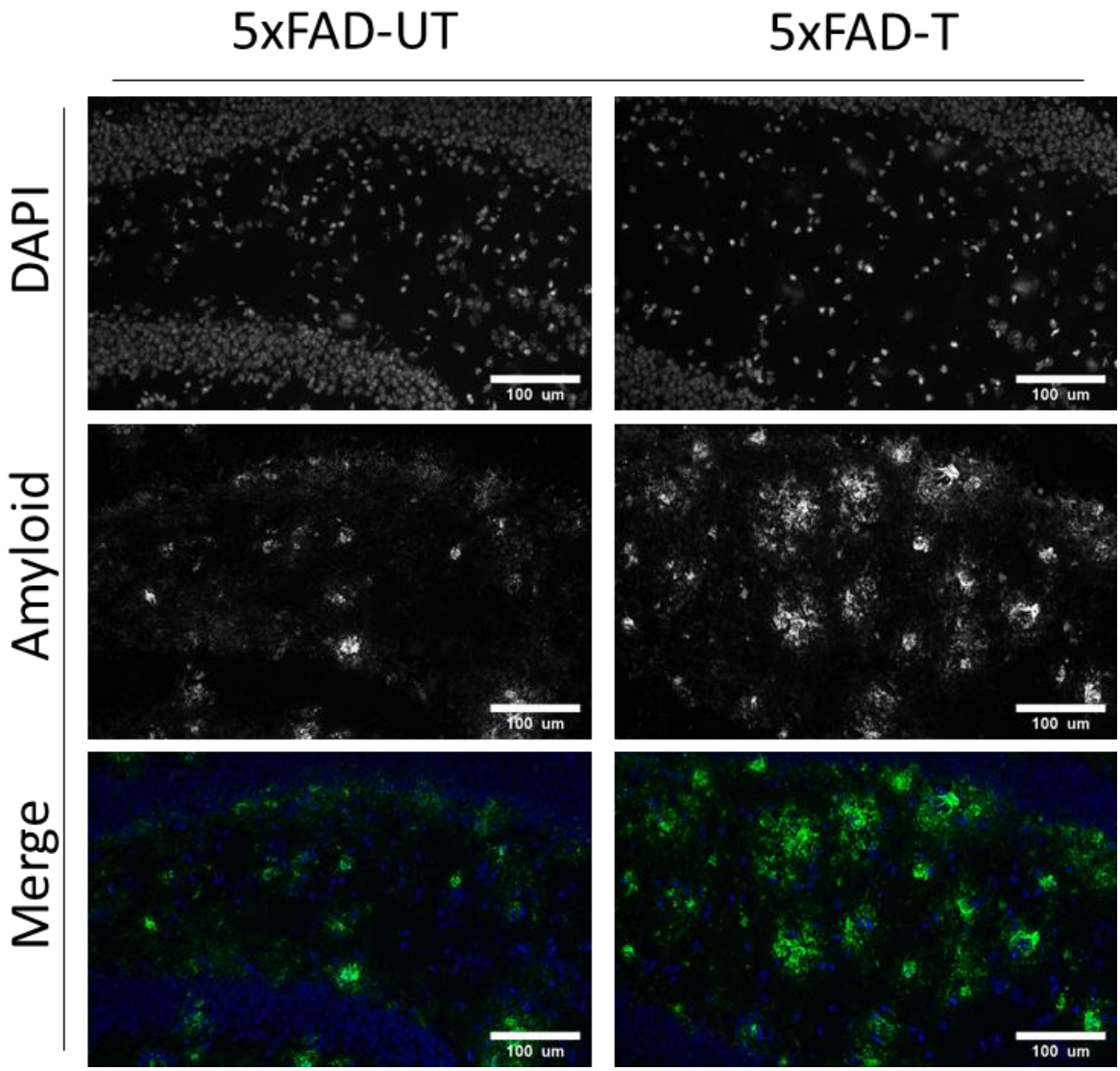

Figure 3.18- Representative Aβ expression in DG of treated and untreated 5xFAD mice after 5 days of 40Hz treatment. *9-month-old 5xFAD female animals were exposed to 1 hour of 40Hz light flicker (5xFAD-T) or 1 hour of darkness (5xFAD-UT) for 5 consecutive days, then animals were sacrificed, and brains were removed. Sagittal sections at 10μm were immunofluorescence stained using a pan-amyloid antibody. All images were taken at 20x objective of DG. Representative images for DAPI staining (top row), Aβ staining (mid row) and the merged images showing Aβ in green and DAPI in blue (bottom row). Scale bar shows 100μm.*

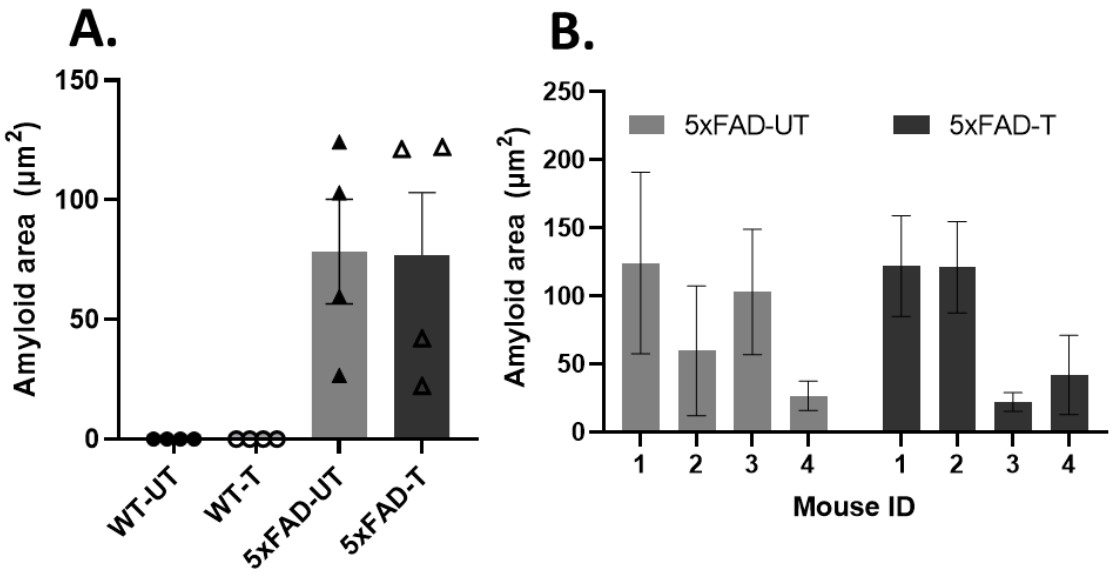

Figure 3.19- Aβ expression in the dentate gyrus of treated and untreated mice after 5 days of treatment. *9-month-old WT and 5xFAD female animals were exposed to 1hr of 40Hz light flicker (5xFAD-T & WT-T) or 1hr of darkness (5xFAD-UT & WT-UT) for 5 consecutive days, then animals were sacrificed, and brains were removed. Sagittal sections at 10µm were immunofluorescence stained using a pan-amyloid antibody. All images were taken at 20x objective of the DG.* ***A****: representative images for DAPI staining (left), Aβ staining (mid) and the merged images showing Aβ in green and DAPI in blue (right).* ***B:*** *Average Aβ burden in the DG of 4 mice per group (±S.E.M.) Each point represents 1 animal.* ***C:*** *Average amyloid in µm² of 3 reps for each individual animal per group (±S.E.M.) n=4 female mice per group. Two-Way ANOVA with Tukey's multiple comparisons performed; no statistical significance found between treated and untreated groups. Genotype: F (1,32)= 31.24, P=<0.0001., Treatment: F (1,32) =0.002, P=0.96*

Finally, we averaged the results obtained for each animal's amyloid levels per region and compared treated and untreated groups (Fig 3.20). We found no significant difference of the overall amyloid plague burden across brain regions between animals treated with 40Hz light flicker and the untreated animals. As expected, significant differences were found between 5xFAD and WT animals- however this data is well-established, thus significance values not shown.

As this was an initial pilot study to determine the effectiveness of treatment in our animals, we used a small group of single-sex animals without a g-power calculation as we had no values to estimate effectiveness. However, our treatment under these circumstances proved ineffective.

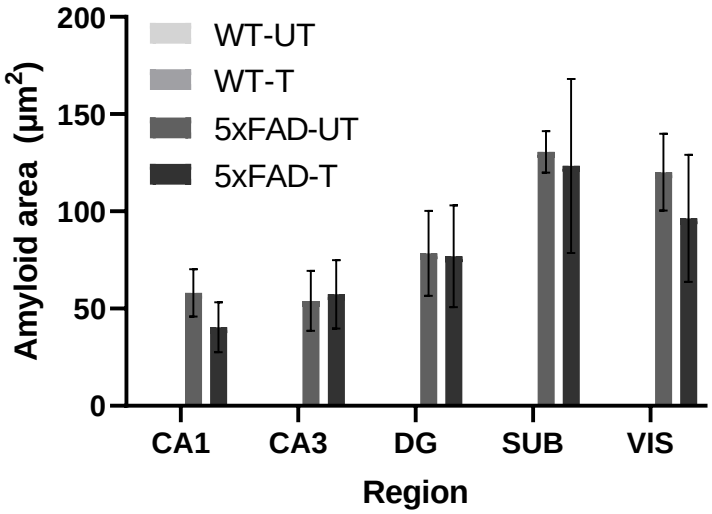

Figure 3.20- Total Aβ plaque area across all brain regions after 5-day light treatment

9-month-old WT and 5xFAD female animals were exposed to 1hr of 40Hz light flicker (5xFAD-T & WT-T) or 1 hour of darkness (5xFAD-UT & WT-UT) for 5 consecutive days, then animals were sacrificed, and brains were removed. Sagittal sections at 10µm were immunofluorescence stained using a pan-amyloid antibody. Images for pan-amyloid-β in the brain regions of CA1, CA3, DG, SUB and Vis were captured at 20x magnification, 3 images per region per animal were quantified using imageJ analysis. Only plaques larger than 3µm were counted to calculate total area per image. All data shows mean area ±S.E.M, *n=4 female mice per group. Data analysed using Two-Way ANOVA with Tukey's multiple comparisons, no statistical significance found between treated and untreated groups. WT data is presented but was below measurable range.*

3.2.4 Effect of 5-day oscillating light treatment on CD45+ cells in the brain regions of 9-month-old mice

AD is associated with chronic inflammation in the associated brain regions, and previous studies showed that 40Hz light flicker increases inflammation via microglial activity (Singer *et al.,* 2018). We therefore used CD45 expression as a preliminary measure of inflammation. CD45 is a widely expressed marker observed on basophils, macrophages, monocytes, and microglial cells (Hermiston, Xu and Weiss, 2003), so data gathered would be a measure of general cellular inflammation rather than identifying the specific cells involved. We used IHC and AMEC-Red (a HRP substrate) to stain CD45 in 10µm thick fresh-frozen sections of treated and untreated WT (Fig 3.21) and 5xFAD (Fig 3.22) mice to measure inflammation in the brain, specifically within the visual cortex where we expect to see the largest changes induced by treatment. Our hypothesis was that higher CD45 expression would suggest more inflammatory responses from immune cells within the region.

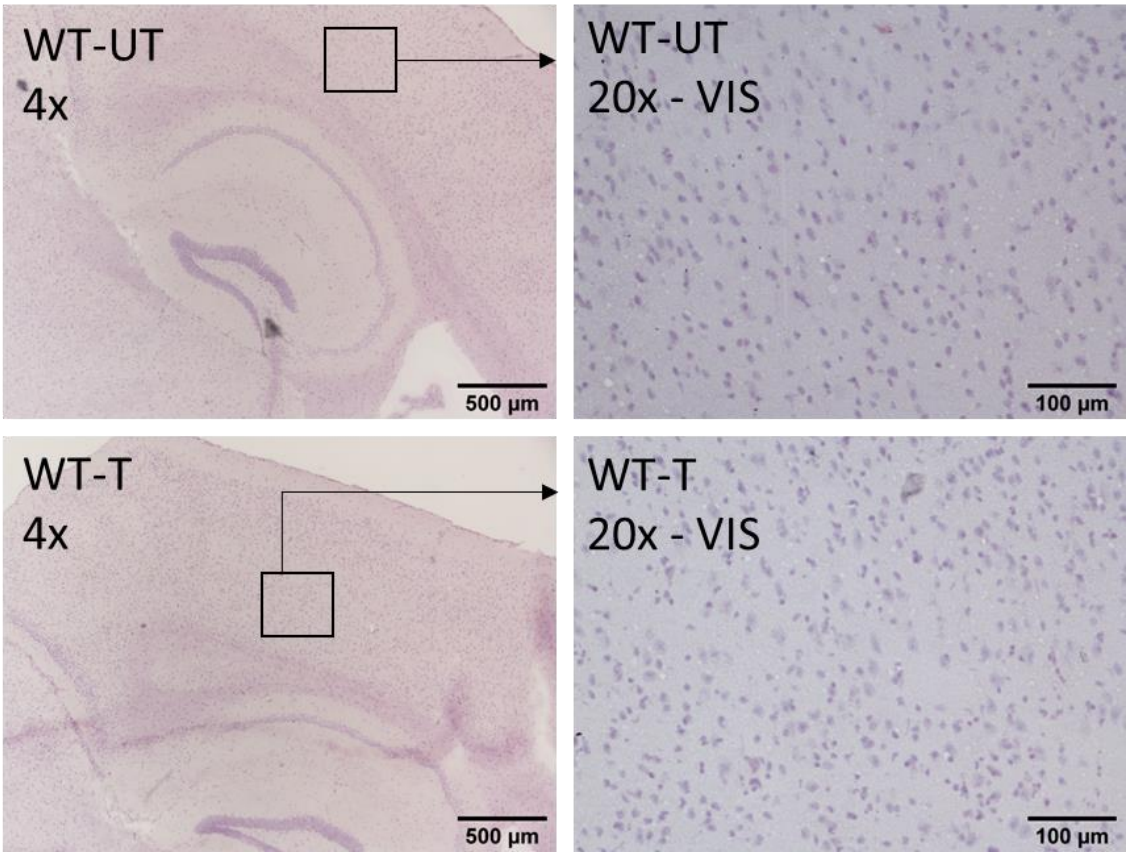

Figure 3.21- Representative images of CD45 in the brain of wild-type mice after 5 days of light treatment. *WT female animals were exposed to 1 hour of 40Hz light flicker (WT-T) or 1 hour of darkness (WT-UT) for 5 consecutive days. Mice were then sacrificed, and brains were removed. Sagittal sections were stained with CD45 antibody, followed by a biotin conjugated antibody and AMEC substrate. Nuclei were stained with haematoxylin. Left column shows representative 4x microscopy images of hippocampus and VC, right column shows representative 20x magnification of the VC. n=4 females in each group.*

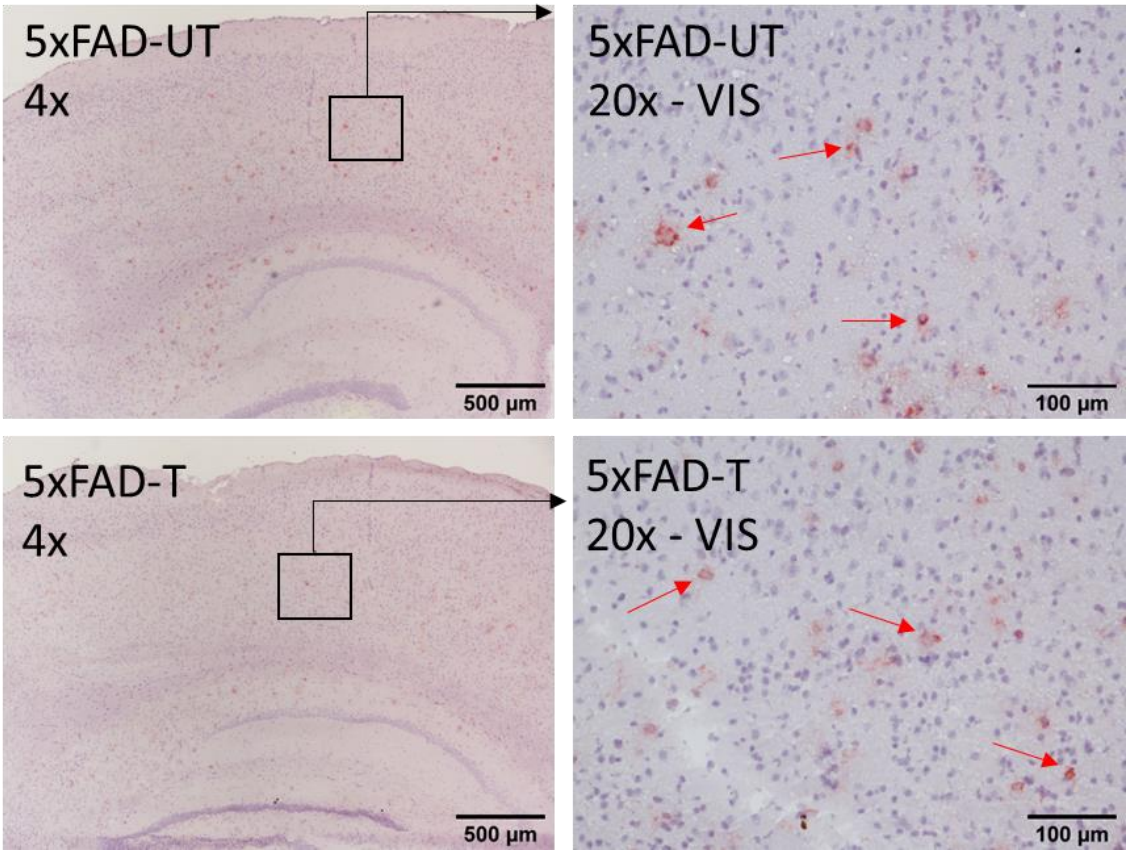

Figure 3.22- Representative images of CD45 in the brain of 5xFAD mice after 5 days of light treatment. *WT female animals were exposed to 1 hour of 40Hz light flicker (5xFAD-T) or 1 hour of darkness (5xFAD-UT) for 5v consecutive days. Mice were then sacrificed, and brains were removed. Sagittal sections were stained with CD45 antibody, followed by a biotin conjugated antibody and AMEC substrate. Nuclei were stained with haematoxylin. Left column shows representative 4x microscopy images of hippocampus and VC, right column shows representative 20x magnification of the VC. n=4 females in each group.*

We observed significantly more CD45+ cells in both untreated and treated 5xFAD animals compared to both WT groups which showed few CD45+ cells in all regions (Fig 3.23 A) consistent with previously published work exhibiting the inflammatory state of the 5xFAD brain. We then analysed the total number of CD45+ cells in each of the four mice (Fig 3.23 B). In the VC no significant difference was found between treated and untreated 5xFAD mice nor between treated and untreated WT (0 in both groups). Similarly, no significant differences were found between treated and untreated 5xFAD mice in the DG, the subiculum, the CA3 region or the CA1 region (Table 3.2).

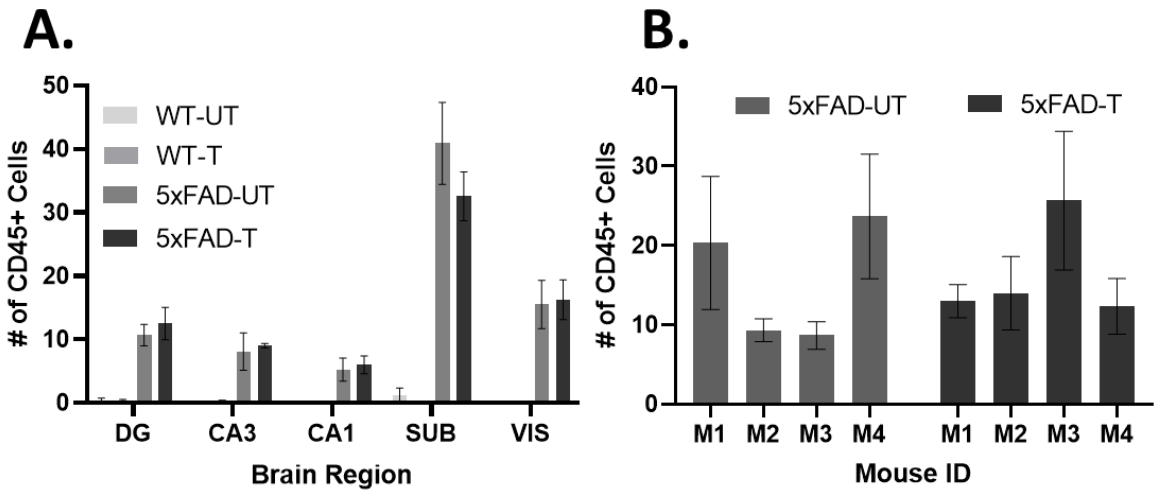

Figure 3.23- Total CD45 cell counts in brain regions of 5 day treated and untreated 5xFAD and WT mice. *CD45 cells were stained via IHC using a CD45 antibody and 20x magnification images collected using a brightfield microscope, then quantified manually using ImageJ.* ***A****: Total number of CD45+ cells in various brain regions of treated and untreated groups, n=4 for each group.* ***B****: Total number of CD45+ cells in the visual region of each individual mouse of 5xFAD treated and untreated groups. All data shows mean ±S.E.M, n=3 sections for each mouse. Two way-ANOVA with Tukey's multiple comparisons performed on both sets of data, no significant difference was found for treatment (F(1,60)=0.26, P=0.6). Genotype (F(1,60)=223.4, P=<0.0001) and region (F(4,60)=29.7, P=<0.0001) shown to be significant factors however individual comparisons showed no significant differences.*

Table 3.2 -CD45+ cell counts in the hippocampus and VC of 9-month-old animals treated with 40Hz light flicker for 5 days.

Images of brain sections immunostained for CD45 were quantified using ImageJ software by manually counting positive cells. 3 sections were imaged per animal then averaged. Data here shows the average of all animals in each group (n=4).

All units shown are total cell count in each brain region ±S.E.M.

CD45- all units are CD45+ cell counts		**Brain region**				
		VC	**SUB**	**CA1**	**CA3**	**DG**
Untreated	**Wild-type**	0	1.2 ± 1.1	0.2 ±0.1	0.2 ±0.1	0.4 ±0.3
	5xFAD	15.5 ±3.8	40.9 ±6.5	5.3 ±1.8	9 ±0.4	10.7 ±1.7
40Hz light treated	**Wild-type**	0	0.1 ±0.1	0.1 ±0.1	0.3 ±0.2	0.3 ±0.2
	5xFAD	16.3 ± 3.2	32.6 ±3.9	6 ±3.9	8.1 ±2.9	12.5 ±2.6

3.2.5 Effect of 15-day light flicker treatment on amyloid burden in 9-month-old animals

The treatment regime of 5 consecutive days did not show any effect on Aβ burden in the brain, therefore we increased the treatment for 15 days to determine if this would improve the effectiveness. The increase to 15 days was based on the fact that while the original publications used 7 days minimum in younger animals, we were unable to repeat this due to limited weekend working due to the COVID-19 lockdown. We therefore hypothesised that a longer treatment duration may prove more effective in our aged animals. Both male and female 5xFAD and WT mice were used for treated and untreated groups (n=3 per group). In this next experiment we continued to use mice aged 9 months as some mice bred during the lockdown period were reaching this age, and we again used the level of Aβ in the brain regions as our measure of treatment effectiveness. Similar to the findings presented in section 3.3, both treated and untreated WTs consistently showed no plaques, and so repetitive data has not been displayed here. We observed no significant difference in the Aβ burden between treated and untreated animals in the VC (Fig 3.24, 3.25, 3.26), the SUB (Fig 3.27, 3.28, 3.29) CA1 (Fig 3.30, 3.31, 3.32), CA3 (Fig 3.33, 3.34, 3.35) or the DG (Fig 3.36, 3.37, 3.38).

We next wanted to determine if there was a difference of Aβ expression between male and female mice to determine whether response to treatment is influenced by biological sex. We first measured the combine totals across each region (Fig 3.39A) and found no significant differences. The data was then divided by sex and post-hoc analysis performed. We observed no significant difference of Aβ burden in the visual region, CA1, CA3 or dentate gyrus regions after treatment in male mice (Fig 3.39B) However, the level of amyloid in the subiculum region of treated male 5xFAD mice was significantly reduced compared with untreated controls ($p^* < 0.05$).

We observed no changes in Aβ burden in any region of treated female 5xFAD compared to their untreated controls (Fig 3.39C).

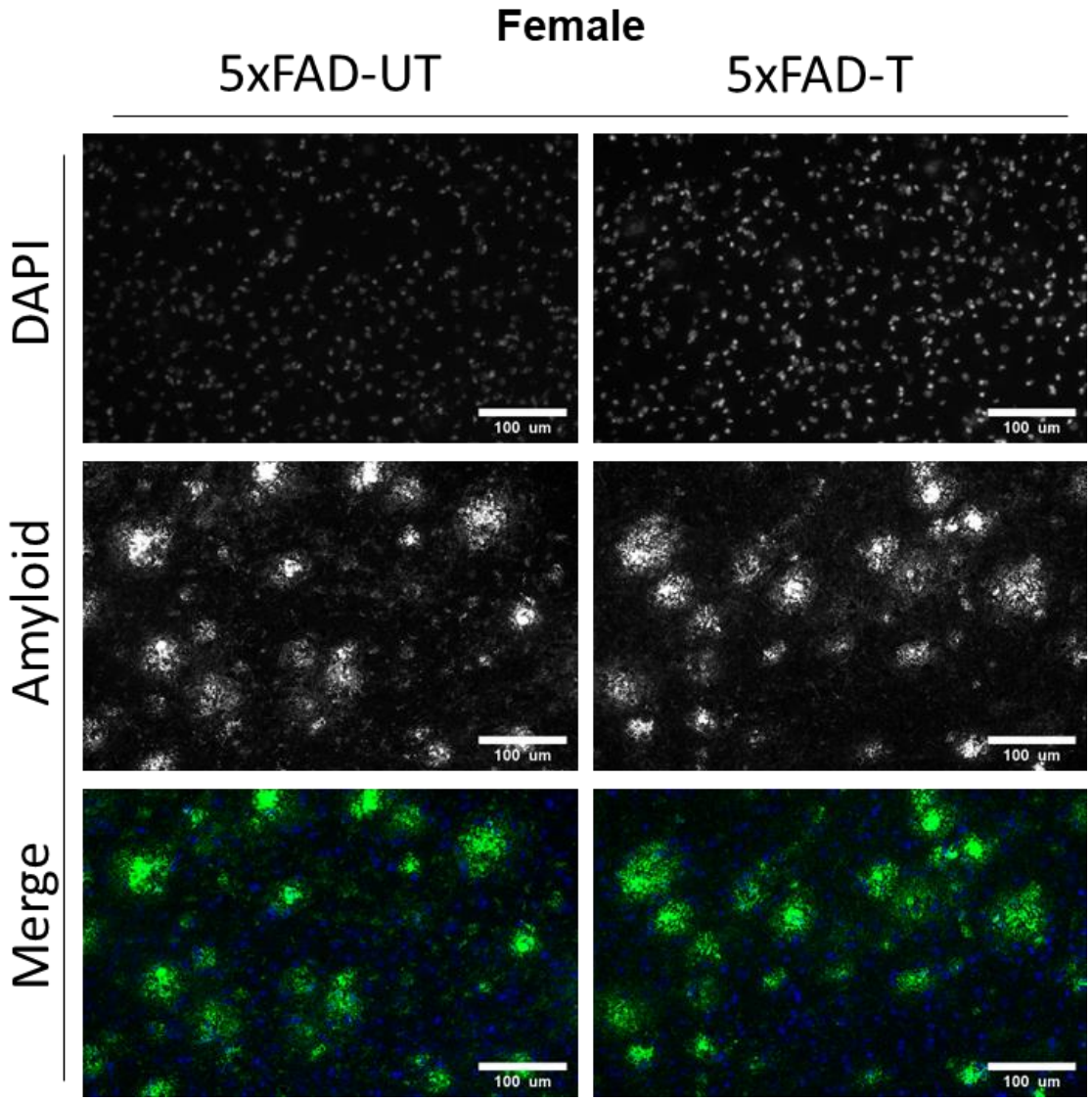

Figure 3.24- Representative Aβ expression in the visual cortex of 40Hz treated and untreated female 5xFAD mice after 15 days of treatment. *9-month-old female 5xFAD were exposed to 1 hour of 40Hz light flicker (5xFAD-T) or 1 hour of darkness (5xFAD-UT) for 15 days, then animals were sacrificed and brains were removed. Sagittal sections at 10μm were immunofluorescence stained using a pan-amyloid antibody. All images were taken at 20x objective of the visual cortex. Representative images for DAPI staining (top row), Aβ staining (mid row) and the merged images showing Aβ in green and DAPI in blue (bottom row). Scale bar shows 100μm.*

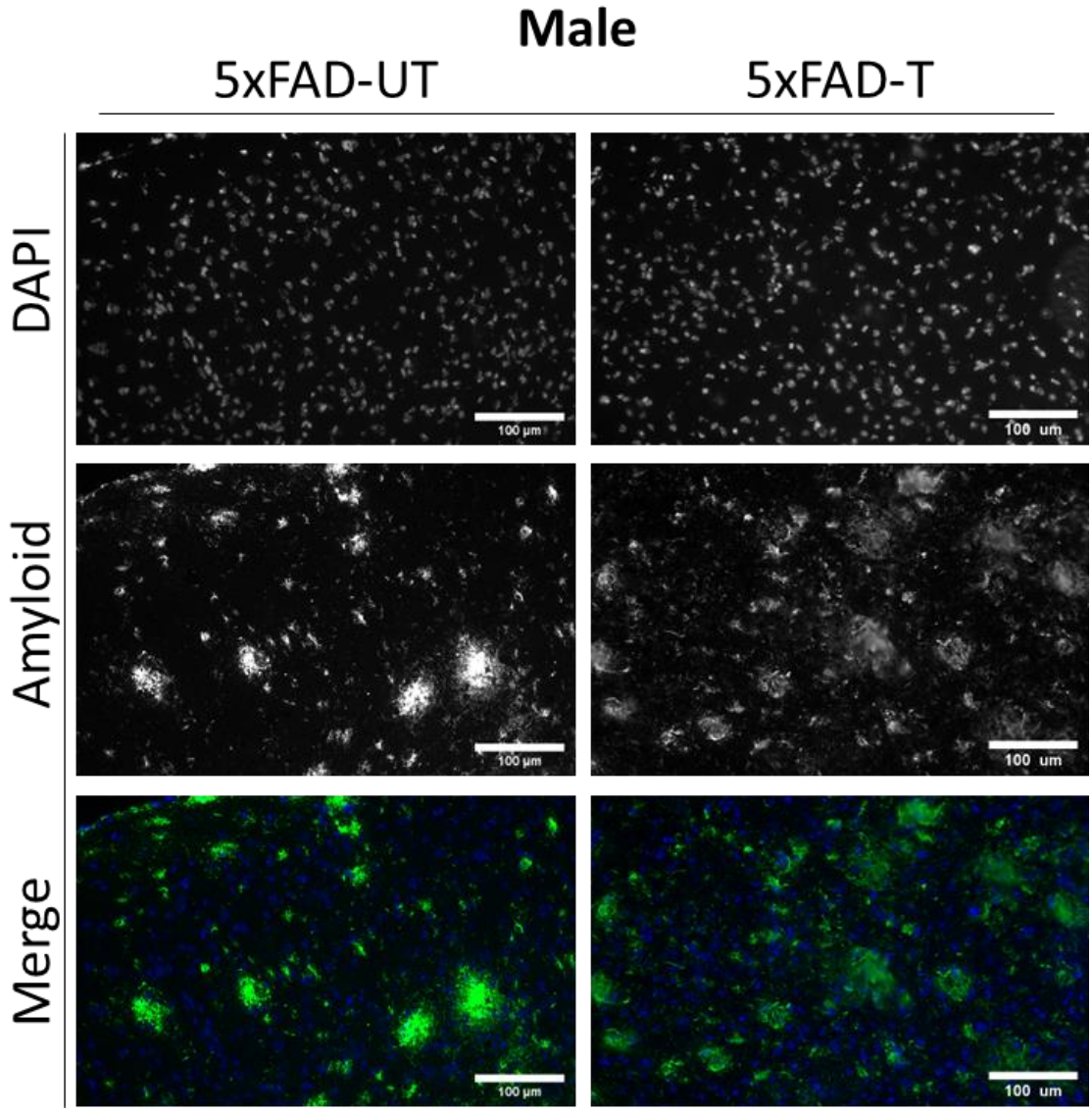

Figure 3.25- Representative Aβ expression in the visual cortex of 40Hz treated and untreated male 5xFAD mice after 15 days of treatment.

9-month-old male 5xFAD were exposed to 1 hour of 40Hz light flicker (5xFAD-T) or 1 hour of darkness (5xFAD-UT) for 15 days, then animals were sacrificed and brains were removed. Sagittal sections at 10µm were immunofluorescence stained using a pan-amyloid antibody. All images were taken at 20x objective of the visual cortex. Representative images for DAPI staining (top row), Aβ staining (mid row) and the merged images showing Aβ in green and DAPI in blue (bottom row). Scale bar shows 100µm.

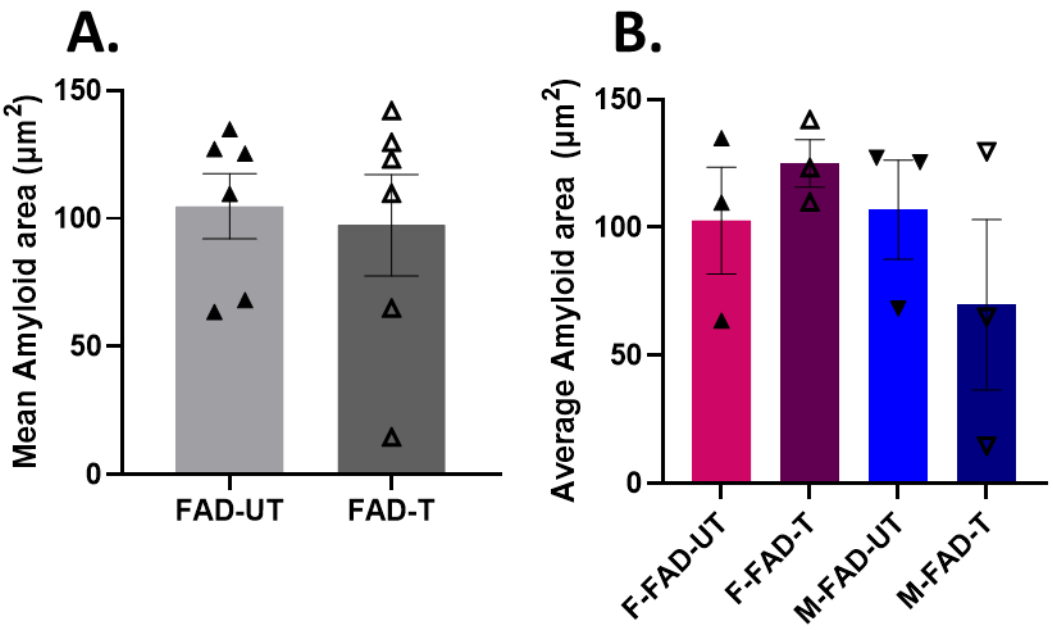

Figure 3.26- Aβ expression in the visual cortex of 40Hz treated and untreated male and female 5xFAD mice after 15 days of treatment. *9-month-old WT and 5xFAD animals of both sexes were exposed to 1 hour of 40Hz light flicker (5xFAD-T) or 1 hour of darkness (5xFAD- UT) for 15 days, then animals were sacrificed and brains were removed. 10µm thick sagittal sections were immunofluorescence stained using a pan-amyloid antibody. All images were quantified at 20x objective of the visual cortex.* ***A****: Total Aβ burden within the visual cortex measured as µm^2 of male and female data combined.* ***B****: Average Aβ burden in the visual cortex of 3 female (F-) or male (M-) mice per group. All data shows mean ±S.E.M. Two-way ANOVA performed with Tukey's multiple comparisons- Treatment: F (1,8) =3.56, P=0.65, Sex: F (1,8) F=2.63, P=0.14. No significant differences found.*

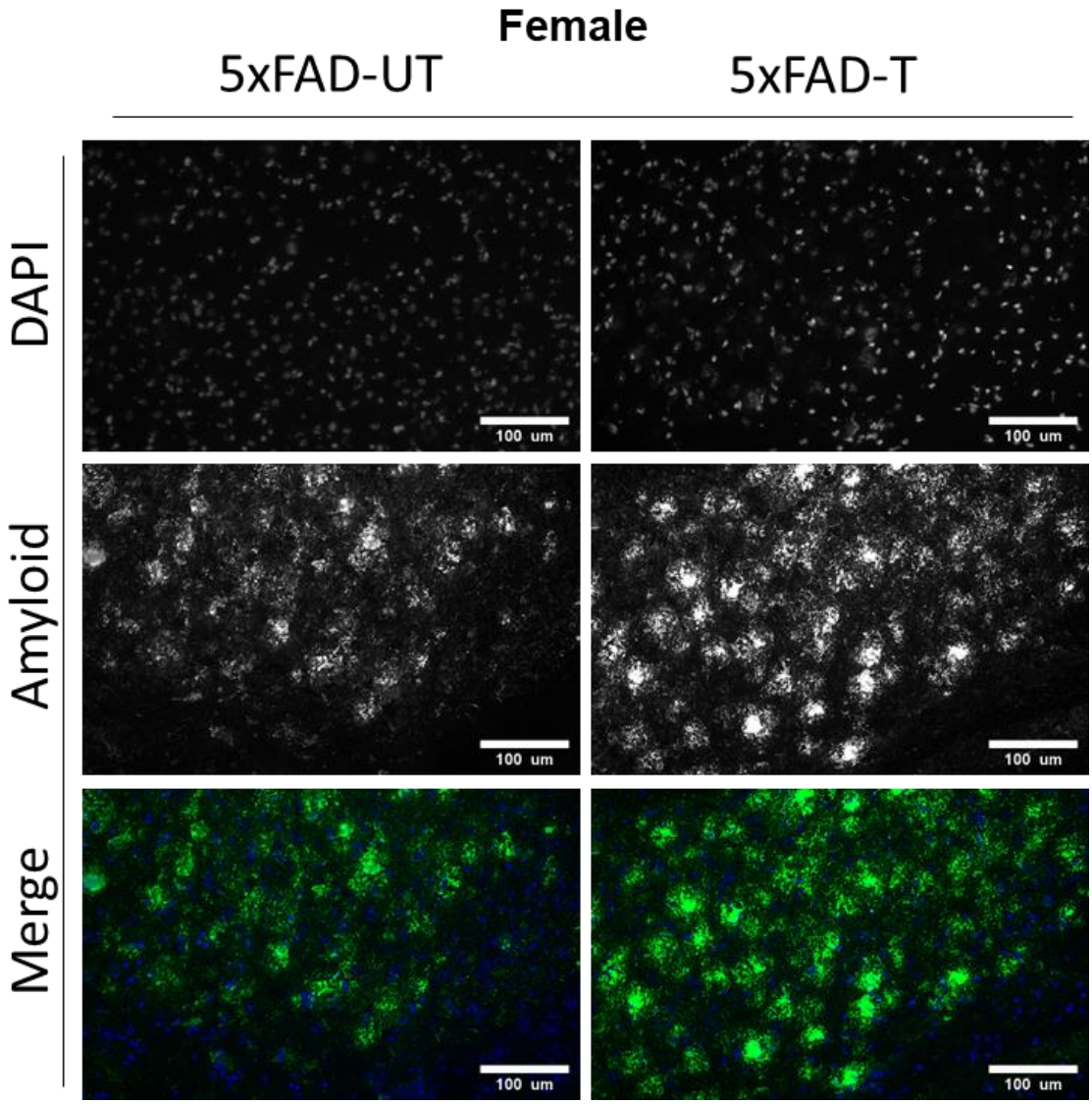

Figure 3.27 Representative Aβ expression in the subiculum of 40Hz treated and untreated female 5xFAD mice after 15 days of treatment. *9-month-old female 5xFAD were exposed to 1 hour of 40Hz light flicker (5xFAD-T) or 1 hour of darkness (5xFAD-UT) for 15 days, then animals were sacrificed, and brains were removed. Sagittal sections at 10μm were immunofluorescence stained using a pan-amyloid antibody. All images were taken at 20x objective of the subiculum. Representative images for DAPI staining (top row), Aβ staining (mid row) and the merged images showing Aβ in green and DAPI in blue (bottom row). Scale bar shows 100μm.*

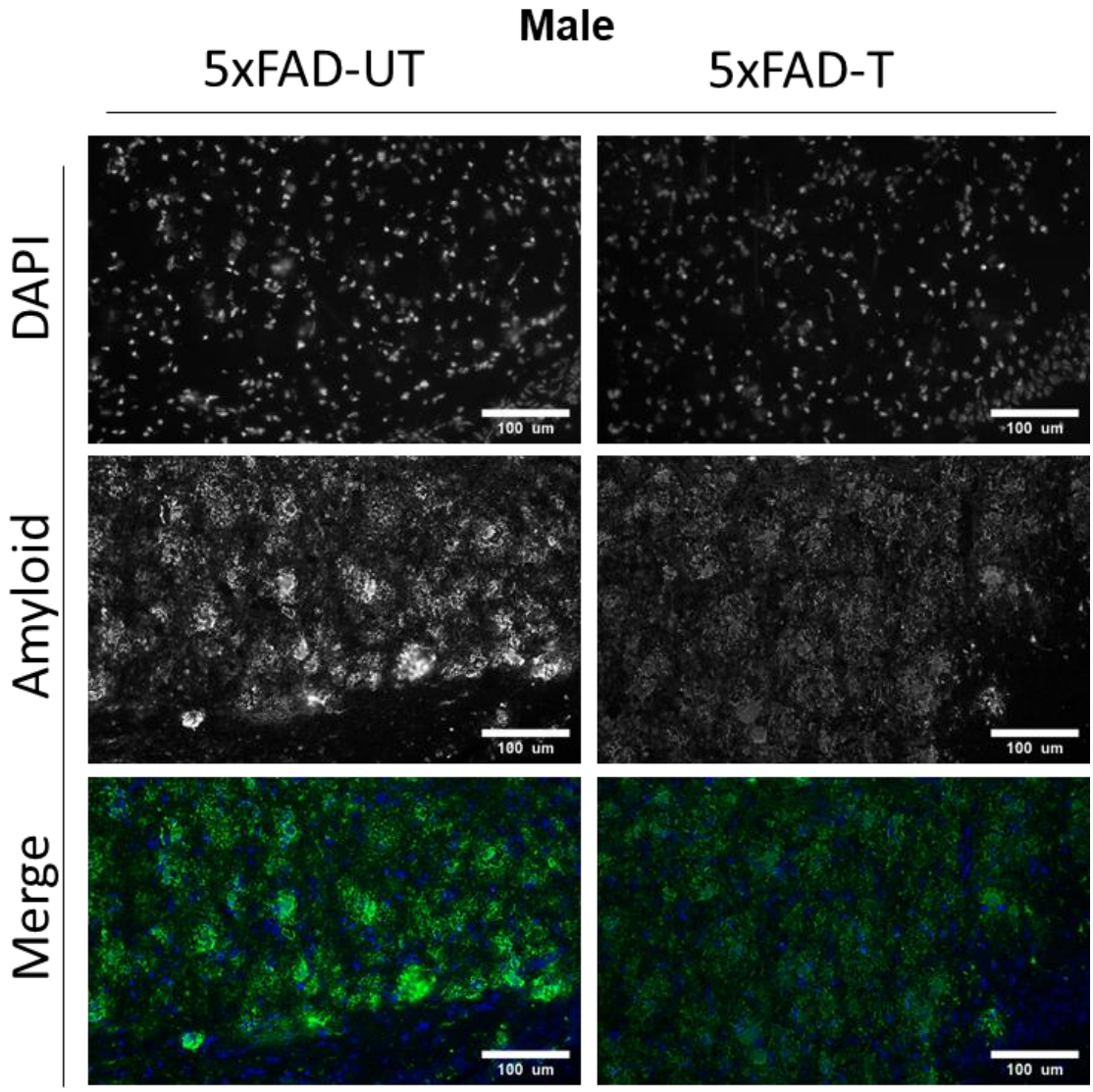

Figure 3.28 - Representative Aβ expression in the subiculum of 40Hz treated and untreated male 5xFAD mice after 15 days of treatment. *9-month-old male 5xFAD were exposed to 1 hour of 40Hz light flicker (5xFAD-T) or 1 hour of darkness (5xFAD-UT) for 15 days, then animals were sacrificed and brains were removed. Sagittal sections at 10μm were immunofluorescence stained using a pan-amyloid antibody. All images were taken at 20x objective of the subiculum. Representative images for DAPI staining (top row), Aβ staining (mid row) and the merged images showing Aβ in green and DAPI in blue (bottom row). Scale bar shows 100μm.*

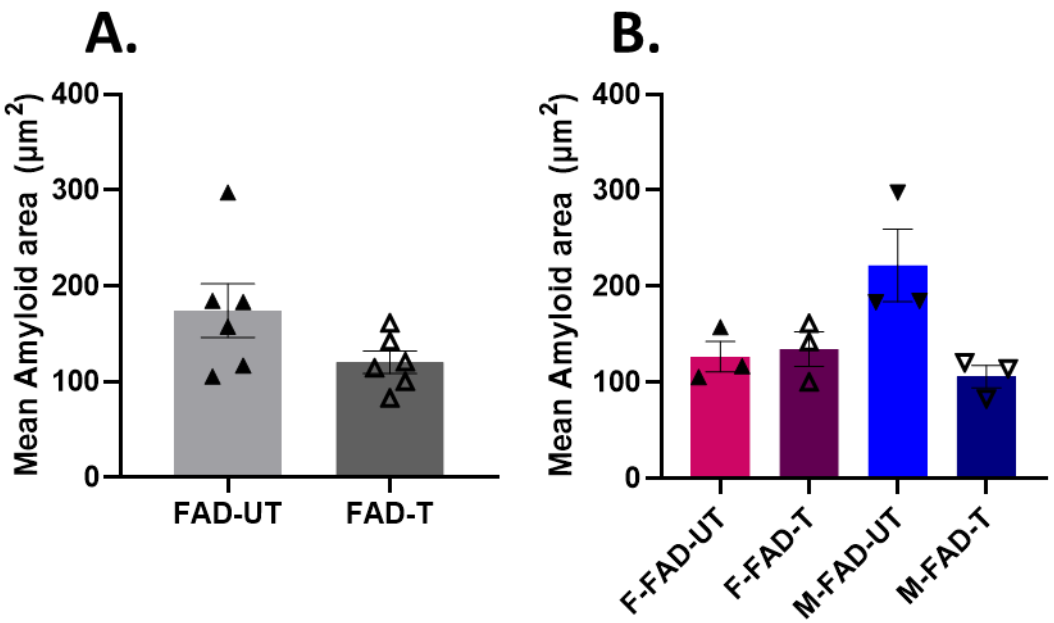

Figure 3.29- Aβ expression in the subiculum of 40Hz treated and untreated mice after 15 days of treatment. *9-month-old 5xFAD animals of both sexes were exposed to 1 hour of 40Hz light flicker (5xFAD-T) or 1 hour of darkness (5xFAD-UT) for 15 days, then animals were sacrificed and brains were removed. 10µm thick sagittal sections were immunofluorescence stained using a pan-amyloid antibody. All images were analysed at 20x objective of the subiculum, and Aβ burden quantified using ImageJ.* ***A****: Total Aβ burden within the subiculum measured as µm² of male and female data combined (n=6 per group)* ***B****: Average Aβ burden in subiculum of 3 female (F-) or male (M-) mice per group. All data shows mean ±S.E.M. Two-Way ANOVA performed; Treatment: F (1,8) =3.35. Sex: F (1,8) =1.27, P=0.29. No significant differences found.*

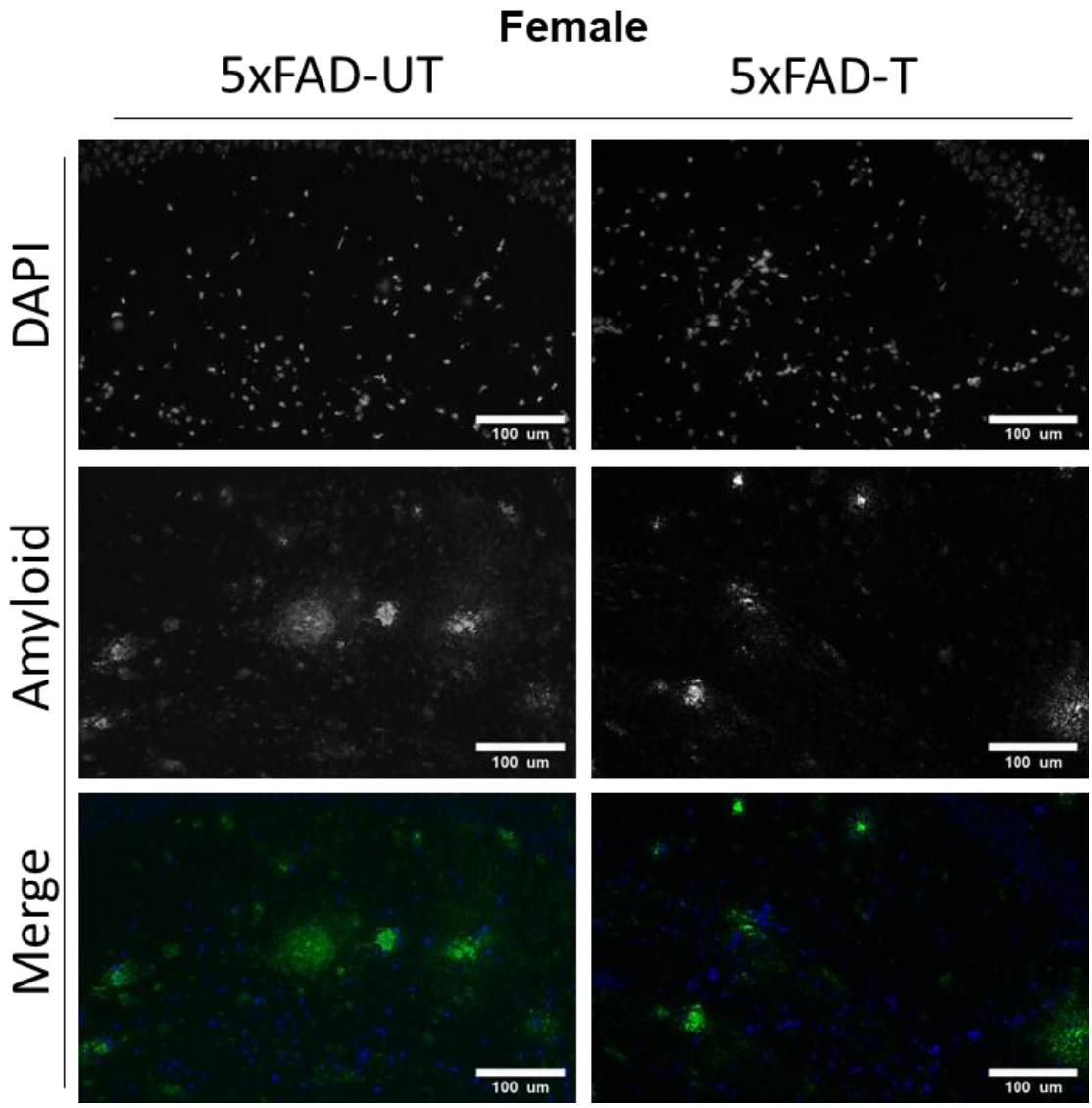

Figure 3.30- Representative Aβ expression in CA1 of 40Hz treated and untreated female 5xFAD mice after 15 days of treatment. *9-month-old female 5xFAD were exposed to 1 hour of 40Hz light flicker (5xFAD-T) or 1 hour of darkness (5xFAD-UT) for 15 days, then animals were sacrificed and brains were removed. Sagittal sections at 10μm were immunofluorescence stained using a pan-amyloid antibody. All images were taken at 20x objective of CA1. Representative images for DAPI staining (top row), Aβ staining (mid row) and the merged images showing Aβ in green and DAPI in blue (bottom row). Scale bar shows 100μm.*

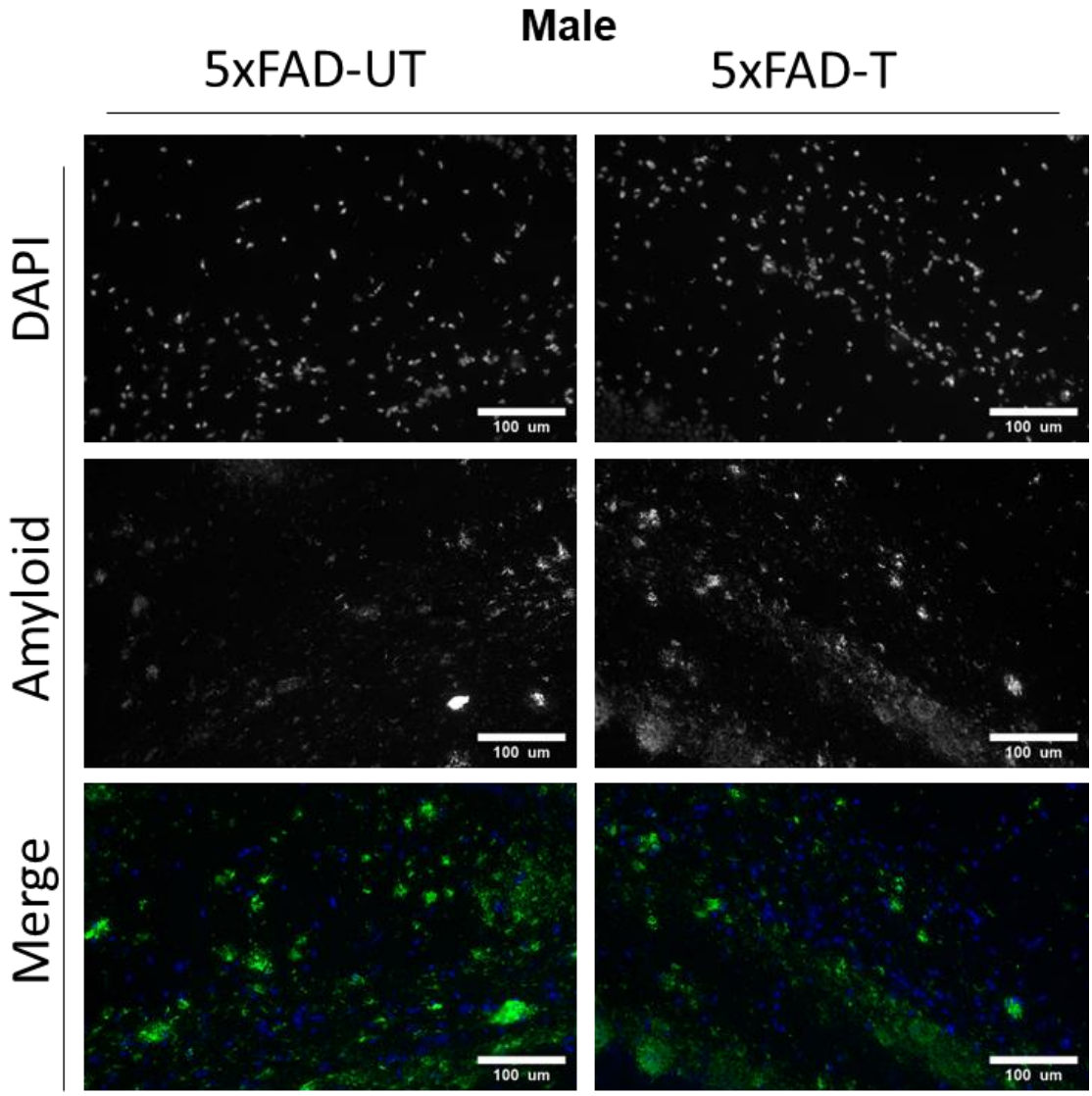

Figure 3.31- Representative Aβ expression in CA1 of 40Hz treated and untreated male 5xFAD mice after 15 days of treatment. *9-month-old male 5xFAD were exposed to 1 hour of 40Hz light flicker (5xFAD-T) or 1 hour of darkness (5xFAD-UT) for 15 days, then animals were sacrificed and brains were removed. Sagittal sections at 10µm were immunofluorescence stained using a pan-amyloid antibody. All images were taken at 20x objective of CA1. Representative images for DAPI staining (top row), Aβ staining (mid row) and the merged images showing Aβ in green and DAPI in blue (bottom row). Scale bar shows 100µm.*

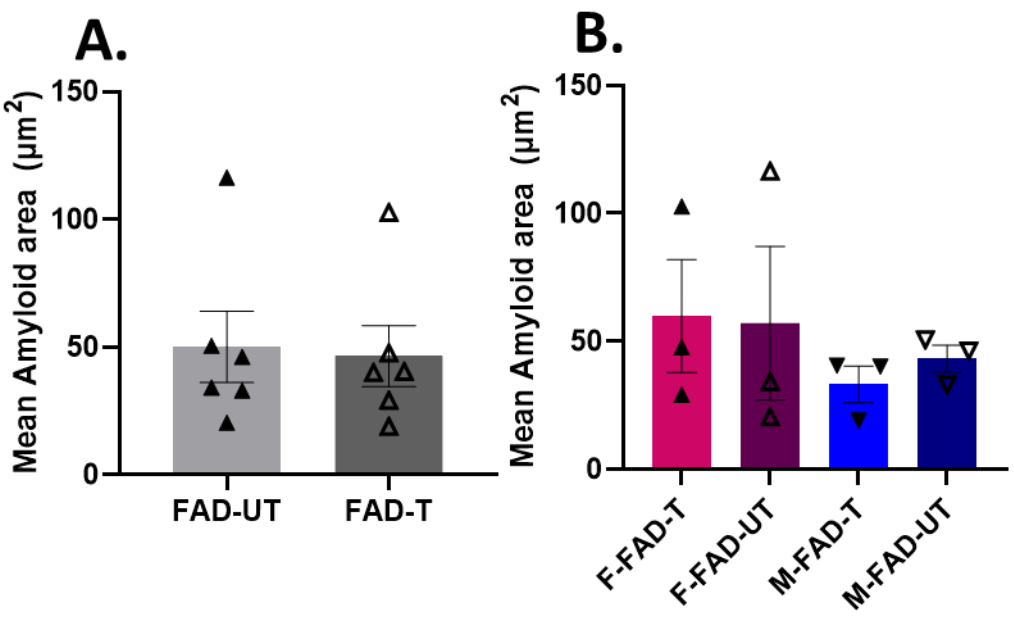

Figure 3.32- Aβ expression in CA1 of 40Hz treated and untreated mice after 15 days of treatment. *9-month-old 5xFAD animals of both sexes were exposed to 1 hour of 40Hz light flicker (5xFAD-T) or 1 hour of darkness (5xFAD-UT) for 15 days, then animals were sacrificed, and brains were removed. 10µm thick sagittal sections were immunofluorescence stained using a pan-amyloid antibody. All images were analysed at 20x objective of CA1, and Aβ burden quantified using ImageJ.* ***A****: Total Aβ burden within CA1 measured as µm^2 of male and female data combined (n=6 per group)* ***B****: Average Aβ burden in CA1 of 3 female (F-) or male (M-) mice per group. All data shows mean ±S.E.M. Two-way ANOVA performed; Treatment: F (1,8) =0.14. Sex: F (1,8) =0.77, P=0.41. No significant differences found.*

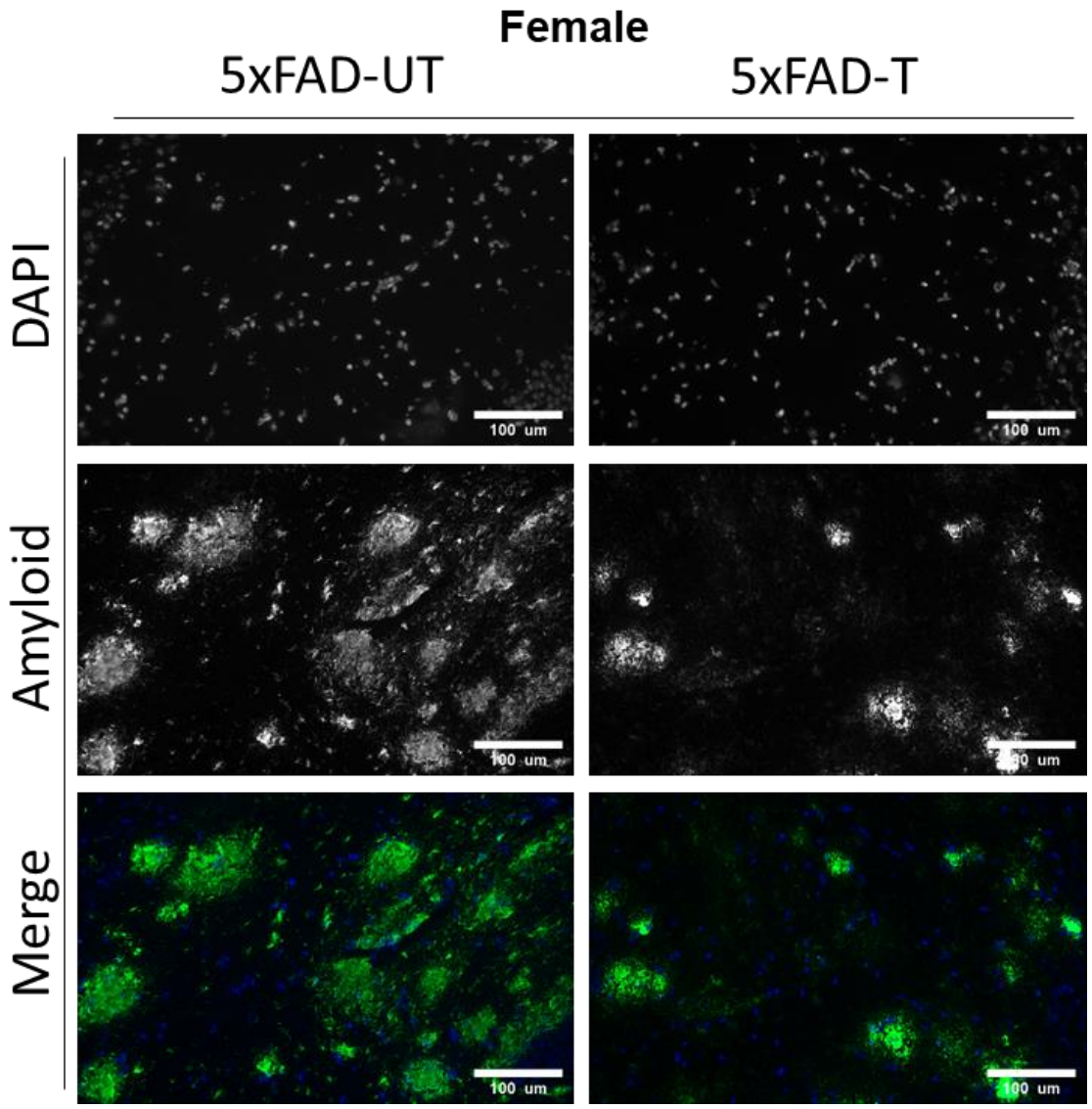

Figure 3.33- Representative Aβ expression in CA3 of 40Hz treated and untreated female 5xFAD mice after 15 days of treatment. *9-month-old female 5xFAD were exposed to 1 hour of 40Hz light flicker (5xFAD-T) or 1 hour of darkness (5xFAD-UT) for 15 days, then animals were sacrificed and brains were removed. Sagittal sections at 10μm were immunofluorescence stained using a pan-amyloid antibody. All images were taken at 20x objective of CA3. Representative images for DAPI staining (top row), Aβ staining (mid row) and the merged images showing Aβ in green and DAPI in blue (bottom row). Scale bar shows 100μm.*

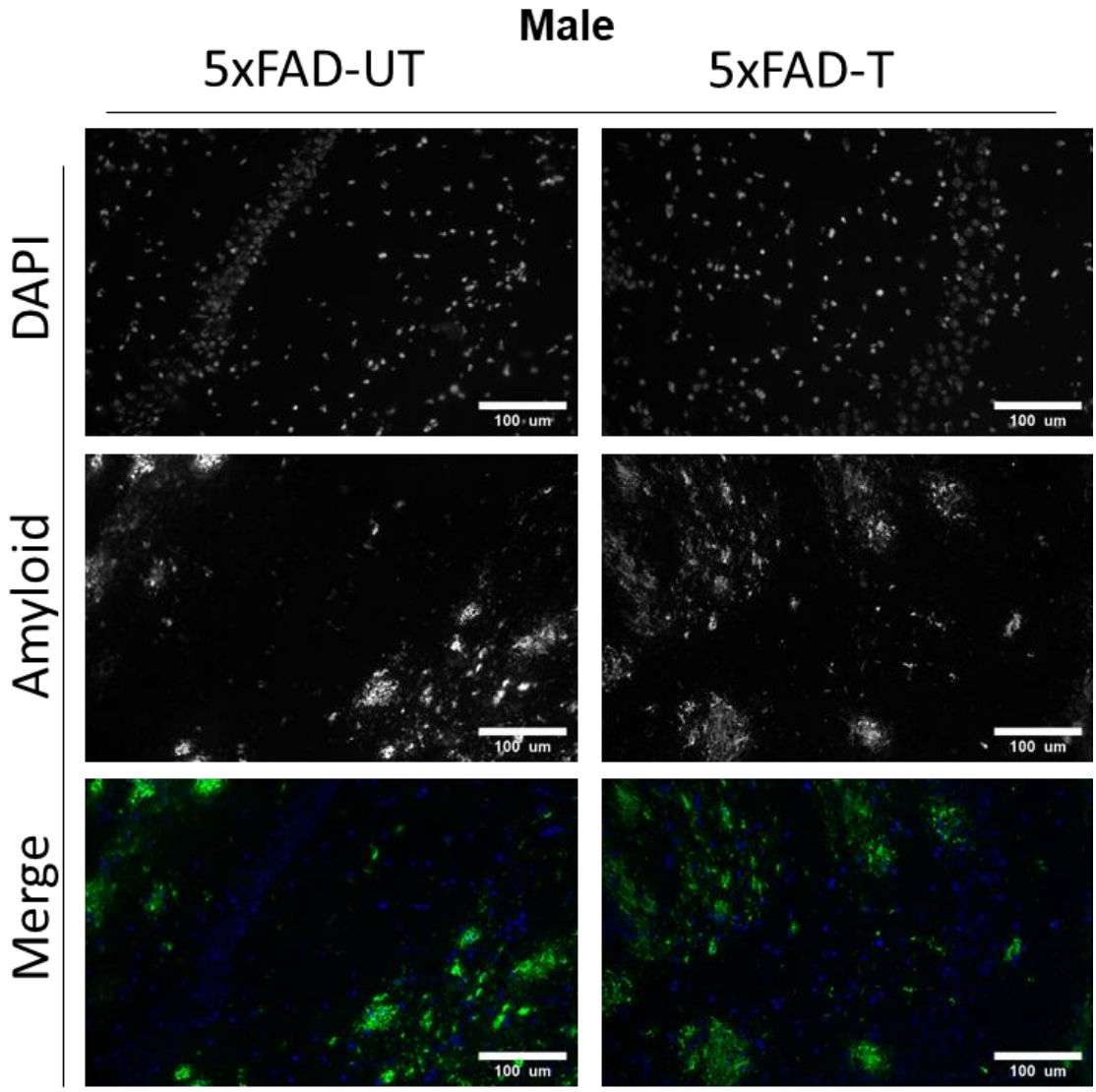

Figure 3.34- Representative Aβ expression in CA3 of 40Hz treated and untreated male 5xFAD mice after 15 days of treatment. *9-month-old male 5xFAD were exposed to 1 hour of 40Hz light flicker (5xFAD-T) or 1 hour of darkness (5xFAD-UT) for 15 days, then animals were sacrificed and brains were removed. Sagittal sections at 10µm were immunofluorescence stained using a pan-amyloid antibody. All images were taken at 20x objective of CA3. Representative images for DAPI staining (top row), Aβ staining (mid row) and the merged images showing Aβ in green and DAPI in blue (bottom row). Scale bar shows 100µm.*

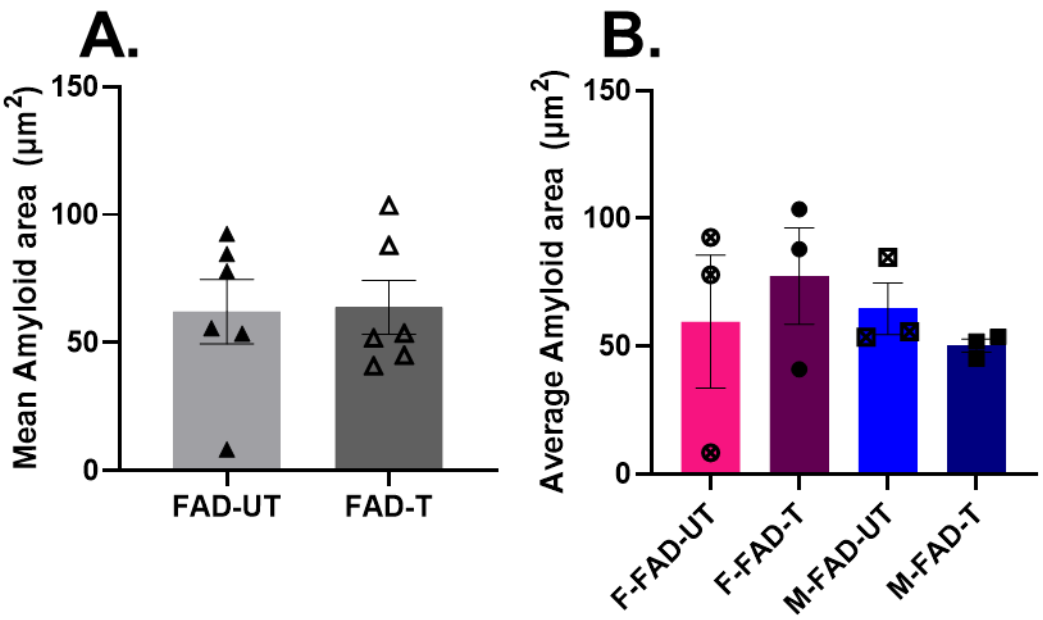

Figure 3.35- Aβ expression in CA3 of 40Hz treated and untreated mice after 15 days of treatment. *9-month-old 5xFAD animals of both sexes were exposed to 1 hour of 40Hz light flicker (5xFAD-T) or 1 hour of darkness (5xFAD-UT) for 15 days, then animals were sacrificed, and brains were removed. 10µm thick sagittal sections were immunofluorescence stained using a pan-amyloid antibody. All images were analysed at 20x objective of CA3, and Aβ burden quantified using ImageJ.* ***A****: Total Aβ burden within CA3 measured as µm^2 of male and female data combined (n=6 per group)* ***B****: Average Aβ burden in CA3 of 3 female (F-) or male (M-) mice per group. All data shows mean ±S.E.M. Two-way ANOVA performed; Treatment: F=0.74, P=0.42. Sex: F=0.35, P=0.57. No significant differences found.*

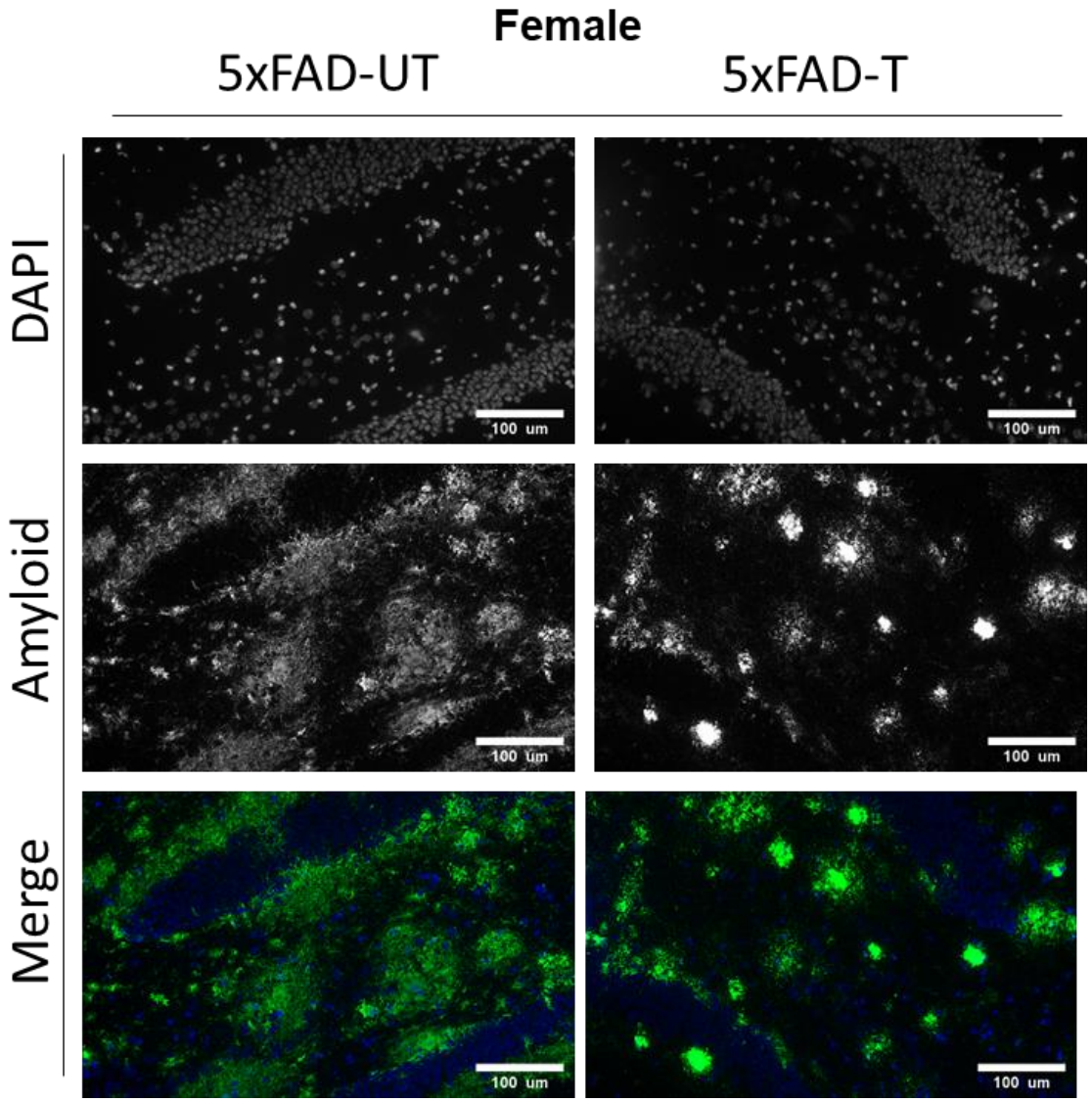

Figure 3.36- Representative Aβ expression in the dentate gyrus of 40Hz treated and untreated female 5xFAD mice after 15 days of treatment. *9-month-old female 5xFAD were exposed to 1 hour of 40Hz light flicker (5xFAD-T) or 1 hour of darkness (5xFAD-UT) for 15 days, then animals were sacrificed and brains were removed. Sagittal sections at 10μm were immunofluorescence stained using a pan-amyloid antibody. All images were taken at 20x objective of the dentate gyrus. Representative images for DAPI staining (top row), Aβ staining (mid row) and the merged images showing Aβ in green and DAPI in blue (bottom row). Scale bar shows 100μm.*

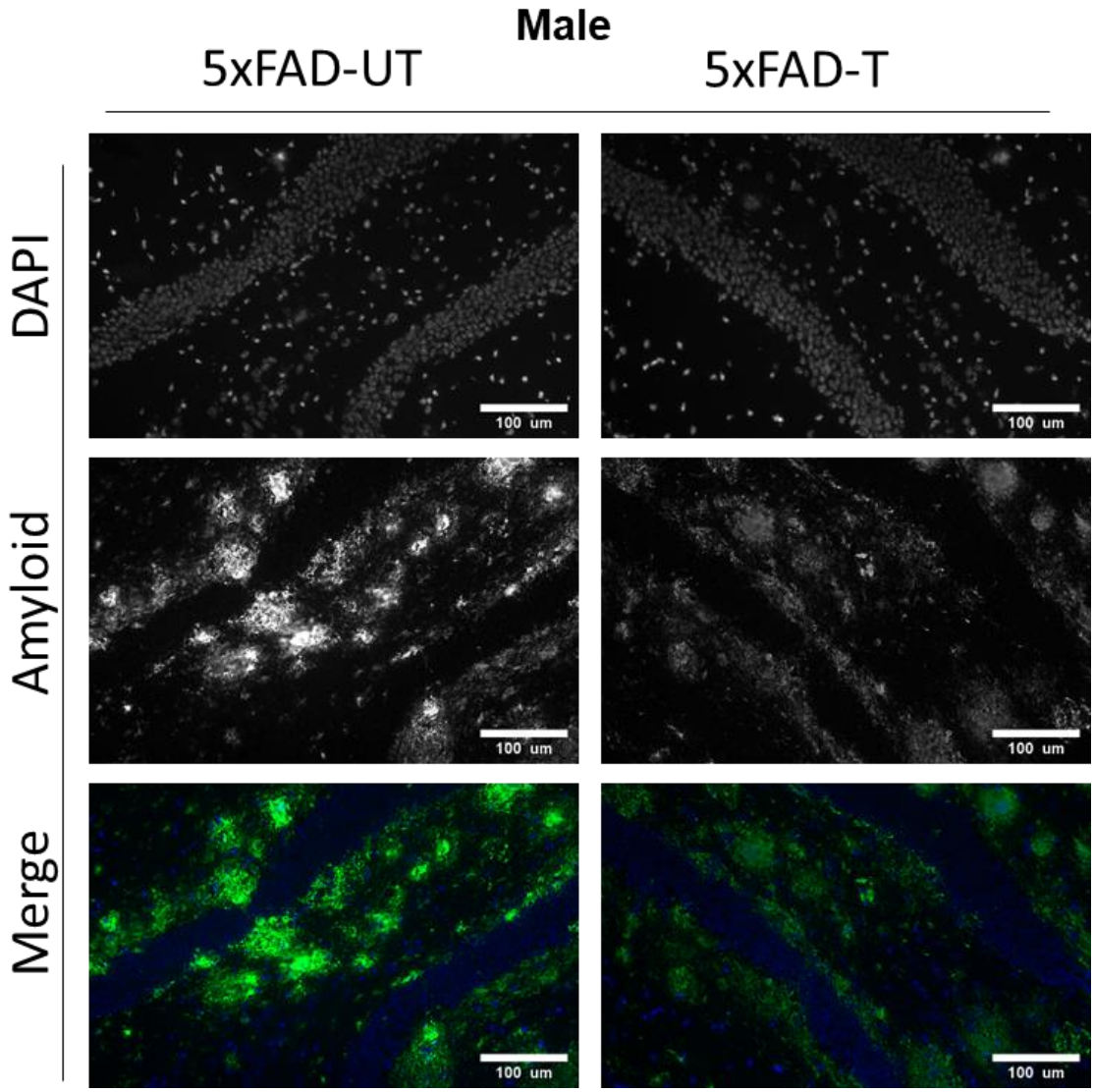

Figure 3.37- Representative Aβ expression in the dentate gyrus of 40Hz treated and untreated male 5xFAD mice after 15 days of treatment. *9-month-old male 5xFAD were exposed to 1 hour of 40Hz light flicker (5xFAD-T) or 1 hour of darkness (5xFAD-UT) for 15 days, then animals were sacrificed and brains were removed. Sagittal sections at 10μm were immunofluorescence stained using a pan-amyloid antibody. All images were taken at 20x objective of the dentate gyrus. Representative images for DAPI staining (top row), Aβ staining (mid row) and the merged images showing Aβ in green and DAPI in blue (bottom row). Scale bar shows 100μm.*

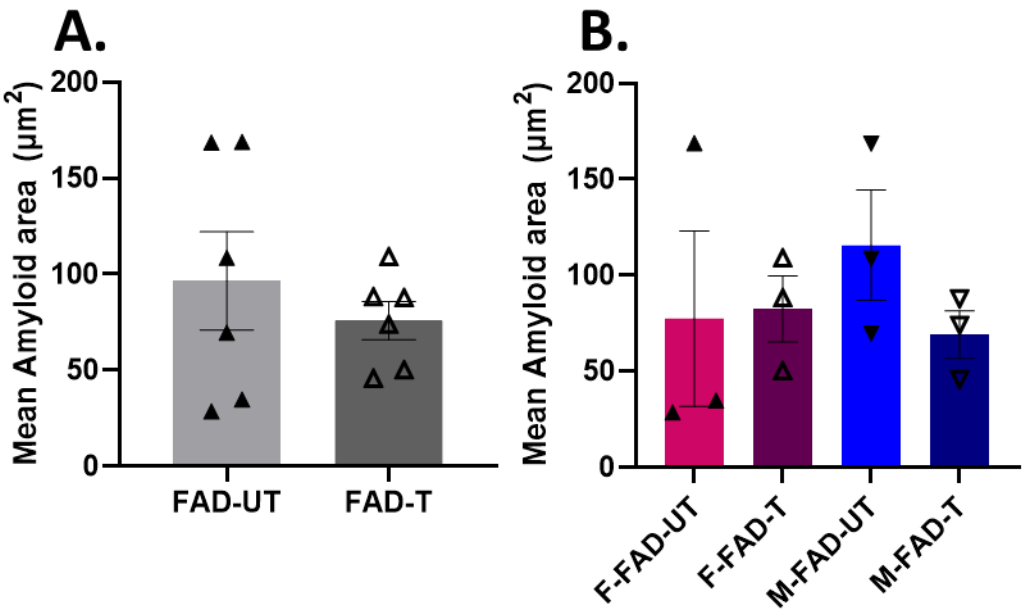

Figure 3.38- Aβ expression in the dentate gyrus of 40Hz treated and untreated mice after 15 days of treatment. *9-month-old 5xFAD animals of both sexes were exposed to 1 hour of 40Hz light flicker (5xFAD-T) or 1 hour of darkness (5xFAD-UT) for 15 days, then animals were sacrificed, and brains were removed. Sagittal sections at 10µm were immunofluorescence stained using a pan-amyloid antibody. All images were analysed at 20x objective of the dentate gyrus, and Aβ burden quantified using ImageJ.* ***A****: Total Aβ burden within DG measured as µm² of male and female data combined (n=6 per group)* ***B****: Average Aβ burden in DG of 3 female (F-) or male (M-) mice per group. All data shows mean ±S.E.M. Two-Way ANOVA performed; Treatment: F (1,8)=0.63, P=0.45. Sex: F (1,8) =0.23, P=0.65. No significant differences found.*

Table 3.3 – Aβ measurements in the HPF and VC of 9-month-old 5xFAD animals treated with light flicker for 15 days.

Frozen brain sections were immunostained for Aβ, then positive area measured using ImageJ software, counting only plaques >3 μm^2. 3 sections were analysed per mouse, and an average calculated. Table shows average Aβ of all mice within each group, exact Aβ area measurements in μm^2 ± S.E.M. Values rounded to 1 decimal place. n=6 animals for all groups and regions.

Aβ area – all units in μm^2		Brain Region				
		VC	**SUB**	**CA1**	**CA3**	**DG**
Untreated	**5xFAD**	104.8 ±12.8	174.2 ± 28.1	50.2 ± 14	62.1 ± 30.7	96.5 ± 25.7
Treated	**5xFAD**	97.38 ±19.8	120.2 ± 11.6	46.5 ± 12	63.8 ±10.5	75.8 ± 10

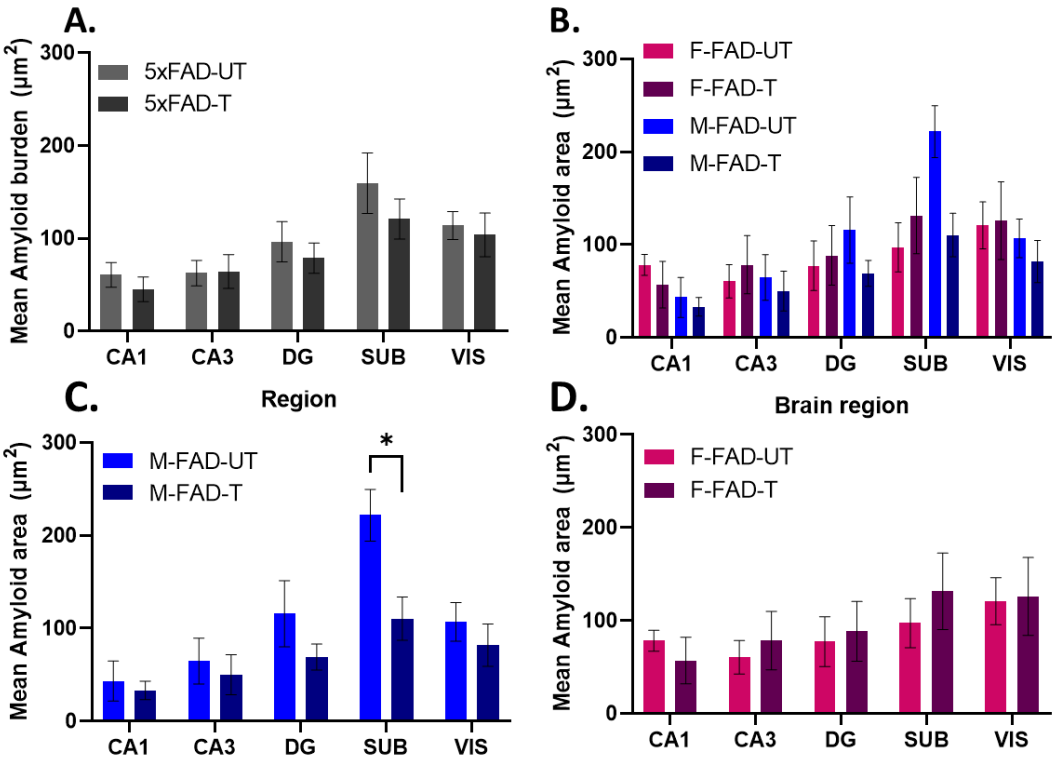

Figure 3.39- Average Aβ plaque area per region in the brains of 40Hz treated and untreated 5xFAD mice after 15-day treatment. *Images from 488nm stained for pan-amyloid-β were captured at 20x magnification for each region, 3 images captured per animal and quantified using imageJ analysis. Only plaques larger than 3µm were counted to calculate total area per image.* ***A:*** *Average amyloid burden per region of untreated and treated 5xFAD mice, n=6 mice per group, combined data of 3 male and 3 female. Treatment not significant (F=1,50)=1.6, P=0.2)* ***B****: Male and female animals plotted together for direct comparison. 3-way ANOVA performed, no significant differences between sexes or treatment group detected.* ***C:*** *Amyloid burden in various brain regions of male 5xFAD mice with or without treatment. n=3. Two-way ANOVA performed. Treatment (F(1,20)=8.025, P=0.01) found to be significant. Tukey's multiple comparisons then performed, SUB region P=0.0142.* ***D:*** *Amyloid burden in various brain regions of female 5xFAD mice with or without treatment. n=3. No significant differences detected. (P*<0.05.)*

3.2.6 Effect of 15-day oscillating light treatment on CD45+ cells in the brain regions of 9-month-old mice

To determine the inflammation level in the brain, we again performed immunohistochemical staining with CD45 antibody in the brain sections. Qualitatively there was no difference of CD45+ staining cells in the brain regions between 5xFAD treated and untreated animals (Fig 3.40 & 3.41). CD45+ cells in different regions of brain were manually counted in each mouse (with 3 sections per mouse). Our data show there was no significant difference of CD45+ cell counts between 40Hz treated 5xFAD and untreated 5xFAD controls in the DG, CA3 or CA1 regions (Table 3.4). However, there was a significant increase in the number of CD45+ cells in the VC of treated female 5xFAD (Fig 3.42.C P*<0.05), mice compared to untreated female 5xFADs (Fig 4.32C). 40Hz treated male 5xFADs did not show this increase compared to untreated male 5xFAD mice (Fig 3.42.B) When data was combined and analysed together, this significant increase in CD45+ cells in the VC was still significant (Fig 3.42.A, P*<0.05).

Table 3.4 Total number of CD45+ cells in the HPF and VC of 9-month-old 5xFAD animals after 15-day 40Hz light treatment.

Brain sections were immunostained for CD45+ and analysed using ImageJ software, positive cells counted manually. Table shows total number of CD45 cells in each area of the HPF (SUB, CA1, CA3 and DG) and the VC ± S.E.M. Values rounded to 1 decimal place. n=6 animals for all groups and regions.

Total no. CD45+ cells		Brain Region				
		VC	**SUB**	**CA1**	**CA3**	**DG**
Untreated	**5xFAD**	6.0 ± 1.1	29.9 ± 3.6	3.4 ± 0.9	6.8 ±1.0	8.9 ± 1.3
Treated	**5xFAD**	12.9 ± 2.1(*)	24.2 ±2.0	3.5 ±1.0	6.8 ±1.1	7.9 ± 0.8

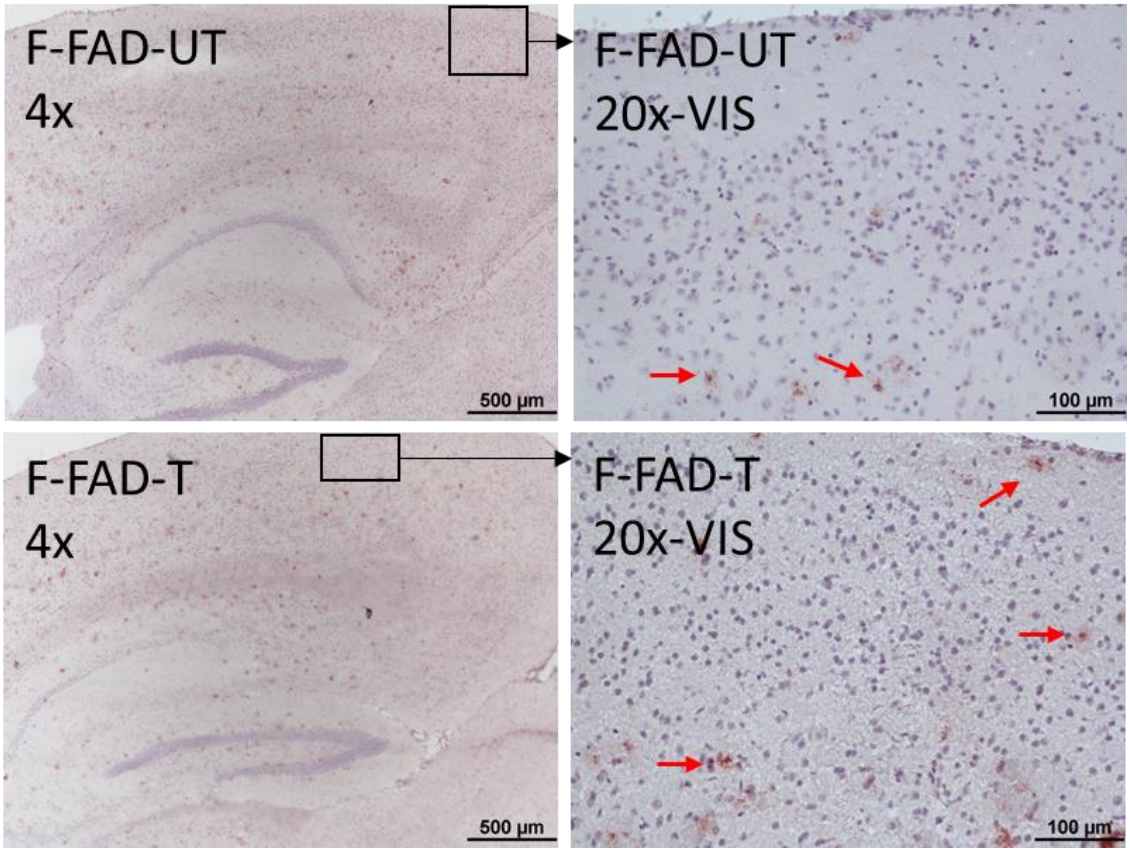

Figure 3.40- Representative images of CD45 in the brain of female 5xFAD mice after 15 days of 40Hz light treatment. *5xFAD female animals were exposed to 1 hour of 40Hz light flicker (5xFAD-T) or 1 hour of darkness (5xFAD-UT) for 15 days. Mice were then sacrificed, and brains were removed. Sagittal sections were stained with CD45 antibody, followed by a biotin conjugated antibody and AMEC substrate. Nuclei were stained with haematoxylin. Left column shows representative 4x microscopy images of hippocampus and VC, right column shows representative 20x magnification of the VC*

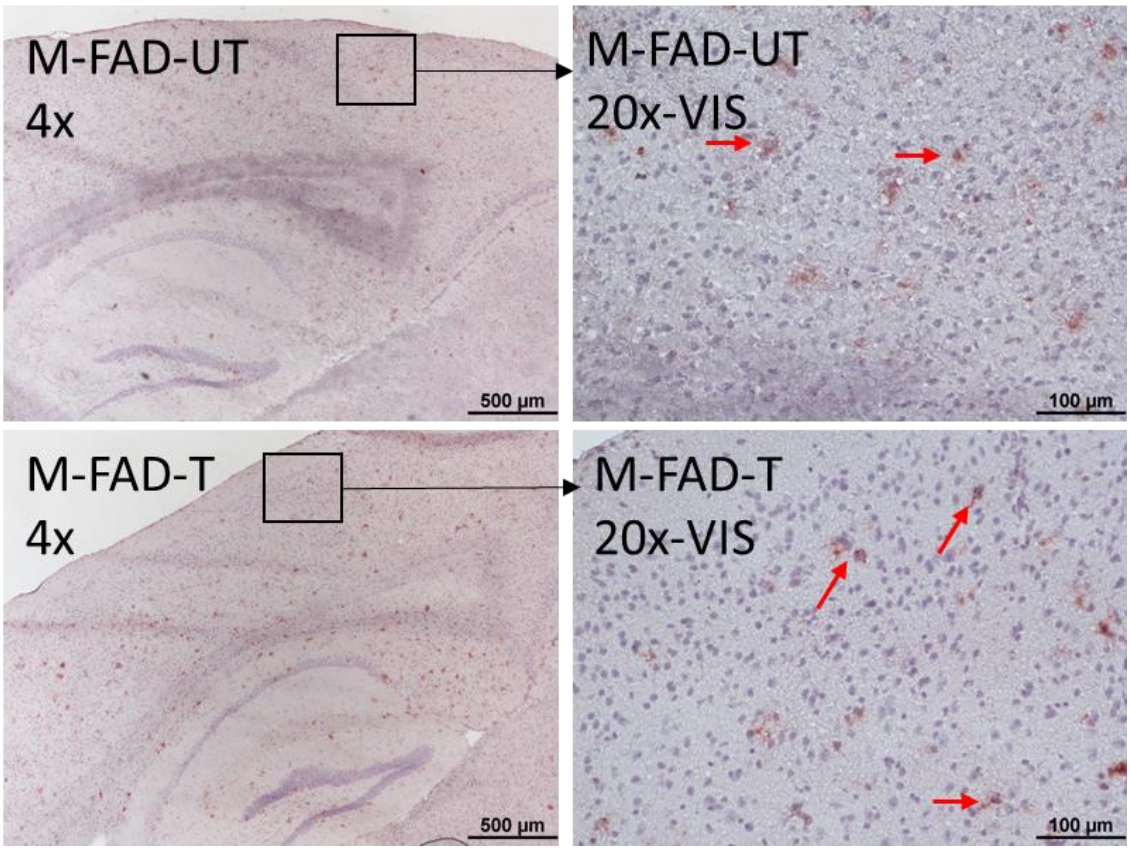

Figure 3.41- Representative images of CD45 in the brain of male 5xFAD mice after 15 days of 40Hz light treatment. *5xFAD male animals were exposed to 1 hour of 40Hz light flicker (5xFAD-T) or 1 hour of darkness (5xFAD-UT) for 15 days. Mice were then sacrificed, and brains were removed. Sagittal sections were stained with CD45 antibody, followed by a biotin conjugated antibody and AMEC substrate. Nuclei were stained with haematoxylin. Left column shows representative 4x microscopy images of hippocampus and VC, right column shows representative 20x magnification of the VC.*

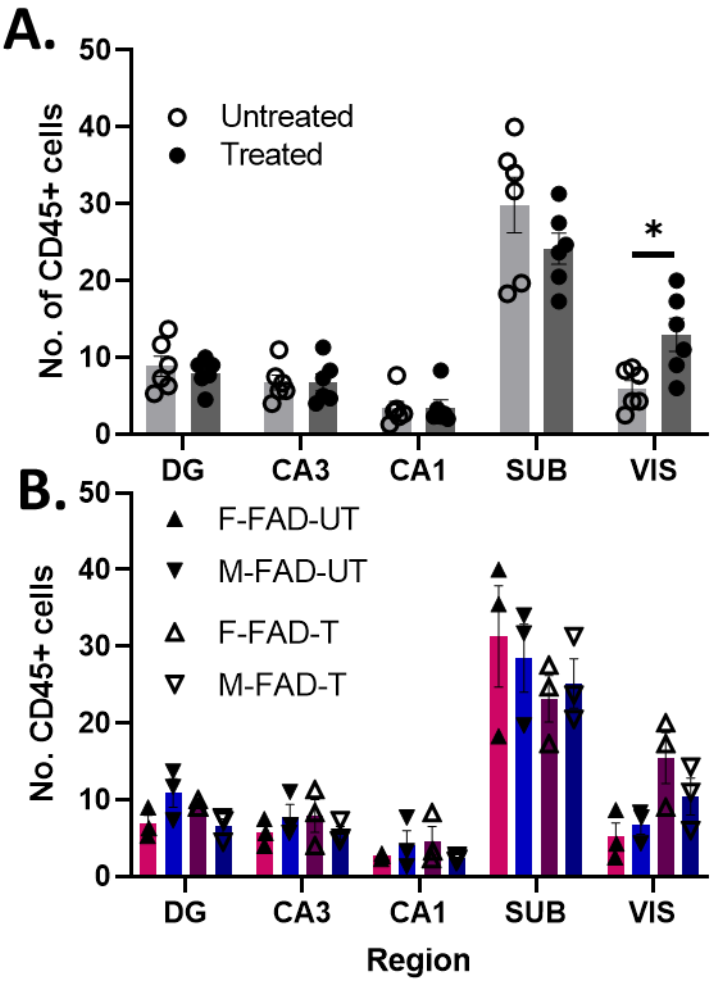

Figure 3.42- Total CD45 cell counts for 9-month-old 5xFAD animals treated with 40Hz light for 15-days. *CD45 cells were stained via IHC using a CD45 primary antibody and 20x magnification images collected using a brightfield microscope, then quantified manually using imageJ. Experimenter was blind to animal genotype and treatment group when quantifying. n=3 mice used per group, and 3 replicate images quantified per mouse.* ***A*** *Shows the combined data from both male and female 5xFAD mice comparing treated and untreated groups ± S.E.M. Two-way ANOVA performed. Treatment (F(1,20)=1.27, P=0.2) caused no significant change however an interaction between treatment and genotype (F(4,50)=3.5, P=0.01) was noted. Sidak's multiple comparison test performed, VC difference P=0.02.* ***B:*** *Data from 40Hz treated male and female 5xFAD mice presented separately. 3-way ANOVA performed, no significant differences in sex (F(1,40)=0.006, P=0.9) or treatment (F(1,40)=0.13, P=0.7) found.*

3.3 Discussion

To begin, a protocol for genotyping 5xFAD mice was adapted from the JAX laboratories website and the manufacturer instructions for the kit. After testing our protocol compared to external genotyping service, we confirmed it was working effectively, and routine genotyping of new litters was conducted throughout the project when new litters were born. This strain offers a powerful model for on-going studies in the group and formed the basis of my subsequent PhD research.

We then had to develop the circuitry for the light-flicker treatment. Following the previously published protocol (Yao *et al.,* 2020) we constructed the circuit board exactly as the protocol indicated, only to find that it was unable to power the LED lights. We therefore adapted the board using additional wires to facilitate the power and Arduino-mediated flickering of the lights. A suitable treatment chamber was then constructed by wrapping black paper around a "home-cage" and found to be suitable for the initial treatment procedure.

Following 5-day treatment, animals were sacrificed, tissue harvested, and brain sections were stained and analysed for the expression of Aβ and CD45. Our data showed all 5xFAD mice exhibited high levels of Aβ in various regions of brains while WT mice had no expression of Aβ, confirming the presence of disease in previously genotyped animals. However, we observed no difference in Aβ levels between treated and untreated 5xFAD animals after 5 days of light treatment. These results do not replicate what was observed by Iaccarino et al (Iaccarino et al*.,* 2016). There are two potential explanations for this difference. Firstly, the difference in the duration of treatment as Iaccarino et al. used 7 days continuous treatment, while we only performed 5 days which may not be a sufficient exposure to the light therapy to induce the changes observed. The second difference was the age of animals used at the time of the treatment. Iaccarino et al used animals aged 6 months in their initial study while we used animals aged 9 months old where AD pathology is more severe (Oakley *et al.,* 2006). More likely however is that the issue is a combination of the two factors; while 5 days of treatment may have been sufficient for 6-month-old animals a longer treatment period is required for 9-month-old animals to compensate for the more severe pathology.

It is also possible that our equipment was not inducing the oscillations required- either due to mechanical fault on the end of the light setup or that it was not inducing the oscillations due to behaviour in the mice (hiding from light, excessive moment etc.).

After the unpromising results from the 5-day treatment, we next decided to extend treatment to 15 days. The revised plan used 15 days total, over 3 sets of 5 consecutive treatments each week for three weeks, again due to restricted weekend working. Our theory was that if 5 days was insufficient to induce any significant change in amyloid burden in the CNS then extended exposure to the light flicker may lead to the expected changes. We again used the levels of Aβ in the visual cortex as our measure of treatment effectiveness and performed CD45 staining to determine if 15 days had an increased or decreased effect on neuroinflammation in AD associated brain regions. Our results showed that there was no significant reduction in the Aβ burden in any region of the brain we investigated and expected to respond to the light flicker treatment. However, we did observe a significant decrease in the SUB region of male 5xFAD mice after 15 days of treatment. This was unexpected as the light flicker treatment would first need to effect the VC before reaching the SUB to induce changes, thus these findings are likely due to variation in animals and low statistical power. Overall the results suggest that the treatment was ineffective at reducing AD pathology.

We did, however, observe a significant increase in the number of inflammatory CD45+ cells within the VC of female mice treated for 15 days, potentially indicating the beginning of a light-induced response which may be hypothesised to be insufficient to affect the amyloid burden within any brain regions of these mice. Previous publications did not examine expression of this marker, thus these findings are novel. The fact that the males showed no such increased in CD45+ cells within the VC suggests there is a sex-dependent response, which may be caused by the more readily-inflammatory female immune system (Klein and Flanagan, 2016; Osborne, Turano and Schwarz, 2018) or the more severe pathology observed in female 5xFAD mice (Oakley *et al.,* 2006). This pro-inflammatory response is in keeping with other publications which have shown 40Hz light flicker induces inflammatory cytokine and marker expression within the CNS (Garza *et al.,* 2020), and thus further validates our model.

When 9-month-old 5xFAD mice were treated with 1-hour 40Hz light flicker or 1 hour of darkness there was no change in the levels of Aβ in any region of the brain. One of the key questions we asked was whether or not the treatment was inducing gamma oscillations within the brain of the mice- either due to mechanical fault or experimental setup and design. We confirmed the light flicker was oscillating at 40Hz using an oscillometer (data transiently displayed on screen, no recorded data available), and that the light levels emitted by the LEDs was sufficient at the front of the cage (approximately 1000 lux, consistent with other published methods (Iaccarino, et al., 2016)). However due to the length of the cages it is possible animals were "hiding" at the back of the cage where only 5-10 lux could penetrate, thus no oscillations would occur. This behaviour may also explain the obvious variation of some of the results within the treated groups if some mice had hidden from the light while others had not. Reports from other labs (Iaccarino et al., 2016) use the same size cages laid with the broad size adjacent to the light to limit how far the animals could travel away from the light. However due to space restrictions this was not feasible for us. Our equipment was further modified as described in Chapter 4 to improve light exposure and ensure mice could not hide for future experiments, as well as improvements to circuitry to improve light output.

3.4 Limitations

The original plan for the experiments was to treat mice at 5/6 months old when the pathology is relatively moderate and severe neuronal damage has not yet occurred (Buskila, Crowe and Ellis-Davies, 2013). However due to the global outbreak of COVID-19, the University was closed unexpectedly for 4 months, meaning the original research plans to treat the mice at 5/6 months were no longer feasible. To avoid wasting the mice we decided to conduct experiments using the 9-month-old mice which had severe pathology. While this theoretically would be harder to treat, we reasoned that it also more closely reflects the neuropathology change in human AD which is not usually detected until significant pathology has already occurred. When the university was partially opened after the summer 2020, the original 7 days of treatment was revised to 5 days due to the additional COVID-19 restrictions on weekend working. During the lockdown we were also unable to test any of the equipment prepared at home (light flicker equipment, breadboard setup etc.) and once we returned the animals were already at the 9-month-old timepoint, so there was very little time to test equipment before experiments began.

As previously mentioned, the cage-setup for these animals was adapted from, but different to the original publications. It is very likely that the home cages used for these experiments were too long, resulting in low light levels at the back of the cage where the animals tended to be. Increasing the intensity of the light was not an option at this stage due to concerns for animal wellbeing (damage to eyes from excessive light levels at the front of the cage) and due to a lack of means (lights were battery operated at this stage, and thus power output was not controllable.) This likely had a significant impact on the effectiveness of the treatment, though some changes were still observed.

Chapter 4

15-day 40Hz light exposure on 4-5-month-old 5xFAD animals

4 15-day 40Hz light exposure to 4-5-month-old 5xFAD animals

After negative results from the first experiments outlined in Chapter 3, it was decided that the equipment and methodology of administering treatment needed to be refined. Our methods in chapter 3 were different from published methods in several key ways- the alignment of the animal chambers to the light (they used horizontal, we used vertical) which may limit the exposure to the levels of light required to induced changes, as well as the ages of our animals (they used 3-6 month old animals, where we used 9 month old). We also used a cardboard chamber to adhere the lights to, while other groups used white background which reflects more light, making for a brighter treatment chamber. We aimed to replicate the initial findings of Iaccarino et.al of reduced Aβ, and thus improved our treatment equipment to align more closely with their methods. We constructed a new light administration chamber, constructed new individual chambers for the animals and used a mains-powered benchtop power unit to power the lights.

We then performed the experiments outline in Chapter 3 (Aβ histology, CD45 histology) to determine any changes induced in these younger animals as compared to the 9 month old animals previously used, as well as confirming the Aβ expression using ELISA. We investigated coexpression of IL-33 with Olig2, an oligodendrocyte protein expressed by both astrocytes and oligodendrocytes We finally used qPCR to measure genes of the Aβ processing pathway such as *BACE1, PSEN1* and *mAPP*. Given the role of *IL-33* we also measured expression of this gene to determine if it was associated with changes in the Aβ pathway, or with AD and sex. We also measured expression of microglial-associated genes such as *TMEM119*, chemotactic receptor *P2YR12* to determine if microglia were migrating in a purine-dependent manner, and AD-associated gene Gpnmb (Ripoll *et al.,* 2007). Our final target for qPCR was *Cst7* which recently published work showed sex-dependent differences in expression of this pro-inflammatory lyosomal product in 5xFAD mice (Baleviciute and Keane, 2023)

4.1 Aims of Chapter

Our primary aims were similar to Chapter 3. We then had additional aims after we confirmed the 40Hz light flicker was reducing Aβ in the VC.

1. To adapt the 40Hz light-treatment circuit and administration chambers to more closely align with published work.

2. To determine if 40Hz light flicker treatment administered for 15 days in 4-5-month-old 5xFAD animals is capable of reduce Aβ burden in the brain

3. To determine if 40Hz light flicker affects the expression of genes associated with the amyloid pathway, and genes associated with microglia.

4. To determine the impact of 40Hz light flicker on expression of IL-33 protein and *IL33* gene expression.

4.2 Results

Having reviewed the differences between our treatment (outlined in Chapter 3) and published methods, we adapted our plan to treat animals at 4-5-months and changed the treatment administration equipment and light-flicker circuit.

To begin, the first 2 litters of animals were weighed daily after 40Hz treatment to determine if the smaller cages or overall treatment procedure was having an adverse effect on the animals' eating habits which can be indicative of stress. After treatment animals were sacrificed, brain tissue harvested and used to measure Aβ burden in ½ brains (via ELISA) and within the VC (via IF), CD45 inflammation via IHC, IL33 and Olig2 expression (via IF) and expression of various AD-related genes within the VC (via qPCR).

4.2.1 Changes to the treatment method

The lack of difference between the treated and untreated groups is potentially explained by sub-optimal light levels not inducing sufficient oscillations to stimulate immune cells to promote clearance of amyloid. Other laboratories use light levels of approximately 1500lux at the side of the cage closest to the light, using the minimum cage size mandated by the home office per mouse (33cm long, 12cm wide and 13cm deep) faced horizontally to the light- allowing for increased exposure. Due to space limitations, we were unable to accommodate the mice using the cages in this format. To compensate for this, smaller experimental chambers were constructed which prevent the animal from “hiding” at the darker end of the previously used cages whilst still allowing ample space for mice to navigate comfortably. Other laboratories also used white or reflective backing which may increase the light reflection into the cages, whereas the previous format of our construction used cardboard which potentially reduced the light levels compared to other studies.

4.2.2 Construction of new light administration chamber

For the second iteration of treatment administration a new chamber was constructed from matte-white PVC foam cut to measure around a set of shelves, with doors made of the same material to create a self-contained chamber. White packaging tape was used where required to limit contrast. The LED lights from the previous build (Chapter 3, Section 3.1) were salvaged and replaced in a similar format- 3 tiers with 2 LED strips per tier.

To power the LEDs, we also purchased a benchtop power supply which can provide more consistent and adjustable power to the lights, unlike the previous iteration which used a battery pack (Fig 4.1). Battery packs reduce power output over time, resulting in dimming of the lights- by using a benchtop power supply this effect was negated and allowed fine control over the output.

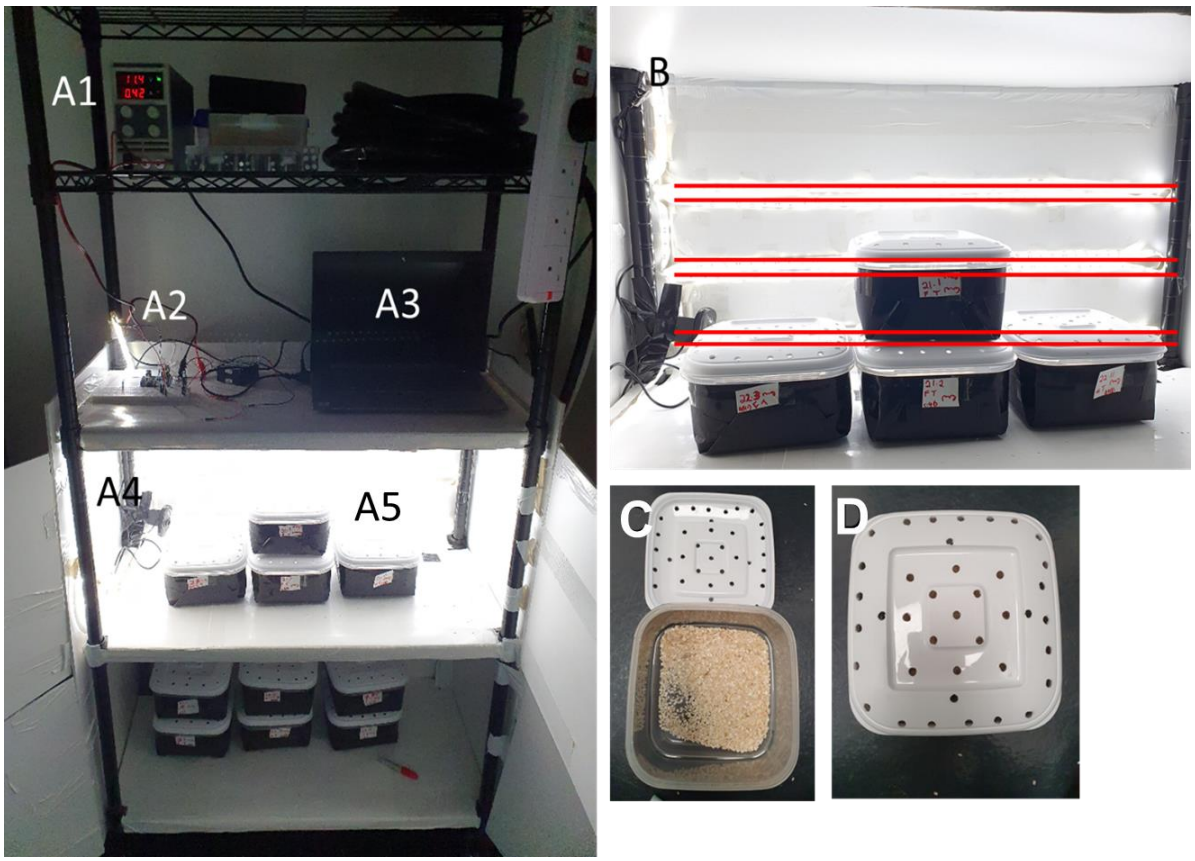

Figure 4.1- New treatment administration chamber setup. *The full setup of the revised light-administration chamber.* ***A1:*** *New benchtop power supply unit, used to provide consistent power output to the LEDs.* ***A2****: The new circuit setup on a breadboard. Circuit setup was identical to Chapter 3 design.* ***A3:*** *Laptop exclusively for treatment, which connects to the webcam.* ***A4:*** *Camera setup to observe animals to ensure safety and activity during the treatment.* ***B:*** *The setup of the LEDs in red - 2 strips of LEDs ran parallel in each "tier" with 3 tiers- measured to align with the middle of each experimental chamber which is exposed to the light. No significant changes were observed in lux levels between each level.* ***C&D*** *show the inside and outside of the experimental chambers respectively. Holes were drilled in the plastic lids and filed until smooth to prevent harm to the animals and discourage teething.*

The experimental cages were constructed from clear plastic containers measuring 17cm wide, 17cm long and 10cm high with opaque white plastic lids (Fig 4.1C and D). Air holes were drilled into the plastic using an electric drill and the edges softened using a fine file to prevent animals harming themselves on sharp edges. The experimental cages were then wrapped on 4 sides (including the bottom of the chamber) using black paper held together with black adhesive tape, leaving only one face of the container exposed to the light.

To ensure sufficient lux levels, a sensitive lux meter (Isotech ILM-01 light meter) was used. Light levels immediately beside the LEDs were 6000 lux, within the cage at the face exposed to the light the lux was approximately 1200 lux, and at the darker end of the cage wrapped in black paper the lux levels were approximately 600 lux. We confirmed that the lux levels at each tier and cage location were comparable using the lux meter.This is comparable with what previous publications used and therefore was deemed to be sufficient. An oscillometer was also used again to confirm that changes to the circuitry had not caused changes to the oscillation, and no changes were found- oscillations still occur at 40Hz as coded. A webcam (Fig 4.1 A4) was also used to ensure animals moved around the cage and did not fall asleep or remain facing away from the light for the duration of the treatment.

4.2.3 Treatment process refinements

While previous publications suggest not using bedding for the duration of treatment, it was found that the cages become unreasonably dirty after only 1 hour within the smaller treatment chambers. This was felt to be a source of unnecessary stress to the animals and so a small amount of bedding was placed into each chamber after the chamber was cleaned with 70% ethanol. This was repeated daily. A sunflower seed was also placed into each chamber at the start of the habituation period to encourage positive association. Animals were rewarded with sunflower seeds upon return to their home cage and allowed to settle for 20 minutes before being returned to the holding room. At the start of treatment, animals were assigned a chamber and remained using this chamber for the duration of treatment to limit exposure to scents from other animals which may cause stress. Throughout treatment, the location of the chamber (i.e., where they were positioned to the light) was randomised.

Due to concerns regarding stress and boredom within the smaller container, several groups of animals were also weighed daily after each treatment to ensure no long-term pathology induced by stress was caused.

4.2.4 Animals weight was unaffected by 15 days of 40Hz light treatment.

Mice were weighed daily to assess the impact of treatment on eating habits (Fig 4.2) which can be indicative of stress in mice. Data is separated by sex due to large differences in weight in male and female, and 5xFAD animals showed reduced weight relative to WT counterparts. Untreated WT female (Fig. 4.2A) animals showed no significant change in weight across treatment duration. Female 5xFAD mice (Fig 4.2C) were lighter than their WT counterparts at the beginning of treatment, though neither untreated controls nor 40Hz treated mice showed a significant change in weight. Male WTs (Fig. 4.2B) were heavier than their female counterparts at the beginning of treatment. The untreated control group showed no significant changes in weight over the course of treatment. The 40Hz treated WT group also showed no significant drop in weight though did show more variation in weights due to several larger animals being in this group. Male 5xFAD mice (Fig. 4.2D) were lighter than their WT counterparts, though no change was observed across treatment in either the untreated controls or the 40Hz treated group. Overall, we determined the 40hz light treatment did not significantly affect the weight of the animals.

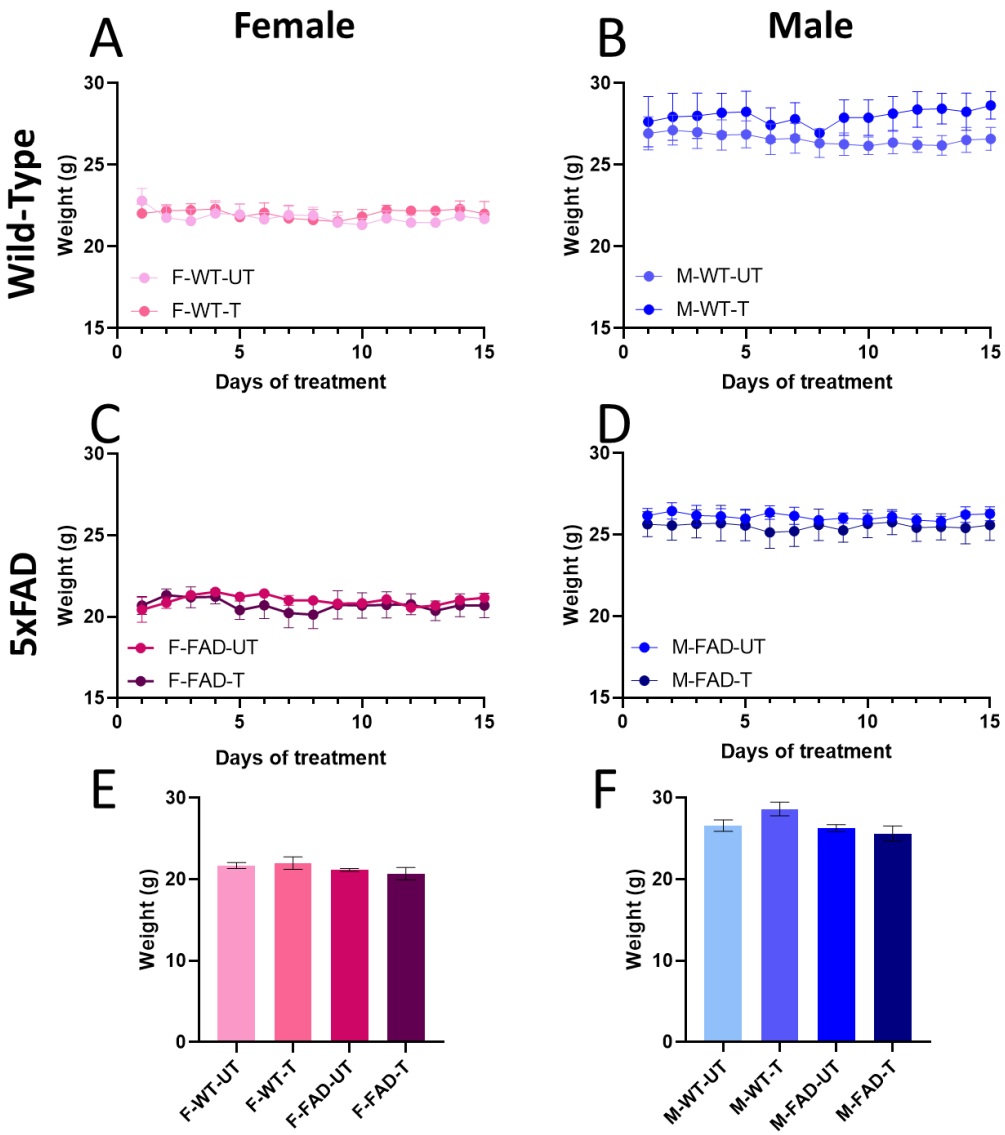

Figure 4.2 - Weight values for 5xFAD and WT animals over 3-week 40Hz light treatment period. *Female (left, pink) and male (right, blue) 5xFAD and wild-type (WT) animals were weighed daily while being treated with 40Hz light (T) or left in darkness (UT) for 1 hour per day for 15 days.* ***A:*** *Changes in weight over 15 days for untreated (F-WT-UT, n=3) and treated (F-WT-T, n=3) wild-type females.* ***B:*** *Changes in weight over 15 days for untreated (M-WT-UT, n=3) and treated (M-WT-T, n=3) wild-type males,* ***C:*** *Changes in weight over 15 days for untreated (F-FAD-UT, n=3) and treated (F-FAD-T, n=3) heterozygous 5xFAD females,* ***D:*** *Changes in weight over 15 days for untreated (M-FAD-UT, n=4) and treated (M-FAD-T, n=4) heterozygous 5xFAD males.* ***E,F:*** *Final weight (day 15) of female (E) and male (F) animals. Multiple t-tests performed, no significant differences found between treated and untreated groups in each figure.*

4.2.5 Effects of 15-day light treatment on Aβ burden in the brain of 4/5-month-old mice

After confirming the new treatment process was not affecting the weight of the animals, we next studied the Aβ burden of the treated and untreated animals. Animals were sacrificed via CO2, brain tissue harvested and used to measure Aβ burden in ½ brains (via ELISA) and within the VC (via IF).

4.2.5.1 Effect of 40Hz light flicker on soluble Aβ 1-40 and Aβ 1-42 proteins in brain of 5xFAD mice

We first wanted to determine if the 40Hz treatment was having an effect on the Aβ burden in the brain "at large". We measured the levels of Aβ fragments 1-40 and Aβ 1-42 in brain samples from 40Hz-light treated and untreated 5xFAD and WT. WT and 5xFAD mice between 4 and 5 months old were treated with 40Hz light or left in dark conditions for 1 hour per day for 15 days over three weeks. On the day of the last treatment, mice were sacrificed and the left hemisphere of each mouse brain was harvested and weighed and then homogenised as described in methods (Chapter 2.7.2). ELISA was used to measure the soluble Aβ fragments only. Results show that 5xFAD mice exhibited significantly higher levels of Aβ 1-40 and Aβ 1-42 in the brain than the WT mice (Fig 4.3, P*<0.001) as expected.

We also found that the level of Aβ1-42 was significantly higher than Aβ1-40 (Fig 4.3) in both groups of 5xFAD. The average Aβ1-40 being 3.61ng/ml in untreated 5xFAD animals and 3.9ng/ml in treated 5xFADs, while the average Aβ1-42 was 67.2ng/ml in untreated 5xFADs 82.9ng/ml in treated 5xFADs. This is expected as 5xFAD animals show heavy bias towards Aβ1-42 production (Oakley *et al.,* 2006).

However, we found no significant difference between the levels of Aβ1-40 or Aβ1-42 in treated 5xFADs and untreated 5xFADs, suggesting treatment did not reduce the Aβ burden in 1 hemisphere of the brain.

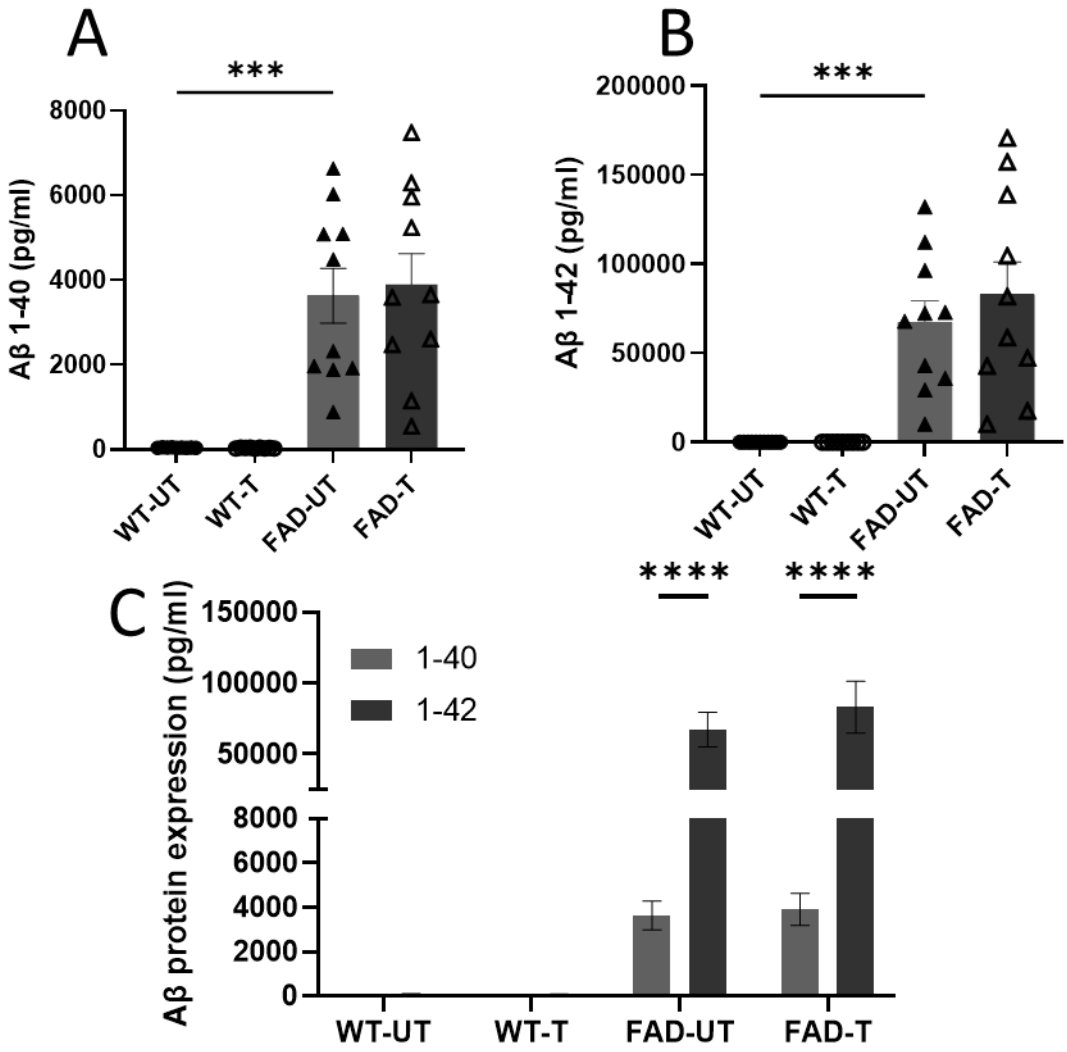

Figure 4.3 - Aβ 1-40 and Aβ 1-42 levels did not change across whole brain after 40Hz light treatment. 5x*FAD mice between 4 and 5 months old were treated with 40hz light (WT-T, FAD-T) or left in dark conditions (WT-UT, FAD-UT) for 1 hour per day for 15 days over three weeks. Brain samples were harvested and processed to measure Aβ 1-40 and Aβ 1-42 using ELISA. Half brains were weighed and samples normalised for weight.* ***A:*** *Aβ 1-40 protein level in ½ brain samples from 5xFAD and WT animals, n=5 in all four groups.)* ***B****: Aβ 1-42 protein level in 1/2 brain samples of 5xFAD and WT animals (F-FAD-UT n=6, n=5 in all other groups) C: Comparison of Aβ 1-40 to Aβ 1-42 between all groups. All figures show mean ± S.E.M. Two-way ANOVA with Tukey's multiple comparisons performed.* A**;** *Treatment: F (1,34) = 0.07, P=0.79, Genotype: F (1,34)=52.9, P=<0.0001.* B; Treatment: F (1,36) = 0.51, P=0.48. Genotype F (1,36)= 46.6, P=<0.001.

4.2.5.2 Histological measurement of Aβ levels in the visual cortex

Having found that the 40Hz light treatment had no significant impact on the protein levels of Aβ1-40 or Aβ1-42 in brain samples, we then used immunofluorescence staining using an Aβ antibody to quantify all Aβ fragment lengths in the VC of 5xFAD animals as used in Chapter 3 (Section 4.3.1). We quantified the total number of plaques greater than 10μm^2 in area in each layer of the VC as well as the extent of Aβ coverage using Qupath software. We used 10μm^2 in this chapter due to improvement of methods and software being used, allowing for more refined measurement of all plaques resulting in a higher threshold being set.

Our data shows that the treatment caused no significant impact in the total number of plaques in the VC (Fig 4.4 A) or in each individual layer of the VC (Fig 4.4B, Table 4.1) However, we did find that the total % coverage of Aβ was significantly reduced after 40Hz treatment (Fig 4.4 C, $p^*<0.05$). Upon further analysis by individual layer, there was no significant difference in layers 1-5, with the significant difference being on deep VC layer 6 (Fig 4.4, Table 4.2).

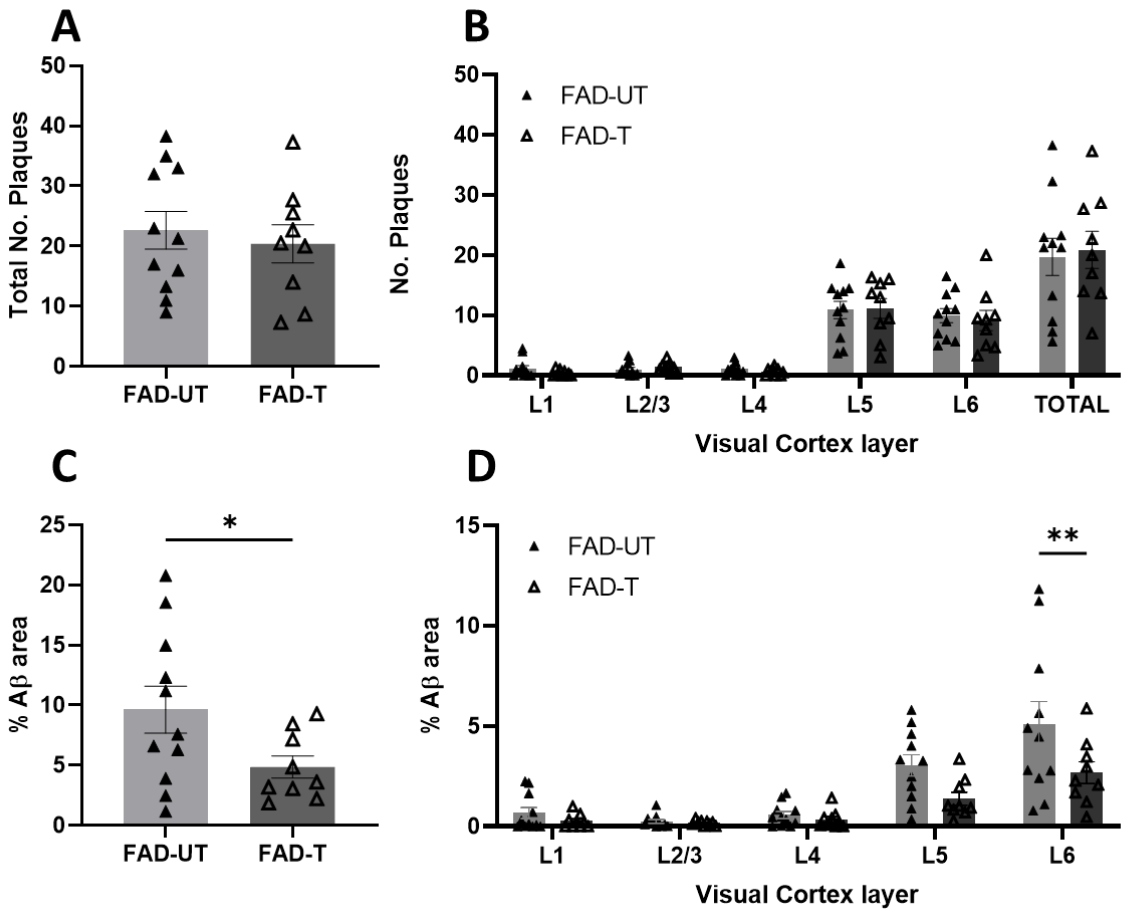

Figure 4.4 - Effect of 40Hz treatment on Aβ burden in visual cortex. *Data from both male and female 5xFAD animals was used (Female: FAD-UT n=6, FAD-T=6, Male FAD-UT n=5, FAD-T n=3)* ***A:*** *Total number of Aβ plaques in the VC for untreated (UT n=11) and treated (T n=9) 5xFAD animals* ***B:*** *Number of Aβ plaques present in each layer of the VC.* ***C:*** *Total % area Aβ coverage in the VC of untreated (UT n=11) and treated (T n=9) 5xFAD animals****.*** ***D****: % area Aβ coverage in each layer of the VC of untreated (UT n=11) and treated (T n=9) 5xFAD animals. Ordinary One-Way ANOVA performed. No significant differences found. A,C: Student's unpaired two-tailed T-test with Welch's correction performed; F (10,8) = 5.15, P=0.027.. B,D: Two-Way ANOVA with Tukey's multiple comparisons performed; D: Treatment: F(1,95)=9.2, P=0.0032. (P*<0.05, P**<0.01)*

Our results suggest that while the 40Hz light flicker did not appear to affect Aβ levels across multiple brain regions, it was sufficient to reduce the expression of Aβ within the VC, specifically within the deep cortical layer 6 (and to a slight but insignificant degree, layer 5). Representative images for these graphs are located on p154 and 156.

Table 4.1 Number of plaques present in each layer of the visual cortex in 4-5month old 5xFAD animals treated with 40Hz light flicker for 15 days.

Table shows mean values for each layer of the VC, as well as combined total number of plaques across the whole VC. Values rounded to 1 decimal place. All units shown are average plaque counts ±S.E.M. n=11 5xFAD-UT, n=9 5xFAD-T.

Total no. plaques		Visual Cortex layer					
		LI	**LII/III**	**L IV**	**LV**	**LVI**	**Total**
Untreated	**5xFAD**	1.2 ± 0.5	1.0 ±0.3	1.1 ± 0.3	10.9 ± 1.5	10.0 ±1.2	22.16 ± 3.1
Treated	**5xFAD**	0.4 ± 0.2	1.4 ±0.3	0.7 ±0.2	11.2 ±1.6	9.2 ±1.7	20.41 ± 3.2

Table 4.2- Aβ measurements in each layer of the visual cortex in 4-5month old 5xFAD animals treated with 40Hz light flicker for 15 days.

Table shows mean values for each layer of the VC, as well as combined total Aβ measurements in the VC. Values rounded to 2 decimal places. All units shown are average μm^2 ±S.E.M from n=11 5xFAD-UT, n=9 5xFAD-T.

Aβ burden (μm^2)		Visual Cortex layer					
		LI	**LII/III**	**L IV**	**LV**	**LVI**	**Total**
Untreated	**5xFAD**	0.67±0.27	0.25 ±0.09	0.6 ±0.17	3.05 ±0.54	5.09 ±1.14	9.63 ±1.96
Treated	**5xFAD**	0.27 ±0.11	0.18 ±0.04	0.35 ±0.15	1.39 ±0.33	2.69 ±0.55	4.86 (*) ±2.77

4.2.6 qPCR analysis of Amyloid processing pathway genes

Having confirmed that treatment appeared to be causing a reduction in Aβ levels within the VC (specifically within deep cortical layers) we sought to understand the underlying molecular mechanisms and any changes that may occur in gene transcription after 40Hz light treatment. Genes of the amyloid processing pathway were examined using quantitative PCR on mRNA extracted from the VC of WT and 5xFAD animals, converted into cDNA as described in methods (Chapter 2.8)

We first sought to determine if the reduction in Aβ in the VC was due to changes in the APP processing pathway. We investigated mRNA expression of endogenous mouse APP (mAPP), the APP gene native to all mice (compared to the 5xFAD human transgene insert) and observed that there was a significant upregulation of *mAPP* mRNA in treated 5xFAD animals compared to untreated 5xFAD animals (Fig 4.5A, P***=0.0005). We then measured expression of *PSEN1* mRNA due to its role in the gamma secretase protein and found that treated 5xFAD animals had significantly reduced expression of *PSEN1* mRNA compared to untreated 5xFADs (Fig 4.5B, P**<0.0002). Having investigated the gamma-secretase protein, we then looked to the beta-secretase gene *BACE1* and found no significant difference between treated and untreated 5xFAD animals (Fig 4.5C).

Because of the role IL-33 has been suggested to play in AD, we wanted to determine if there 40Hz light treatment changes the expression of the IL-33 gene in the VC. We investigated the mRNA expression of *IL33* (Fig 4.5D). We observed that treated WT animals significantly upregulated *IL33* mRNA (P*=0.048) compared to untreated WT mice, and that untreated 5xFAD animals had significantly more *IL33* mRNA than untreated WTs (P*<0.02)- however despite a slight trend towards reduced mRNA expression there was no significant change in 40Hz treated 5xFAD animals.

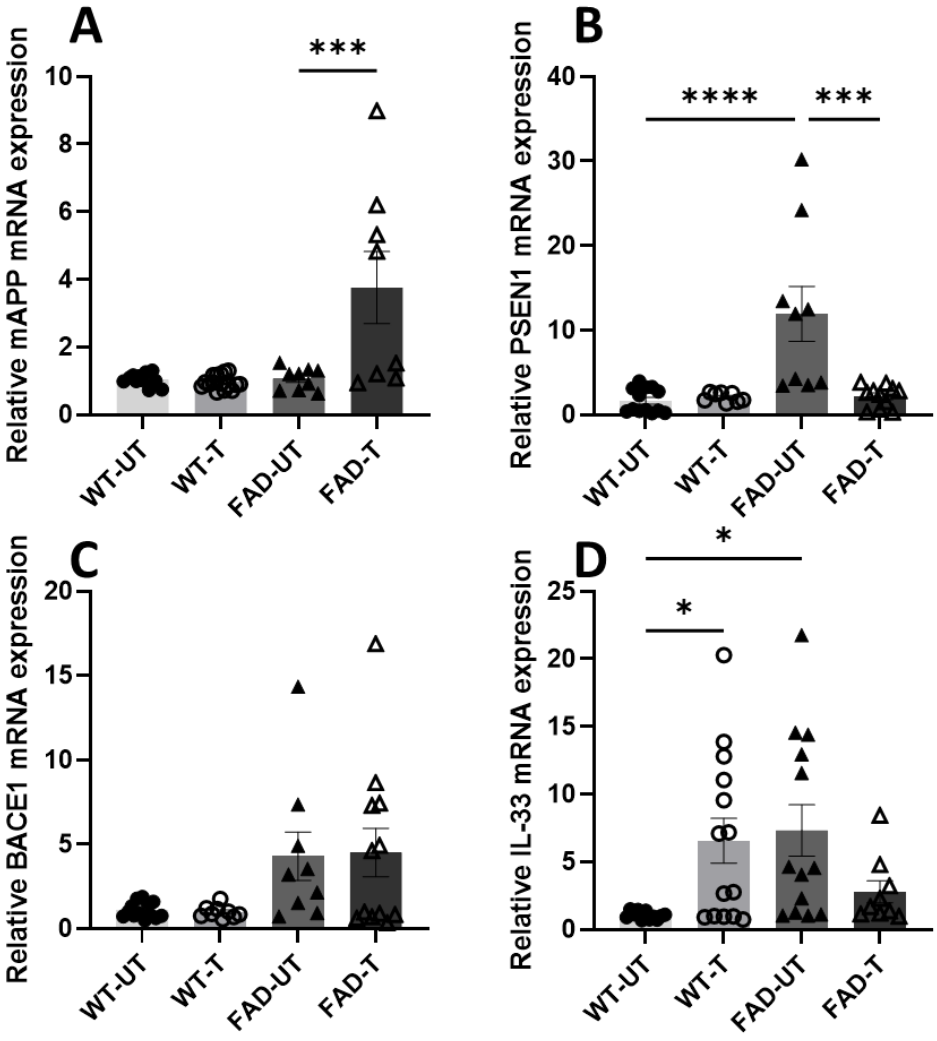

Figure 4.5- Relative expression of genes mAPP, PSEN1, mBACE1 and IL33. *Untreated wild-type (WT-UT), untreated 5xFAD (FAD-UT) and 40hz light treated wild-type (WT-T) and 5xFAD (FAD-T) visual cortices were harvested from ½ brain and mRNA extracted.* ***A****: Relative expression of mouse APP mRNA (WT-UT n=13, WT-T n=15, FAD-UT n=9, FAD-T n=8)* ***B:*** *Relative expression of PSEN1 mRNA (WT-UT n=13, WT-T n=8, FAD-UT n=10 FAD-T n=11)* ***C****: Relative expression BACE1 mRNA, (WT-UT n=13, WT-T n=9, FAD-UT n=9, FAD-T n=13)* ***D:*** *Relative expression of IL-33 mRNA. (WT-UT n=11, WT-T n=14, FAD-UT n=13, FAD-T n=9) All CT values normalised to mean WT-UT value using 2–ΔΔCt method. Ordinary one-way ANOVA with Tukey's multiple comparisons test performed. Treatment: mAPP (A)- F (3,40)=10.1, P=<0.0001. PSEN1 (B)- F(3,38)= 12.1, P=<0.0001. BACE1 (C): F(3,39)= 4.13, P=0.012. IL-33 (D): F (3,43) = 4.1. (P=0.01. P*<0.05, P**<0.01, P***<0.001, P****<0.0001).*

We then sought to determine if there was a change in the expression of microglia related genes that may suggest the 40Hz light treatment was affecting these immune cells within the VC. We first measured expression of 2 DAM genes, Gpnmb (encoding for GPNMB, an inflammatory glycoprotein associated with microglia) (Fig 4.6A) and Cst7 (encoding for Cystatin F, a protein known to be upregulated in AD and associated with inflammation)(Fig 4.6C) We observed a significantly more (P*<0.05) mRNA in untreated 5xFAD animals compared to WT-UT controls for both *Cst* and *Gpnmb*. Cst7 was significantly upregulated in both treated and untreated 5xFAD animals (P***<0.001, P****<0.0001). This is in keeping with published findings on Cst7 (Landel *et al.,* 2014) and Gpnmb (Hüttenrauch *et al.,* 2018) and suggests that 40Hz light flicker treatment did not significantly change the expression of DAM genes in our 5xFAD mice. Next, we measured the expression of microglia-specific genes TMEM119 (Fig 4.6C) and P2YR12 (Fig 4.6D) and observed no significant difference between any of the treatment groups.

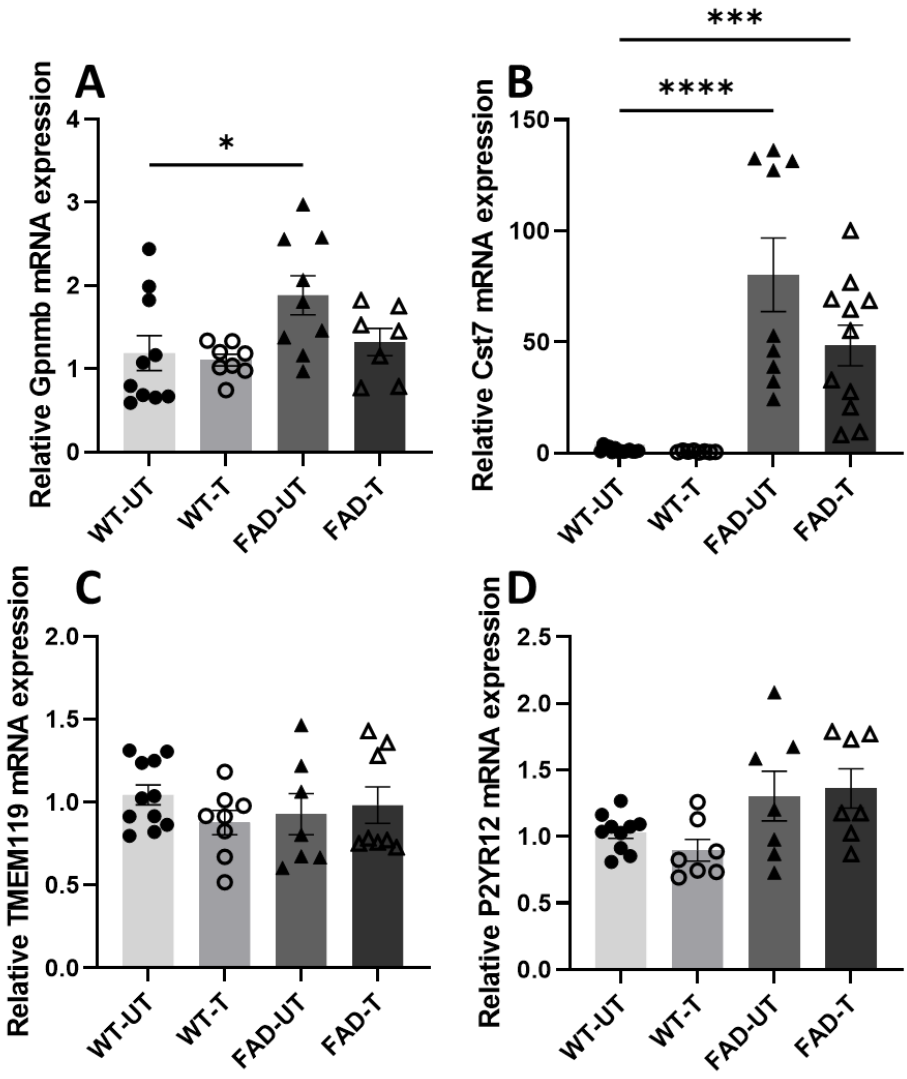

Figure 4.6- Relative expression of microglia-associated genes Gpnmb, Cst7, TMEM119 and P2YR12. *Untreated wild-type (WT-UT), untreated 5xFAD (FAD-UT) and 40hz light treated wild-type (WT-T) and 5xFAD (FAD-T) visual cortices were harvested from ½ brain and mRNA extracted.* ***A****: Relative expression of Gpnmb mRNA (WT-UT n=7-10 for all groups).* ***B:*** *Relative expression of Cst7 mRNA (n=8-12 for all groups).* ***C****: Relative expression TMEM119 mRNA, (n=7-11 for all groups).* ***D:*** *Relative expression of P2YR12 mRNA. (n=7-10 for all groups) All CT values normalised to mean WT-UT value using 2–ΔΔCt method. Ordinary one-way ANOVA with Tukey's multiple comparisons test performed to determine treatment effect. Gpnmb (A): F(3,30)=0.9, P=0.45. Cst7 (B): F(3,32)=19.17, P=<0.001. TMEM119 (C): F(3,30)=0.7, P=0.56. P2YR12 (D): F(3,32)=3.4, P=0.03.(P*<0.05, P***<0.001, P****<0.0001)*

4.2.7 Correlations between IL33, AD-related genes and microglia genes expression.

Having analysed the results from qPCR, it appeared that there may be correlations between changes in gene expression before and after treatment- particularly given the changes in *IL33* which appeared to affect WT and 5xFAD animals differently after treatment. We therefore collected the data from animals which had qPCR results for multiple genes to determine if there was a significant correlation.

We first investigated if there was any significant correlation between *IL33* and the AD related genes *mAPP*, *PSEN1* and *BACE1* between the treated WTs, and treated and untreated 5xFAD animals. We observed a significant negative correlation between *PSEN1* and *IL33* (r= -0.73, p*=0.04) in treated WT animals, and a moderate negative correlation between *mAPP* and *IL33* (r= -0.73). In untreated 5xFAD animals we observed a significant positive correlation between *IL33* and *mAPP* (r=0.87 P*=0.01) and *IL33* and *BACE1* (r=0.99, p***=0.0006), and a moderate but insignificant positive correlation between *IL33* and *PSEN1 (*Fig 4.7A*)*. Finally in treated 5xFADs we observed no significant differences, however a moderate negative correlation was observed between mAPP (r= -0.59), PSEN1 (r= -0.55) and BACE1 (r= -0.54).

We also investigated the correlation between the AD genes. We found significant positive correlation between *mAPP* and *PSEN1* in treated WTs (r=0.96, p=0.0001) (Fig 4.7B). In untreated 5xFADs we found significant positive correlation between *mAPP* and *BACE1* (r=0.99, p=0.002). In treated 5xFADs we found significant positive correlation between *mAPP* and *PSEN* (r=0.98, p=0.0009) *mAPP* and *BACE1* (r=0.92, p=0.0092) and *BACE1* and *PSEN1* (r=0.94, p=0.005).
Though not statistically significant, at least a moderately strong correlation was observed between all genes in all groups.

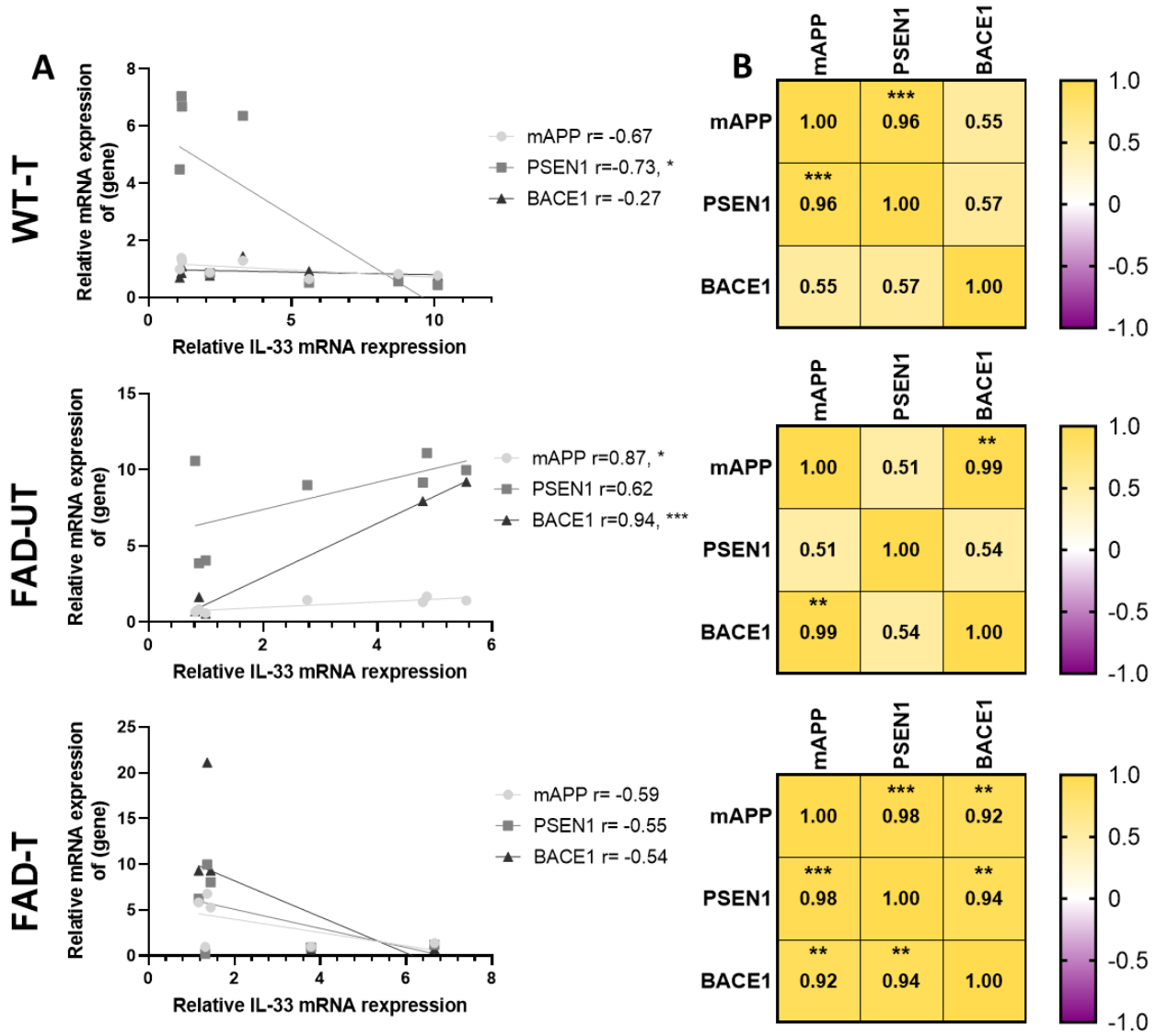

Figure 4.7- Correlations between AD-related genes and IL33 mRNA expression in untreated 5xFADs and 40hz-light treated 5xFADs and WT animals. *Animals with qPCR results for IL33, mAPP, PSEN1 and BACE1 were plotted to determine if gene expression correlated. Any animals missing a result were excluded from analysis.* ***A****: Scatter plots showing correlation between IL33 and mAPP, PSEN1 and BACE1 in 40Hz treated WT (top, n=8) untreated 5xFADs (middle, n=5) and 40Hz treated 5xFADs (bottom, n=6). Legend shows corresponding r values and significance values for each group.* ***B:*** *Heatmap of Pearson's correlation r values when AD related genes were compared to each other.*

Pearson's r value calculated via prism. P values calculated using two-tailed analysis with a 95% confidence interval. P<0.05, P**<0.01, P***<0.001.*

We then investigated any correlation between *IL33* mRNA and microglial genes *Cst7*, *Gpnmb*, *TMEM119* and *P2YR12*. We observed no significant correlation between any of the genes and *IL33* mRNA in treated WTs. In untreated 5xFADs we observed a significant positive (r=0.84 p*=0.038) correlation between expression of *IL33* mRNA and *Cst7* mRNA. In treated 5xFADs this correlation was lost, as 5xFADs exhibited no significant correlation between *IL33* and any of the microglial genes, however there was a strong positive correlation between *TMEM119* and *IL33* (r=0.82) and a moderate positive correlation between P2YR12 and *IL33* (r=0.74) (Fig 4.8A)

We then compared the microglial genes with each other to determine if any of these may be correlated. In treated WTs we observed a significant correlation between *P2YR12* and *TMEM119* (r= -0.88, p*=0.046). Although there was no statistically significant difference between any other genes, there was a moderate correlation between *P2YR12* and *Cst7 (r*=0.69). (Fig 4.8B)

In untreated 5xFADs we observed no statistically significant correlations between any of the microglial genes, though a strong positive correlation was found between *P2YR12* and *Gpnmb (r*=0.83), and a moderate positive correlation between *Gpnmb* and *Cst7 (r*=0.67), and between *P2YR12* and *TMEM119* (r=0.64).

Finally in treated 5xFADs we observed a significant positive correlation between *TMEM119* and *P2YR12* (r=0.96, p=0.008). A strong negative correlation was also observed between *P2YR12* and *Gpnmb* (r=-0.80), and a moderate negative correlation between *TMEM119* and *Gpnmb* (r= -0.61). A moderate positive correlation was found between *TMEM119* and *Cst7 (r*=0.6).

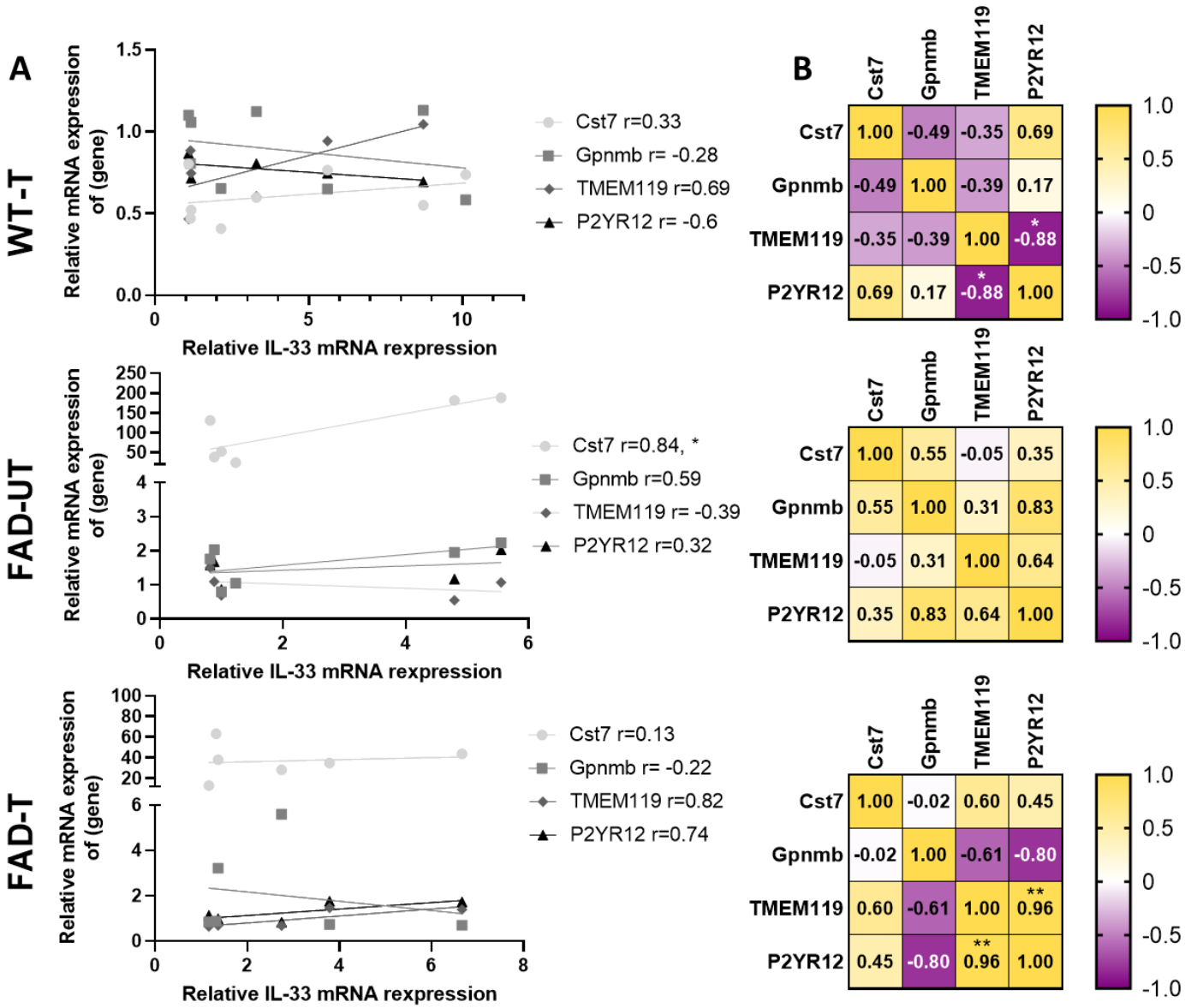

Figure 4.8- Correlations between microglia-related genes and IL33 mRNA expression in untreated 5xFADs and 40hz-light treated 5xFADs and WT animals. *Animals with qPCR results for IL33, Cst7, Gpnmb, TMEM119 and P2YR12 were plotted to determine if gene expression correlated. Any animals missing a result for any gene were excluded from analysis.*

***A**: scatter plot showing correlation between IL33 and Cst7, Gpnmb, TMEM119 and P2YR12. Legend shows corresponding r values and significance values for each gene compared to IL33. WT-T (n=8), FAD-UT (n=5) and FAD-T (n=6).*

***B:** Heatmap of Pearson's correlation r values when microglia related genes were compared to each other.*

Pearson's r value calculated via prism. P values calculated using two-tailed analysis with a 95% confidence interval. P<0.05,*

4.2.8 Effects of 15-day light treatment on CD45 expression in the visual cortex of 5xFAD mice

Next, we sought to determine if the 40Hz light treatment had any effect on inflammation, measured via the expression of CD45+ cells in the VC (Fig 4.9). We observed no significant difference in the overall number of CD45+ cells in the visual cortex between treated and untreated 5xFAD animals. Representative images found on page 184 and 185.

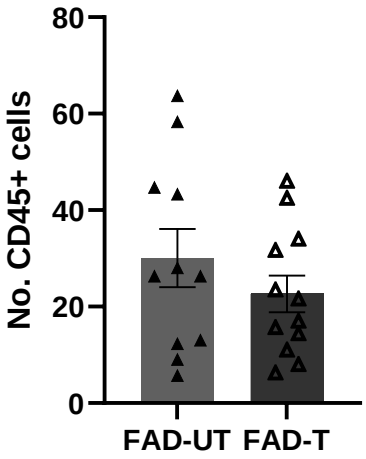

Figure 4.9 – Effect of 15-day light treatment on CD45 expression in the VC *Data from both male and female 5xFAD animals was used (Female: FAD-UT n=5 FAD-T=4, Male FAD-UT n=5, FAD-T n=7). Brain sections were stained for CD45 using immunohistochemistry and images taken using an upright brightfield microscope. Images were quantified at 10x magnification using Qupath software. Unpaired 2-tailed T-test with Welch's correction performed, no significant difference found (P=0.3).*

4.2.9 Effects of 15-day light treatment on expression of IL-33 and OLIG2 proteins in the brain of 4/5-month-old mice

Finally, we sought to determine if IL-33 protein levels were different between both WT and 5xFAD animals, and if the 40Hz light flicker treatment changed this protein expression in line with our previous mRNA findings. We used immunofluorescence staining using antibodies against IL-33 as well as Olig2, an oligodendrocyte-associated protein to determine if any changes in the expression of IL-33 may be linked to oligodendrocytes. The total number of IL-33+, Olig2+ cells were both quantified both in the total VC as well as in each cortical layer using Qupath software and measured as expression per μm^2. As in previous experiments, WT-T, FAD-UT, and FAD-T were compared to WT-UT, and FAD-T also compared to FAD-UT.

We observed no significant difference in the total level of IL-33 (Fig 4.10A) or Olig2 (Fig 4.10C) in the VC between any compared groups. However, when measured in each individual cortex layer we found a significant increase in the IL-33 level in WT-T animals in cortical layer 2/3 (Fig 4.10B, P*<0.05) and a significant reduction in IL-33 expression in layer 4 in FAD-UT (P**<0.01) compared to WT-UT, and in 40Hz treated 5xFADs (P*<0.01) compared to WT-UT. Similarly, there was a significant decrease in Olig2 expression in layer 4 of the VC in untreated 5xFADs (P*<0.05) compared to WT-UT, and in 40Hz treated 5xFADs (P**<0.01) compared to WT-UT controls.

These results combined suggest there is a decrease in the number of IL-33+ or Olig2+ specifically in layer 4 of the VC in 5xFAD animals compared to WTs, and that 40Hz treatment upregulated expression in layer 2/3 in treated WTs compared to untreated WT controls.

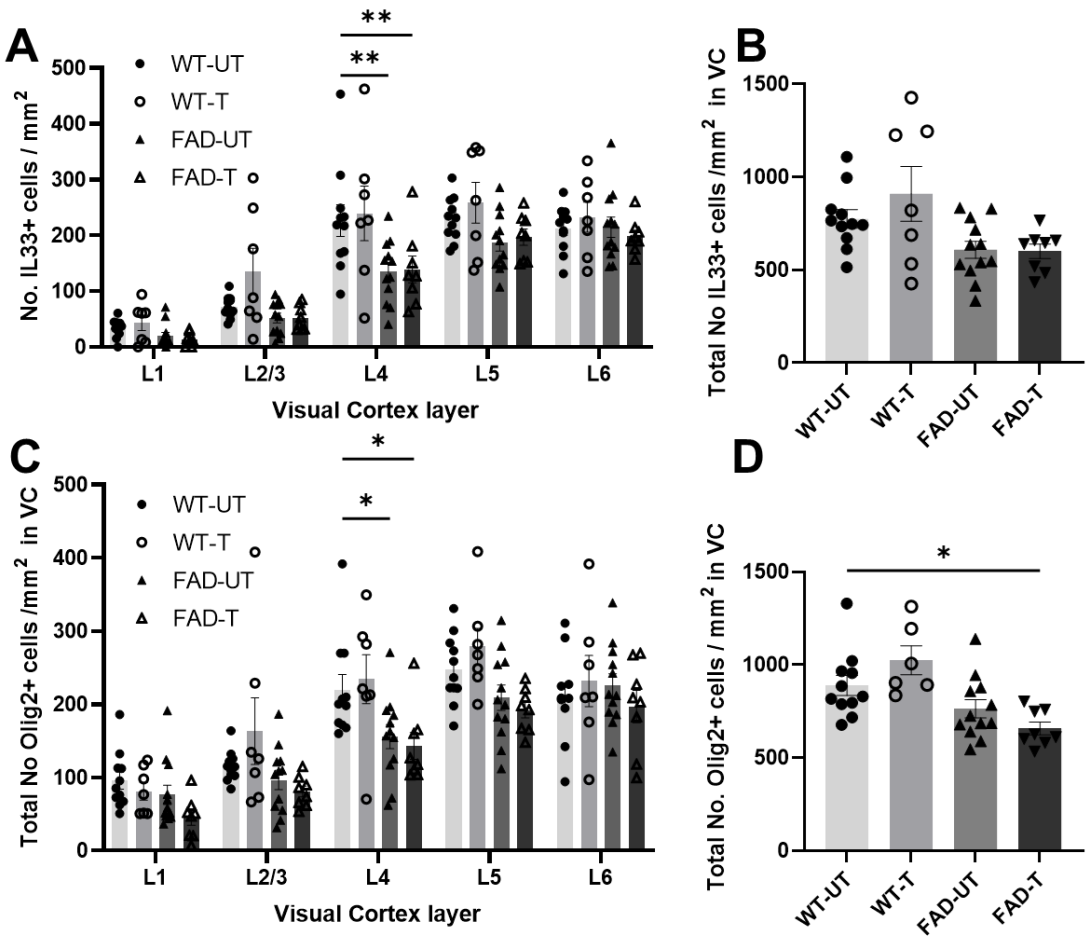

Fig 4.10 – Expression of IL-33+ and Olig2+ cells within the VC of 40hz light-treated and untreated animals. *Data from both male and female 5xFAD animals was used (Female: FAD-UT n=6, FAD-T=6, Male FAD-UT n=5, FAD-T n=3) Brain sections were co-stained for IL33 and Olig2 and visualised using fluorescence microscopy. Images were quantified at 10x magnification using Qupath software.* ***A:*** *Total number of IL33+ cells in the VC for untreated (UT WT=11, FAD n=10) and treated (T WT n=6, FAD n=6) 5xFAD animals* ***B:*** *Number of Aβ plaques present in each layer of the VC.* ***C:*** *Total % area Aβ coverage in the VC of untreated (UT n=11) and treated (T n=9) 5xFADs.* ***D****: % area Aβ coverage in each layer of the VC of untreated (UT n=11) and treated (T n=9) 5xFAD animals.* ***A&C****: Three-way ANOVA with Tukey's multiple comparisons performed- A: Genotype: F (1,170) = 30.24, P=<0.0001. Cortical layer x genotype: F (4,170) = 2.7, P=0.03. C: Genotype: F(4,170)=28.94, P=<0.0001.* ***B&D****: Two-way ANOVA with Tukey's multiple comparisons performed. B: Genotype: F(1,22) = 14.7, P=0.0009. D: Genotype: F (1,33) = 19.56, P=0.0001. (P*<0.05, P**<0.01)*

4.3 Discussion

This chapter used younger 5xFAD mice aged between 4 and 5 months to determine the effectiveness of 40Hz light-flicker treatment in reducing Aβ burden and altering AD pathology.

Aβ is a hallmark of AD in the brains of human patients as well as a measure of the progression of disease in the 5xFAD model. We first measured protein expression in the brains of 5xFAD animals using ELISA, then more specifically measured Aβ in the VC region using immunofluorescence as a measure of our treatment's effectiveness.

4.3.1 Changes in Aβ burden across brain

Our first goal was to determine the effectiveness of the 40Hz light flicker treatment in reducing Aβ burden in 5xFAD animals. We first measured the protein expression in brain samples from 5xFAD animals using ELISA and found no significant changes in Aβ in our 40Hz light treated animals compared to untreated 5xFAD controls. This is, however, in keeping with previous publications which suggest that the visual 40Hz treatment primarily affects the VC, with effectiveness diminishing further into the brain (and a similar pattern for audio-only stimulation). Given we only used visual stimulation, we did not expect to see highly significant changes across the entire brain. We also observed that Aβ 1-42 expression was significantly higher in our 5xFAD animals than Aβ1-40. Again, this is in keeping with previous studies into the 5xFAD model which rapidly deposits Aβ1-42 (Oakley *et al.,* 2006).

We then measured the Aβ burden within the VC alone using immunofluorescence. It is here we found a significant reduction in Aβ in the total area measured across the whole VC, and specifically within deep cortical layer 6 (level 5 showed a reduction trend but was not significant.) Our data thus suggests that the 40Hz light treatment administered over 15 days was having an effect on the Aβ burden in the deep cortical layers of the VC in our 4-5-month-old 5xFAD animals.

Recently there has been a great deal of debate surrounding the 40Hz stimulation, with conflicting reports. While the Tsai lab has multiple publications showing the treatment effectively reducing Aβ (Iaccarino, Annabelle C. Singer, *et al.,* 2016; Martorell *et al.,* 2019) other labs were unable to replicate these results despite using extensive n-numbers and multiple models (Soula *et al.,* 2023). While our data does suggest a small but significant decrease in Aβ in the overall VC, the data was highly variable between

animals and it is possibly an artefact of the data that would be removed if n numbers were increased in this study. However, it is equally possible that this is a true replication of the original findings, as other labs have reported positive outcomes from 40Hz treatment (albeit with different treatment methods (Bobola *et al.,* 2020) or measuring different outcomes (Yao *et al.,* 2020). The field of gamma oscillation treatment remains controversial, and there is a dire need for standardisation (in animal model used, sex of animals and treatment method) and publishing of negative results.

The reduction only in layer 6 is novel, as previous publications did not examine individual cortical layers. This reduction in layer 6 specifically is interesting, as layer 6 is reported to have the broadest diversity of cell-types compared to other layers (Brumberg, Hamzei-Sichani and Yuste, 2003). This may explain why we only see a significant change in level 6, and a slight but insignificant reduction in cortical layer 5.

4.3.2 No changes in CD45 expression after light treatment

CD45 is a pan-leukocyte marker expressed by macrophages and microglia in the CNS. It is generally known as an "M1" activation marker, and a regulator of T-cell signalling (Courtney *et al.,* 2019b) and cytokine receptor signalling (Irie-Sasaki *et al.,* 2001). CD45 is upregulated by microglia in human AD patients (Hopperton *et al.,* 2018) and is expressed by DAMs in 5xFAD models (Rangaraju *et al.,* 2018). We used CD45 to investigate the inflammatory state of microglia in 5xFADs before and after treatment, however we observed no significant changes between groups after treatment, further showing a lack of changes in microglial activation. This is contradictory to what we observed previously in Chapter 3. It is possible that given the younger age of the animals, the microglia were more capable of shifting to an alternative activation state and thus did not upregulate expression of inflammation-associated CD45, whilst in older animals the severe pro-inflammatory state of the CNS may have primed the microglia towards a pro-inflammatory response.

4.3.3 Changes in gene expression after 40Hz treatment

4.3.3.1 AD-related genes

Our findings of significantly reduced Aβ in the VC region suggested the 40Hz light treatment over 15 days was working as expected. To understand the underlying molecular mechanisms, we next used qPCR to determine if the light treatment was having a post-transcriptional effect on genes related to the APP processing pathway.

We observed a significant increase in endogenous mouse APP mRNA in treated 5xFADs compared to untreated 5xFADs and untreated WT controls. Similarly, a significant decrease in *PSEN1* mRNA (which was for both mouse *PSEN1* and the human transgene insert) and no change in the expression of BACE1. Our results were initially surprising, however when combined there are several possible mechanisms to explain our findings.

a.) mAPP

APP is the precursor to Aβ in both humans and mice, though each species expresses its own version of the gene. 5xFAD animals express both the human transgene insert and the endogenous mouse APP protein.

Our first finding was the significant increase in *mAPP* mRNA. Untreated 5xFADs exhibited similar levels of *mAPP* to the untreated WT controls, though this finding is in agreement with published literature in humans in which *huAPP* mRNA was not found to be significantly increased in AD patients compared to healthy controls (Matsui *et al.,* 2007). This is also a measure of endogenous mouse APP, the native gene to C57BL/6 mice and therefore should not be increased in 5xFAD animals where the human transgene insert produces the increased human APP protein and associated mRNA (Oblak *et al.,* 2021).

Interestingly, while we observed the significant reduction in levels of Aβ in the VC 40Hz treated 5xFAD animals expressed significantly (P***<0.001) increased mAPP expression. It could be hypothesised that this increase in treated 5xFAD *mAPP* mRNA is potentially due to a decrease in the human transgene expression, therefore requiring more endogenous APP to compensate for the decrease (though human APP expression was not investigated in this study). Logically, this would also suggest that untreated 5xFAD mice express less *mAPP* to compensate for the increased huAPP, so this hypothesis does not seem applicable.

Studies have shown that endogenous mAPP regulates the deposition of Aβ in APP transgenic mice (such as 5xFADs), where mice devoid of endogenous mAPP exhibit higher deposition of Aβ and diminished microglial response to Aβ plaques (Steffen *et al.,* 2017) Overexpression of endogenous mAPP does not increase total Aβ deposition, however, instead exerting its effect by changing the solubility of the transgenic protein (Jankowsky *et al.,* 2007). This seemingly regulatory effect of mAPP on transgenic hAPP

in these mice may explain why we observed a decrease in overall amyloid deposition, despite increases in *mAPP* mRNA. It is also possible that increased mAPP increased the solubility of the amyloid, resulting in less deposition.

b.) PSEN1 and BACE1

BACE1 is the β-secretase protein responsible for the first amyloidogenic cleavage of the APP protein, while PSEN1 is the γ-secretase protein responsible for the secondary cleavage in both the amyloidogenic and non-amyloidogenic pathways.

We observed a reduction in *PSEN1* despite the increase in *mAPP*, suggesting that while mouse APP increases, transcripts for the γ-secretase catalytic subunit PSEN1 decrease. γ-secretase is the second cleaving enzyme associated with the both the amyloidogenic and non-amyloidogenic pathways. The reduction in *PSEN1* has several possible downstream effects- while PSEN1 and the γ-secretase complex is most frequently associated with the cleavage of APP, the complex is also responsible for cleaving of other proteins (Güner and Lichtenthaler, 2020) including Notch signalling (linked to downstream transcriptional changes in immune regulation (Azimi, Le and Brown, 2018) and calcium signalling (Bezprozvanny, 2013) It has also been linked to microglial function (Lau *et al.,* 2020).

PSEN1 also has a link to IL-33 expression via its cleavage of the notch receptor, leading to intracellular notch signalling and thus this downregulation in PSEN1 may explain the slight (but insignificant) downregulation in our treated 5xFAD animals. Further evidence towards this is that IL-33 expression is inhibited by γ-secretase inhibitors (Sundlisæter *et al.,* 2012); therefore, a decrease in PSEN1 would logically correlate with a decrease in IL-33.

c.) IL33

IL-33 is a pleiotropic protein with many immune-regulatory and inflammatory functions, as well as acting as a transcription factor. Given its multiple roles, published data around the role of IL-33 in AD has been conflicting. Some studies have found that IL-33 is increased in AD patients, specifically around plaques (Xiong *et al.,* 2014) and has been linked to increased inflammation (Reverchon *et al.,* 2020) and therefore it could be suggested that this cytokine contributes to the pathology of AD. However, IL-33 has also been found to be decreased in the brains of AD patients, with higher

cognitive preservation associated with higher IL-33 expression (Liang *et al.,* 2020). It has also been suggested that IL-33 is linked with microglial clearance of Aβ (Lau *et al.,* 2020). These directly contradictory results highlight the complexity of the role of IL-33 in the CNS and AD.

After 40Hz light treatment we observed a slight but insignificant decrease in IL-33 mRNA expression in our 5xFAD animals. Our untreated wild-type animals also expressed significant increased *IL33* mRNA, which did translate to a minor increase in protein expression detected by IF. A previous study used male C57BL/6 mice to measure cytokine expression after 40Hz visual stimulation and observed that the resulting immune-signalling-profile was distinct from LPS-induced inflammation, measured by differing expression of multiple genes including IL-10, TNF-α, IL-17 and IL-1β (Garza *et al.,* 2020) suggesting there is inflammation induced by the light treatment, but it is distinctly different to LPS-induced inflammation. Our findings agree with this, as we did not observe any changes to genes in the APP processing pathway from our WT-C57BL/6 animals but did observe a significant increase in *IL33* mRNA. Although both WT and 5xFAD animals received the same treatment, the resulting post-transcriptional changes for the two groups appears to be different. This suggests that the 40Hz light flicker has different effects on gene transcription dependent on the inflammatory state of the brain prior to treatment.

4.3.3.2 Changes in microglia gene expression after treatment

Considering the important role microglial cells play during the development and progression of AD, we next investigated genes associated with microglia activity. *Gpnmb* is generally associated with an immune-regulatory function (Ripoll *et al.,* 2007) and has been shown to be increased in AD and 5xFAD animals and therefore associated with DAMs (Hüttenrauch *et al.,* 2018). We observed that our untreated 5xFAD animals exhibited significantly higher levels of *Gpnmb* than untreated WTs, consistent with published findings in AD (Hüttenrauch *et al.,* 2018) While treated 5xFADs showed a slight reduction in Gpnmb expression, this difference did not reach statistical significance. Therefore, our light treatment did not affect expression of *Gpnmb*, as neither our treated WTs nor treated 5xFADs exhibited any significant changes relative to untreated WTs.

Cst7 is a pro-inflammatory marker that has been shown to be upregulated 5xFAD animals (Landel *et al.,* 2014; D Daniels *et al.,* 2022), which is in agreement with our findings as 5xFAD animals exhibited significantly higher levels of Cst7 mRNA than WT controls. Our data exhibited two distinct populations within the 5xFAD-UT group; something that we planned to expand upon in the following chapter. We did not notice any changes in mRNA expression of *Cst7* induced by the 40hz light flicker treatment. This suggests that the previous inflammatory state associated with AD is not changed by 40Hz light treatment, and that microglia populations did not upregulate or downregulate these regulatory or inflammatory markers.

The precise function of TMEM119 has yet to be identified, but studies have shown this microglia-exclusive marker is highly expressed in homeostatic microglia but downregulated in DAM, thus it is used as a DAM marker associated with AD (Bennett *et al.,* 2016; Kenkhuis *et al.,* 2022) P2YR12 is a G-protein-coupled purinergic receptor which mediates chemotaxis of microglia towards ATP, and is similarly associated with homeostasis but downregulated in AD (Gómez Morillas, Besson and Lerouet, 2021; Maeda *et al.,* 2021) Despite the literature showing that these genes are downregulated in AD patients, we did not find any significant difference in expression of *TMEM119* nor *P2YR12* in our 5xFAD mice compared to WT-UT controls. This is partially explainable by the fact this data is mRNA and not protein expression, and the majority of published literature focuses on protein expression. It is also possible our mouse model has slightly different expression of these markers.

We also did not observe any significant changes in either gene after 40Hz light treatment, suggesting that any changes in Aβ deposition were not associated with a shift in microglial expression of these genes- this is of particular interest, given the role of P2YR12 as a chemotactic receptor, and further suggests the microglia were not responding to increased levels of ATP/ADP in the CNS of our 40Hz treated mice.

4.3.3.3 Correlation between AD genes and IL33 mRNA expression

We used a pearson's r-test to determine if there were correlations between several APP-processing genes and *IL33* across WT-T, 5xFAD UT and 5xFAD T animals relative to WT-UT CT values. We found interesting correlations between these genes, suggesting that IL33 mRNA expression is connected to the APP processing pathway genes.

Both PSEN1 and BACE1 have roles as transcription factors via their interaction with notch signalling (De Strooper *et al.,* 1999; He *et al.,* 2014) In brief, "Notch" proteins are intracellular signalling proteins which trigger transcription of DNA into proteins after interaction with their extra-cellular receptor. Jag1 (Jagged 1) is one of the proteins associated with the binding of notch, and these proteins are highly conserved across most animals, and so is applicable in both humans and mice. In AD, Notch signalling has been shown to be dysregulated (Cho *et al.,* 2019).

IL33 transcription is regulated by notch signalling, but it too exerts effects as a transcription factor by its effects on PU.1 (a transcription factor frequently found in microglia which has been linked to AD) and NF-kb (Sundlisæter *et al.,* 2012; Rustenhoven *et al.,* 2018; Lau *et al.,* 2020) and thus we expected to find a correlation between these genes. Interestingly, we found that the correlation patterns vary between the different disease states. In 40Hz light treated wild-types we observed that *PSEN1* and *mAPP* both exhibited a significant negative correlation, suggesting that increased *IL33* reduced expression of AD-related genes and altered APP processing. When we analysed correlation between the three genes we found that *PSEN1* and *mAPP* showed a highly significant positive correlation in WT-T mice, with BACE1 expressing only moderately strong correlation with both *PSEN1* and *mAPP*. Meanwhile in untreated 5xFADs we observed the opposite trend. *IL33* showed a positive correlation with all 3 genes, though most significantly with *BACE1*. When the APP-processing genes were compared, we found that in untreated 5xFADs the strongest correlation was between *BACE1* and *mAPP*, whereas *PSEN1* showed only a moderately strong correlation.
In 40Hz treated 5xFADs we observed changes more similar to the *WT*-T group; all 3 genes expressed a strong negative correlation with *IL33* mRNA expression. Interestingly, all 3 genes also showed strong positive correlation with each other (*BACE1* with *mAPP* and *PSEN1*, and *PSEN1* with *mAPP*) in contrast to the WT-T group.

From these data we can suggest several hypotheses, though they also create several more questions. Firstly, expression of BACE1 and mAPP are highly correlated in 5xFAD animals. This is perhaps unsurprising, given that it has been well established that 5xFAD animals express increased BACE1 around amyloid deposits (Zhao *et al.,* 2007) and its role as the initial mis-cleaving enzyme on the path to producing Aβ. More

interesting however, is the strong positive correlation between BACE1 and IL33. IL33 expresses transcription inhibition on transcription factor NF-κB (Choi *et al.,* 2012), which in turn has been suggested to increase BACE1 expression (Qiao *et al.,* 2021). Why, then, do we find a positive correlation in these genes?

Combined, these results suggest that 40Hz light treatment does alter the transcription of these genes, and that *IL33* may be involved in this response as a transcription factor, which may in turn have a downstream impact of transcription of other genes.

4.3.3.4 Correlations between microglia genes and IL33

We then wanted to investigate any correlations between *IL33,* and the expression of genes associated with microglia markers.

The pro-inflammatory gene *Cst7* showed no correlation in 40Hz treated WTs or 5xFAD animals but showed a significant correlation with *IL33* in untreated 5xFAD animals. This is potentially explained by the significant differences in *Cst7* expression in these two groups compared to WT-UT, as *Cst7* expression is very low in treated WTs, and reduced in 40Hz treated 5xFADs. However, the correlation with untreated 5xFADs suggests that *IL33* and inflammatory *Cst7* are linked. It has been well established that *IL33* expresses both inflammatory (Xiong *et al.,* 2014) and anti-inflammatory (Saresella, Marventano, Piancone, La Rosa, *et al.,* 2020) role depending on the level of expression and other transcriptional factors. It is likely that another, as yet unidentified in this study, factor is influencing the balancing act of *IL33* and its role in inflammation, causing it to correlate with inflammatory *Cst7* before, but not after, 40Hz light treatment. *Cst7* also expressed a moderate but insignificant correlation with *Gpnmb* only in our untreated 5xFADs, with a moderate negative correlation found in the treated WTs.

4.3.4 Expression of IL-33 and OLIG2 proteins in the VC of 40Hz treated 5xFAD and WT mice

Having measured expression of IL-33 mRNA, we next wanted to determine if this increase in mRNA expression was translated into an increase in protein expression in the visual cortex. We also measured Olig2 to identify an
d quantify the number of OPCs and oligodendrocytes in the VC expressing IL-33.

When measuring the total number of IL-33+ cells within each individual layer of the VC, we observed that the highest protein expression was within the deep cortical layers (L4-L6), with reduced expression in L1-3. We also found a significant decrease in IL-33 expression specifically (and exclusively) in layer 4 of 5xFAD mice when compared to WT controls. Whilst there was a pattern of reduced expression in every layer, these did not reach significance. This is of significant interest, as layer 4 is involved in cortical information processing (Scala *et al.,* 2019).

Surprisingly, we did not find any increase in IL-33 protein levels between 40Hz treated and 40Hz untreated animals of either genotype. When we measured the total IL-33+ expression across the whole VC we again found no significant differences. This suggests the changes in *IL33* mRNA was limited to post-transcriptional increases and was not further translated into protein increases. It is possible that there are changes in IL-33 protein regulation through sST2, oxidation or inflammatory proteases, but these were not measured in this study.

Olig2 is a transcription factor that is expressed almost exclusively by subsets of astrocytes, OPCs and mature myelinating oligodendrocytes. Its role is to activate expression of myelinisation (Zhang *et al.,* 2022) as well as determining oligodendrocyte differentiation (Liu *et al.,* 2007). We therefore used it as a means of identifying glial expression of IL-33. We found a similar pattern in Olig2 expression was in IL-33 expression. The deep cortical layers 4-6 showed the highest expression, with layers 1-3 showing reduced expression. We again found a significant reduction in Olig2 expression in layer 4 of the VC in our 5xFAD animals compared to our WT-UT. However, we also found a significant difference when we measured the total number of Olig2+ cells in the VC. Our 40Hz treated 5xFAD animals showed significantly fewer Olig2+ cells when compared to our WT-UT animals, whereas the untreated 5xFAD animals showed no such difference. This suggests that the treatment was affecting oligodendrocytes; either through changing maturation of oligodendrocytes or through reduction in overall oligodendrocyte population- though this difference may simply be an artefact of the variability in the data, as untreated 5xFADs showed (non-significantly) lower overall Olig2 expression also.

4.3.5 Overall conclusion

Overall, we have shown here that the 40Hz light flicker stimulation significantly reduces Aβ in the VC of 4–5-month-old mice, although to a lower extent than observed in the initial publication. It's possible this difference is due to the weekend-interruptions used in our studies, as the original publication showed that Aβ returned to pre-treatment levels within 24 hours showing the 40hz reduction to be transient. Contrary to the original study however, we did not observe a decrease in the total number of plaques- again this may be explained by the breaks in our treatment.

Another large difference between our study and the original publications is that we included female 5xFAD animals in our study, while they only included male AD-model mice throughout the 3 publications. Female 5xFAD animals are well known to produce more severe pathology than male littermates (Bundy *et al.,* 2019) and so this may have affected the skew of our data. This may also explain why we saw a less significant drop in Aβ1-40 and Aβ1-42 within the VC compared to the original studies, as there is little data on the 40hz light-treatment in female 5xFADs. Given that female 5xFADs experience more severe pathology and inflammation (Murtaj *et al.,* 2019) it could be hypothesised that they respond differently to the light treatment.

Whilst our treatment was less effective at reducing Aβ protein levels, it was still sufficient to show pre-translational changes within the VC, showing effects on the APP processing pathway and expression of *IL33*. This suggests a role for IL-33 in the 40Hz flicker treatment which is differentially expressed based on the inflammatory profile of the brain at the beginning of the light treatment.

While we observed pre-transcriptional changes in the APP processing pathway and a reduction of Aβ in the VC, we still found some data sets had distinct groupings. We suspected this may be due to sexual dimorphism in response to treatment.

We also found interesting correlations between expression of *IL33* mRNA and APP-processing gene mRNA, and inflammatory microglia marker Cst7 mRNA. Our findings suggest that the 40Hz light flicker treatment induces changes at the transcriptional level and suggests a role for *IL33* in this change- though more in-depth study into the intra-cellular signalling pathways needs to be conducted.

4.3.6 Limitations

Given the complexity of the role of IL-33, many more experiments could be conducted to determine whether the non-significant decrease in our treated 5xFAD animals (and our significant increase in WTs) is pro or anti-inflammatory. The measurement of mRNA does not necessarily translate to protein expression, and so western blotting may elucidate if there is an increase in protein. This cytokine has many functions from nuclear signalling and immunomodulation, to serving as an alarmin- therefore the precise role of this cytokine in 40Hz light flicker stimulation remains unclear. We are also unable to determine specifically which cells are producing these between oligodendrocytes and astrocytes.

Given the nature of the 2-ΔΔCt method we were unable to determine correlations in gene expression between WT-UT, which would have established a baseline to which the other groups can be compared- this would clarify if the 40Hz treatment is inducing the negative correlations, or if the negative correlations are inherent in WT mice- this is an unfortunate limitation to our analysis. We are also unable to tell exactly which cells are up / downregulating these genes due to the homogenisation of brain tissue. While the changes in overall gene expression in the VC give us an indication of what is happening, they cannot tell us specifically which cells are responding.

Chapter 5

Sex based differences in response to 40Hz light treatment

5. Sex based differences in response to 40Hz light treatment.

Alzheimer's disease disproportionately affects women (Brookmeyer *et al.,* 2011; Fisher, Bennett and Dong, 2018) due to a variety of suspected factors including genetics, sex hormones and differences in baseline inflammatory responses. The 5xFAD model we used in this study also exhibits this dimorphism, with female 5xFAD animals exhibiting earlier and faster deposition of Aβ (Oakley *et al.,* 2006; Bundy *et al.,* 2019). This is of particular significance given the association with hormone changes exhibited during menopause in women and the increased AD prevalence in women. However, recent studies have found links between estrogen, hormone-replacement therapy (HRT) and reductions in AD risk (Song *et al.,* 2020). Despite these findings there is still very limited understanding as to why women may be more susceptible to AD, and many publications continue to use only male animals in their studies despite changes to many funding bodies requiring both sexes be used. There remains a need to increase our understanding of sex-based responses in both humans and animal research models.

Given the clear link between sex-based hormones in AD, combined with publications which suggest males and females respond differently to light (Chellappa *et al.,* 2017) we suspected that there would be a difference in responses to the 40Hz light treatment.

Studying the sex-based response to 40Hz light is novel, as no study to date has analysed the 40Hz light flicker in terms of sex-based response and the majority of studies have used only male animals across several AD mouse models.

In this chapter, male and female 5xFAD and WT mice were treated with 40Hz light or darkness for 1 hour a day for 15 days, then data analysed to determine sex-based responses to 40Hz light as well as innate differences between 5xFAD animals and their WT littermates.

5.1 Aims

The primary aim of this chapter is to examine results from male and female animals seperately to determine if there is any difference between the responses of male and female animals to 40Hz light flicker treatment.

5.2 Results

In this chapter we post-analysed our data sets to account for biological sex as an additional factor, as re-use of the data already available to us is aligned with the core principles of the 3Rs- the guiding principles of animal research (Specifically, the reduction of animal numbers used) (NC3Rs; Hubrecht and Carter, 2019). This allowed us to maximise the use of each individual animal to understand the effect of genotype, 40Hz light flicker and biological sex whilst also limiting the number of animals sacrificed.

5.2.1 Sex-dimorphic expression of Aβ 1-40 and Aβ 1-42 in brains of 5xFAD mice

To understand the differences in expression of Aβ1-40 and Aβ1-42 between male and female 5xFAD animals we first used ELISA to measure the protein level in the brain. WT and 5xFAD animals at 4-5 months old of both sexes were treated with 40Hz light flicker for 1 hour per day, for 15 days before being sacrificed. Brain tissue was collected, and processed for ELISA.

To begin, all data was analysed using a 3-way ANOVA with Tukey's multiple corrections. This identified that both sex (P****<0.0001) and genotype (P****<0.0001) were significant factors in Aβ 1-40, and similarly for Aβ 1-42 (sex P**=0.032, genotype P****<0.0001) (Appendix B). We therefore first compared the levels of Aβ protein expression between the sexes. We observed that there was no significant differences in levels of Aβ protein of either fragment length in WTs of male or female animals (Fig 5.1A,B) when compared, in both 40Hz light treated and untreated groups. We found that in both treated and untreated female 5xFADs there was significantly higher Aβ 1-40 (Fig 5.1C, P**<0.01) than their male counterparts. However, when we compared expression of Aβ 1-42 between sexes we found there was significantly more Aβ protein in treated 5xFAD females than treated 5xFAD males (Fig 5.1D, P*<0.05), with no significant difference between untreated animals of each sex.

To evaluate the effectiveness of the 40Hz treatment within each sex to determine if either sex responded differently to treatment, the data for treated and untreated groups were next compared within each sex. We found untreated 5xFAD animals of both female (Fig 5.2A,B) and male (Fig 5.2C,D) mice exhibited significantly more Aβ protein compared to WT-UT animals as expected. However, there were no significant changes in Aβ protein level in female or male 5xFAD animals after 40Hz light flicker treatment.

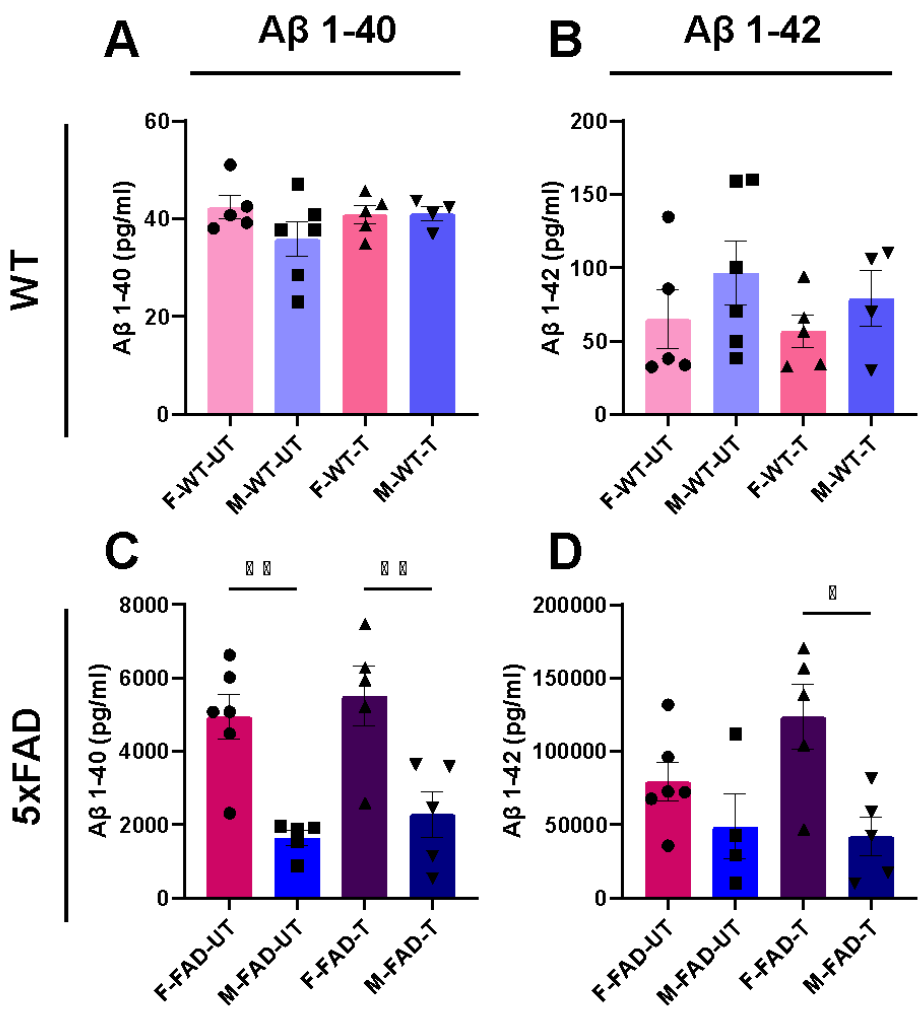

Figure 5.1 - Aβ 1-40 and Aβ 1-42 expression differs by sex in 5xFAD animals. *Female and male WT and 5xFAD mice between 4 and 5 months old were treated with 40Hz light (WT-T, FAD-T) or left in dark conditions (WT-UT, FAD-UT) for 1 hour per day for 15 days over three weeks. Following final treatment brain samples were harvested and processed to measure Aβ 1-40 and Aβ 1-42 using ELISA.* ***WT (A,B):*** *Aβ 1-40(A) and 1-42 (B) protein level in brain samples of female animals, n=5-6 in all four groups.* ***5xFAD (C,D)*** *Aβ 1-40 (C) and 1-42 (D) protein expression from male animals (n=4-6 in all groups.) Each data point represents 1 animal. All figures show mean ± S.E.M. Three-way ANOVA performed (DFn=1, DFd=32) to compare sex (F=26.88, P=<0.0001) genotype (F=127.1, P=<0.0001) and treatment (F=0.93. P=0.34). Tukey's multiple comparisons then performed; C: F-FAD-UT vs M-FAD-UT P=<0.0001. F-FAD-T vs M-FAD-T P=0.0003. D: F-FAD-T vs M-FAD-UT P=0.0012. (P*<0.05, P***<0.001, P****<0.0001)*

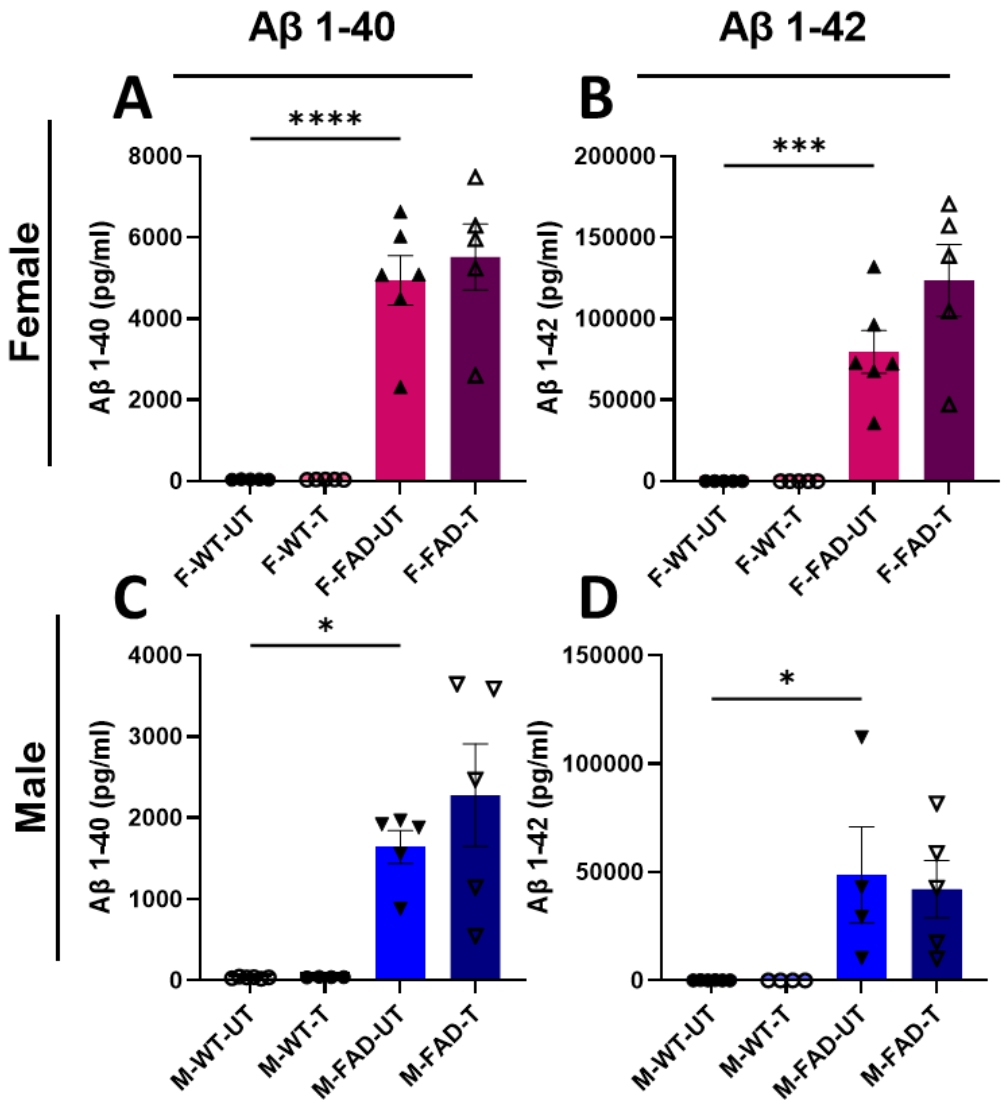

Figure 5.2 - No significant changes across ½ brain Aβ burden in either sex. *Female (pink, A,B) and male (blue, C,D) WT and 5xFAD mice between 4 and 5 months old were treated with 40hz light (WT-T, FAD-T) or left in dark conditions (WT-UT, FAD-UT) for 1 hour per day for 15 days over three weeks. Brain samples were harvested and processed to measure Aβ 1-40 and Aβ 1-42 using ELISA.* ***Female (A,B)****: Aβ 1-40 protein (A) and Aβ 1-42 (B) protein level in brain samples of female animals, (n=5-6 for all groups)* ***Males (C,D)*** *Aβ 1-40 (C) and Aβ 1-42 (D) protein levels from male animals (n=4-6 for all group). Each data point represents 1 animal. Data represented as pg/ml. All figures show mean ± S.E.M. Three-way ANOVA with Tukey's multiple comparisons performed to compare genotype (F=26.9, P=<0.0001), sex (F=127.1, P=<0.0001) and treatment (F=0.93, P=0.34). (P*<0.05, P***<0.001, P****<0.0001)*

5.2.2 Aβ histology in visual cortex of female and male 5xFAD mice

Our ELISA results showed that female 5xFADs express significantly higher levels of Aβ than male 5xFADs, showing a clear sexual dimorphism. We therefore questioned if this difference would be expressed within the VC and if there was a difference between the sexes in Aβ protein levels across cortical layers. To begin, we first sought to determine if male and female 5xFAD animals responded to 40Hz light treatment differently when compared to untreated same-sex controls.

Female mice were treated with 40Hz light for 15 days, then culled, tissues harvested and Aβ levels measured using a pan-Aβ antibody (Fig 5.3A) to evaluate the overall area of Aβ within the VC. These data show that the superficial cortical layers showed the lowest level of Aβ, with layers 5 and 6 expressing the highest Aβ burden (Fig 5.3B) and the highest overall number of plaques (Fig 5.3C). Overall, there was no statistically significant difference between untreated and treated female 5xFAD animals in any layer of the VC either by the extent of Aβ coverage (Table 5.1), nor by the total number of plaques (Table 5.2).

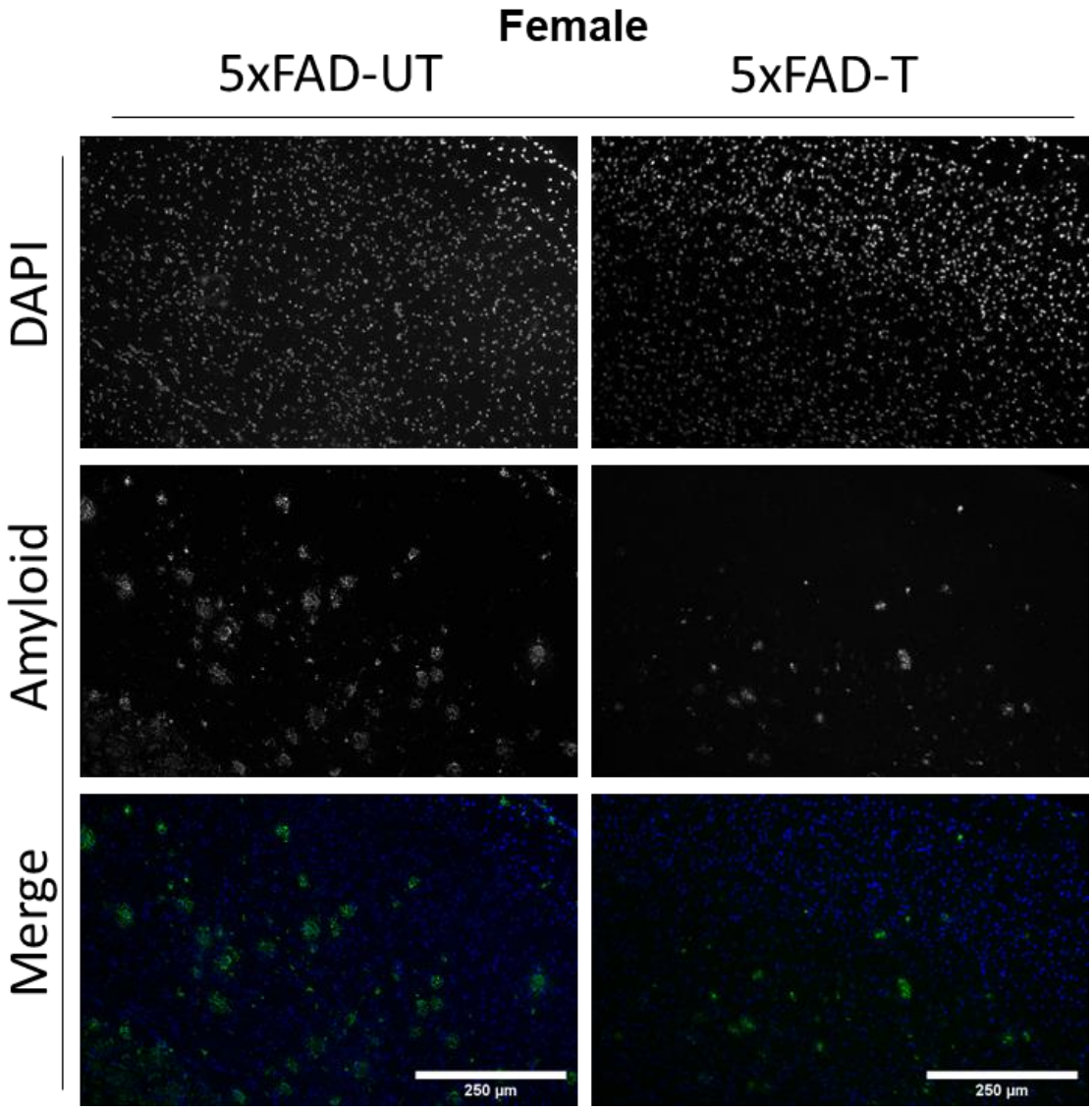

Figure 5.3 - Effect of 40Hz light flicker on Aβ burden in primary visual cortex of 4-5-month-old female 5xFAD mice. *Female 5xFAD animals between 4 and 5 months old were treated with 40hz light (5xFAD-T, n=6) or left in dark conditions (5xFAD-UT, n=6) for 1-hour per day for 15 days over three weeks. Brain tissues were harvested on the day, following the final treatment, and were sectioned for staining with a pan-Aβ antibody. Immunofluorescence images were taken and the total area positive for Aβ was measured using Qupath Software. 10x images show representative immunofluorescence images of VC of untreated and treated female mice showing DAPI (blue) and amyloid-β (green), scale bar shows 250µm.*

Male mice were treated alongside females for 15 days then sacrificed, tissues harvested and Aβ levels measured using a pan-Aβ antibody (Fig 5.4A). Untreated male 5xFADs showed slightly more Aβ than their treated counterparts, although this difference did not reach statistical significance (Table 5.1). Similar to females, the superficial cortical layers showed the lowest Aβ protein levels (Fig 5.4B). L4 showed minimal Aβ coverage given the size of this layer, and deep cortical layer 6 showed the highest levels of Aβ. None of the individual layers reached a statistically significant difference between untreated male 5xFAD and 40Hz treated male 5xFAD animals for Aβ coverage, nor for the number of plaques (Fig 5.4C)

Table 5.1- Area of Aβ in each layer of the visual cortex in 4-5month old female and male 5xFAD mice treated with 40Hz light flicker for 15 days.

Aβ burden (% of area)			Visual Cortex layer					
			LI	**LII/III**	**L IV**	**LV**	**LVI**	**Total**
Female	**Untreated**	**5xFAD**	0.86 ± 0.4	0.36 ± 0.2	0.74 ±0.3	2.5 ± 0.8	4.8 ±1.6	7.8 ± 3.1
	Treated	**5xFAD**	0.35 ±0.2	0.22 ±0.05	0.26 ±0.1	1.5 ± 0.4	2.6 ±0.5	4.9 ±0.9
Male	**Untreated**	**5xFAD**	0.44 ±0.3	0.13 ± 0.04	0.37 ±0.7	3.7 ±0.7	5.4 ±1.8	7.6 ± 1.7
	Treated	**5xFAD**	0.11 ±0.1	0.079 ±0.06	0.52 ±0.5	1.1 ±0.5	2.9 ±1.5	4.7 ±2.3

Table shows mean values for each layer of the VC, as well as combined total Aβ measurements in the VC. Values rounded to 2 decimal places ± S.E.M. All units shown are a percentage of the area covered.

Table 5.2- Number of Aβ plaques in each layer of the visual cortex in 4-5month old female and male 5xFAD mice treated with 40Hz light flicker for 15 days.

Total no. plaques			Visual Cortex layer				
			LI	**LII/III**	**L IV**	**LV**	**LVI**
Female	**Untreated**	**5xFAD**	1.1 ±0.6	1.4 ±0.5	1.1 ±0.3	10.7 ±2.3	9.3 ± 1.8
	Treated	**5xFAD**	0.94 ± 0.3	2.3 ± 0.7	0.9 ±0.2	13 ± 2.1	8.7 ±1.8
Male	**Untreated**	**5xFAD**	1.3 ±0.2	0.6 ±0.4	1.0 ±0.6	11 ± 1.9	10.8 ± 1.6
	Treated	**5xFAD**	0.1 ± 0.1	0.89 ± 0.6	0.5 ±0.3	10.7 ±3.9	11.7 ±4.4

Table shows mean plaque counts within the VC. Values rounded to 2 decimal places ± S.E.M. All units shown are total plaque number.

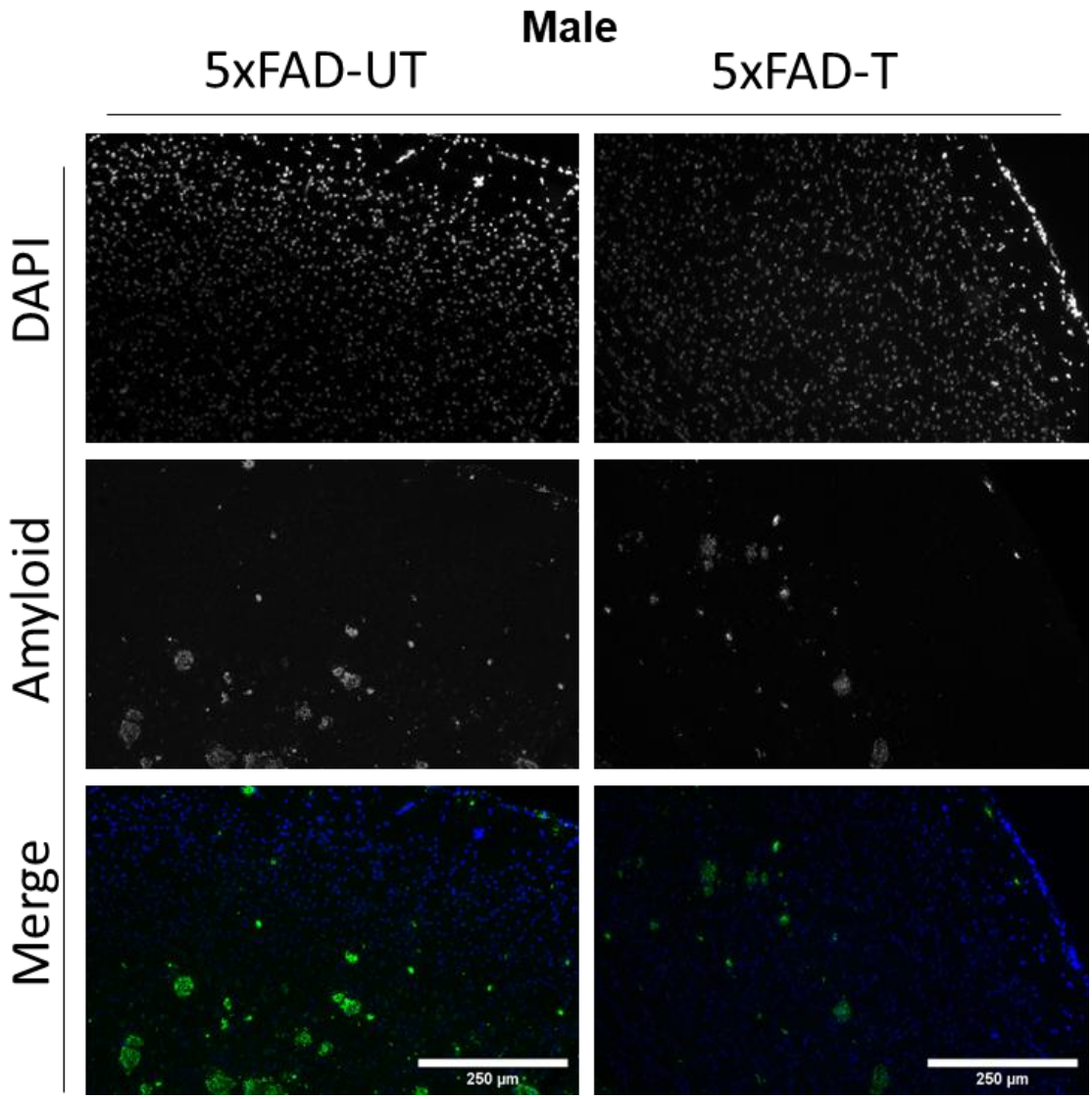

Figure 5.4 - Effect of 40Hz light flicker on Aβ burden in visual cortex of 4/5-month-old male 5xFAD mice. *Male 5xFAD animals between 4 and 5 months old were treated with 40hz light (5xFAD-T, n=6) or left in dark conditions (5xFAD-UT, n=6) for 1-hour per day for 15 days over three weeks. Brain tissues were harvested on the day after the last treatment and were sectioned for staining with a pan-Aβ antibody. Immunofluorescence images were taken and the total area positive for Aβ was measured using Qupath Software. Images show representative immunofluorescence images of VC of untreated and treated male mice showing DAPI (blue) and amyloid-β (green), scale bar shows 250µm.*

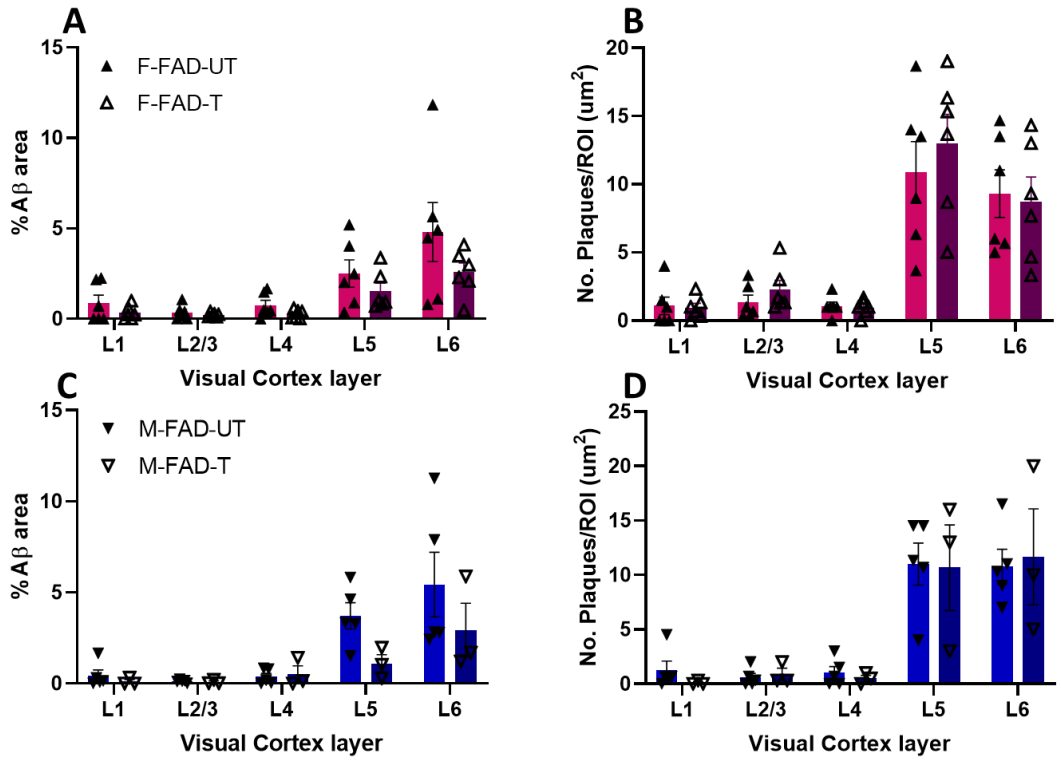

Figure 5.5 – Effects of 40Hz light flicker treatment on the Aβ burden of each layer of the VC in female and male 5xFAD mice. 5xFAD animals of both sexes were treated with 40Hz light flicker or left in darkness for 1hr per day for 15 days. Animals were then sacrificed and IF staining performed using a pan-Aβ antibody. Immunofluorescence images were captured and the Aβ burden quantified using Qupath software. ***A:*** *The level of Aβ calculated as a % of coverage of the layer of the visual cortex of female 5xFADs.* ***B:*** *Number of plaques counted manually in each layer of the VC in female 5xFADs.* ***C:*** *The % of each visual cortex layer that was positive for Aβ.* ***D:*** *Number of plaques counted in each layer of the VC of treated and untreated male 5xFADs. Each data point represents one animal. Data shows mean of 3 replicates per animal* ± S.E.M. *Three-way ANOVA with Tukey's multiple comparisons performed, no significant differences found for %coverage for sex (F=0.023,, P=0.96) but a significant difference found for treatment group (F=7.99m, P**=0.0059).*

While the three-way ANOVA indicated treatment may have a significant effect, this was further analysed using Tukey's multiple comparison test. We found no significant difference between treated and untreated 5xFAD groups. Overall, there was no statistically significant difference in the expression of Aβ in any layer of the visual cortex between 40Hz treated 5xFADs of either sex, either by the extent of Aβ coverage, nor by the total number of plaques.

We then compared the level of Aβ coverage and the number of plaques in each layer of the visual cortex between males and females. We found no statistically significant difference in Aβ% area coverage on any individual layer of the VC between male and female 5xFADs with or without 40Hz treatment (Fig 5.5, top) nor in the number of Aβ plaques on each layer (Fig 5.5, bottom).

We finally compared the total Aβ coverage and number of Aβ plaques in the entire VC between male and female 5xFADs with or without 40Hz treatment. This data showed no statistically significant difference between males and females of either 5xFAD treatment group (Fig 5.6). Interestingly, despite reports that female 5xFADs exhibit higher levels of Aβ in the brain than males we found each sex exhibited similar Aβ levels in the VC when measured by histology.

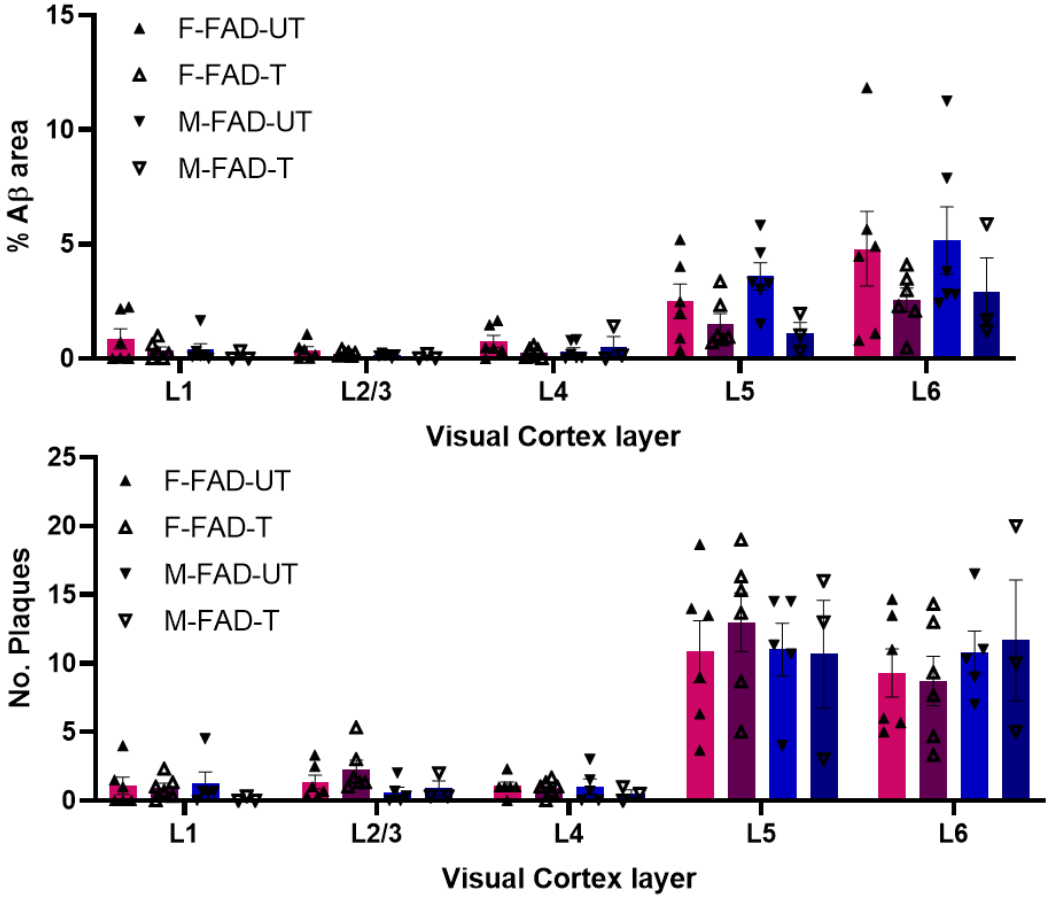

Figure 5.6- Comparison of Aβ levels and plaque numbers between male and female 5xFAD animals in each layer of the visual cortex

Statistical tests were performed to compare the male and female %Aβ area (top) and the total number of Aβ plaques (bottom) in each layer of the VC. Each data point represents one animal. Three-way ANOVA (DFn=4, DFd=85) with Tukey's multiple comparisons performed. %Aβ area: cortical layer (F=18.83, P=<0.0001) sex (F=0.002, P=0.97), treatment (F=7.99, P=0.0059)

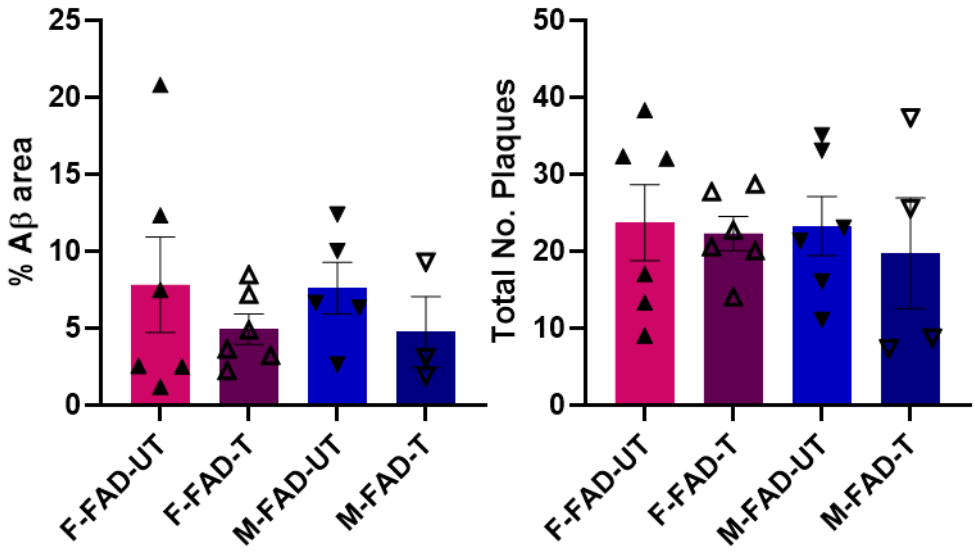

Figure 5.7- Total levels of Aβ and total number of plaques in the whole visual cortex for male and female, 40Hz treated and untreated 5xFAD mice. *Histological Aβ data from individual layers of the VC was summed to estimate the total Aβ across the area measured.* ***Left:*** *total % of VC that was Aβ+.* ***Right****: Total number of plaques across the entire VC between male and female 5xFADs. Each data point represents one animal. Error bars shown mean ± S.E.M. Two-way ANOVA (DFn=1, DFd=16) with Tukey's multiple comparisons performed to compare treatment (F=0.08, P=0.8) and sex (F=0.28, P=0.12) no significant differences detected.*

5.2.3 Effect of sex on gene expression in female and male 5xFAD mice after 40Hz treatment.

To understand the molecular mechanisms of the response between female and male mice to 40Hz treatment, we performed RT-PCR to measure the level of mRNA expressed in the VC of male and female WT and 5xFAD animals that were treated with 40Hz light or left in darkness as a control. All data for each group was normalised to its respective WT-UT group (E.g., female WT-T, female FAD-UT and female FAD-T all normalised to average CT values for female WT-UT) for each gene.

We again started with the AD-related genes. *PSEN1* was significantly (P****<0.0001, 5-fold-increase) elevated in female 5xFADs compared to WT controls and was significantly decreased in female 5xFAD animals after 40Hz light flicker treatment (Fig 5.7A, P****<0.0001, 0.1-fold-decrease). We found no difference in female WTs after treatment. In males the untreated 5xFAD group was significantly (Fig 5.7B, P*<0.05, 29-fold-increase) higher than the WT controls, but the decrease in the treated 5xFADs did not reach significance due to high variation in results (Fig 5.7A). Similar to females, there was no significant difference between treated and untreated male WTs.

In *BACE1* we saw more sexually dimorphic results. There were no significant differences in female WTs after treatment (Fig 5.7C), however female 5xFADs exhibited a decrease in mRNA levels after light flicker treatment (P*<0.05, 0.45-fold-decrease) compared to untreated 5xFADs and untreated wild-types. Male animals showed no significant difference between untreated 5xFADs compared to untreated WTs, nor in treated and untreated 5xFADs (Fig 5.7D).

In *mAPP* we observed that female untreated 5xFADs expressed significantly less mRNA (Fig 5.7E, P*<0.05, 0.7-fold-decrease) than their WT-UT counterparts. After 40Hz light treatment the WT group showed no significant changes, while the 5xFAD group increased their mRNA expression compared to untreated 5xfADs (P*<0.05, 1.04-fold-increase). In both sexes mRNA for endogenous mouse APP was increased in 5xFAD animals after treatment, though males increased expression to a much higher extent than their untreated counterparts (Fig 5.7E, P****<0.0001, 6.5-fold-increase) while females only returned to baseline (WT-UT) levels of expression

(P*<0.05, Fig 5.7E). Untreated 5xFAD males also didn't express the same decreased level of *mAPP* (relative to WT-UT) that female 5xFADs did.

Finally, we examined *IL33* mRNA expression. Female 5xFAD animals expressed significantly more *IL33* than untreated female WTs (Fig 5.7F, P*<0.05, 7.8-fold-increase). After 40Hz light treatment, female WTs significantly increased *IL33* expression (Fig 5.7G, P*<0.05, 9-fold-increase) compared to WT-UT, while 5xFAD females exhibited slightly lower *IL33* than their untreated counterparts, though this did not reach significance. Male animals showed a similar trend. Male untreated 5xFADs showed significantly more *IL33* than WT controls (Fig 5.7H, P**<0.01, 4-fold-increase), and 40Hz treated 5xFADs showed a pattern of reduced *IL33* mRNA that did not reach significance.

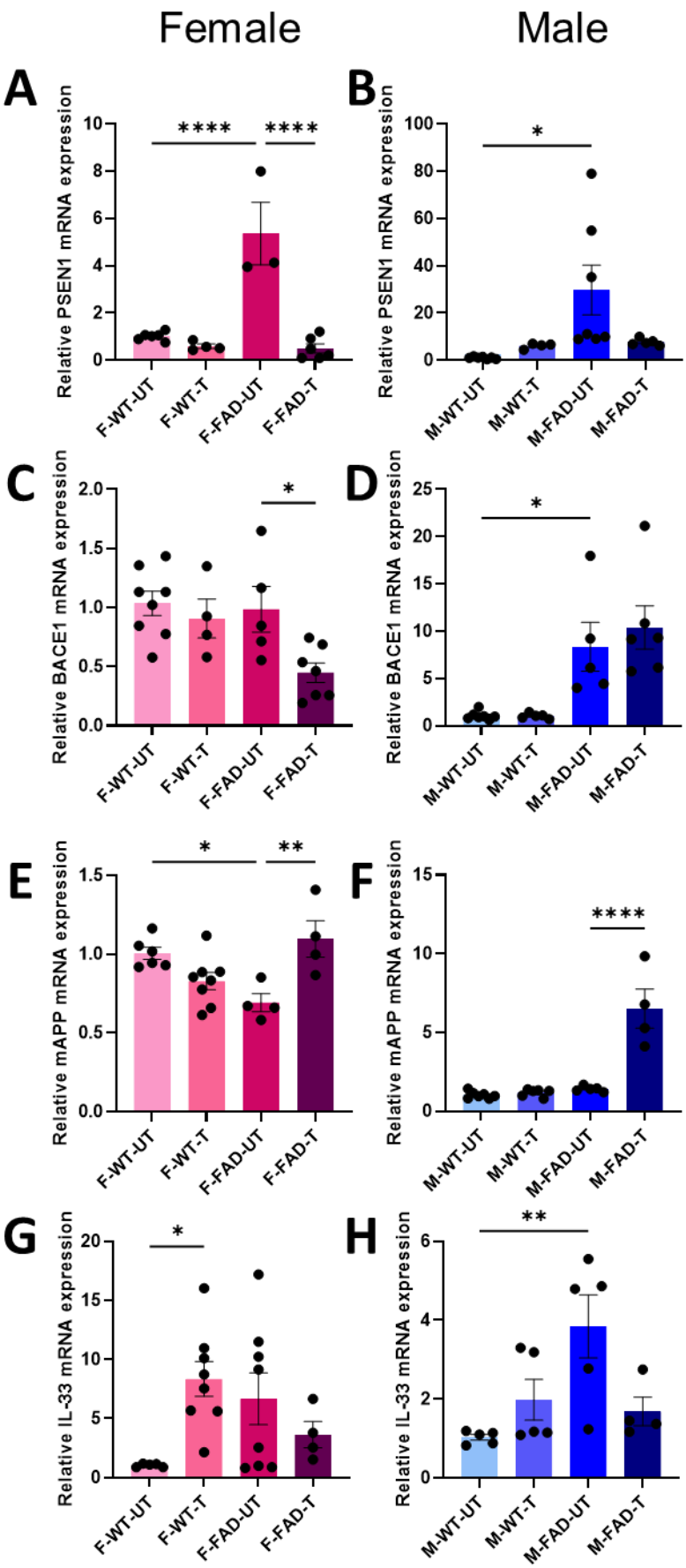
Female
Male
A
B
C
D
E
F
G
H
Relative PSEN1 mRNA expression
Relative BACE1 mRNA expression
Relative mAPP mRNA expression
Relative IL-33 mRNA expression
F-WT-UT
F-WT-T
F-FAD-UT
F-FAD-T
M-WT-UT
M-WT-T
M-FAD-UT
M-FAD-T
****
*
**

Figure 5.8- Sex-dependent expression of genes PSEN1, BACE1, mAPP, IL-33 after 40Hz treatment. *Female (left column, pink) and male (right column, blue) untreated wild-type (WT-UT), untreated 5xFAD (FAD-UT) and 40hz light treated wild-type (WT-T) and 5xFAD (FAD-T) visual cortices were harvested from ½ brain and mRNA extracted and qPCR performed for PSEN1 (A,B), BACE1 (C,D) endogenous mAPP (E,F) and IL-33 (G,H). All CT values normalised to sex-specific mean WT-UT value using 2–ΔΔCt method. Each data point represents one mouse. Error bars shown mean* ± S.E.M. *One-way ANOVAs performed with Tukey's multiple comparisons, as data is normalised to WT-UT group* ***A****- Treatment: F(3,15)=23.41, P=<0.0001, F-WT-UT vs F-FAD-UT P=<0.0001, F-FAD-UT vs F-FAD-T P=<0.0001.* ***B-*** *Treatment: F(3,19)=4.4, P=0.016, M-WT-UT vs M-FAD-T P=0.0142.* ***C****- Treatment: F(3,20) =5.1, P=0.009, F-FAD-UT vs F-FAD-T P=0.038.* ***D****- Treatment: F (3,19) =2.16, P=0.0006, M-WT-UT vs M-WT-T P=0.023.* ***E-*** *Treatment: F (3,18)=6.32, P=0.04, F-WT-UT vs F-FAD-UT P=0.023, F-FAD-UT vs F-FAD-T P=0.0068.* ***F-*** *Treatment: F (3,18)= 29.2, P=<0.0001, M-FAD-UT vs M-FAD-T: P=<0.001****.*** ***G-*** *Treatment: F (3,21)= 3.26, P=0.042, F-WT-UT vs F-FAD-T P=0.383.* ***H-*** *Treatment: F (3,15)= 5.47, P=0.009, M-WT-UT vs M-FAD-UT P=0.0073. . (P*=<0.05, P**=<0.01, P****=<0.0001)*

Next, we examined the sex-dependent expression of microglia-related genes in female and male mice with and without 40Hz treatment.

We observed no significant changes in *Gpnmb* expression before or after treatment in either females (Fig 5.8A) or males (Fig 5.8B) of either genotype, suggesting that 40Hz light flicker treatment did not affect expression of *Gpnmb* in males or females of either genotype.

We next looked at expression of *Cst7,* a gene that has been recently reported to show sexual-dimorphism. We observed that female 5xFAD animals expressed significantly (P****<0.0001, 54-fold change) more *Cst7* mRNA than their WT-UT controls, and this expression was unchanged by 40hz treatment (Fig 5.8C). However, while untreated 5xFAD males showed similar significantly higher expression of C*st7* (P**<0.01, 115-fold increase, Fig 5.8D) relative to WT-UT controls this expression was significantly reduced (P*<0.05, 31-fold-decrease) after treatment with 40Hz light. There were no changes in *Cst7* expression in WTs after 40Hz treatment in either sex.

In *P2YR12* we observed that female 5xFADs did not express significantly higher mRNA levels compared to untreated WTs. Neither WT nor 5xFAD females changed their expression of *P2YR12* after 40Hz light treatment, although female 40Hz treated 5xFAD animals did show significantly more mRNA when compared to untreated WTs (Fig 5.8E, P*<0.05, 2-fold-increase) In males, we observed no significant changes between any genotype or treatment group (Fig 5.8F).

There were no significant changes in any treatment group of any genotype of female animals in expression of *TMEM119* mRNA (Fig 5.8G). However, there were no differences between untreated 5xFADs and WTs but both male WT (0.7-fold-decrease) and 5xFAD (0.7-fold-decrease) decreased expression of *TMEM119* mRNA after 40hz light treatment (both P*<0.05, Fig 5.8H)

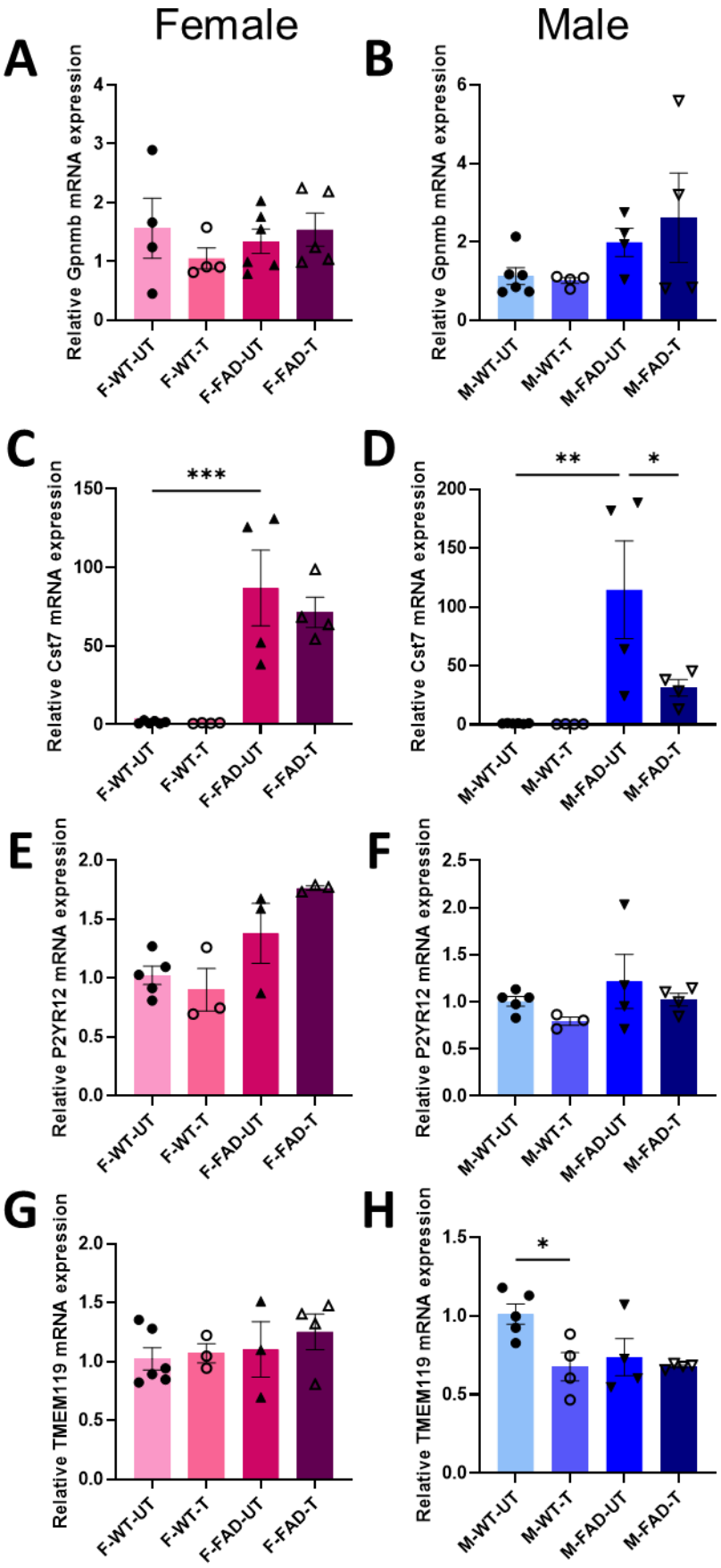
Female
Male
A
B
C
D
E
F
G
H
Relative Gpnmb mRNA expression
Relative Cst7 mRNA expression
Relative P2YR12 mRNA expression
Relative TMEM119 mRNA expression
F-WT-UT
F-WT-T
F-FAD-UT
F-FAD-T
M-WT-UT
M-WT-T
M-FAD-UT
M-FAD-T
***
**
*
*

Figure 5.9- Sex-dependent expression of microglia genes Gpnmb, Cst7, P2YR12 and TMEM119 after 40Hz treatment. *Female (left column, pink) and male (right column, blue) untreated wild-type (WT-UT), untreated 5xFAD (FAD-UT) and 40hz light treated wild-type (WT-T) and 5xFAD (FAD-T) visual cortices were harvested from ½ brain and mRNA extracted and qPCR performed for Gpnmb (top row), Cst7(2nd row), P2YR12 (3rd row) and TMEM119 (Bottom row). All CT values normalised to sex-specific mean WT-UT value using 2–ΔΔCt method. Each data point represents one animal. Error bars shown mean* ± S.E.M. *Ordinary one-way ANOVA with Tukey's multiple comparisons test performed.* ***A****- Treatment: F (3,15)=0.55, P=0.65* ***B-*** *Treatment: F(3,14)=1.86, P=0.18* ***C****- Treatment: F(3,14) =15.78, P=<0.0001, F-WT-UT vs F-FAD-UT P=0.0004* ***D****- Treatment: F (3,14) =8.11, P=0.002, M-WT-UT vs M-FAD-UT P=0.024, M-FAD-UT vs M-FAD-T P=0.04* ***E-*** *Treatment: F (3,10)=6.87, P=0.008, F-WT-UT vs F-FAD-UT P=0.023.* ***F-*** *Treatment: F (3,12)= 1.110, P=<0.383, no significance found.* ***G-*** *Treatment: F (3,12)= 0.57, P=064, no significance found.* ***H-*** *Treatment: F (3,13)= 4.47, P=0.023, M-WT-UT vs M-WT-T P=0.04. (P*<0.05, P**<0.01, P****<0.0001)*

5.2.3.1 Relative mRNA expression between males and females in each treatment group

Next, we determined if there were significant differences in gene expression between male and female mice in response to treatments. This would allow us to determine if the changes observed in gene expression within sex were comparable or significantly different across sexes. We conducted post-hoc analysis on the data by normalising the male Ct values to the average female CT values for each group (Male WT-UT normalised to average female WT-UT, etc).

First, we compared relative *PSEN1* expression from males, normalised to the CT values obtained for the relevant female group. We found that WT males express significantly lower *PSEN1* mRNA than their female counterparts (P****<0.0001, Fig 5.9), however this difference was not found in WT-T, FAD-UT, or FAD-T comparison groups. This suggests an innate difference in PSEN1 expression between male and female C57BL/6 mice. We next compared the expression of *mAPP* mRNA between males and females. In the WT mice we found no significant differences in mAPP mRNA expression between treated or untreated wild-type animals. However, in male 5xFADs we found that both treated and untreated mice expressed significantly higher levels of *mAPP* mRNA than the female mice with or without 40Hz treatment. (P***<0.001, Fig 5.10), suggesting expression of endogenous *mAPP* in 5xFADs is sexually dimorphic, and this difference was exacerbated after 40Hz light treatment.

There was a similar pattern of *BACE1* expression. While WT animals showed no significant differences, we found significantly higher levels in male 5xFADs than female 5xFADs in both treatment groups (Fig 5.11). Given that we previously found no difference in females when treatment groups were compared within the same sex, this is not surprising, as male 5xFADs expressed higher *BACE1* than their WT counterparts (Fig 5.7). Female 5xFADs also decreased *BACE1* expression after treatment, further emphasising this sex-based response to 40Hz light treatment.

We then compared expression of *IL33* mRNA and found the opposite trend. Male wild-types in both treated and untreated groups expressed significantly lower levels of *IL33* than their female counterparts. While there appeared to be lower levels in the 5xFAD group, these results did not reach statistical significance (Fig 5.12).

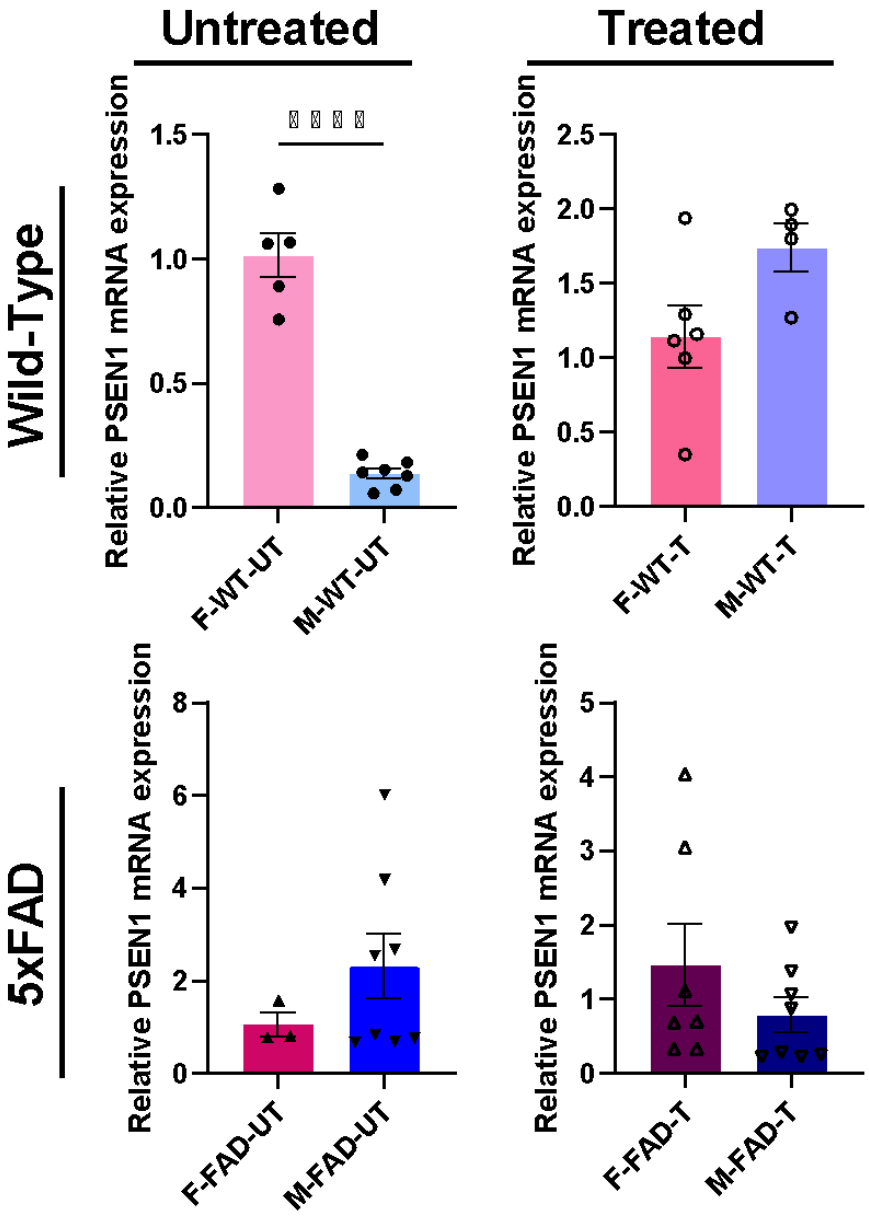

Figure 5.10 – Expression of PSEN1 mRNA in males relative to females from all treatment groups. *CT values from previous experiments were first separated by sex, then male ΔCT values normalised to the average ΔCT value for the corresponding female group. WT-UT males (n=7) were normalised to WT-UT females (n=5), WT-T males (n=4) were normalised to WT-T females (n=6), Untreated 5xFAD (FAD-UT) males (n=9) were normalised to untreated 5xFAD females (n=3) and treated 5xFAD (FAD-T) males (n=4) were normalised to treated 5xFAD females (n=7). All CT values normalised to sex-specific mean WT-UT value using 2–ΔΔCt method. All data shown as mean ± S.E.M. Unpaired t-test performed, (P****<0.0001).*

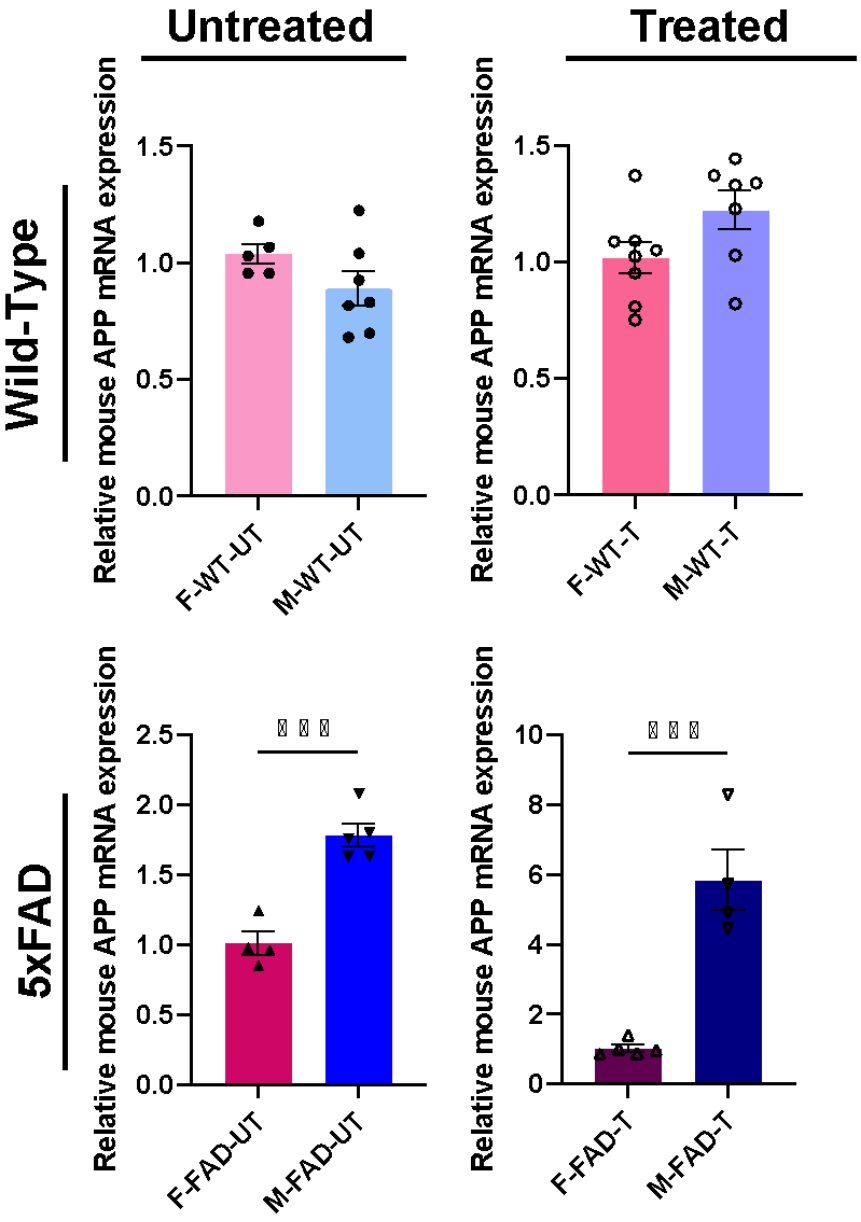

Figure 5.11 Expression of mAPP mRNA in males relative to females from all treatment groups. *CT values from previous experiments were first separated by sex, then male ΔCT values normalised to the average ΔCT value for the corresponding female group. WT-UT males (n=7) were normalised to WT-UT females (n=5), WT-T males (n=7) were normalised to WT-T females (n=7), Untreated 5xFAD (FAD-UT) males (n=5) were normalised to untreated 5xFAD females (n=4), and treated 5xFAD (FAD-T) males (n=4) were normalised to treated 5xFAD females (n=5). All data shown as mean ± S.E.M. Unpaired t-test performed, (P***<0.001).*

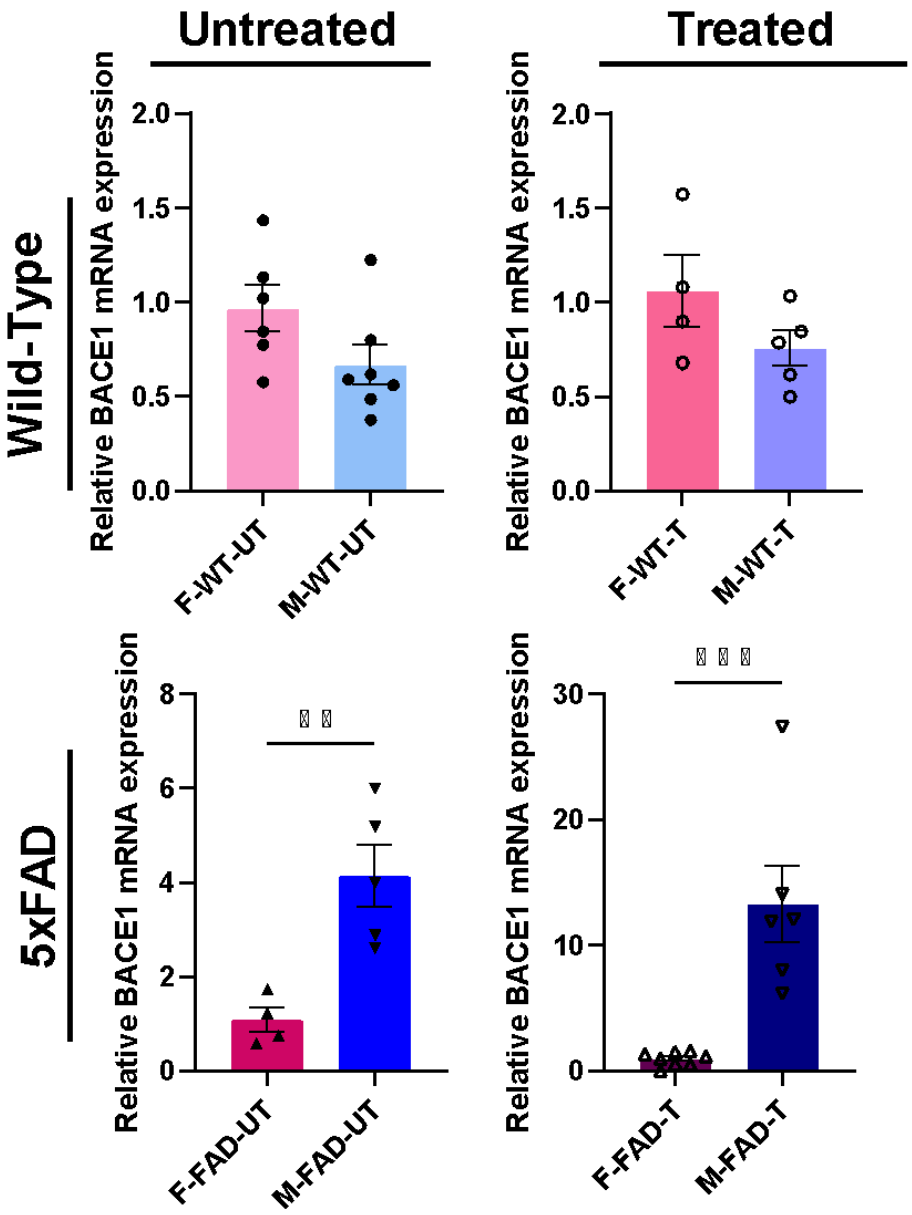

Figure 5.12 Expression of BACE1 mRNA in males relative to females from all treatment groups. *CT values from previous experiments were first separated by sex, then male ΔCT values normalised to the average BACE1 ΔCT value for the corresponding female group. WT-UT males (n=7) were normalised to WT-UT females (n=6), WT-T males (n=5) were normalised to WT-T females (n=4), Untreated 5xFAD (FAD-UT) males (n=5) were normalised to untreated 5xFAD females (n=4), and treated 5xFAD (FAD-T) males (n=6) were normalised to treated 5xFAD females (n=8). All data shown as mean ± S.E.M. Unpaired t-test performed, (P**<0.01, P***<0.001).*

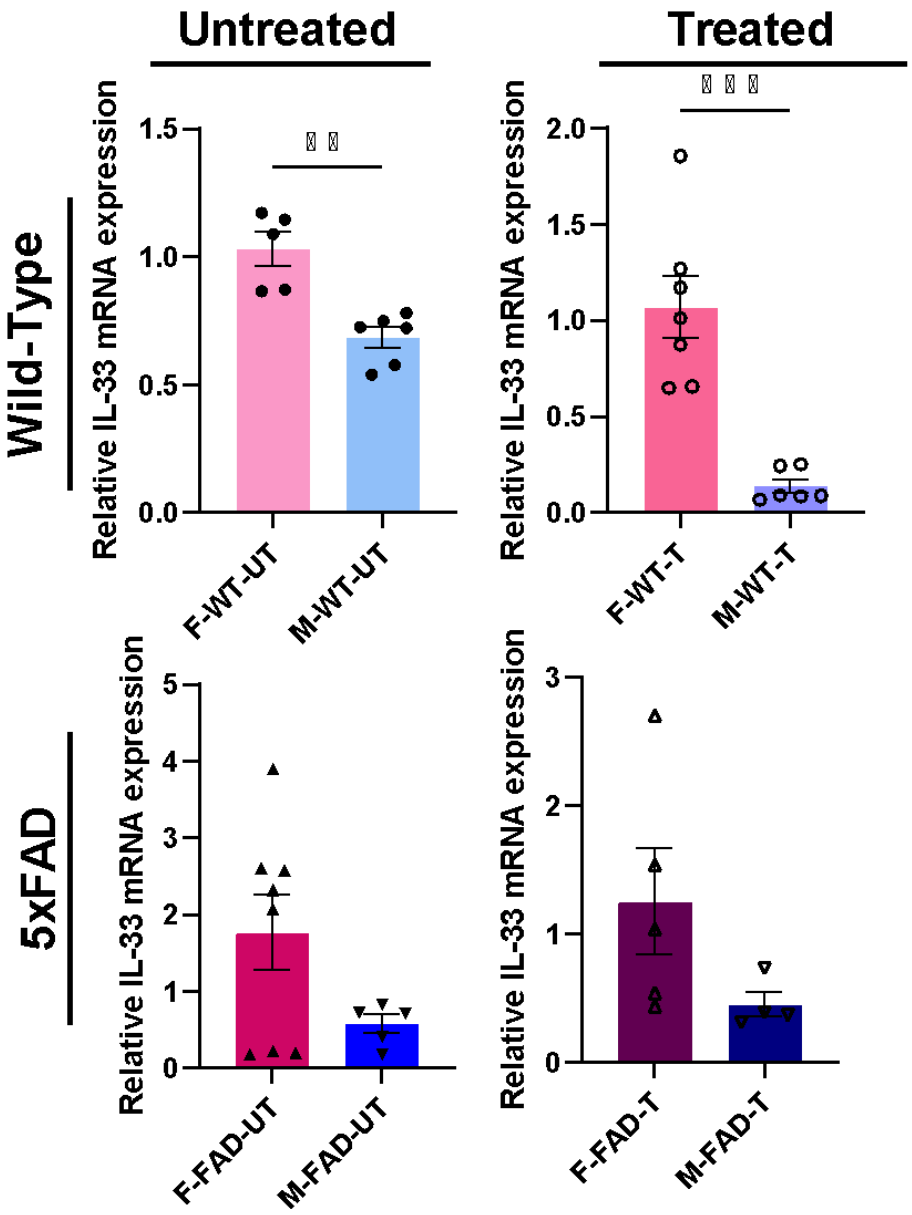

Figure 5.13 Expression of IL33 mRNA in males relative to females from all treatment groups. *CT values from previous experiments were first separated by sex, then male ΔCT values normalised to the average IL33 ΔCT value for the corresponding female group. WT-UT males (n=6) were normalised to WT-UT females (n=5), WT-T males (n=6) were normalised to WT-T females (n=7), Untreated 5xFAD (FAD-UT) males (n=5) were normalised to untreated 5xFAD females (n=8),and treated 5xFAD (FAD-T) males (n=4) were normalised to treated 5xFAD females (n=5). All data shown as mean ± S.E.M. Unpaired t-test performed, (P**<0.01, P***<0.001).*

Next, we investigated the expression levels of microglia-related genes between female and male mice, and their response for the 40Hz treatment. We again first looked at expression of *Gpnmb* mRNA between males and females. We observed no significant differences in gene expression between male and female WT mice that were treated or untreated, nor between treated or untreated 5xFAD animals.

In *Cst7* expression we observed that there was no significant difference between female and male WT mRNA level. After 40Hz treatment both WT and 5xFAD males expressed lower levels of *Cst7* than their female counterparts (P**<0.01, P***<0.001 respectively, Fig 5.14) however the female data for each group exhibited high variation across samples. Untreated male and female 5xFADs showed similar levels of *Cst7* mRNA, suggesting the baseline expression is not different between these two groups. Whilst the results from the single-sex comparisons (Fig 5.8) suggest this is not surprising as treated male 5xFADs downregulated *Cst7* expression while females did not, the data from both treated WTs and 5xFADs suggest that males express lower *Cst7* than females after (but not before) treatment.

In *TMEM119* (Fig 5.15) expression there was no significant differences between male and female WT-UT, WT-T, or 5xFAD-UT groups. 40Hz treated male 5xFADs expressed significantly (P*<0.05) lower *TMEM119* mRNA than treated 5xFAD females. This difference is potentially explained by the very slight (but insignificant) increase in F-FAD-T compared to F-WT-UT mRNA (Fig 5.8G) or the significant decrease in M-FAD-T compared to M-WT-UT (Fig 5.8H). However, given the lack of difference between the WT-UT, WT-T and FAD-UT groups when males were compared to females, it may also be a sex-dimorphic difference induced by the 40Hz light flicker treatment.

In expression of *P2YR12 (*Fig 5.15*)* we observed no differences between female and male in any genotype or treatment group, suggesting this remains consistent between sexes and neither sex responded differently to 40Hz treatment in *P2YR12* mRNA level.

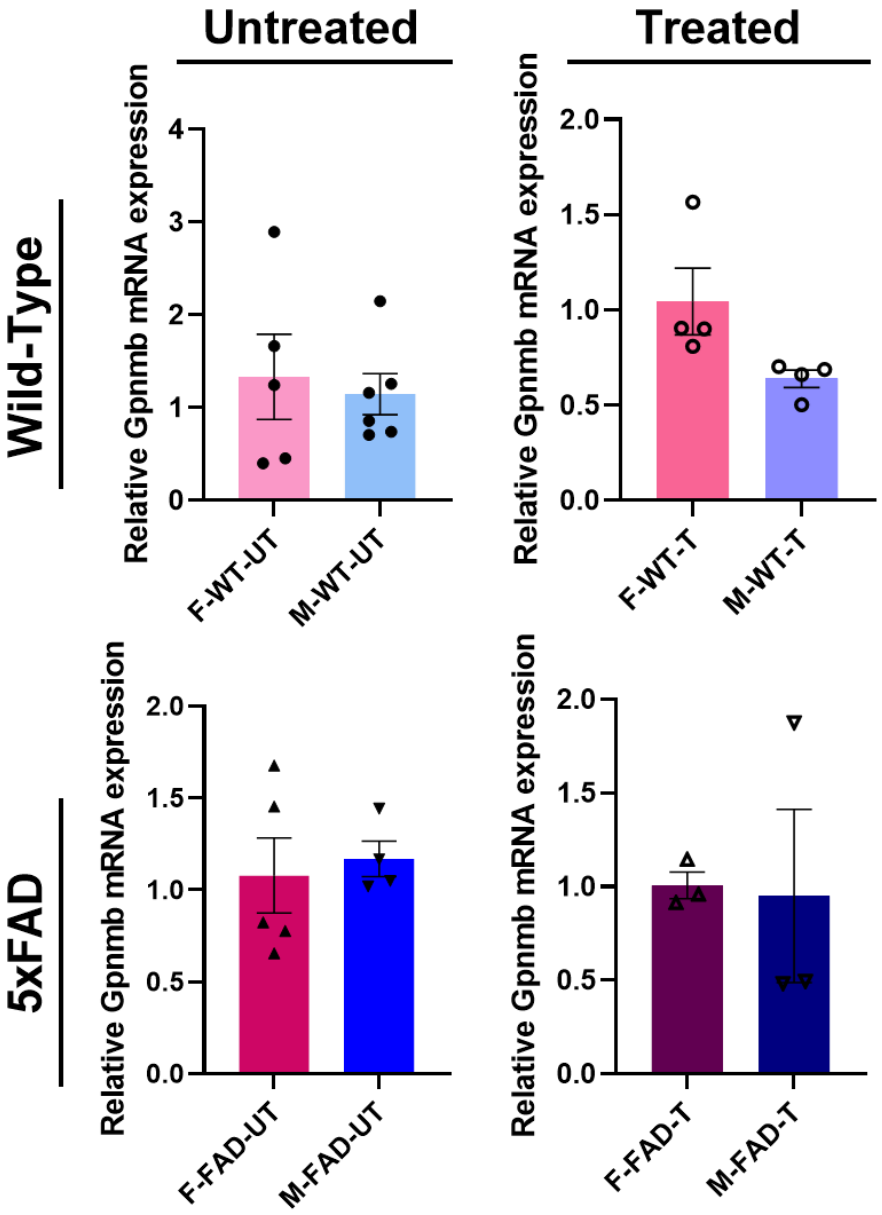

Figure 5.14 Expression of Gpnmb mRNA in males relative to females from all treatment groups. *CT values from previous experiments were first separated by sex, then male ΔCT values normalised to the average Gpnmb ΔCT value for the corresponding female group. WT-UT males (n=6) were normalised to WT-UT females (n=5), WT-T males (n=4) were normalised to WT-T females (n=4), Untreated 5xFAD (FAD-UT) males (n=4) were normalised to untreated 5xFAD females (n=5),and treated 5xFAD (FAD-T) males (n=3) were normalised to treated 5xFAD females (n=3). All data shown as mean ± S.E.M. Unpaired t-test performed, no significant differences found)*

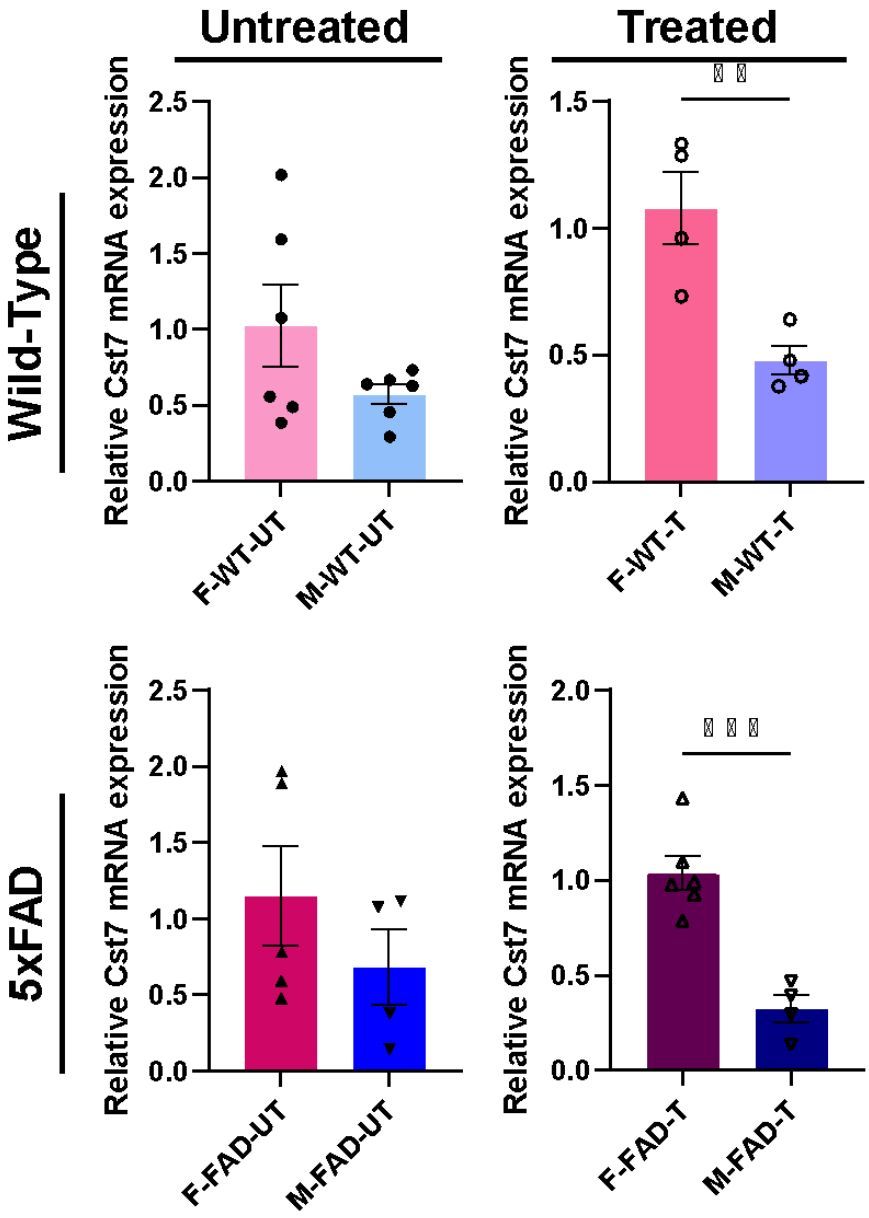

Figure 5.15 Expression of Cst7 mRNA in males relative to females from all treatment groups *CT values from previous experiments were first separated by sex, then male ΔCT values normalised to the average Cst7 ΔCT value for the corresponding female group. WT-UT males (n=6) were normalised to WT-UT females (n=6), WT-T males (n=4) were normalised to WT-T females (n=4), Untreated 5xFAD (FAD-UT) males (n=5) were normalised to untreated 5xFAD females (n=5) and treated 5xFAD (FAD-T) males (n=4) were normalised to treated 5xFAD females (n=6). All data shown as mean ± S.E.M. Unpaired t-test performed, (P**<0.01, P***<0.001)*

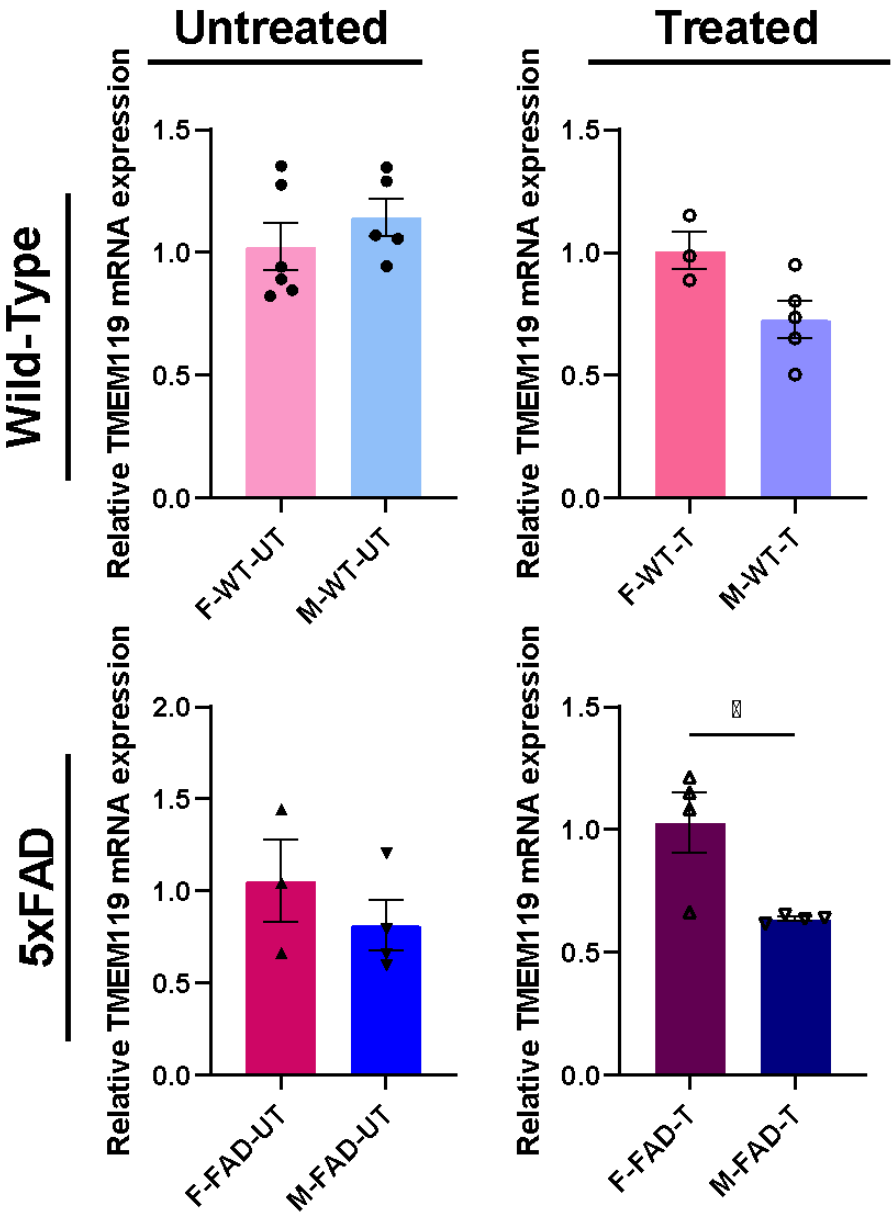

Figure 5.16 Expression of TMEM119 mRNA in males relative to females from all treatment groups. *CT values from previous experiments were first separated by sex, then male ΔCT values normalised to the average Tmem119 ΔCT value for the corresponding female group. WT-UT males (n=5) were normalised to WT-UT females (n=6), WT-T males (n=5) were normalised to WT-T females (n=3), Untreated 5xFAD (FAD-UT) males (n=4) were normalised to untreated 5xFAD females (n=3) and treated 5xFAD (FAD-T) males (n=4) were normalised to treated 5xFAD females (n=4). All data shown as mean ± S.E.M. Unpaired t-test performed, (P*<0.05).*

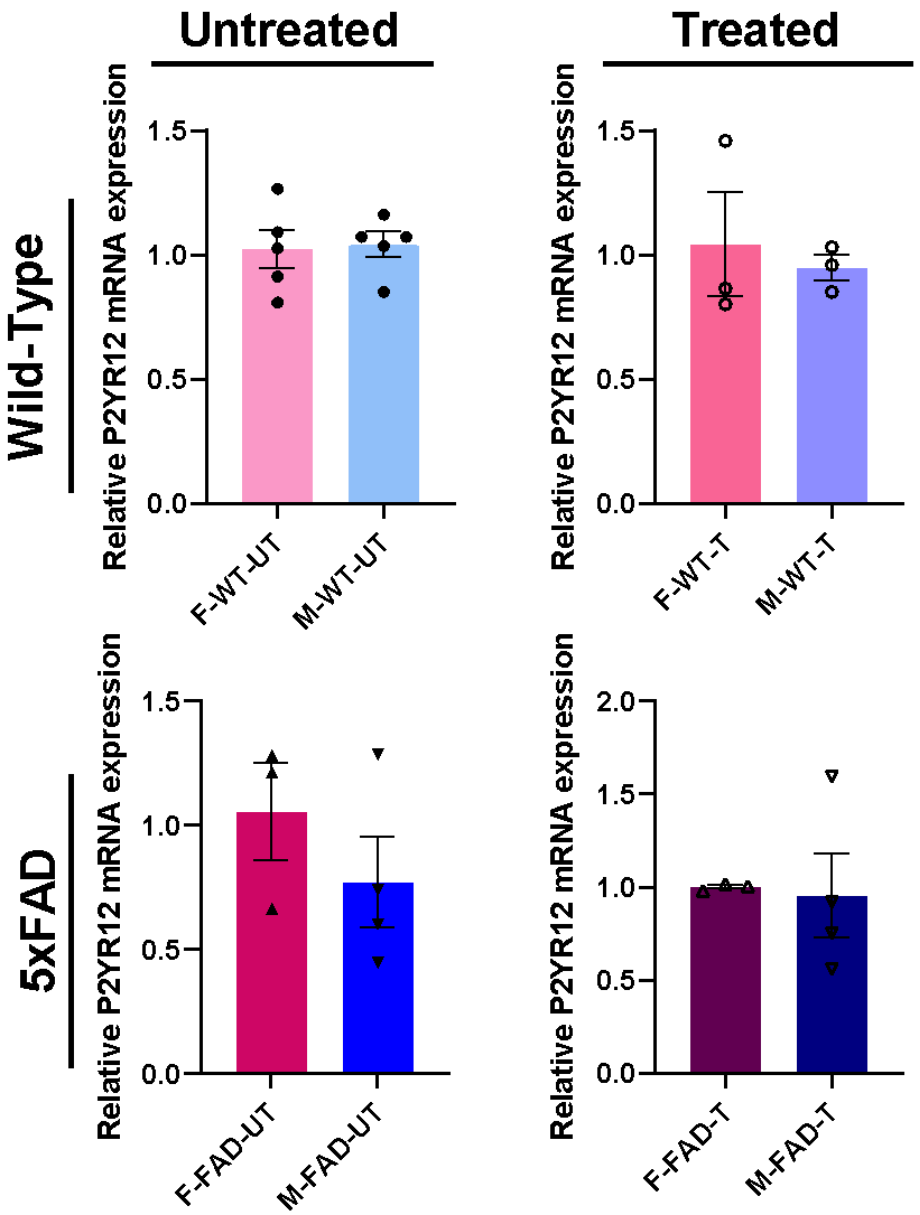

Figure 5.17 Expression of P2Y12 mRNA in males relative to females from all treatment groups. CT values from previous experiments were first separated by sex, then male ΔCT values normalised to the average P2Y12 ΔCT value for the corresponding female group. WT-UT males (n=5) were normalised to WT-UT females (n=5), WT-T males (n=3) were normalised to WT-T females (n=3), Untreated 5xFAD (FAD-UT) males (n=4) were normalised to untreated 5xFAD females (n=3) and treated 5xFAD (FAD-T) males (n=4) were normalised to treated 5xFAD females (n=3). All data shown as mean ± S.E.M. Unpaired t-test performed; no significant differences found.

5.2.4 CD45+ inflammation in 40Hz light flicker treated female and male 5xFAD mice.

As we mentioned previously, inflammation plays a key role in the pathology of AD and given there are innate differences in neuroinflammation between males and females (Beagley and Gockel, 2003) we next decided to compare inflammation between the sexes. Here, we evaluated the level of neuroinflammation by measuring the expression of CD45 in the VC of female (Fig 5.17) and male (Fig 5.18) animals, and their response to 40Hz light treatment.

Qualitatively, images from untreated 5xFAD animals of both genders appeared to show less intense staining, suggesting lower CD45 expression and thus lower inflammation prior to 40Hz treatment. However, after quantification (Fig 5.19) we found that untreated male 5xFAD animals exhibited significantly higher levels of CD45 (P*0.01) than untreated female 5xFADs. After 40Hz light treatment female 5xFAD mice showed no change in CD45 level, while male 5xFAD mice downregulated expression of CD45 compared to untreated controls (P*<0.0456). Overall statistics found that while treatment was not a significant factor, sex and the interaction between sex and treatment were.

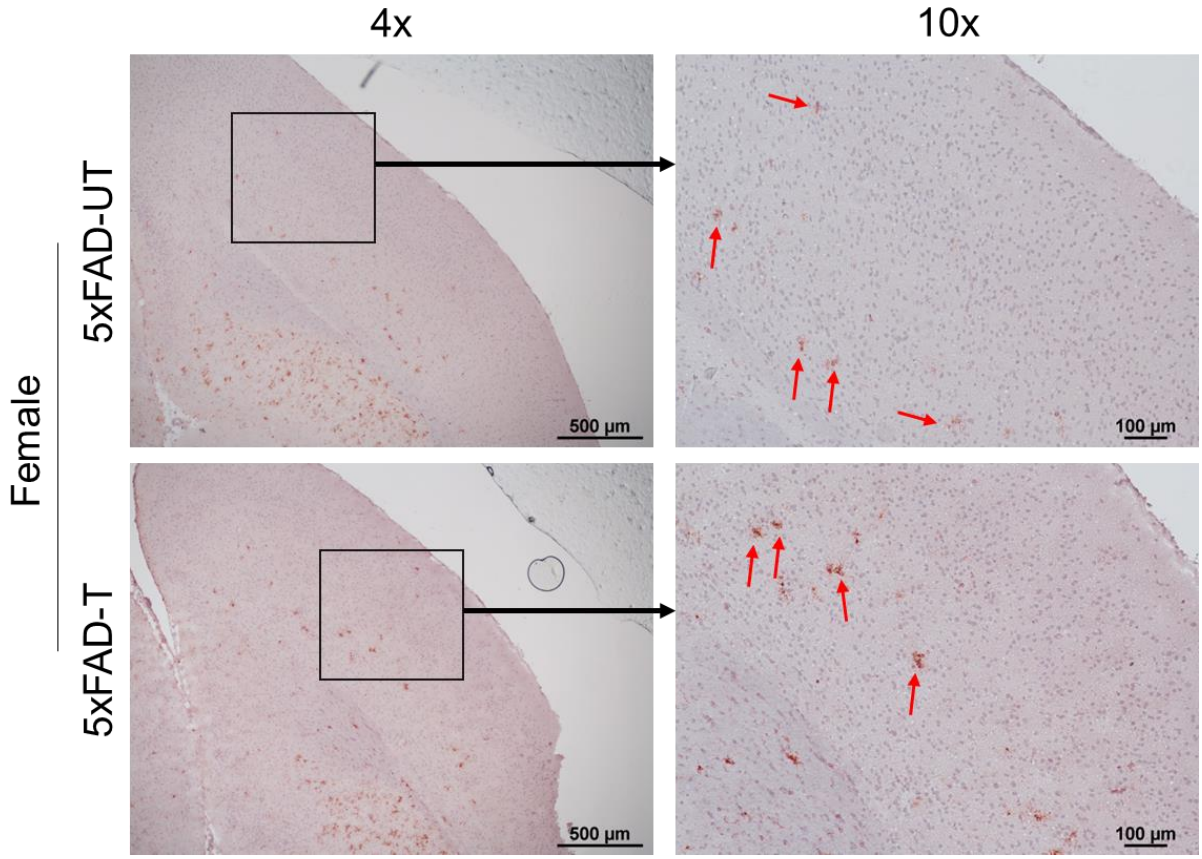

Figure 5.18- Representative CD45 IHC images of the visual cortex of 4-5-month-old female 5xFAD mice after 15 days 40hz light treatment. *5xFAD female animals were exposed to 1 hour of 40Hz light flicker (5xFAD-UT) or 1 hour of darkness (5xFAD-T) for 15 days. Mice were then sacrificed, and brains were removed. Sagittal sections were stained with CD45 antibody, followed by a biotin conjugated antibody and AMEC substrate. Nuclei were stained with haematoxylin. Left column shows representative 4x microscopy images of coronally cut VC, right column shows representative 10x magnification of the highlighted region in VC. Arrows point to CD45+ expression.*

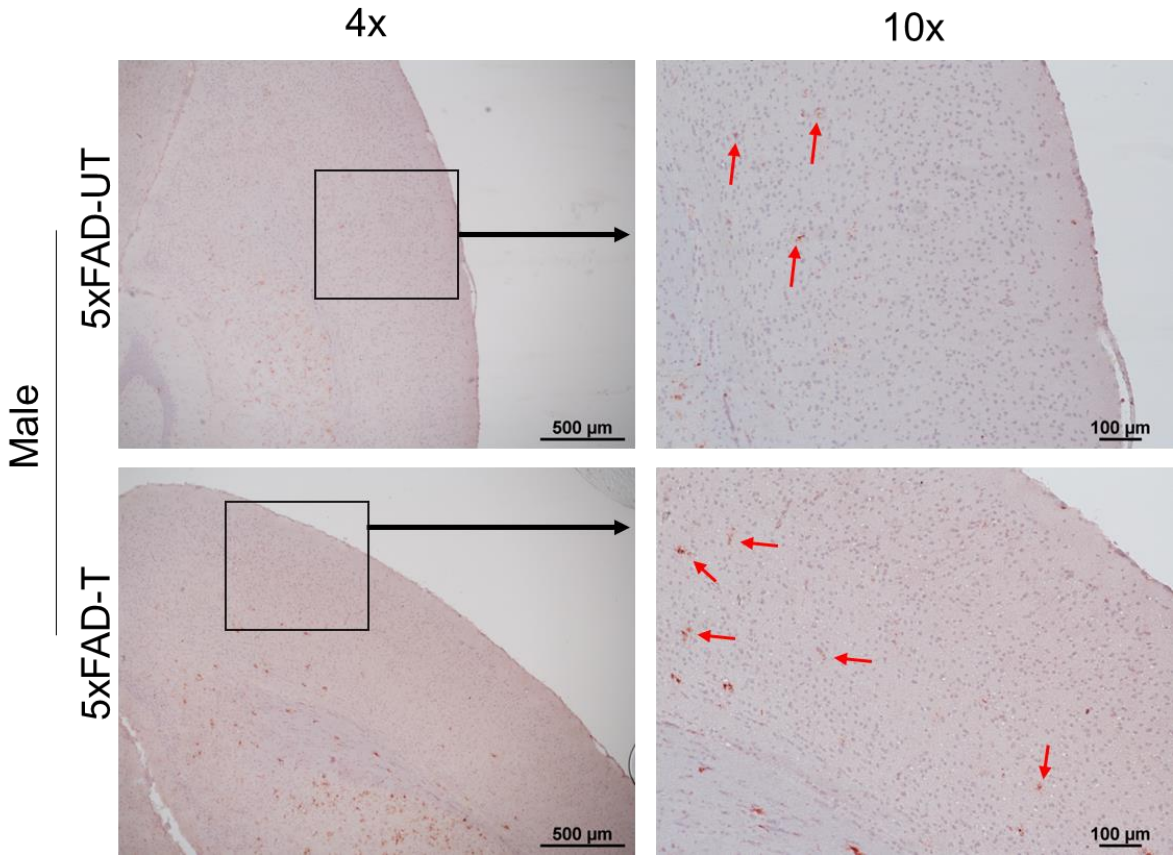

Figure 5.19- Representative CD45 IHC images of the visual cortex of 4-5-month-old male 5xFAD mice after 15 days 40hz light treatment. *5xFAD male animals were exposed to 1 hour of 40Hz light flicker (5xFAD-UT) or 1 hour of darkness (5xFAD-T) for 15 days. Mice were then sacrificed, and brains were removed. Sagittal sections were stained with CD45 antibody, followed by a biotin conjugated antibody and AMEC substrate. Nuclei were stained with haematoxylin. Left column shows representative 4x microscopy images of coronally cut VC, right column shows representative 10x magnification of the highlighted region in VC. Arrows point to CD45+ expression.*

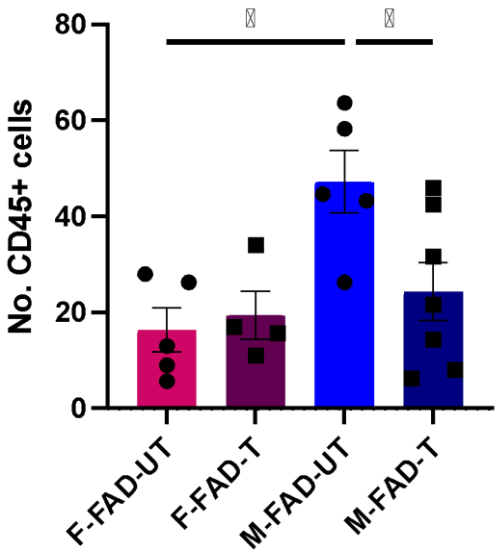

Figure 5.20 – Total number of CD45+ cells in the VC of 4-5-month-old male and female 5xFADs after 15-day 40Hz light treatment. *CD45 cells were stained via IHC using a CD45 primary antibody and 10x magnification images collected using a brightfield microscope, then quantified manually using Qupath software. n= minimum 4 mice per group. Each data point represents 1 mouse, error bars show mean CD45+ cell count* ± S.E.M. *2-way ANOVA performed. Treatment not found to be significant factor (F(1,17=2.7, P=0.1) however sex was significant (F(1,17)=8.8, P=0.009) as was the interaction between sex and treatment (F(1,17)=4.6) p=0.046) Tukey's multiple comparisons found significant differences between F-FAD-UT and M-FAD-UT (P=0.01) and M-FAD-UT and M-FAD-T (P=0.046) (P****<0.0001, P***<0.001).*

5.2.5 Expression of IL-33 and Olig2 in the visual cortex of female and male 5xFAD and WT mice

Next, we sought to determine if there were differences in protein expression of IL-33 and Olig2 between the sexes. IL-33 has been previously suggested to be influenced by sex (Russi *et al.,* 2018) and considering our previous RT-PCR findings of *IL33* mRNA we hypothesised there would be differences in protein expression in the VC between the treatment groups.

Next, we sought to determine if there were differences in protein expression of IL-33 and Olig2 between the sexes. IL-33 has been previously suggested to be influenced by sex (Russi *et al.,* 2018) and considering our previous RT-PCR findings of *IL33* mRNA we hypothesised there would be differences in protein expression in the VC between the treatment groups.

Mice were treated with 40Hz light flicker or spent time in darkness as a control 1 hour per day for 15 days, then sacrificed and brain tissue collected for histology. Tissue samples were co-stained using antibodies for IL-33 and Olig2. We collected our immunofluorescent images then quantified the total number of cells using Qupath cell-counting software. IL-33+ or Olig2+ cells were first quantified on each layer of the VC, then a total calculated.

We first analysed the data from our female animals of WT (Fig 5.20) and 5xFAD (Fig 5.21) mice treated with 40Hz light flicker or darkness controls. No significant difference in total IL-33+ or Olig2+ cell counts in the VC was found between untreated 5xFAD mice and untreated WT controls (Fig 5.22 A,B). However, when we assessed each layer of the VC separately, we found that 5xFAD animals (both treated and untreated) exhibited significantly (Fig 5.23A, P***<0.001) fewer IL-33+ cells than WT controls. A similar pattern of reduced expression in L4 of 5xFAD tissue was observed for Olig2 (Fig 5.23B, P*<0.05).

We next performed the same analysis on data from our male WT (Fig 5.24) and 5xFAD (Fig 5.25) mice. We observed no significant difference in the total number of IL-33+ (Fig 5.26A) or Olig2+ (Fig 5.26B) within the VC between our untreated 5xFAD mice and our untreated WT controls, nor between 40Hz light treated and untreated controls of either genotype.

When we assessed the data from each layer of the VC, we again observed no significant differences in IL-33+ (Fig 5.27A) or Olig2+ (Fig 5.27B) cells in any layer of the VC. Despite the lack of significance, there was a trend of increased IL-33 and Olig2 expression in layers 2/3 in 40hz treated WT male animals, and a slightly increased (but not significant) number of IL-33+ and Olig2+ cells across the entire VC in 40Hz treated WT male animals.

In both males and females we observed the highest levels of IL-33 and Olig2 in the deeper cortical layers 4-6, with lower expression in layers 1-3. Interestingly, the comparison between genotype and treatment showed a small degree of significance in male mice, suggesting the treatment had a small interaction with the expression of both IL-33 and Olig2 varied after treatment within one genotype in males but not in females. Females also showed a higher degree of variation between WT and 5xFAD animals (P=<0.0001).

These data combined suggest that our 40Hz treatment did not have any impact on expression of IL-33 or Olig2 in either WT or 5xFAD males or females. This is surprising considering our findings in *IL33* mRNA expression, and suggests the changes are limited to a post-transcriptional but pre-translational change.

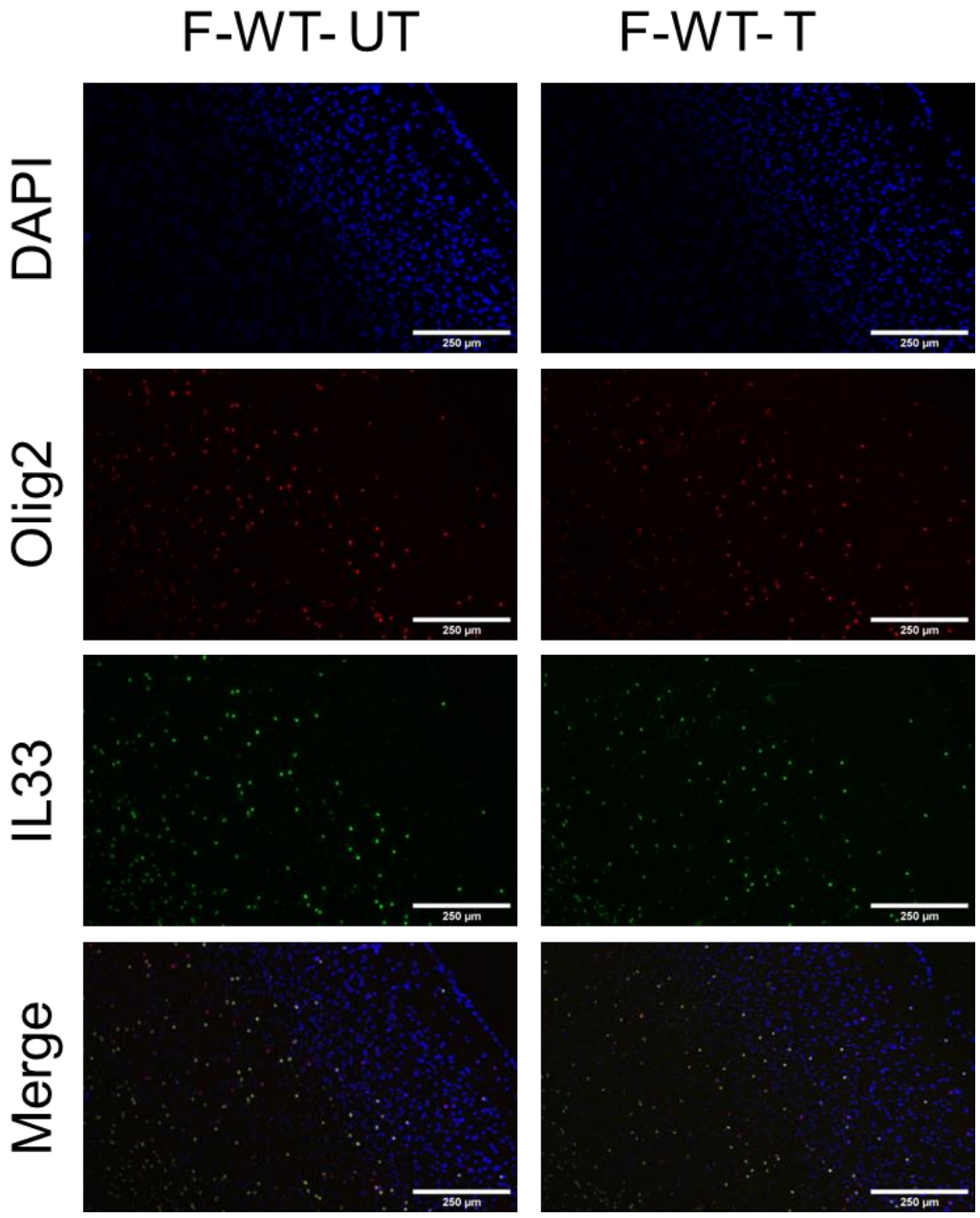

Figure 5.21- Representative IL-33 and Olig2 expression in the visual cortex of treated and untreated female wild-type mice after 15 days of 40Hz treatment. *4-5-month-old female wild-type mice were exposed to 1 hour of 40Hz light flicker (5xWT-T) or 1 hour of darkness (5xWT-UT) for 15 days, then animals were sacrificed, and brains were removed. Sagittal sections of brain tissues at 10µm thickness were immunofluorescence stained using antibodies for IL-33 and Olig2. All images were taken at 10x objective of the visual cortex. Images show representative images for DAPI staining (left), Olig2 (second column), IL-33 (right) and the combined image (right). Scale bar represents 250µm*

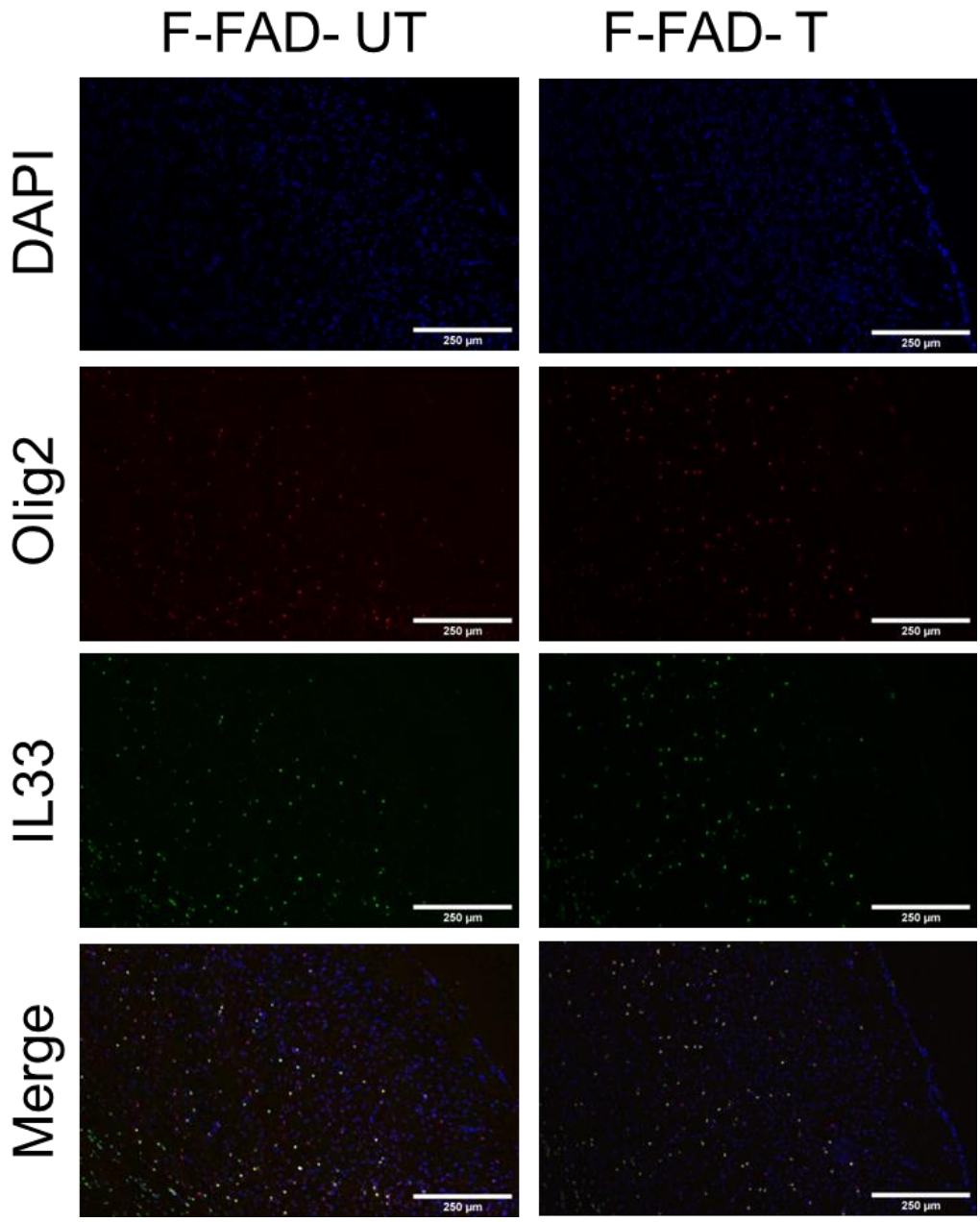

Figure 5.22- Representative IL-33 and Olig2 expression in the visual cortex of treated and untreated female 5xFAD mice after 15 days of 40Hz treatment. *4-5-month-old female 5xFAD mice were exposed to 1 hour of 40Hz light flicker (5xFAD-T) or 1 hour of darkness (5xFAD-UT) for 15 days, then animals were sacrificed, and brains were removed. Sagittal sections of brain tissues at 10µm thickness were immunofluorescence stained using antibodies for IL-33 (green, 488nm) and Olig2 (red, 555nm). All images were taken at 10x objective of the visual cortex. All images were taken at 10x objective of the visual cortex. Images show representative images for DAPI staining (left), Olig2 (second column), IL-33 (right) and the combined image (right). Scale bar represents 250µm.*

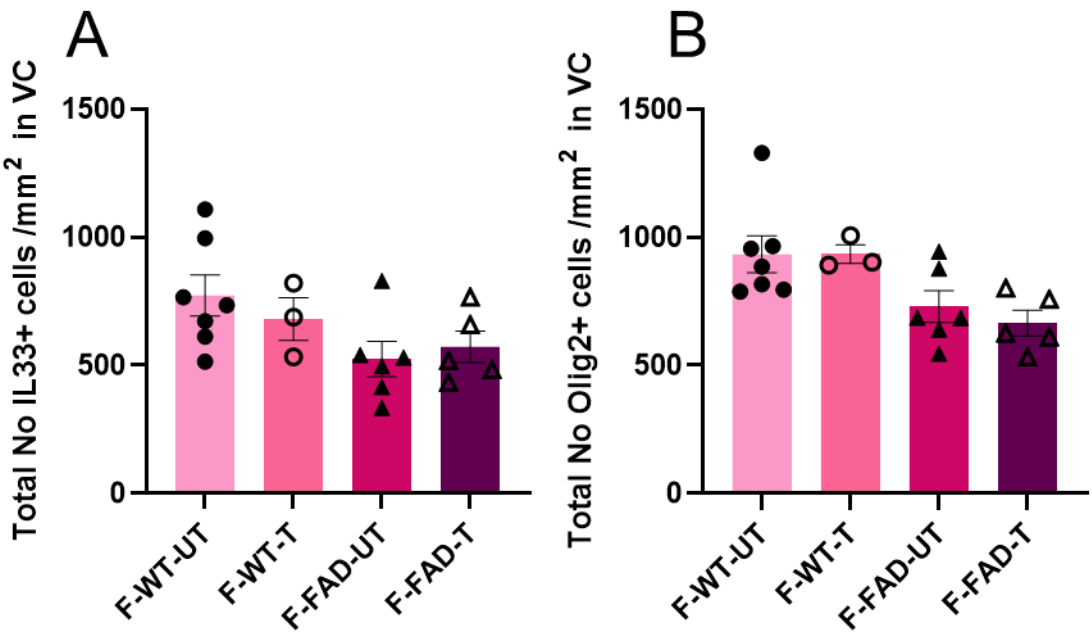

Figure 5.23 – Total number of IL-33+ and Olig2+ cells in the visual cortex of female WT and 5xFAD mice after 15 days of 40Hz light treatment. *5xFAD animals between 4 and 5 months old were treated with 40hz light (WT-T n=3, 5xFAD-T, n=5) or left in dark conditions (WT-UT n=7, 5xFAD-UT, n=6) for 1-hour per day for 15 days over three weeks. Brain tissues were harvested on the day, following the final treatment, and were sectioned for staining with antibodies against IL-33 and Olig2. Immunofluorescence images were taken and the total positive cells for each marker were quantified using Qupath automated cell-counting software* ***A****: Total IL-33+ cells in the whole VC.* ***B****: Total Olig2+ cells in the whole VC. Each data point represents one animal. Data=mean of 3 images per mouse ± S.E.M. Two-way ANOVA with Tukey's multiple corrections performed. A: Genotype: F(1,17)=4.9, P=0.04. B: Genotype: F(1,17)=11.7, P=0.003.*

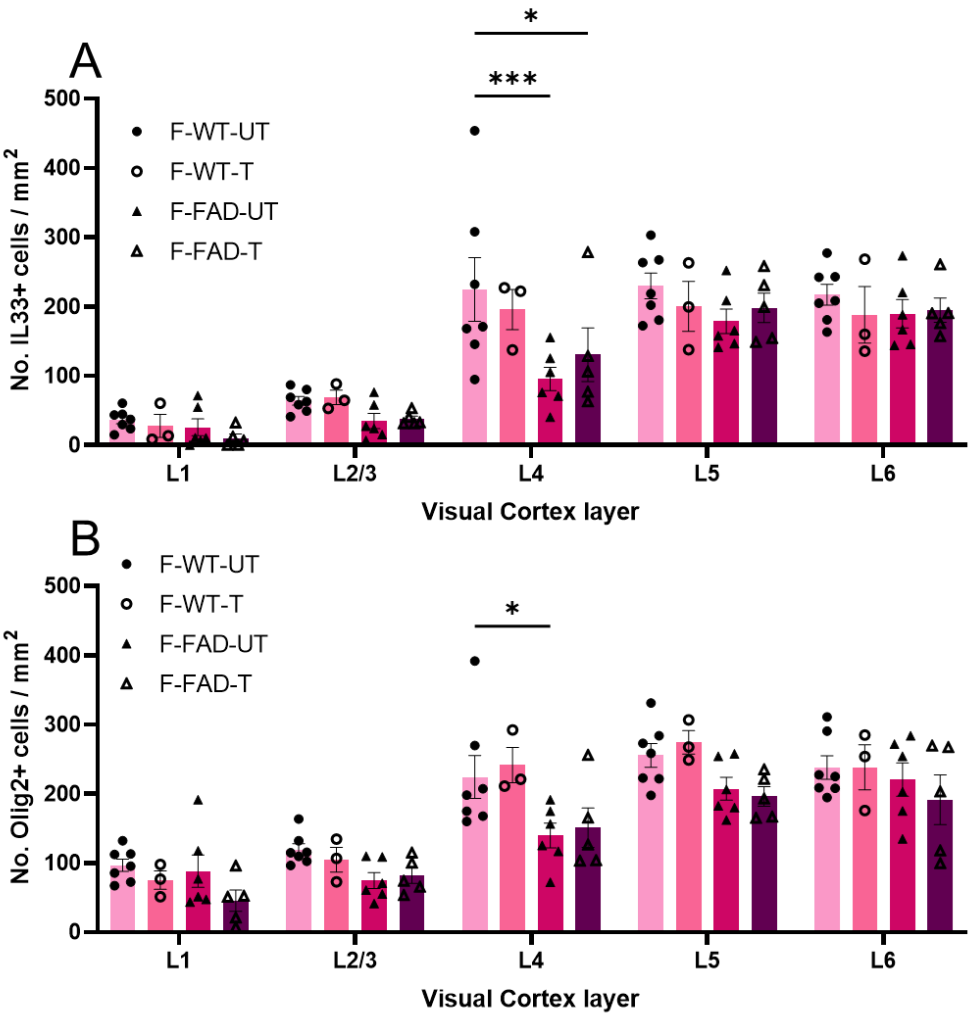

Figure 5.24 – Number of IL-33+ and Olig2+ cells in each layer of the visual cortex of female WT and 5xFAD mice after 15 days of 40Hz light treatment. *Female 5xFAD animals between 4 and 5 months old were treated with 40hz light (WT-T n=3, 5xFAD-T, n=5) or left in dark conditions (WT-UT n=7, 5xFAD-UT, n=6) for 1-hour per day for 15 days over three weeks. Brain tissues were harvested on the day, following the final treatment, and were sectioned for staining with antibodies against IL-33 and Olig2. Immunofluorescence images were taken and the total positive cells for each marker were quantified using Qupath automated cell-counting software* ***A****: Total IL-33+ cells in each layer of the VC.* ***B****: Total Olig2+ cells in each layer of the VC. Each data point represents one animal. Data=mean of 3 images per mouse ± S.E.M. Three-way ANOVA with Tukey's multiple comparisons performed. A: Genotype: F(1,85)=11.38, P=0.0011. B: Genotype: F(1,85)=22.94, P=<0.001. (p*<0.05, p***<0.001**).*

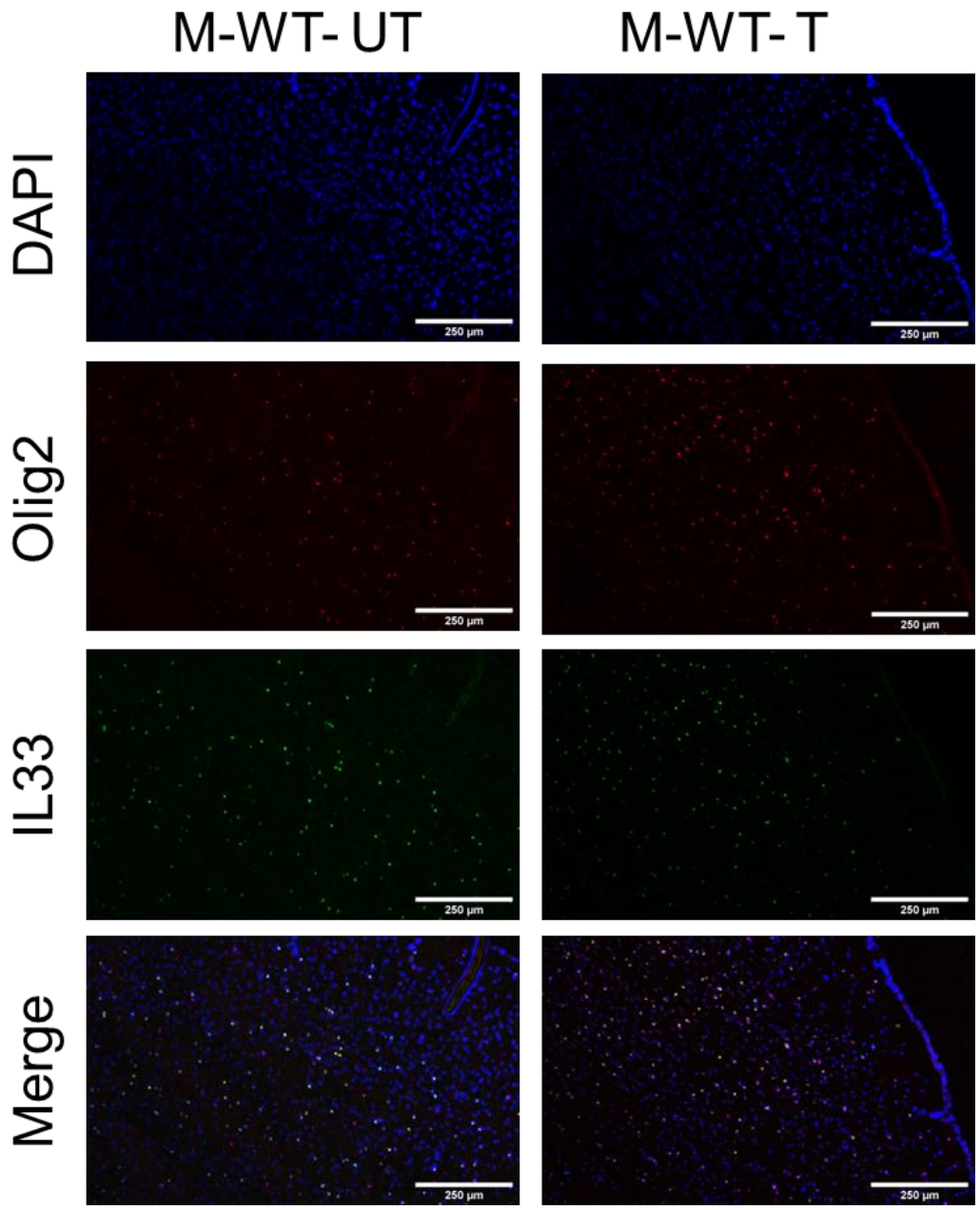

Figure 5.25- Representative IL-33 and Olig2 expression in the visual cortex of treated and untreated male wild-type mice after 15 days of 40Hz treatment. *4-5-month-old male wild-type mice were exposed to 1 hour of 40Hz light flicker (5xWT-T) or 1 hour of darkness (5xWT-UT) for 15 days, then animals were sacrificed, and brains were removed. Sagittal sections of brain tissues at 10µm thickness were immunofluorescence stained using antibodies for IL-33 (green, 488nm) and Olig2 (red, 555nm). All images were taken at 10x objective of the visual cortex. Images show representative images for DAPI staining (left), Olig2 (second column), IL-33 (right) and the combined image (right). Scale bar represents 250µm*

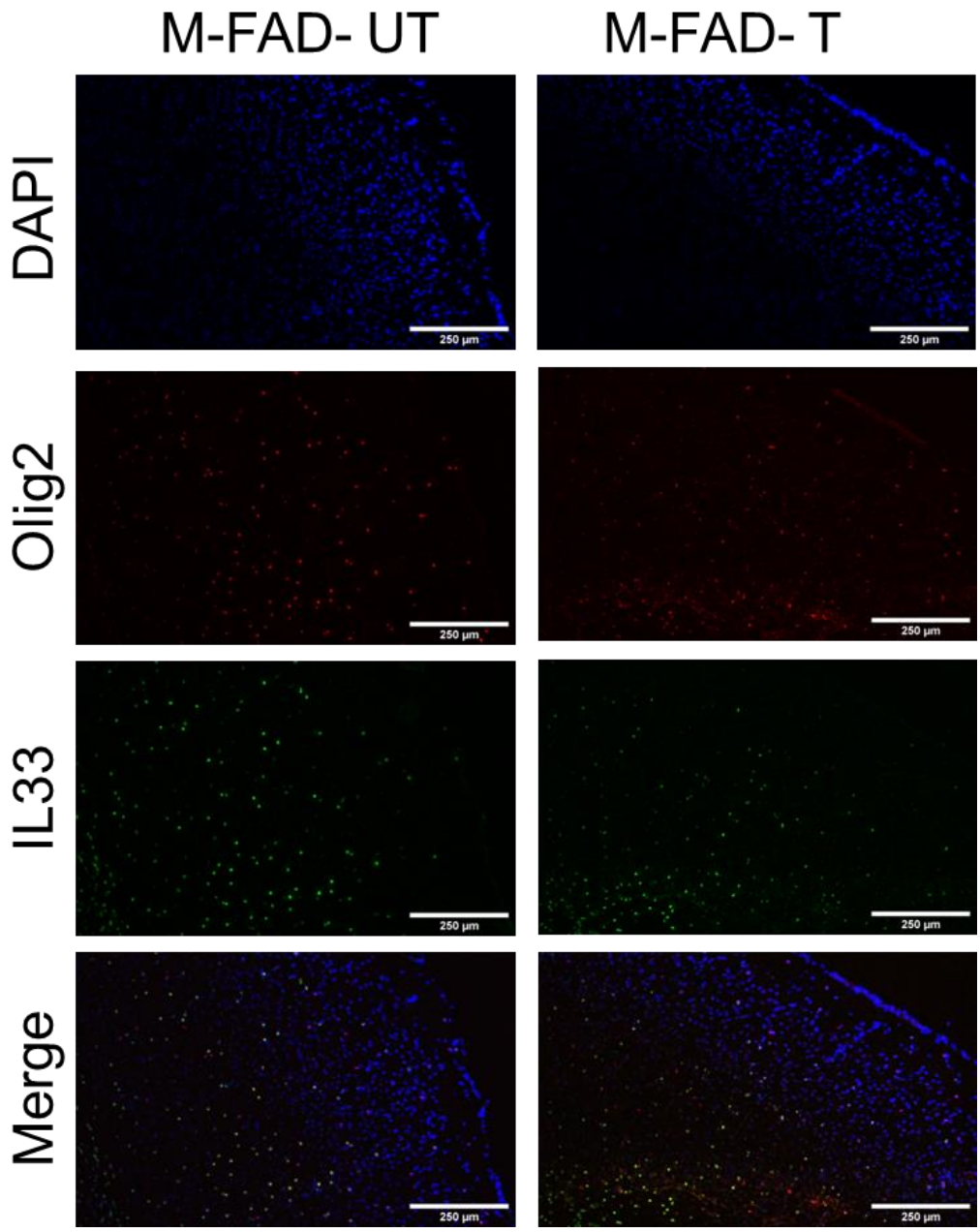

Figure 5.26- Representative IL-33 and Olig2 expression in the visual cortex of treated and untreated male 5xFAD mice after 15 days of 40Hz treatment. *4-5-month-old male 5xFAD mice were exposed to 1 hour of 40Hz light flicker (5xFAD-T) or 1 hour of darkness (5xFAD-UT) for 15 days, then animals were sacrificed, and brains were removed. Sagittal sections of brain tissues at 10µm thickness were immunofluorescence stained using antibodies for IL-33 (green, 488nm) and Olig2 (red, 555nm). All images were taken at 10x objective of the visual cortex. Images show representative images for DAPI staining (left), Olig2 (second column), IL-33 (right) and the combined image (right). Scale bar represents 250µm.*

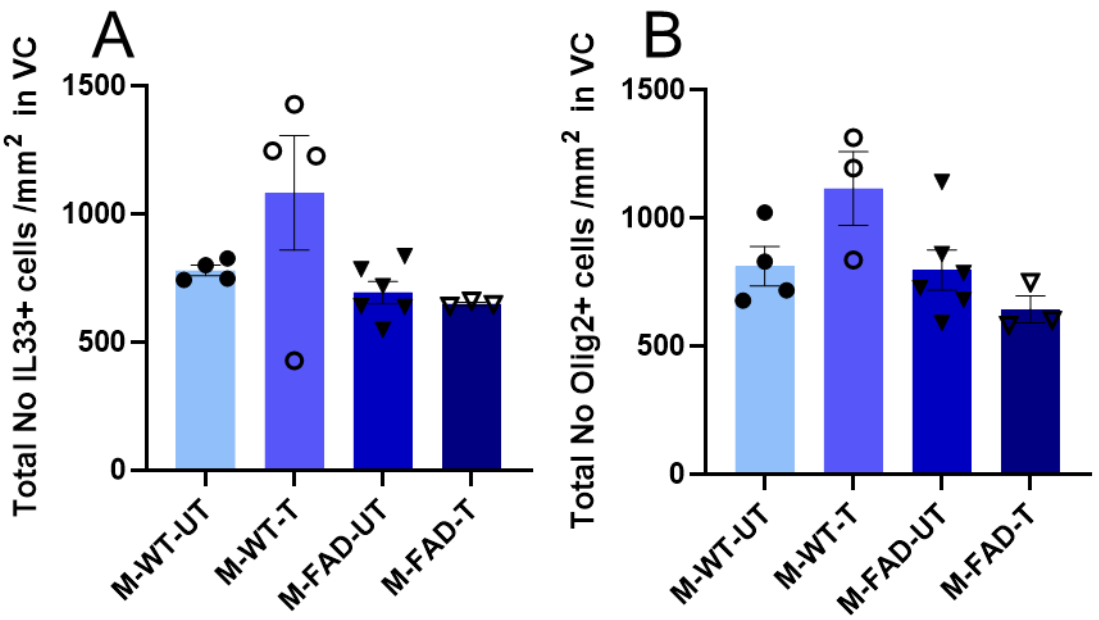

Figure 5.27 – Number of IL33+ and Olig2+ cells in the visual cortex of male WT and 5xFAD mice after 15 days of 40Hz light treatment. *Male 5xFAD animals between 4 and 5 months old were treated with 40hz light (WT-T n=4, 5xFAD-T, n=3) or left in dark conditions (WT-UT n=4, 5xFAD-UT, n=6) for 1-hour per day for 15 days over three weeks. Brain tissues were harvested on the day, following the final treatment, and were sectioned for staining with antibodies against IL-33 and Olig2. Immunofluorescence images were taken and the total positive cells for each marker were quantified using Qupath automated cell-counting software* ***A****: Total IL-33+ cells in the whole VC.* ***B****: Total Olig2+ cells in the whole VC. Each data point represents one animal. Data= mean of 3 images per mouse ± S.E.M. Two-way ANOVA with Tukey's multiple comparisons performed. A: Genotype: F(1,13)=5.3, P=0.038 B: Genotype: F(1,12)=6.7, P=0.0241).*

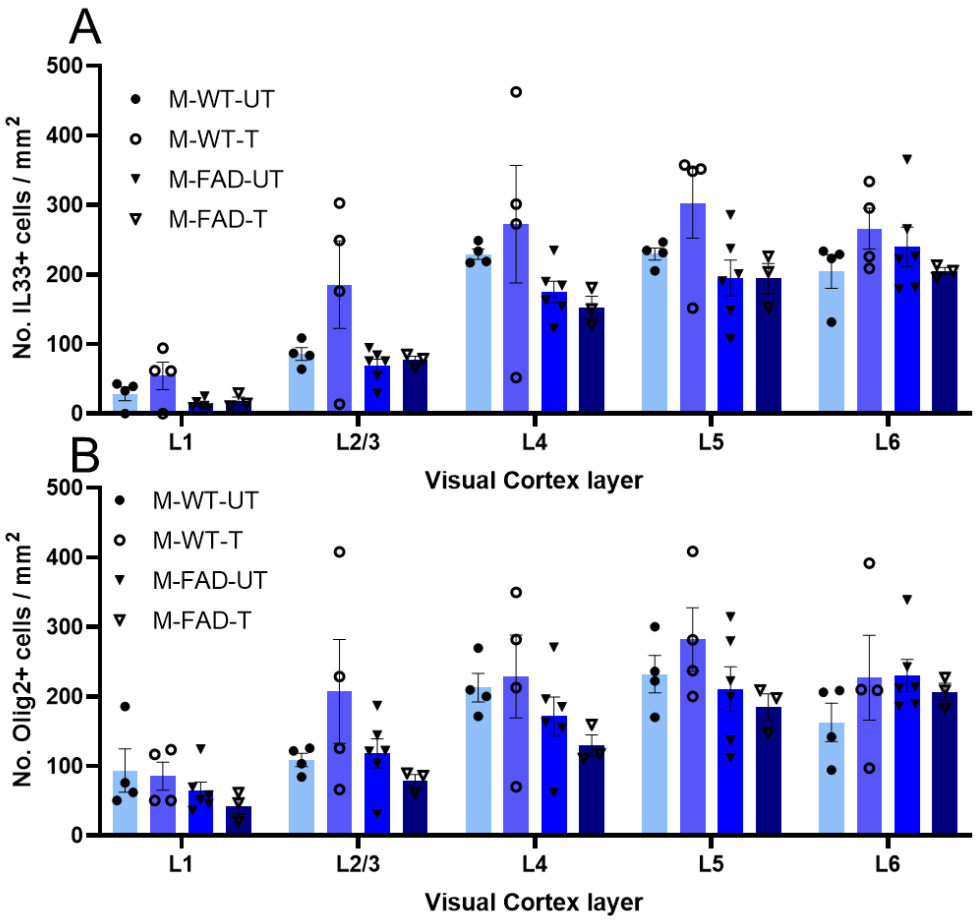

Figure 5.28 – Number of IL-33+ and Olig2+ cells in the visual cortex of male WT and 5xFAD mice after 15 days of 40Hz light treatment. *Male 5xFAD animals between 4 and 5 months old were treated with 40hz light (WT-T n=4, 5xFAD-T, n=3) or left in dark conditions (WT-UT n=4, 5xFAD-UT, n=6) for 1-hour per day for 15 days over three weeks. Brain tissues were harvested on the day, following the final treatment, and were sectioned for staining with antibodies against IL-33 and Olig2. Immunofluorescence images were taken and the total positive cells for each marker were quantified using Qupath automated cell-counting software* ***A****: Total IL-33+ cells in each layer of the VC.* ***B****: Total Olig2+ cells in each layer of the VC. Each data point represents one animal. Data=mean of 3 images per mouse ± S.E.M. Three-way ANOVA with Tukey's multiple comparisons performed. A: Genotype: F(1,65)=14.10, P=0.0004. Genotype x treatment: F(1,65)= 6.3, P=0.014. B: Genotype: F(1,65)=14.10, P=0.004. Genotype x treatment: F(1,65)=6.3, P=0.01*

5.3 Discussion

AD is the leading cause of death in women in the UK (Alzheimer's Research UK, 2015). AD disproportionately affects women through a number of suggested mechanisms and displays a clear sexual dimorphism affected by hormones and innate biological differences between men and women. However, precise mechanisms remain unknown and the area of research into sex-based responses is a relatively new one. Thus, it is essential that research focuses not only on treatment, but also on how both biological sexes respond to treatment, to further inform potential clinical studies in humans.

In this thesis we used both male and female animals in our experiments so we could study any sexually dimorphic responses to the 40Hz light flicker treatment as well as innate differences between the sexes that may explain some aspects of the disparity in AD prevalence between men and women.

5.3.1 Differences in Aβ expression in the brain between sexes

5.3.1.1 Aβ in the whole brain

We began by analysing the data from male and female animals, including sex as an additional factor. We observed no significant changes in expression of Aβ 1-40 or Aβ 1-42 after treatment in 5xFADs in either males or females. This suggests that the data in previous chapters combined results remained accurate and that the 40Hz light flicker was unable to affect Aβ burden across the entire brain regardless of sex.

We next compared the data from males and females to each other, across each treatment group. We observed that there was no difference in expression of Aβ 1-40, or Aβ 1-42 in wild-type animals (although there was a slight pattern of male WTs expressing higher Aβ 1-42 this did not reach significance). However, when 5xFAD animals were compared we found that both treated and untreated female 5xFADs exhibited significantly more Aβ 1-40 than their male counterparts, in keeping with published works (Oakley *et al.,* 2006; Bundy *et al.,* 2019) We also observed that 5xFAD animals exhibit significantly more Aβ 1-42 than Aβ 1-40 in both sexes, also in keeping with published work. However, we observed no significant difference in Aβ 1-42 between untreated 5xFAD males and females, only in treated 5xFADs did we see the significantly lower results from males than females.

Despite the fact that our 40Hz light treatment did not reduce Aβ expression in the brain “at-large” all of our ELISA results were in keeping with previously published results, further confirming our model was working as expected and that our females were expressing the more severe AD pathology than males, as is well established.

5.3.1.2 Aβ expression in the visual cortex of male and female 5xFAD animals treated with 40Hz-light flicker for 15 days.

Having established that our ELISA data did not exhibit significant differences, we next separated the Aβ histological data from the VC to determine if the 40Hz flicker affected the Aβ levels in the VC of either sex differently.

First, we looked at the Aβ coverage between sexes. Both male and female 5xFADs exhibited higher Aβ deposition within the deep cortical layers (L5 & L6). However, neither sex showed a significant decrease in Aβ after 40Hz light treatment when measured in each individual layer, or as a total in the VC. The most likely explanation for this lack of significance is the reduced statistical power than comes from separating the data points into individual sexes. While no results reached statistical significance, there was still a trend towards reduced Aβ in 40Hz light treated male and female 5xFAD mice in deep cortical layers, but not in superficial layers 1-3. We then measured the number of plaques separated by sex. There was no significant difference in the number of plaques after 40Hz light treatment in 5xFADs, nor did males and females exhibit significantly different number of plaques in any layer of the VC. In both sexes the highest Aβ burden and number of plaques were the deep cortical layer 5 and 6.

These data combined with our ELISA data suggest that while female 5xFAD animals exhibit higher total Aβ deposition across the whole brain, they do not exhibit significantly higher levels of Aβ, nor higher numbers of Aβ plaques in the VC when compared to males. It also confirms that the 40Hz light flicker treatment did not affect Aβ deposition in either sex differently. Interestingly, the total number of plaques remained unchanged after treatment, despite a trend towards reducing Aβ. We suggest that while the treatment was unable to completely eliminate any of the plaques, the plaques that were present were slightly smaller in 40Hz treated mice. Iaccarino et.al found that their 40Hz treatment reduced both plaque number and

plaque size- however this experiment used only male animals aged 6 months and treated for a continuous time period. These differences in method may explain the differences in our results.

5.3.2 Sex-based differences in gene expression

Although our Aβ measurements did not show any significant reduction when separated by sex, we hypothesised that females and males would respond differently to 40Hz light treatment on a post-transcriptional, pre-translational level- given the innate differences between males and females.

5.3.2.1 Aβ pathway genes PSEN1, mAPP, and BACE1.

To begin we analysed the differences in sex-based response to 40Hz light flicker treatment within the Aβ processing pathway.

The γ-secretase protein PSEN1 has previously been shown to be downregulated by estrogen in human glial cells (Csöregh Nord *et al.,* 2010) and within the mouse cerebellum (Ghosh and Thakur, 2008) suggesting this gene is regulated in a sexually-dimorphic fashion.

We found that *PSEN1*, showed a similar pattern between males and females, where untreated 5xFAD animals showed significantly higher *PSEN1* expression than WT-UT controls, and this was reduced to non-significant after 40Hz light treatment. Both male and female 5xFADs responded with a decrease in expression after 40Hz light treatment, suggesting that expression of *PSEN1* was not affected by sex in our study. Neither our study nor previous publications accounted for conversion of testosterone into estrogen via aromatase activity, so while PSEN1 is regulated by sex hormones it is implied that both males and females show a similar pattern of regulation- something our data also suggests.

We also observed that untreated female WTs expressed significantly more *PSEN1* than their male counterparts, though this difference in expression was not found in 5xFADs. This difference has been previously shown in WT rats (Piscopo *et al.,* 2013) and WT mice (Placanica, Zhu and Li, 2009) and shows a sex-based difference in the APP processing pathway in animals out-with disease conditions.

mAPP showed a similar pattern, though with some sexual dimorphism. Female 5xFAD animals showed a decreased level of *mAPP* expression compared to WT-UT females. After 40Hz light treatment, the levels of *mAPP* in female 5xFADs was then increased to become comparable to the WT-UT expression. Male 5xFADs however displayed equivalent level of *mAPP* to their WT-UT counterparts. After 40Hz light treatment this expression was highly significantly increased. When we directly compared male animals to their respective female counterparts, we found that while there was no different in *mAPP* expression in WTs between males and females, and female 5xFAD animals consistently expressed lower *mAPP* than their male counterparts. Given that *mAPP* has been shown to regulate Aβ deposition in other AD mouse models (Steffen *et al.,* 2017), this decrease in female 5xFADs may contribute to the more severe pathology observed in female AD models (Sil *et al.,* 2022).Unfortunately, there is very limited information available on mAPP as it is a relatively new area of research, and thus there are even fewer studies into the effects of sex on gene *mAPP* expression. This makes our findings somewhat novel and improves on our understanding of the impact of sex in the 5xFAD model.

In *Bace1* we found a stark contrast between males and females after treatment. Female 5xFAD animals displayed a level of *Bace1* that was comparable to untreated WTs, suggesting that *BACE1* mRNA expression is not affected by the transgenic mutations in female animals. In contrast to this, male 5xFAD animals showed slightly higher levels of *BACE1* compared to male untreated WTs. When we further compared male mRNA expression to the equivalent female group, we found that both treated and untreated male 5xFADs express significantly higher *BACE1* levels than their female counterparts. This is in keeping with published findings which suggest that BACE1 expression is affected by estrogen levels (Placanica, Zhu and Li, 2009).The response to 40Hz light flicker in *Bace1* expression was also sexually dimorphic. While female 5xFADs downregulated *Bace1* after treatment, males appeared to slightly increase *BACE1* (though not significantly) in response to treatment.

Lower estrogen in female patients and AD mouse models has been associated with increased Aβ deposition (Yue *et al.,* 2005) and further studies suggest that estrogens regulate BACE1 expression (Cui *et al.,* 2022). Testosterone (specifically testosterone not converted into estrogen via aromatase) in male mouse models has also been shown to regulate BACE1 expression (McAllister *et al.,* 2010) , while age-related

reduced testosterone has been linked with increased AD risk (Bianchi, 2022).These studies emphasise that *BACE1* is regulated through sex-specific mechanisms. While unexpected, If the 40Hz light treatment affected sex-hormone expression within the brain, it may explain the sex-dimorphic response to the treatment. Indeed, recent studies have shown that men and women express different responses to and preferences to light levels and wavelength (Chellappa *et al.,* 2017) which may also apply to mice.

We have shown that our 40Hz light treatment affected the Aβ processing pathway in a sexually dimorphic pattern, with *mAPP* and *PSEN1* showing similar patterns between the sexes, but *BACE1* showing a sex-based difference in response. This difference may expand upon our current understand of why women have higher incidence of AD, but the complex relationship between biological sex and these 3 genes needs to be expanded to cover humans.

5.3.2.2 Expression of *IL33* mRNA

Previous publications have established that IL-33 responses are regulated by sex-hormones androgen and estrogen both in the peripheral body (Vasanthakumar *et al.,* 2020) and within the CNS (Russi *et al.,* 2018). A recent study into IL-33 administration in an AD mouse model also used animals of both sexes but did not investigate if this response was affected by the sex of the animal. (Amy K.Y. Fu *et al.,* 2016). Having established that in our combined data we saw a response to 40Hz light in both WT and 5xFAD animals, we next sought to determine if the groupings observed in our data were caused by sexually-dimorphic changes in *IL33* mRNA expression.

Surprisingly, we found that the highest level of *IL33* dimorphism in response to 40Hz light treatment was in WT animals. Female WT animals significantly upregulated *IL33* mRNA, and males showed a trend upward - though this was not significant. When we directly compared these groups, the females of both treated and untreated WTs expressed significantly more *IL33* than their male counterparts. This difference in response to the light treatment in WT C57BL/6 animals suggests a sexually dimorphic response in *IL33* expression.

In contrast, 5xFAD animals showed significantly more *IL33* mRNA than WT-UT controls in both sexes, in keeping with published findings. (Liang *et al.,* 2020) Both 40Hz treated and untreated female 5xFADs expressed slightly more *IL33* when compared

to male counterparts, but the high degree of variation in their results meant the difference did not reach significance. While there was a slight trend towards reduced *IL33* mRNA expression after 40Hz treatment of 5xFAD mice, this did not reach significance in either sex.

From these data we have shown that 40Hz light flicker changes expression of IL-33 mRNA, and these changes display a sex-based dimorphism. This is perhaps unsurprising, given the evidence that IL-33 is closely linked to hormone expression, but suggests a role for IL33 in the effects of the 40Hz light flicker.

5.4.2.3 Sexually dimorphic expression of *Cst7* mRNA after 40Hz light flicker treatment

Cst7 is upregulated in AD models in DAMs and has been shown to play a sexually dimorphic role in microglial regulation in an APP mutation mouse model. This published study found that *Cst7* was upregulated more highly in female animals than in males. When the *Cst7* gene was knocked-out, female animals exhibited higher Aβ burden, while males exhibited reduced inflammation but no change in Aβ burden. We therefore hypothesised that the response in *Cst7* expression to the 40Hz light flicker would also be sexually dimorphic.

Interestingly, we found that our baseline 5xFAD females did not exhibit significantly higher levels of *Cst7* (though there was a slight difference) which is in contrast to the previous studies. However, after 40Hz light-flicker treatment our female 5xFADs exhibited no change in *Cst7* mRNA, while the males showed a significant decrease. In the 2022 study (D Daniels *et al.,* 2022), deletion of *Cst7* resulted in a lower inflammatory profile in male mice (measured by a decrease in transcripts for inflammatory cytokines such as *Il1b*, *Cscl2* and *tnf*) therefore it is within reason to suggest that our males may also have decrease inflammation after 40Hz treatment.

When we directly compared mRNA levels between males and females of corresponding treatment groups, we found that females in both treatment groups exhibited significantly higher levels of *Cst7* mRNA than their male counterparts, despite finding no significant changes in treated WTs when compared to their sex-corresponding WT-UT groups. It is possible that the 40Hz flicker decreased *Cst7*

expression in WT males, or further increased in WT females such that the difference reached significance.

5.3.2.4 Expression of TMEM119 and P2Y12 *mRNA*

P2YR12 has been shown to exhibit some sexual-dimorphism in C57BL/6 mice previously (D Daniels *et al.,* 2022) where it peaked in both sexes at 4 months, but then rapidly decreased in males after 4 months. Another study in mice found that P2YR12 is more highly expressed in males than females, suggesting male microglia may be more mobile and responsive to Aβ. We hypothesised that our males would increase P2YR12 in response to 40Hz treatment, however we observed no significant differences in our male groups. Instead, we found it was female 5xFADs who upregulated P2YR12 after 40Hz treatment. This may explain how both groups showed a slight decrease in Aβ, but through different mechanisms.

In contrast, TMEM119 only showed a significant change in male animals relatively to male WT-UT animals. We observed that all groups (WT-T, 5xFAD and 40Hz treated 5xFAD) showed reduced TMEM119 mRNA expression relative to the WT-UT controls. This suggests that the 40Hz treatment reduced WT-T levels to equivalent of 5xFADs but did not lower the expression in 5xFADs. This is of interest given that TMEM119 is considered a “homeostatic” marker, and previous studies into sex-based microglia marker expression suggest that TMEM119 is upregulated more in female AD model mice than in males (Guillot-Sestier *et al.,* 2021).

5.3.3 40Hz treatment reduced CD45+ Inflammation only in male animals

In CD45 expression we again found sexual-dimorphism in responses. We observed that our untreated male 5xFAD animals expressed significantly more CD45+ cells than our female untreated 5xFAD animals, and that this increased expression was reduced after 40Hz light flicker treatment.

Previous studies have found that microglia increase CD45 expression when in close proximity to Aβ plaques and is associated with increased phagocytosis of plaques by microglia and macrophages (Zhu *et al.,* 2011). Studies into other inflammatory brain conditions such as traumatic brain injury have shown that males animals expressed higher CD45+ cell responses (Doran *et al.,* 2019), which is in agreement with our findings.

Our findings of decreased CD45+ cell numbers is in agreement with findings from the lab which published the original 40Hz findings, though the sex of the animals used for this original finding is unclear (Iaccarino, Annabelle C. Singer, *et al.,* 2016). This is further evidence that we successfully replicated some aspects of this study, however the reduction only being found in male mice is further evidence that the response to 40Hz treatment expresses sexual-dimorphism.

5.3.4 Expression of IL-33 and OLIG2 protein unchanged in the VC by 40Hz light flicker

We showed in the previous chapter that there were no significant differences in IL-33 or Olig2 protein expression within the VC after 40Hz light treatment, however we also found significant differences between 5xFAD and WT animals. We therefore sought to determine if this difference was influenced by sex.

Interestingly, we found that there were differences when the data was analysed separately. We found that IL-33 expression layer 4 of the VC was only significantly reduced in female 5xFADs relative to female WT-UT, but not in males. While differences in expression of IL-33 between sexes in the CNS have been previously reported (Rurak *et al.,* 2022) these differences were in early stages of development and were not expressed in adulthood. There is very limited data on sex-based differences in IL-33 expression within the CNS- however studies have been conducted outwith the CNS focusing mainly on peripheral immune cells. Several studies have shown that testosterone induces immune cells (mast cells (Russi *et al.,* 2018) and innate lymphoid cells (Blanquart *et al.,* 2022) to release type 2 cytokines (regulatory) as opposed to type 1 (inflammatory).

Similarly, there is little data available on the effects of estrogens and androgens on the primary visual cortex in mice. One available study found that L2/3 of the audio cortex expressed the highest levels of estrogen receptors (Tremere *et al.,* 2011) and the distribution of estrogen and androgen receptors across specific brain regions have been shown to be sex-dependent.

5.4.5 Overall conclusions

We first showed the same well-documented differences in Aβ 1-40 and Aβ 1-42 expression between male and female 5xFAD mice. While our 40Hz treatment did not affect whole brain Aβ expression, this confirmed our animal model was in keeping with published findings. We next showed that 40Hz light treatment did not exhibit sex-based differences in the reduction of Aβ in the VC. While these results did not reach significance once split by sex, it is likely this is the result of reduced statistical power from reduced n-numbers for the data set.

We next showed that gene expression in C57BL/6 and 5xFAD mice was sexually dimorphic. We observed increased expression of *PSEN1* and *IL33* in our female WT animals when compared to our males. In untreated 5xFADs we observed that male animals expressed higher *mAPP* and *BACE1* than females but decreased *IL33* relative to females.

We then found that 40Hz treatment induces changes in gene expression in both WT and 5xFAD mice, and these changes are sex-dependent. While female WT animals upregulated IL33 mRNA after treatment, male WTs did not. Male WTs decreased expression of TMEM119 after 40Hz light treatment while females showed no changes.

In our 5xFAD mice we observed that only females showed reduction in *PSEN1* and *BACE1* after 40Hz treatment, while only male mice reduced expression of *Cst7*. We also found that 5xFADs of both sexes upregulated *mAPP* expression after treatment.

In protein measurement we found male 5xFADs reduced CD45+ cells in the VC after 40Hz treatment while females did not, however we found no differences in Olig2 and IL-33 expression before or after treatment in either 5xFAD or WT animals.

Overall, we found that 40Hz light treatment appears to have the same outcome (slightly reduced Aβ) but through different mechanisms depending on the sex of the animal. These differences in expression and response to 40Hz light may have many complex explanations.

Firstly, female animals are more subject to stress (Marrocco *et al.,* 2017), and while we took every step possible to limit the stress in our animals it is possible that our female animals responded less favourably to the treatment procedure. Indeed, it was observed that female animals took considerably longer (approx. 2 weeks) than males

(approx. 3 days) to habituate to handling and transfer into experimental chambers (though these observations were recorded it was not quantifiable). Increased stress in our females could have potentially altered our findings. Female animals also have an estrous cycle which affects estrogen level, which were not measured throughout this study. Given the impact of estrogen on IL-33 and other markers previously discussed, it is possible this was a factor. However, mice were used at age points regardless of their estrus cycle.

The final potential difference-and the most likely- is the largest; the innate differences in brain circuitry and chemical signalling between males and females. In both humans (Krolick, Zhu and Shi, 2018) and mice (Khaliulin, Kartawy and Amal, 2020) there are differences in neurotransmission, gamma oscillations (Pu *et al.,* 2020) and immune signalling (Osborne, Turano and Schwarz, 2018) all of which affect gene expression and the inflammatory profile of the brain. We have shown that male and female 5xFAD animals responded to 40Hz light flicker differently. We also showed innate differences in WT animals between sexes which have not been reported previously.

5.5 Limitations

One key limitation of this chapter was our inability to measure the expression of hormone levels in the brain. The processing of our brain samples for Aβ ELISA used guanidine hydrochloride, and this made the samples unsuitable for use with other ELISA targets. Ideally, we would have measured the expression of androgens and estrogens within the CNS to allow us to measure their correlation with gene and protein expression.

Similarly, the oestrus cycles of our female animals was not tracked. In future studies, after the female animals are sacrificed a vaginal swab should be performed (Byers *et al.,* 2012) and analysed so the stage of oestrus can be accounted for in analysis. This should be done after sacrificing the animal to prevent undue stress which may affect results. It may also be of interest to determine the effectiveness of 40Hz light flicker at different stages of oestrus.

As with previous chapters, mRNA data is limited in that the relationship between mRNA level and protein expression is not yet fully understood. While we have shown changes in gene expression these do not necessarily translate to protein changes.

Due to limited numbers of animals with data points for multiple genes we were also unable to perform the correlation analysis between genes. This would have been of particular interest, as we suspect the correlation of *IL33* and AD genes *PSEN1*, *mAPP* and *BACE1* is heavily impacted by sex.

Chapter 6
Final Discussion

6. General discussion.

AD is a chronic neurodegenerative disease which, as our population ages with new medical advancements, is becoming more of a significant problem both economically and individually. There are currently no therapies which target multiple pathologies of the disease with the majority of treatments aimed at managing symptoms such as depression and anxiety or excitatory signalling. The few treatments that do exist are currently experimental, and still only target one aspect of the disease. There is therefore a dire need to develop new treatments and understand the mechanisms of these treatments to help us further understand this disease.

Previous reports stated that gamma-oscillatory treatments (via sound or light) are capable of reducing Aβ burden in the brains of several mouse models of AD, though the underlying mechanisms of this were unclear. However, the treatment appeared to stimulate microglia cells to clear the plaques, suggesting the response was mediated by the neuroimmune system.

This project aimed to investigate the effectiveness of a 40Hz light flicker treatment in modulating neuroimmune cell activity to reduce Aβ burden in AD-model mice and determine the pathways through which these changes occur. The study used a 5xFAD model exhibiting 5 mutations in APP processing and the γ-secretase protein PSEN1, using both male and female animals to determine sex-based responses to the treatment as well as innate differences in gene expression between the two. This study was limited to the immunological factors and did not focus on the neural circuitry, or any changes induced in neurons.

6.1 Effect of 40Hz gamma oscillatory light treatment on Aβ pathology in 5xFAD mice

Our first goal was to confirm the results as reported by Iaccarino et.al however our study used a few changes to the original methods. Primarily, we used both male and female animals in comparison to the original study which appear to use only male animals- this was done to determine if males and females would respond differently to the treatment, given the differences in pathology between the sexes. We also had alterations to the treatment method in terms of the administration chambers.

We first attempted the treatment in 9-month-old animals for 1 hour a day for 5 days (Chapter 3, section 2) or 15 days (Chapter 3, section 3) due to the COVID-19

lockdown. We observed no significant reduction of Aβ in any region of the brain analysed for either treatment duration. As previous reports from Iaccarino et al used male 5xFAD animals at 6 months old old and administered 40Hz treatment for 1hr a day for 7 days, while Marotell et.al used 1 hr a day of auditory and visual 40Hz stimulation in 6-month-old 5xFAD males. We hypothesised our lack of changes induced by 40Hz gamma was likely due to the advanced age of our animals, where pathology is too severe to be affected by the light and associated oscillations (Oakley *et al.,* 2006). We therefore investigated the effect of treatment in female and male mice aged 4-5 months.

It was in these younger mice we successfully replicated the Aβ reduction-measured by histology- though our hypothesis was correct in that the reduction was significantly less than originally published. We also did not observe the reduction in Aβ plaque count (Chapter 4, Figure 4.4). Regardless however, even without the PV-Cre mutation, the 40Hz light flicker treatment appears to have modestly reduced the Aβ burden in the VC only. In similar published data, the light flicker alone was insufficient to affect deeper brain regions such as the hippocampus.

Since this project began, other groups have published negative findings from using the 40Hz stimulation protocol published by Tsai et.al. In 2023 Soula et.al published an attempted replication, which stated they found no changes in plaque count, changes in microglia nor the reduced Aβ 1-40/42 after 40Hz stimulation (Soula *et al.,* 2023). They investigated using 5xFAD mice at 4 and 7 months old of both sexes, and measured Aβ burden, gamma entrainment in the brain and microglia changes across several AD models, measuring the plaque size before and after 7 days of 40Hz treatment to determine changes in individual animals induced by the treatment and reported that after multiple replicates there were no significant changes, contrasting with the original publication and our own findings.

While our findings showed a significant (albeit small) reduction in total Aβ coverage after 16 days of daily one hour treatment, the significant reduction of Aβ was limited only to the VC and did not affect the overall number of plaques in the VC or in any other brain region. Our data was also highly variable, and it is possible this significant reduction was an artifact induced by the inherent variability of animal research- as Soula et al suggested of their own findings. Even though our reduction in Aβ may not be a “true” finding, the changes in mRNA expression are considerable and suggest

that the treatment was still causing some changes, albeit only at a post-transcriptional level.

The findings are therefore controversial- does 40Hz stimulation truly offer a potential non-invasive therapy for AD? Studies have already begun into human responses to 40Hz, finding that 40Hz light flicker can indeed cause changes in the brain (Zhang *et al.,* 2021) and in AD patients caused changes in sleep patterns (Cimenser *et al.,* 2021), helping to restore the normal sleeping pattern which is interrupted in AD. In one small study of 9 human participants, improvements in mood and cognitive scoring were observed after 40Hz audio stimulation (Sharpe *et al.,* 2020). We did not observe any significant changes in behaviour of our animals, though constant observation was not performed after the animals were returned to their home cages- therefore it is possible there was a change that we could not measure in the 2-hour daily window. These publications suggest there is still potential for this treatment even if it does not directly impact the Aβ burden, although significantly more research should be conducted into this field given the variation in published findings.

6.2 Post-transcriptional changes were induced by 40Hz light flicker treatment and were sex dependent.

Despite the controversy surrounding this treatment, we did observe interesting changes in mRNA expression of genes involved in the Aβ processing pathway which suggest how 40Hz light flicker may inducing changes to Aβ protein levels- although it is important to note that changes in mRNA expression do not necessarily result in changes in protein expression (Liu, Beyer and Aebersold, 2016).The mechanism of these changes in gene expression remains unclear, though is most likely induced via the optical nerve pathway through the LGN. However, it may also involve circadian regulation of gene expression as the treatment is light based and the circadian rhythm is highly responsive to changes in light exposure. Regardless, these findings are novel and expand our understanding of the impact of the 40Hz light flicker on gene transcription.

We observed changes to key genes in the amyloid processing pathway, showing the 40Hz light had a post-translational but pre-transcriptional effect on gene expression. Light has long been known to regulate gene expression in cortical layers (Nedivi *et al.,* 1996) and regulate the circadian rhythm- the internal clock that regulates gene

expression and cell behaviour (Saeed and Abbott, 2017) Previous studies suggested that the 40Hz light flicker directly impacted expression of circadian clock genes in the SCN (Yao *et al.,* 2020) however this is the first evidence of the 40Hz light flicker directly affecting genes in the APP-pathway within the VC. While this may be good news, it is important to note that changes in genes with multiple functions (such as PSEN1) may result in unforeseen downstream consequences, given PSEN1s suspected roles in cell differentiation and division.

We found differences in both WT and 5xFAD animals in *IL33* mRNA expression. The increase from WTs and decrease from 5xFADs suggest that the 40Hz light treatment has differential effects depending on the inflammatory profile of the brain prior to treatment- this will need to be considered prior to exposing individuals to the light therapy.
Given the extensive role each of the genes investigated plays in homeostatic neuronal function, changes in these may have long-term consequences beyond reduction in Aβ- long term observation may be advisable to determine if these are transient changes or if these have effects on other neurological function.

6.3 Sex differences in AD, 5xFAD mice and response to 40Hz treatment.

AD is a disease that is affected by both estrogen and testosterone and affects more women than men- thus there appears to be a sex-based risk factor. Despite this, the majority of studies in mouse-models of AD only used male animals (Waters and Laitner, 2021). We used both male and female animals to investigate any innate differences caused by biological sex and any differences in response to the 40Hz light flicker treatment as we suspected the innate differences in neuroinflammation between sexes (Osborne, Turano and Schwarz, 2018).

By using both sexes in our study we found differing responses from our males and females in specific genes- namely *Bace1* and *Cst7*. While there are previous reports that both of these genes express sex-dependent expression (Cui *et al.,* 2022; Baleviciute and Keane, 2023) the response of these genes to 40Hz light flicker has never been previously documented, making our findings here novel. These previous publications also help to explain our findings given that expression of these proteins are dependent on sex-hormones, and specifically seem to affect microglia function. What is interesting however, is that we still observed slight decreases in Aβ in both sexes

despite these differences, suggesting that despite the divergence in gene expression between sexes after 40Hz light treatment, the end result was the same. This points to a mechanism that may explain the higher prevalence of AD in female patients than males and is an interesting point of further research.

6.4 Limitations

This research study was heavily impacted by the COVID-19 pandemic which limited access to animals, resources, and lab-work. Our original experimental plan was significantly altered, and the entire outcome of the thesis revised. Our original plan was to use 6-month-old animals and investigate the effects of auditory treatment, however as 5xFAD lose a significant portion of their hearing by 9 months old we had to use a light-based treatment instead. Upon our return to the University, we were limited to working weekdays, thus our use of 15-day treatment over a 3-week period in contrast to other publications uninterrupted treatment regimen. Future studies would ideally not have interruptions in the treatment schedule, as Iaccarino et.al showed the reduction in Aβ they observed was transient and returned to expected levels within 24 hours after 40Hz treatment.

One intrinsic limitation is the use of an animal model- however exposing patients to experimental treatment and then “harvesting” brain tissue is, obviously, not an option. We used a 5xFAD mouse model which only displays one aspect of AD pathology (rapid Aβ deposition) and so we are limited to measuring the effects of 40Hz light on this single aspect of the disease.

Finally, due to time constraints and limited access, we were unable to experiment using other frequency oscillations as a control. The previous studies used other frequencies (10Hz, random Hz, 80Hz etc) to confirm the 40Hz frequency was the one inducing changes, however in this thesis it would have been useful to include as a control to similarly confirm the changes were not being induced by any of the treatment setup. Similarly, due to schedule conflicts and timing we were unable to arrange training for the surgical procedure required to install the headcaps to the animal required to monitor the brain oscillations. This would have confirmed if that 40Hz light treatment was inducing the gamma oscillations in the animals- although it’s worth observing this would have been performed in a much smaller subset of the animals.

6.5 Future work and directions

The administration of 40Hz light treatment has many variables to consider given the complexity of this treatment method, and the limitations of this study. There are therefore many unexplored directions in which this research could be taken further.

The first potential angle would be to further investigate the sex-based differences in response to the treatment. Future experiments should check the oestrus cycle via vaginal swab after culling the animal, so stage in the cycle can be accounted for in estrogen expression. CNS levels of both mRNA (PCR or RNA-seq) and protein (Immunoblotting / ELISA / metabolomics) levels of estrogen and androgen can then be checked to determine if the 40Hz treatment was indeed causing changes in this. Whilst we checked for evidence of stress by assessing changes in weight induced by treatment, cortisol levels should also be checked to determine if either sex (or all animals) were experiencing measurable stress from the treatment.

Given the multiple variables in this study, there are also several directions in changing the duration of the light exposure (which may be cumulative in its effect and lead to longer-lasting results), the frequency and wavelength of the light (which may require optimisation based on human or animal subjects) and the intensity of the light (which again may require optimisation between humans and animals, particularly nocturnal animals which are light sensitive). The age of the animals should also be closely considered, as the ideal treatment for AD would begin before symptoms begin to show, as by that stage pathology is already severe. If this treatment is incapable of treating older animals, it would be interesting to see how treating very young animals over an extended time period would affect the development of their disease as well as any other downstream effects from chronic treatment. Studies using alternative mouse models exhibiting different pathologies and gene mutations could also expand on our understanding of how this treatment affects different genetic mutations and pathologies of AD. This study used 5xFAD mice which exhibit 5 mutations- 3 APP mutations (KM670/671NL, 1716V, V717I) and 2 PSEN1 mutations (M146L, L286V) (M.Hall and D.Roberson, 2009). Further studies could use tauopathy models such as 3xTG mice which have mutations on APP (KM60/671NL), MAPT (P301L) and PSEN1 (m146v) or single mutation models. There are a wide variety of mouse models expressing transgenic or knock-in mutations of AD and expanding our knowledge on how the 40Hz treatment affects different mutations would provide to more effective

treatment of patients who express widely different mutations leading to the same disease. While previous groups have studied APP/PS1 and Tau P301s models, there remains more mutations in models which could be used to develop our understanding of this treatment.

Another potential study could investigate the intra-cellular signalling pathways involved in the 40Hz responses. As previously discussed there appears to be an interplay between IL-33, PSEN1, BACE1 and notch signalling and Nf-κb signalling. By further expanding on our understanding of how these proteins and genes interact we may be able to further understand the role of IL-33 in AD and develop further insight into treating the disease. A metabolomic or proteomic analysis may of significant interest to unravel changes in metabolism in the CNS induced by 40Hz light flicker.

Finally, studies to elucidate the innate differences in brain circuitry may shed some light on the different responses we observed between the sexes to 40Hz light flicker treatment. There is evidence that males and females have inherently different circuitry induced by expression of sex-hormones. This is evident from responses to stress (Furman, Tsoory and Chen, 2022), circadian rhythms (Duffy *et al.,* 2011), working memory (Hill, Laird and Robinson, 2014) and immune responses (Osborne, Turano and Schwarz, 2018) all of which have a profound impact on the brain. This is a very broad, and yet relatively new area of research, with the NIH only requiring that sex be considered as a biological variable in 2015 and so there is still much to be done to fully understand the differences in circuitry and pathways in male and female brains.

6.6 Final thoughts

The administration of 40Hz light flicker remains highly controversial within the field. This study was an attempt at replication of previous work, and a further exploration into changes in gene expression and sex-based differences in response.

This treatment would have provided an ideal therapy given its non-invasive nature, and the behavioural challenges encountered with late-stage Alzheimer's patients. However, given the findings of both this thesis and other research publications, it appears there is a great deal more to unveil around this treatment, its impacts on neural circuits and intracellular signalling and the optimum treatment duration and age of exposure. Alzheimer's Disease is a long-term, chronic disease whose pathologies begin developing well before symptoms present- therefore this treatment may be more effective in younger individuals before the onset of symptoms. onset of symptoms. However, given the changes we observed in treatment of WT animals, as well as other groups findings in treatment of WT animals (Garza *et al.,* 2020) that may have additional complications. The brain is intrinsically complex, and much research remains to be done to unravel the mechanisms behind this treatment.

References

7. References

'2022 Alzheimer's disease facts and figures' (2022) *Alzheimer's & Dementia*, 18(4), pp. 700–789. doi: 10.1002/alz.12638.

Adaikkan, C. *et al.* (2019) 'Gamma Entrainment Binds Higher-Order Brain Regions and Offers Neuroprotection', *Neuron*, 102(5), pp. 929-943.e8. doi: 10.1016/j.neuron.2019.04.011.

Adams, M. M. *et al.* (2004) 'Estrogen modulates synaptic N-methyl-D-aspartate receptor subunit distribution in the aged hippocampus', *Journal of Comparative Neurology*, 474(3), pp. 419–426. doi: 10.1002/cne.20148.

Aimo, A. *et al.* (2019) 'Clinical and Prognostic Significance of sST2 in Heart Failure: JACC Review Topic of the Week', *Journal of the American College of Cardiology*. Elsevier USA, pp. 2193–2203. doi: 10.1016/j.jacc.2019.08.1039.

Aizenstein, H. J. *et al.* (2008) 'Frequent Amyloid Deposition Without Significant Cognitive Impairment Among the Elderly', *Archives of Neurology*, 65(11), p. 1509. doi: 10.1001/archneur.65.11.1509.

Allen, M. *et al.* (2014) 'Association of MAPT haplotypes with Alzheimer ' s disease risk and MAPT brain gene expression levels', *Alzheimer's Research & Therapy*, 6(4), pp. 1–14.

Alzforum (2018) *TREM2 mutations*. Available at: https://www.alzforum.org/mutations/trem2-r62h.

Alzforum (2023a) *MAPT mutations*. Available at: https://www.alzforum.org/mutations/mapt.

Alzforum (2023b) *PSEN1 Mutations*. Available at: https://www.alzforum.org/mutations/psen-1.

Alzheimer's Research UK (2015) *A Marginalised Majority: Women and Dementia*. Available at: https://www.alzheimersresearchuk.org/about-us/our-influence/policy-work/reports/women-dementia/ (Accessed: 4 May 2023).

Anstey, K. J. *et al.* (2021) 'Association of sex differences in dementia risk factors with sex differences in memory decline in a population-based cohort spanning 20–76 years', *Scientific Reports*, 11(1), p. 7710. doi: 10.1038/s41598-021-86397-7.

Atagi, Y. *et al.* (2015) 'Apolipoprotein E is a ligand for triggering receptor expressed on myeloid cells 2 (TREM2)', *Journal of Biological Chemistry*, 290(43), pp. 26043–26050. doi: 10.1074/jbc.M115.679043.

Ayodele, T. *et al.* (2021) 'Early-Onset Alzheimer's Disease: What Is Missing in Research?', *Current Neurology and Neuroscience Reports*, 21(2), p. 4. doi: 10.1007/s11910-020-01090-y.

Azcoitia, I., Mendez, P. and Garcia-Segura, L. M. (2021) 'Aromatase in the Human Brain', *Androgens*. Mary Ann Liebert Inc., pp. 189–202. doi: 10.1089/andro.2021.0007.

Azimi, M., Le, T. T. and Brown, N. L. (2018) 'Presenilin gene function and Notch signaling feedback regulation in the developing mouse lens', *Differentiation*, 102, pp. 40–52. doi: 10.1016/j.diff.2018.07.003.

Baleviciute, A. and Keane, L. (2023) 'Sex-specific role for microglial CST7 in Alzheimer's disease', *Nature Reviews Immunology*, 23(2), pp. 73–73. doi: 10.1038/s41577-022-00830-0.

Barbier, P. *et al.* (2019) 'Role of Tau as a Microtubule-Associated Protein: Structural and Functional Aspects', *Frontiers in Aging Neuroscience*, 11. doi: 10.3389/fnagi.2019.00204.

Başar, E. *et al.* (2016) 'Delay of cognitive gamma responses in Alzheimer's disease', *NeuroImage: Clinical*, 11, pp. 106–115. doi: 10.1016/j.nicl.2016.01.015.

Bature, F. *et al.* (2017) 'Signs and symptoms preceding the diagnosis of Alzheimer ' s disease : a systematic scoping review of literature from 1937 to 2016', *BMJ Open*, 7(8). doi: 10.1136/bmjopen-2016-015746.

Beagley, K. W. and Gockel, C. M. (2003) 'Regulation of innate and adaptive immunity by the female sex hormones oestradiol and progesterone', *FEMS Immunology and Medical Microbiology*. Elsevier, pp. 13–22. doi: 10.1016/S0928-8244(03)00202-5.

Bear, M., Connors, B. and Paradiso, M. A. (2016) *Neuroscience: Exploring the Brain, Enhanced Edition*. Enhanced 4th edition. Burlington, MA: Jones & Barnett Learning. Available at: https://search-ebscohost-com.proxy.lib.strath.ac.uk/login.aspx?direct=true&db=nlebk&AN=2437548&site=ehost-live (Accessed: 15 June 2023).

Beery, A. K. and Zucker, I. (2011) 'Sex bias in neuroscience and biomedical research', *Neuroscience & Biobehavioral Reviews*, 35(3), pp. 565–572. doi: 10.1016/j.neubiorev.2010.07.002.

Belelli, D. *et al.* (2006) 'Neuroactive steroids and inhibitory neurotransmission: Mechanisms of action and physiological relevance', *Neuroscience*, 138(3), pp. 821–829. doi: 10.1016/j.neuroscience.2005.07.021.

Di Benedetto, G. *et al.* (2022) 'Role of Microglia and Astrocytes in Alzheimer's Disease: From Neuroinflammation to Ca2+ Homeostasis Dysregulation', *Cells*. MDPI. doi: 10.3390/cells11172728.

Bennett, M. L. *et al.* (2016) 'New tools for studying microglia in the mouse and human CNS', *Proceedings of the National Academy of Sciences of the United States of America*, 113(12), pp. E1738–E1746. doi: 10.1073/pnas.1525528113.

Benzinger, T. L. S. *et al.* (2013) 'Regional variability of imaging biomarkers in autosomal dominant Alzheimer's disease', *Proceedings of the National Academy of Sciences of the United States of America*, 110(47). doi: 10.1073/pnas.1317918110.

Beydoun, M. A. *et al.* (2021) 'Race, APOE genotypes, and cognitive decline among middle-aged urban adults', *Alzheimer's Research & Therapy*, 13(1), p. 120. doi: 10.1186/s13195-021-00855-y.

Bezprozvanny, I. (2013) 'Presenilins and Calcium Signaling—Systems Biology to the Rescue', *Science Signaling*, 6(283). doi: 10.1126/scisignal.2004296.

Bianchi, V. E. (2022) 'Impact of Testosterone on Alzheimer's Disease', *The World Journal of Men's Health*, 40(2), p. 243. doi: 10.5534/wjmh.210175.

Bianchi, V. E., Herrera, P. F. and Laura, R. (2021) 'Effect of nutrition on neurodegenerative diseases. A systematic review', *Nutritional Neuroscience*, 24(10), pp. 810–834. doi: 10.1080/1028415X.2019.1681088.

Blanquart, E. *et al.* (2022) 'Targeting androgen signaling in ILC2s protects from IL-33–driven lung inflammation, independently of KLRG1', *Journal of Allergy and Clinical Immunology*, 149(1), pp. 237-251.e12. doi: 10.1016/j.jaci.2021.04.029.

Bobola, M. S. *et al.* (2020) 'Transcranial focused ultrasound, pulsed at 40 Hz, activates microglia acutely and reduces Aβ load chronically, as demonstrated in vivo', *Brain Stimulation*, 13(4), pp. 1014–1023. doi: 10.1016/j.brs.2020.03.016.

Boccazzi, M. *et al.* (2021) 'The immune-inflammatory response of oligodendrocytes in a murine model of preterm white matter injury: the role of TLR3 activation', *Cell Death & Disease*, 12(2), p. 166. doi: 10.1038/s41419-021-03446-9.

Brookmeyer, R. *et al.* (2011) 'National estimates of the prevalence of Alzheimer's disease in the United States', *Alzheimer's & Dementia*, 7(1), pp. 61–73. doi: 10.1016/j.jalz.2010.11.007.

Brumberg, J. C., Hamzei-Sichani, F. and Yuste, R. (2003) 'Morphological and Physiological Characterization of Layer VI Corticofugal Neurons of Mouse Primary Visual Cortex', *Journal of Neurophysiology*, 89(5), pp. 2854–2867. doi: 10.1152/jn.01051.2002.

Bundy, J. L. *et al.* (2019) 'Sex-biased hippocampal pathology in the 5XFAD mouse model of Alzheimer's disease: A multi-omic analysis', *Journal of Comparative Neurology*, 527(2), pp. 462–475. doi: 10.1002/cne.24551.

Buskila, Y., Crowe, Sarah. E. and Ellis-Davies, G. C. R. (2013) 'Synaptic deficits in layer 5 neurons precede overt structural decay in 5xFAD mice', *Journal of Neuroscience*, 2254(1), pp. 152–159. doi: doi:10.1016/j.neuroscience.2013.09.016. Synaptic.

Butterfield, D. A. and Pocernich, C. B. (2003) 'The Glutamatergic System and Alzheimer's Disease', *CNS Drugs*, 17(9), pp. 641–652. doi: 10.2165/00023210-200317090-00004.

Byers, S. L. *et al.* (2012) 'Mouse Estrous Cycle Identification Tool and Images', *PLoS ONE*, 7(4), p. e35538. doi: 10.1371/journal.pone.0035538.

Byron, N., Semenova, A. and Sakata, S. (2021) 'Mutual interactions between brain states and Alzheimer's disease pathology: A focus on gamma and slow oscillations', *Biology*, 10(8). doi: 10.3390/biology10080707.

Del C. Alonso, A. *et al.* (2001) 'Interaction of Tau Isoforms with Alzheimer's Disease Abnormally Hyperphosphorylated Tau and in Vitro Phosphorylation into the Disease-like Protein', *Journal of Biological Chemistry*, 276(41), pp. 37967–37973.

Cameron, B. and Landreth, G. E. (2011) 'Inflammation, Microglia and Alzheimer's Disease', *Neurobiology of disease*, 37(3), pp. 503–509. doi: 10.1016/j.nbd.2009.10.006.Inflammation.

Cao, K., Liao, X., Lu, J., Yao, S., Wu, F., Zhu, X., Shi, D. and Wen, S. (2018) 'IL-33 / ST2 plays a critical role in endothelial cell activation and microglia-mediated neuroinflammation modulation', pp. 1–12.

Caraguel, C. G. B. *et al.* (2011) 'Selection of a Cutoff Value for Real-Time Polymerase Chain Reaction Results to Fit a Diagnostic Purpose: Analytical and Epidemiologic Approaches', *Journal of Veterinary Diagnostic Investigation*, 23(1), pp. 2–15. doi: 10.1177/104063871102300102.

Casula, E. P. *et al.* (2022) 'Decreased Frontal Gamma Activity in Alzheimer Disease Patients', *Annals of Neurology*, 92(3), pp. 464–475. doi: 10.1002/ana.26444.

Chapuis, J. *et al.* (2009) 'Transcriptomic and genetic studies identify IL-33 as a candidate gene for Alzheimer's disease', *Molecular Psychiatry*, 14(11), pp. 1004–1016. doi: 10.1038/mp.2009.10.Transcriptomic.

Chellappa, S. L. *et al.* (2017) 'Sex differences in light sensitivity impact on brightness perception, vigilant attention and sleep in humans', *Scientific Reports*, 7(1), p. 14215. doi: 10.1038/s41598-017-13973-1.

Chêne, G. *et al.* (2015) 'Gender and incidence of dementia in the Framingham Heart Study from mid-adult life', *Alzheimer's and Dementia*, 11(3), pp. 310–320. doi: 10.1016/j.jalz.2013.10.005.

Cho, S.-J. *et al.* (2019) 'Altered expression of Notch1 in Alzheimer's disease.', *PloS one*, 14(11), p. e0224941. doi: 10.1371/journal.pone.0224941.

Choi, Y. S. *et al.* (2012) 'Nuclear IL-33 is a transcriptional regulator of NF-κB p65 and induces endothelial cell activation', *Biochemical and Biophysical Research Communications*, 421(2), pp. 305–311. doi: 10.1016/j.bbrc.2012.04.005.

Chu, T. H. *et al.* (2017) 'Axonal and myelinic pathology in 5xFAD Alzheimer's mouse spinal cord', *PLoS ONE*, 12(11). doi: 10.1371/journal.pone.0188218.
Cimenser, A. *et al.* (2021) 'Sensory-Evoked 40-Hz Gamma Oscillation Improves Sleep and Daily Living Activities in Alzheimer's Disease Patients', *Frontiers in Systems Neuroscience*, 15. doi: 10.3389/fnsys.2021.746859.

Condello, C. *et al.* (2015) 'Microglia constitute a barrier that prevents neurotoxic protofibrillar Aβ42 hotspots around plaques', *Nature Communications*, 6(6176), pp. 139–148. doi: https://doi.org/10.1038/ncomms7176.

Correale, J. and Gaitán, M. I. (2019) 'Autoimmune Astrocytopathy', in Mitoma, H. and Manto, M. (eds) *Neuroimmune Diseases: From Cells to the Living Brain*. Cham: Springer International Publishing, pp. 329–355. doi: 10.1007/978-3-030-19515-1_10.

Courtney, A. H. *et al.* (2019a) 'CD45 functions as a signaling gatekeeper in T cells', *Science Signaling*, 12(604). doi: 10.1126/scisignal.aaw8151.

Csöregh Nord, L. *et al.* (2010) 'Analysis of Oestrogen Regulation of Alpha-, Beta- and Gamma-Secretase Gene and Protein Expression in Cultured Human Neuronal and Glial Cells', *Neurodegenerative Diseases*, 7(6), pp. 349–364. doi: 10.1159/000282279.

Cuadros, M. A. *et al.* (2022) 'Microglia and Microglia-Like Cells: Similar but Different', *Frontiers in Cellular Neuroscience*. Frontiers Media S.A. doi: 10.3389/fncel.2022.816439.

Cui, J. *et al.* (2022) 'Sex-Specific Regulation of β-Secretase: A Novel Estrogen Response Element (ERE)-Dependent Mechanism in Alzheimer's Disease', *The Journal of Neuroscience*, 42(6), pp. 1154–1165. doi: 10.1523/JNEUROSCI.0864-20.2021.

D Daniels, M. J. *et al.* (2022) 'Cystatin F (Cst7) drives sex-dependent changes in microglia in an amyloid-driven model of Alzheimer's Disease', *bioRxiv (Preprint)*. doi: 10.1101/2022.11.18.516922.

Danysz, W. and Parsons, C. G. (2012) 'Alzheimer's disease, β-amyloid, glutamate, NMDA receptors and memantine - Searching for the connections', *British Journal of Pharmacology*, 167(2), pp. 324–352. doi: 10.1111/j.1476-5381.2012.02057.x.

Demuro, A. *et al.* (2005) 'Calcium dysregulation and membrane disruption as a ubiquitous neurotoxic mechanism of soluble amyloid oligomers', *Journal of Biological Chemistry*, 280(17), pp. 17294–17300. doi: 10.1074/jbc.M500997200.

Dennison, J. L. *et al.* (2021) 'Sexual Dimorphism in the 3xTg-AD Mouse Model and Its Impact on Pre-Clinical Research', *Journal of Alzheimer's disease : JAD*. NLM (Medline), pp. 41–52. doi: 10.3233/JAD-201014.

Dermaut, B. *et al.* (2004) 'A Novel Presenilin 1 Mutation Associated with Pick's Disease but Not β-Amyloid Plaques', *Annals of Neurology*, 55(5), pp. 617–626. doi: 10.1002/ana.20083.

van Deursen, J. A. *et al.* (2011) '40-Hz steady state response in Alzheimer's disease and mild cognitive impairment', *Neurobiology of Aging*, 32(1), pp. 24–30. doi: 10.1016/j.neurobiolaging.2009.01.002.

DiSabato, D. J., Quan, N. and Godbout, J. P. (2016) 'Neuroinflammation: the devil is in the details', *Journal of Neurochemistry*, 139(S2), pp. 136–153. doi: 10.1111/jnc.13607.

Dong, Y.-X. *et al.* (2018) 'Association between Alzheimer's disease pathogenesis and early demyelination and oligodendrocyte dysfunction', *Neural Regeneration Research*, 13(5), p. 908. doi: 10.4103/1673-5374.232486.

Doran, S. J. *et al.* (2019) 'Sex Differences in Acute Neuroinflammation after Experimental Traumatic Brain Injury Are Mediated by Infiltrating Myeloid Cells', *Journal of Neurotrauma*, 36(7), pp. 1040–1053. doi: 10.1089/neu.2018.6019.
Duffy, J. F. *et al.* (2011) 'Sex difference in the near-24-hour intrinsic period of the human circadian timing system', *Proceedings of the National Academy of Sciences*, 108(supplement_3), pp. 15602–15608. doi: 10.1073/pnas.1010666108.
D'uscio, L. V and Katusic, Z. S. (2019) 'Vascular phenotype of amyloid precursor protein-deficient mice', *Am J Physiol Heart Circ Physiol*, 316, pp. 1297–1308. doi: 10.1152/ajpheart.00539.2018.-The.

van Dyck, C. H. *et al.* (2023) 'Lecanemab in Early Alzheimer's Disease', *New England Journal of Medicine*, 388(1), pp. 9–21. doi: 10.1056/NEJMoa2212948.

Ebneth, A. *et al.* (1998) 'Overexpression of Tau Protein Inhibits Kinesin-dependent Trafficking of Vesicles, Mitochondria, and Endoplasmic Reticulum: Implications for Alzheimer's Disease', *The Journal of cell biology*, 143(3), pp. 777–794.

Ecol, M. (2017) 'Alzheimer's disease: experimental models and reality', *Acta Neuropathologica*, 25(5), pp. 1032–1057. doi: 10.1111/mec.13536.Application.

Elder, G. A., Gama Sosa, M. A. and De Gasperi, R. (2010) 'Transgenic Mouse Models of Alzheimer's Disease', *Mount Sinai Journal of Medicine: A Journal of Translational and Personalized Medicine*, 77(1), pp. 69–81. doi: 10.1002/msj.20159.

Evans, S. *et al.* (1987) 'Muscle acetylcholine receptor biosynthesis', *The Journal of biological chemistry*, 262(10), pp. 4911–6. Available at: http://www.ncbi.nlm.nih.gov/pubmed/2435720.

Fernandez, C. G. *et al.* (2019) 'The Role of APOE4 in Disrupting the Homeostatic Functions of Astrocytes and Microglia in Aging and Alzheimer ' s Disease', *Frontiers in Aging Neuroscience*, 11(February), pp. 1–18. doi: 10.3389/fnagi.2019.00014.

Fielder, E. *et al.* (2020) 'Anti-inflammatory treatment rescues memory deficits during aging in nfkb1−/− mice', *Aging Cell*, 19(10). doi: 10.1111/acel.13188.

Fish, A. M. *et al.* (2020) 'Sex-biased trajectories of amygdalo-hippocampal morphology change over human development', *NeuroImage*, 204, p. 116122. doi: 10.1016/j.neuroimage.2019.116122.

Fisher, D. W., Bennett, D. A. and Dong, H. (2018) 'Sexual dimorphism in predisposition to Alzheimer's disease', *Neurobiology of Aging*, 70, pp. 308–324. doi: 10.1016/j.neurobiolaging.2018.04.004.

Fitzgerald, P. J. and Watson, B. O. (2018) 'Gamma oscillations as a biomarker for major depression: an emerging topic', *Translational Psychiatry*, 8(1). doi: 10.1038/s41398-018-0239-y.

Fontainhas, A. M. *et al.* (2011) 'Microglial morphology and dynamic behavior is regulated by ionotropic glutamatergic and GABAergic neurotransmission', *PLoS ONE*, 6(1). doi: 10.1371/journal.pone.0015973.

Frisoni, G. B. *et al.* (2022) 'The probabilistic model of Alzheimer disease: the amyloid hypothesis revised', *Nature Reviews Neuroscience*, 23(1), pp. 53–66. doi: 10.1038/s41583-021-00533-w.

Fu, Amy K Y *et al.* (2016) 'IL-33 ameliorates Alzheimer ' s disease-like pathology and cognitive decline', *PNAS*, 113(19), pp. 2705–2713. doi: 10.1073/pnas.1604032113.

Fu, Amy K.Y. *et al.* (2016) 'IL-33 ameliorates Alzheimer's disease-like pathology and cognitive decline', *Proceedings of the National Academy of Sciences of the United States of America*, 113(19), pp. E2705–E2713. doi: 10.1073/pnas.1604032113.

Furman, O., Tsoory, M. and Chen, A. (2022) 'Differential chronic social stress models in male and female mice', *European Journal of Neuroscience*, 55(9–10), pp. 2777–2793. doi: 10.1111/ejn.15481.

Gadani, S. P. *et al.* (2015) 'The Glia-Derived Alarmin IL-33 Orchestrates the Immune Response and Promotes Recovery following Report The Glia-Derived Alarmin IL-33 Orchestrates the Immune Response and Promotes Recovery following CNS Injury', *Neuron*, 85(4), pp. 703–709. doi: 10.1016/j.neuron.2015.01.013.

Galanis, C. *et al.* (2021) 'Amyloid-beta mediates homeostatic synaptic plasticity', *Journal of Neuroscience*, 41(24), pp. 5157–5172. doi: 10.1523/JNEUROSCI.1820-20.2021.

Garza, K. M. *et al.* (2020) 'Gamma Visual Stimulation Induces a Neuroimmune Signaling Profile Distinct from Acute Neuroinflammation', *The Journal of Neuroscience*, 40(6), pp. 1211–1225. doi: 10.1523/JNEUROSCI.1511-19.2019.

Gatz, M. *et al.* (2006) 'Role of Genes and Environments for Explaining Alzheimer Disease', *Archives of General Psychiatry*, 63(2), p. 168. doi: 10.1001/archpsyc.63.2.168.

Gharbi-Meliani, A. *et al.* (2021) 'The association of APOE ε4 with cognitive function over the adult life course and incidence of dementia: 20 years follow-up of the Whitehall II study', *Alzheimer's Research and Therapy*, 13(1). doi: 10.1186/s13195-020-00740-0.

Ghosal, K. *et al.* (2016) 'Tau protein mediates APP Intracellular domain (AICD)-Induced Alzheimer's-Like pathological features in mice', *PLoS ONE*, 11(7), pp. 1–22. doi: 10.1371/journal.pone.0159435.

Ghosh, S. and Thakur, M. K. (2008) 'PS1 Expression is Downregulated by Gonadal Steroids in Adult Mouse Brain', *Neurochemical Research*, 33(3), pp. 365–369. doi: 10.1007/s11064-007-9424-8.

Ghoshal, N., Binder, L. I. and Vitek, M. (2001) *Inhibition of neuronal maturation in primary hippocampal neurons from τ deficient mice*, *Article in Journal of Cell Science*. Available at: https://www.researchgate.net/publication/12103742.

Glenner, G. G. and Wong, C. W. (1984) 'Alzheimer's disease: Initial report of the purification and characterization of a novel cerebrovascular amyloid protein', *Biochemical and Biophysical Research Communications*, 120(3), pp. 885–890. doi: 10.1016/S0006-291X(84)80190-4.

Gómez Morillas, A., Besson, V. C. and Lerouet, D. (2021) 'Microglia and Neuroinflammation: What Place for P2RY12?', *International journal of molecular sciences*, 22(4). doi: 10.3390/ijms22041636.

Götz, J. *et al.* (2001) 'Formation of neurofibrillary tangles in P301L tau transgenic mice induced by Aβ42 fibrils', *Science*, 293(5534), pp. 1491–1495. doi: 10.1126/science.1062097

Goyena, R. (2019) 'Loss of tau and Fyn reduces compensatory effects of MAP2 for tau and reveals a Fyn-independent effect of tau on glutamate induced Ca2+ response', *Journal of Chemical Information and Modeling*, 53(9), pp. 1689–1699. doi: 10.1017/CBO9781107415324.004.

Greendale, G. A., Lee, N. P. and Arriola, E. R. (1999) 'The menopause', *The Lancet*, 353(9152), pp. 571–580. doi: 10.1016/S0140-6736(98)05352-5.

Guillot-Sestier, M.-V. *et al.* (2021) 'Microglial metabolism is a pivotal factor in sexual dimorphism in Alzheimer's disease', *Communications Biology*, 4(1), p. 711. doi: 10.1038/s42003-021-02259-y.

Güner, G. and Lichtenthaler, S. F. (2020) 'The substrate repertoire of γ-secretase/presenilin', *Seminars in Cell & Developmental Biology*, 105, pp. 27–42. doi: 10.1016/j.semcdb.2020.05.019.

Haas, L. T. *et al.* (2016) 'Metabotropic glutamate receptor 5 couples cellular prion protein to intracellular signalling in Alzheimer's disease', *Brain*, 139(2), pp. 526–546. doi: 10.1093/brain/awv356.

Habib, N. *et al.* (2020) 'Disease-associated astrocytes in Alzheimer's disease and aging', *Nature Neuroscience*, 23(6), pp. 701–706. doi: 10.1038/s41593-020-0624-8.

Hammes, S. R. and Levin, E. R. (2019) 'Impact of estrogens in males and androgens in females', *Journal of Clinical Investigation*, 129(5), pp. 1818–1826. doi: 10.1172/JCI125755.
Hanisch, U. K. (2002) 'Microglia as a source and target of cytokines', *Glia*, 40(2), pp. 140–155. doi: 10.1002/glia.10161.

Harkin, T. *et al.* (2001) *Drug Safety: Most Drugs Withdrawn in Recent Years Had Greater Health Risks for Women*. Washington D.C. Available at: https://www.gao.gov/assets/gao-01-286r.pdf (Accessed: 29 June 2023).

Harman, S. M. *et al.* (2001) 'Longitudinal Effects of Aging on Serum Total and Free Testosterone Levels in Healthy Men', *Journal of Clinical Endocrinology & Metabolism*, 86(2), pp. 724–731. Available at: https://academic.oup.com/jcem/article/86/2/724/2841070.

He, Q. *et al.* (2021) 'A feasibility trial of gamma sensory flicker for patients with prodromal Alzheimer's disease', *Alzheimer's and Dementia: Translational Research and Clinical Interventions*, 7(1). doi: 10.1002/trc2.12178.

He, W. *et al.* (2014) 'β-Site Amyloid Precursor Protein Cleaving Enzyme 1(BACE1) Regulates Notch Signaling by Controlling the Cleavage of Jagged 1 (Jag1) and Jagged 2 (Jag2) Proteins', *Journal of Biological Chemistry*, 289(30), pp. 20630–20637. doi: 10.1074/jbc.M114.579862

Heneka, M. T. *et al.* (2018) 'Neuroinflammation in Alzheimer' s Disease', *Lancet Neurol*, 14(4), pp. 388–405. doi: 10.1016/S1474-4422(15)70016-5.Neuroinflammation.

Hermiston, M. L., Xu, Z. and Weiss, A. (2003) 'CD45: A critical regulator of signaling thresholds in immune cells', *Annual Review of Immunology*, 21, pp. 107–137. doi: 10.1146/annurev.immunol.21.120601.140946.

Herrmann, C. S. and Demiralp, T. (2005) 'Human EEG gamma oscillations in neuropsychiatric disorders', *Clinical Neurophysiology*, pp. 2719–2733. doi: 10.1016/j.clinph.2005.07.007.

Hill, A. C., Laird, A. R. and Robinson, J. L. (2014) 'Gender differences in working memory networks: A BrainMap meta-analysis', *Biological Psychology*, 102, pp. 18–29. doi: 10.1016/j.biopsycho.2014.06.008.

Hopperton, K. E. *et al.* (2018) 'Markers of microglia in post-mortem brain samples from patients with Alzheimer's disease: a systematic review', *Molecular Psychiatry*, 23(2), pp. 177–198. doi: 10.1038/mp.2017.246.

Horstman, A. M. *et al.* (2012) 'The Role of Androgens and Estrogens on Healthy Aging and Longevity', *The Journals of Gerontology Series A: Biological Sciences and Medical Sciences*, 67(11), pp. 1140–1152. doi: 10.1093/gerona/gls068.

Hsin-Yu Sung *et al.* (2019) 'Issue Cover (September 2019)', *Journal of Neurochemistry*, 150(6). doi: 10.1111/jnc.14522.

Huang, Y. and Mahley, R. W. (2014) 'Apolipoprotein E: Structure and function in lipid metabolism, neurobiology, and Alzheimer's diseases', *Neurobiology of Disease*, 72, pp. 3–12. doi: 10.1016/j.nbd.2014.08.025.

Huber, C. M. *et al.* (2018) 'Cognitive Decline in Preclinical Alzheimer's Disease: Amyloid-Beta versus Tauopathy', *Journal of Alzheimer's Disease*, 61(1), pp. 265–281. doi: 10.3233/JAD-170490.

Hubrecht and Carter (2019) 'The 3Rs and Humane Experimental Technique: Implementing Change', *Animals*, 9(10), p. 754. doi: 10.3390/ani9100754.

Hüttenrauch, M. *et al.* (2018) 'Glycoprotein NMB: a novel Alzheimer's disease associated marker expressed in a subset of activated microglia', *Acta neuropathologica communications*, 6(1), p. 108. doi: 10.1186/s40478-018-0612-3.

Iaccarino, H. F., Singer, Annabelle C., *et al.* (2016) 'Gamma frequency entrainment attenuates amyloid load and modifies microglia', *Nature*, 540(7632), pp. 230–235. doi: 10.1038/nature20587.

Iaccarino, H. F., Singer, Anabelle C., *et al.* (2016) 'Gamma frequency entrainment attenuates amyloid load and modifies microglia', *Nature*, 540(7632), pp. 230–235. doi: 10.1016/j.physbeh.2017.03.040.

Imbimbo, B. *et al.* (2023) 'Initial failures of anti-tau antibodies in Alzheimer's disease are reminiscent of the amyloid-β story', *Neural Regeneration Research*, 18(1), p. 117. doi: 10.4103/1673-5374.340409.

Irie-Sasaki, J. *et al.* (2001) 'CD45 is a JAK phosphatase and negatively regulates cytokine receptor signalling', *Nature*, 409(6818), pp. 349–354. doi: 10.1038/35053086.

Ishizuka, N., Weber, J. and Amaral, D. G. (1990) 'Organization of intrahippocampal projections originating from CA3 pyramidal cells in the rat', *Journal of Comparative Neurology*, 295(4), pp. 580–623. doi: 10.1002/cne.902950407.

Jamali, S. and Ross, B. (2014) 'Sustained changes in somatosensory gamma responses after brief vibrotactile stimulation', *NeuroReport*, 25(7), pp. 537–541. doi: 10.1097/WNR.0000000000000133.

Jankowsky, J. L. *et al.* (2007) 'Rodent Aβ Modulates the Solubility and Distribution of Amyloid Deposits in Transgenic Mice', *Journal of Biological Chemistry*, 282(31), pp. 22707–22720. doi: 10.1074/jbc.M611050200.

Jankowsky, J. L. and Zheng, H. (2017) 'Practical considerations for choosing a mouse model of Alzheimer's disease', *Molecular Neurodegeneration*, 12(1), pp. 1–22. doi: 10.1186/s13024-017-0231-7.

Jay, T. R. *et al.* (2015) 'TREM2 deficiency eliminates TREM2+ inflammatory macrophages and ameliorates pathology in Alzheimer ' s disease mouse models', *Journal of Experimental Medicine*, 212(3), pp. 287–295. doi: 10.1084/jem.20142322.

Ji, C. and Sigurdsson, E. M. (2021) 'Current Status of Clinical Trials on Tau Immunotherapies', *Drugs*, 81(10), pp. 1135–1152. doi: 10.1007/s40265-021-01546-6.

Ji, J., Sundquist, J. and Sundquist, K. (2016) 'Gender-specific incidence of autoimmune diseases from national registers', *Journal of Autoimmunity*, 69, pp. 102–106. doi: 10.1016/j.jaut.2016.03.003.

Jiao, M. *et al.* (2020) 'Neuroprotective effect of astrocyte-derived IL-33 in neonatal hypoxic-ischemic brain injury', *Journal of Neuroinflammation*, 17(251), pp. 1–14.

Jiao, S. S. *et al.* (2016) 'Sex Dimorphism Profile of Alzheimer's Disease-Type Pathologies in an APP/PS1 Mouse Model', *Neurotoxicity Research*, 29(2), pp. 256–266. doi: 10.1007/s12640-015-9589-x.

Jo, S. *et al.* (2014) 'GABA from reactive astrocytes impairs memory in mouse models of Alzheimer's disease', *Nature Medicine*, 20(8), pp. 886–896. doi: 10.1038/nm.3639.

Kamer, A. R. *et al.* (2009) 'TNF-α and antibodies to periodontal bacteria discriminate between Alzheimer's disease patients and normal subjects', *Journal of Neuroimmunology*, 216(1–2), pp. 92–97. doi: 10.1016/j.jneuroim.2009.08.013.

Kawahara, M. *et al.* (2000) 'Alzheimer's β-amyloid, human islet amylin, and priori protein fragment evoke intracellular free calcium elevations by a common mechanism in a hypothalamic GnRH neuronal cell line', *Journal of Biological Chemistry*, 275(19), pp. 14077–14083. doi: 10.1074/jbc.275.19.14077.

Kayed, R. *et al.* (2004) 'Permeabilization of lipid bilayers is a common conformation-dependent activity of soluble amyloid oligomers in protein misfolding diseases', *Journal of Biological Chemistry*, 279(45), pp. 46363–46366. doi: 10.1074/jbc.C400260200.

Keely, S. J. (2011) 'Epithelial acetylcholine - a new paradigm for cholinergic regulation of intestinal fluid and electrolyte transport', *The Journal of Physiology*, 589(4), pp. 771–772. doi: 10.1113/jphysiol.2010.204263.

Kellogg, E. H. *et al.* (2018) 'Near-atomic model of microtubule-tau interactions', *Science*, 360(6394), pp. 1242–1246. doi: 10.1126/science.aat1780.

Kempuraj, D. *et al.* (2013) 'Glia Maturation Factor Induces Interleukin-33 Release from Astrocytes: Implications for Neurodegenerative Diseases', *Journal of Neuroimmune Pharmacology*, 8(3), pp. 643–650. doi: 10.1007/s11481-013-9439-7.

Kenigsbuch, M. *et al.* (2022) 'A shared disease-associated oligodendrocyte signature among multiple CNS pathologies', *Nature Neuroscience*, 25(7), pp. 876–886. doi: 10.1038/s41593-022-01104-7.

Kenkhuis, B. *et al.* (2022) 'Co-expression patterns of microglia markers Iba1, TMEM119 and P2RY12 in Alzheimer's disease', *Neurobiology of Disease*, 167, p. 105684. doi: 10.1016/j.nbd.2022.105684.

Khaliulin, I., Kartawy, M. and Amal, H. (2020) 'Sex Differences in Biological Processes and Nitrergic Signaling in Mouse Brain', *Biomedicines*, 8(5), p. 124. doi: 10.3390/biomedicines8050124.

Killin, L. O. J. *et al.* (2016) 'Environmental risk factors for dementia: a systematic review', *BMC Geriatrics*, 16(1), p. 175. doi: 10.1186/s12877-016-0342-y.

Kim, H. J. *et al.* (2003a) 'Selective neuronal degeneration induced by soluble oligomeric amyloid beta protein.', *The FASEB journal : official publication of the Federation of American Societies for Experimental Biology*, 17(1), pp. 118–120.

Klein, A. S. *et al.* (2016) 'Early cortical changes in gamma oscillations in alzheimer's disease', *Frontiers in Systems Neuroscience*, 10(OCT). doi: 10.3389/fnsys.2016.00083.

Klein, R. S., Garber, C. and Howard, N. (2017) 'Infectious immunity in the central nervous system and brain function', *Nature Immunology*, 18(2), pp. 132–141. doi: 10.1038/ni.3656.

Klein, S. L. and Flanagan, K. L. (2016) 'Sex differences in immune responses', *Nature Reviews Immunology*, 16(10), pp. 626–638. doi: 10.1038/nri.2016.90.

Koenig, T. *et al.* (2005) 'Decreased EEG synchronization in Alzheimer's disease and mild cognitive impairment', *Neurobiology of Aging*, 26(2), pp. 165–171. doi: 10.1016/j.neurobiolaging.2004.03.008.

Koenigsknecht-Talboo, J. and Landreth, G. E. (2005) 'Microglial phagocytosis induced by fibrillar β-amyloid and IgGs are differentially regulated by proinflammatory cytokines', *Journal of Neuroscience*, 25(36), pp. 8240–8249. doi: 10.1523/JNEUROSCI.1808-05.2005.

Kotsiou, O. S., Gourgoulianis, K. I. and Zarogiannis, S. G. (2018) 'IL-33/ST2 axis in organ fibrosis', *Frontiers in Immunology*. Frontiers Media S.A. doi: 10.3389/fimmu.2018.02432.

Krolick, K. N., Zhu, Q. and Shi, H. (2018) 'Effects of Estrogens on Central Nervous System Neurotransmission: Implications for Sex Differences in Mental Disorders', in, pp. 105–171. doi: 10.1016/bs.pmbts.2018.07.008.

Kumar, Devendra *et al.* (2018) 'Secretase inhibitors for the treatment of Alzheimer's disease: Long road ahead', *European Journal of Medicinal Chemistry*, 148, pp. 436–452. doi: 10.1016/j.ejmech.2018.02.035.

Kuperstein, I. *et al.* (2010) 'Neurotoxicity of Alzheimer's disease Aβ peptides is induced by small changes in the Aβ42 to Aβ40 ratio', *The EMBO Journal*, 29(19), pp. 3408–3420. doi: 10.1038/emboj.2010.211.

Landel, V. *et al.* (2014) 'Temporal gene profiling of the 5XFAD transgenic mouse model highlights the importance of microglial activation in Alzheimer's disease', *Molecular Neurodegeneration*, 9(1), p. 33. doi: 10.1186/1750-1326-9-33.

Larson, M. *et al.* (2012) 'The complex PrPc-Fyn couples human oligomeric Aβ with pathological tau changes in Alzheimer's disease', *Journal of Neuroscience*, 32(47), pp. 16857–16871. doi: 10.1523/JNEUROSCI.1858-12.2012.

Lau, S.-F. *et al.* (2020) 'IL-33-PU.1 Transcriptome Reprogramming Drives Functional State Transition and Clearance Activity of Microglia in Alzheimer's Disease', *Cell Reports*, 31(3), p. 107530. doi: 10.1016/j.celrep.2020.107530.

Lee, H. *et al.* (2005) 'Tau phosphorylation in Alzheimer ' s disease : pathogen or protector ?', *TRENDS In Molecular Medicine*, 11(4), pp. 164–9. doi: 10.1016/j.molmed.2005.02.008.

Lee, M., Schwab, C. and Mcgeer, P. L. (2011) 'Astrocytes are GABAergic cells that modulate microglial activity', *Glia*, 59(1), pp. 152–165. doi: 10.1002/glia.21087.

Lewczuk, P. *et al.* (2010) 'Soluble amyloid precursor proteins in the cerebrospinal fluid as novel potential biomarkers of Alzheimer's disease: A multicenter study', *Molecular Psychiatry*, 15(2), pp. 138–145. doi: 10.1038/mp.2008.84.

Lewis, J. *et al.* (2001) 'Enhanced neurofibrillary degeneration in transgenic mice expressing mutant tau and APP', *Science*, 293(5534), pp. 1487–1491. doi: 10.1126/science.1058189.

Li, C. and Götz, J. (2018) 'Pyk2 is a Novel Tau Tyrosine Kinase that is Regulated by the Tyrosine Kinase Fyn', *Journal of Alzheimer's Disease*, 64(1), pp. 205–221. doi: 10.3233/JAD-180054.

Li, T. *et al.* (2016) 'The neuritic plaque facilitates pathological conversion of tau in an Alzheimer's disease mouse model', *Nature Communications*, 7(May), pp. 1–13. doi: 10.1038/ncomms12082.

Liang, C.-S. *et al.* (2020) 'The role of interleukin-33 in patients with mild cognitive impairment and Alzheimer's disease', *Alzheimer's Research & Therapy*, 12(1), p. 86. doi: 10.1186/s13195-020-00652-z.

'Life Expectancy in Scotland 2019-2021' (2022) *Scottish Government*. Available at: https://www.nrscotland.gov.uk/files/statistics/life-expectancy-in-scotland/19-21/life-expectancy-19-21-report.pdf.

Liu, Y., Beyer, A. and Aebersold, R. (2016) 'On the Dependency of Cellular Protein Levels on mRNA Abundance', *Cell*, 165(3), pp. 535–550. doi: 10.1016/j.cell.2016.03.014.

Liu, Z. *et al.* (2007) 'Induction of oligodendrocyte differentiation by Olig2 and Sox10: Evidence for reciprocal interactions and dosage-dependent mechanisms', *Developmental Biology*, 302(2), pp. 683–693. doi: 10.1016/j.ydbio.2006.10.007.

Livak, K. J. and Schmittgen, T. D. (2001) 'Analysis of relative gene expression data using real-time quantitative PCR and the 2(-Delta Delta C(T)) Method.', *Methods (San Diego, Calif.)*, 25(4), pp. 402–8. doi: 10.1006/meth.2001.1262.

Loiola, R. A. *et al.* (2019) 'Estrogen Promotes Pro-resolving Microglial Behavior and Phagocytic Cell Clearance through the Actions of Annexin A1', *Frontiers in Endocrinology*, 10(JUN). doi: 10.3389/fendo.2019.00420.

Lue, L. *et al.* (1999) 'Soluble amyloid β peptide concentration as a predictor of synaptic change in Alzheimer's disease', *American Journal of Pathology*, 155(3), pp. 1–10. Available at: papers2://publication/uuid/FFAA42DB-8D43-4A55-91F6-DBC6B746AD67.

Maeda, J. *et al.* (2021) 'Distinct microglial response against Alzheimer's amyloid and tau pathologies characterized by P2Y12 receptor', *Brain Communications*, 3(1). doi: 10.1093/braincomms/fcab011.

Márquez-Ropero, M. *et al.* (2020) 'Microglial Corpse Clearance: Lessons From Macrophages', *Frontiers in Immunology*. Frontiers Media S.A. doi: 10.3389/fimmu.2020.00506.

Marriott, R. J. *et al.* (2022) 'Lower serum testosterone concentrations are associated with a higher incidence of dementia in men: The UK Biobank prospective cohort study', *Alzheimer's and Dementia*, 18(10), pp. 1907–1918. doi: 10.1002/alz.12529.

Marrocco, J. *et al.* (2017) 'A sexually dimorphic pre-stressed translational signature in CA3 pyramidal neurons of BDNF Val66Met mice', *Nature Communications*, 8(1), p. 808. doi: 10.1038/s41467-017-01014-4.

Marsh, S. E. *et al.* (2016) 'The adaptive immune system restrains Alzheimer's disease pathogenesis by modulating microglial function', *Proceedings of the National Academy of Sciences of the United States of America*, 113(9), pp. E1316–E1325. doi: 10.1073/pnas.1525466113.

Martorell, A. J. *et al.* (2019) 'Multi-sensory Gamma Stimulation Ameliorates Alzheimer's-Associated Pathology and Improves Cognition', *Cell*, 177(2), pp. 256-271.e22. doi: 10.1016/j.cell.2019.02.014.

Mathis, C. A. *et al.* (2013) 'In vivo assessment of amyloid-β deposition in nondemented very elderly subjects', *Annals of Neurology*, 73(6), pp. 751–761. doi: 10.1002/ana.23797.

Matsui, T. *et al.* (2007) 'Expression of APP pathway mRNAs and proteins in Alzheimer's disease', *Brain Research*, 1161, pp. 116–123. doi: 10.1016/j.brainres.2007.05.050.

Mayeux, R. and Stern, Y. (2012) 'Epidemiology of Alzheimer Disease', *Cold Spring Harbour perspectives in medicine*, 2(8), pp. 1–18.

Mazaheri, F. *et al.* (2017) ' TREM 2 deficiency impairs chemotaxis and microglial responses to neuronal injury ', *EMBO reports*, 18(7), pp. 1186–1198. doi: 10.15252/embr.201743922.

McAleese, K. E. *et al.* (2015) 'Cortical tau load is associated with white matter hyperintensities', *Acta Neuropathologica Communications*, 3(1), p. 60. doi: 10.1186/s40478-015-0240-0.

McAllister, C. *et al.* (2010) 'Genetic Targeting Aromatase in Male Amyloid Precursor Protein Transgenic Mice Down-Regulates β-Secretase (BACE1) and Prevents Alzheimer-Like Pathology and Cognitive Impairment', *The Journal of Neuroscience*, 30(21), pp. 7326–7334. doi: 10.1523/JNEUROSCI.1180-10.2010.

Mckhann, G. M. *et al.* (2011) 'The diagnosis of dementia due to Alzheimer ' s disease : Recommendations from the National Institute on Aging-Alzheimer ' s Association workgroups on diagnostic guidelines for Alzheimer ' s disease', *Alzheimer's & Dementia*, 7(3), pp. 263–269. doi: 10.1016/j.jalz.2011.03.005.

Mendez, M. F. (2017) 'Early-Onset Alzheimer Disease', *Neurologic Clinics*, 35(2), pp. 263–281. doi: 10.1016/j.ncl.2017.01.005.

M.Hall, A. and D.Roberson, E. (2009) 'Mouse Models of Alzheimer's Disease', *Brain research bulletin*, 106(5), pp. 2080–2092. doi: 10.1111/j.1471-4159.2008.05558.x.Complement.

Mietelska-Porowska, A. and Wojda, U. (2017) 'T Lymphocytes and Inflammatory Mediators in the Interplay between Brain and Blood in Alzheimer's Disease: Potential Pools of New Biomarkers', *Journal of Immunology Research*, 2017. doi: 10.1155/2017/4626540.

Miller, A. M. (2011) 'Role of IL-33 in inflammation and disease', *Journal of Inflammation*. doi: 10.1186/1476-9255-8-22.

Miyamoto, T. *et al.* (2017) 'Phosphorylation of tau at Y18, but not tau-fyn binding, is required for tau to modulate NMDA receptor-dependent excitotoxicity in primary neuronal culture', *Molecular Neurodegeneration*, 12(1), pp. 1–19. doi: 10.1186/s13024-017-0176-x.

Montagne, A., Zhao, Z. and Zlokovic, B. V (2017) 'Alzheimer ' s disease : A matter of blood – brain barrier dysfunction ? The Journal of Experimental Medicine', *Journal of Experimental Medicine*, 214(11), pp. 3151–3169.

Mrak, R. E., Sheng, J. G. and Griffin, W. S. T. (1996) 'Correlation of astrocytic S100β expression with dystrophie neurites in amyloid plaques of Alzheimer's disease', *Journal of Neuropathology and Experimental Neurology*, 55(3), pp. 273–279. doi: 10.1097/00005072-199603000-00002.

Mullard, A. (2019) 'Anti-amyloid failures stack up as Alzheimer antibody flops', *Nature Reviews Drug Discovery*. doi: 10.1038/d41573-019-00064-1.

Murtaj, V. *et al.* (2019) 'Age and Sex Influence the Neuro-inflammatory Response to a Peripheral Acute LPS Challenge', *Frontiers in Aging Neuroscience*, 11. doi: 10.3389/fnagi.2019.00299.

Nakazono, T. *et al.* (2017) 'Impaired in vivo gamma oscillations in the medial entorhinal cortex of knock-in Alzheimer model', *Frontiers in Systems Neuroscience*, 11(June), pp. 1–12. doi: 10.3389/fnsys.2017.00048.

Nasrabady, S. E. *et al.* (2018) 'White matter changes in Alzheimer's disease: a focus on myelin and oligodendrocytes', *Acta Neuropathologica Communications*, 6(1), p. 22. doi: 10.1186/s40478-018-0515-3.

National Centre for the Replacement, R. and R. of A. in R. (no date) *Who we are: The 3Rs* , *https://nc3rs.org.uk/who-we-are/3rs*.

National Institute for Health and Care Excellence (2018) 'Dementia: assessment, management and support for people living with dementia and their carers', (NG97).
Neddens, J. *et al.* (2018) 'Phosphorylation of different tau sites during progression of Alzheimer's disease', *Acta neuropathologica communications*, 6(1), p. 52. doi: 10.1186/s40478-018-0557-6.

Nedivi, E. *et al.* (1996) 'A set of genes expressed in response to light in the adult cerebral cortex and regulated during development.', *Proceedings of the National Academy of Sciences*, 93(5), pp. 2048–2053. doi: 10.1073/pnas.93.5.2048.

Neu, S. C. *et al.* (2017) 'Apolipoprotein E Genotype and Sex Risk Factors for Alzheimer Disease', *JAMA Neurology*, 74(10), p. 1178. doi: 10.1001/jamaneurol.2017.2188.

Neurochemistry, J. O. F. (2019) 'Down-regulation of interleukin-33 expression in oligodendrocyte precursor cells impairs oligodendrocyte lineage progression', *Journal of Neurochemistry*, (150), pp. 691–708. doi: 10.1111/jnc.14788.

Nugent, B. *et al.* (2012) 'Hormonal Programming Across the Lifespan', *Hormone and Metabolic Research*, 44(08), pp. 577–586. doi: 10.1055/s-0032-1312593.

Nygaard, H. B. (2017) 'Targeting Fyn kinase in Alzheimer's Disease', *Biological Psychiatry*, 25(5), pp. 1032–1057. doi: 10.1111/mec.13536.Application.

Oakley, H. *et al.* (2006) 'Intraneuronal β-amyloid aggregates, neurodegeneration, and neuron loss in transgenic mice with five familial Alzheimer's disease mutations: Potential factors in amyloid plaque formation', *Journal of Neuroscience*, 26(40), pp. 10129–10140. doi: 10.1523/JNEUROSCI.1202-06.2006.

Oblak, A. L. *et al.* (2021) 'Comprehensive Evaluation of the 5XFAD Mouse Model for Preclinical Testing Applications: A MODEL-AD Study', *Frontiers in Aging Neuroscience*, 13. doi: 10.3389/fnagi.2021.713726.

Oddo, S. *et al.* (2003) 'Triple-Transgenic Model of Alzheimer's Disease with Plaques and Tangles', *Neuron*, 39(3), pp. 409–421. doi: 10.1016/S0896-6273(03)00434-3.

Oh, J. *et al.* (2010) 'Astrocyte-derived interleukin-6 promotes specific neuronal differentiation of neural progenitor cells from adult hippocampus', *Journal of Neuroscience Research*, 88(13), pp. 2798–2809. doi: 10.1002/jnr.22447.

Olabarria, M. *et al.* (2011) 'Age-dependent decrease in glutamine synthetase expression in the hippocampal astroglia of the triple transgenic Alzheimer's disease mouse model: Mechanism for deficient glutamatergic transmission?', *Molecular Neurodegeneration*, 6(1), pp. 1–9. doi: 10.1186/1750-1326-6-55.

Osborne, B. F., Turano, A. and Schwarz, J. M. (2018) 'Sex differences in the neuroimmune system', *Current Opinion in Behavioral Sciences*, 23, pp. 118–123. doi: 10.1016/j.cobeha.2018.05.007.

Paoletti, P. and Neyton, J. (2007) 'NMDA receptor subunits: function and pharmacology', *Current Opinion in Pharmacology*, 7(1), pp. 39–47. doi: 10.1016/j.coph.2006.08.011.

Papastavrou, E. *et al.* (2007) 'Caring for a relative with dementia: family caregiver burden', *Journal of Advanced Nursing*, 58(5), pp. 446–457. doi: 10.1111/j.1365-2648.2007.04250.x.

Park, M.-N. *et al.* (2015) 'Insufficient sex description of cells supplied by commercial vendors', *American Journal of Physiology-Cell Physiology*, 308(7), pp. C578–C580. doi: 10.1152/ajpcell.00396.2014.

Park, S. S. *et al.* (2020) 'Physical exercise during exposure to 40-Hz light flicker improves cognitive functions in the 3xTg mouse model of Alzheimer's disease', *Alzheimer's Research and Therapy*, 12(1). doi: 10.1186/s13195-020-00631-4.

Pastor, M. A. *et al.* (2002) *Activation of Human Cerebral and Cerebellar Cortex by Auditory Stimulation at 40 Hz*, *The Journal of Neuroscience*.

Piller, C. (2022) 'Revised clinical trial form for Alzheimer's antibody warned of fatal brain bleeds', *Science.org*, 30 December.

Piscopo, P. *et al.* (2013) 'Sex effect on presenilins expression in post-natal rat brain', *Advances in Bioscience and Biotechnology*, 04(12), pp. 1086–1094. doi: 10.4236/abb.2013.412145.

Placanica, L., Zhu, L. and Li, Y.-M. (2009) 'Gender- and Age-Dependent γ-Secretase Activity in Mouse Brain and Its Implication in Sporadic Alzheimer Disease', *PLoS ONE*, 4(4), p. e5088. doi: 10.1371/journal.pone.0005088.

Prendergast, B. J., Onishi, K. G. and Zucker, I. (2014) 'Female mice liberated for inclusion in neuroscience and biomedical research', *Neuroscience & Biobehavioral Reviews*, 40, pp. 1–5. doi: 10.1016/j.neubiorev.2014.01.001.

Pu, Y. *et al.* (2020) 'Gender differences in navigation performance are associated with differential theta and high-gamma activities in the hippocampus and parahippocampus', *Behavioural Brain Research*, 391, p. 112664. doi: 10.1016/j.bbr.2020.112664.

Puzzo, D. *et al.* (2011) 'Endogenous amyloid-β is necessary for hippocampal synaptic plasticity and memory', *Annals of Neurology*, 69(5), pp. 819–830. doi: 10.1002/ana.22313.

Qiao, A. *et al.* (2021) 'Reduction BACE1 expression via suppressing NF-κB mediated signaling by Tamibarotene in a mouse model of Alzheimer's disease', *IBRO Neuroscience Reports*, 10, pp. 153–160. doi: 10.1016/j.ibneur.2021.02.004.

Qiu, T. *et al.* (2015) 'Aβ42 and Aβ40: similarities and differences', *Journal of Peptide Science*, 21(7), pp. 522–529. doi: 10.1002/psc.2789.

Radde, R. *et al.* (2006) 'Aβ42-driven cerebral amyloidosis in transgenic mice reveals early and robust pathology', *EMBO reports*, 7(9), pp. 940–946. doi: 10.1038/sj.embor.7400784.

Rangaraju, S. *et al.* (2018) 'Differential Phagocytic Properties of CD45low Microglia and CD45high Brain Mononuclear Phagocytes—Activation and Age-Related Effects', *Frontiers in Immunology*, 9. doi: 10.3389/fimmu.2018.00405.

Rashad, A. *et al.* (2022) 'Donanemab for Alzheimer's Disease: A Systematic Review of Clinical Trials', *Healthcare*, 11(1), p. 32. doi: 10.3390/healthcare11010032.

Raz, L. and Miller, V. M. (2013) 'Considerations of Sex and Gender Differences in Preclinical and Clinical Trials', in Dathe, S. and Michel, M. C. (eds) *Sex and Gender Differences in Pharmacology. Handbook of Experimental Pharmacology*. Berlin: Springer, Berlin, Heidelberg, pp. 127–147. doi: 10.1007/978-3-642-30726-3_7.

Reverchon, F. *et al.* (2020) 'Hippocampal interleukin-33 mediates neuroinflammation-induced cognitive impairments', *Journal of Neuroinflammation*, 17(1), p. 268. doi: 10.1186/s12974-020-01939-6.

Ribary, U. *et al.* (1991) 'Magnetic field tomography of coherent thalamocortical 40-Hz oscillations in humans', *Proceedings of the National Academy of Sciences of the United States of America*, 88(24), pp. 11037–11041. doi: 10.1073/pnas.88.24.11037.

Richard, B. C. *et al.* (2015) 'Gene dosage dependent aggravation of the neurological phenotype in the 5XFAD mouse model of Alzheimer's disease', *Journal of Alzheimer's Disease*, 45(4), pp. 1223–1236. doi: 10.3233/JAD-143120.

Ripoll, V. M. *et al.* (2007) 'Gpnmb Is Induced in Macrophages by IFN-γ and Lipopolysaccharide and Acts as a Feedback Regulator of Proinflammatory Responses', *The Journal of Immunology*, 178(10), pp. 6557–6566. doi: 10.4049/jimmunol.178.10.6557.

Roberson, E. D. *et al.* (2011) 'Amyloid-β/fyn-induced synaptic, network, and cognitive impairments depend on tau levels in multiple mouse models of alzheimer's disease', *Journal of Neuroscience*, 31(2), pp. 700–711. doi: 10.1523/JNEUROSCI.4152-10.2011.

Rogers, J. and Lue, L. F. (2001) 'Microglial chemotaxis, activation, and phagocytosis of amyloid β-peptide as linked phenomena in Alzheimer's disease', *Neurochemistry International*, 39(5–6), pp. 333–340. doi: 10.1016/S0197-0186(01)00040-7.

Roy, A. *et al.* (2013) 'Cardiomyocyte-secreted acetylcholine is required for maintenance of homeostasis in the heart', *The FASEB Journal*, 27(12), pp. 5072–5082. doi: 10.1096/fj.13-238279.

Rubio-Perez, J. M. and Morillas-Ruiz, J. M. (2012) 'A Review: Inflammatory Process in Alzheimer's Disease, Role of Cytokines', *The Scientific World Journal*, 2012, pp. 1–15. doi: 10.1100/2012/756357.

Rurak, G. M. *et al.* (2022) 'Sex differences in developmental patterns of neocortical astroglia: A mouse translatome database', *Cell Reports*, 38(5), p. 110310. doi: 10.1016/j.celrep.2022.110310.

Russi, A. E. *et al.* (2018) 'Male-specific IL-33 expression regulates sex-dimorphic EAE susceptibility', *Proceedings of the National Academy of Sciences*, 115(7). doi: 10.1073/pnas.1710401115.

Rustenhoven, J. *et al.* (2018) 'PU.1 regulates Alzheimer's disease-associated genes in primary human microglia', *Molecular Neurodegeneration*, 13(1), p. 44. doi: 10.1186/s13024-018-0277-1.

Rustgi, S. D., Kayal, M. and Shah, S. C. (2020) 'Sex-based differences in inflammatory bowel diseases: a review', *Therapeutic Advances in Gastroenterology*, 13, p. 175628482091504. doi: 10.1177/1756284820915043.

Rynearson, K. D. *et al.* (2021) 'Preclinical validation of a potent γ-secretase modulator for Alzheimer's disease prevention', *Journal of Experimental Medicine*, 218(4). doi: 10.1084/jem.20202560.

Sadleir, K. R. *et al.* (2015) 'Aβ reduction in BACE1 heterozygous null 5XFAD mice is associated with transgenic APP level', *Molecular Neurodegeneration*, 10(1). doi: 10.1186/1750-1326-10-1.

Sadleir, K. R., Popovic, J. and Vassar, R. (2018) 'ER stress is not elevated in the 5XFAD mouse model of Alzheimer's disease', *Journal of Biological Chemistry*, 293(48), pp. 18434–18443. doi: 10.1074/jbc.RA118.005769.

Saeed, Y. and Abbott, S. M. (2017) 'Circadian Disruption Associated with Alzheimer's Disease', *Current Neurology and Neuroscience Reports*. Current Medicine Group LLC 1. doi: 10.1007/s11910-017-0745-y.

Saha, P. and Sen, N. (2019) 'Tauopathy: A common mechanism for neurodegeneration and brain aging', *Mechanisms of Ageing and Development*, 178(January), pp. 72–79. doi: 10.1016/j.mad.2019.01.007.

Sala Frigerio, C. *et al.* (2019) 'The Major Risk Factors for Alzheimer's Disease: Age, Sex, and Genes Modulate the Microglia Response to Aβ Plaques', *Cell Reports*, 27(4), pp. 1293-1306.e6. doi: 10.1016/j.celrep.2019.03.099.

Salazar, S. V. *et al.* (2019) 'Alzheimer's Disease Risk Factor Pyk2 Mediates Amyloid-β-Induced Synaptic Dysfunction and Loss', *The Journal of Neuroscience*, 39(4), pp. 758–772. doi: 10.1523/JNEUROSCI.1873-18.2018.

Saresella, M., Marventano, I., Piancone, F., Rosa, F. La, *et al.* (2020) 'IL-33 and its decoy sST2 in patients with Alzheimer ' s disease and mild cognitive impairment', *Journal of Neuroinflammation*, 4(17), pp. 1–10.

Saresella, M., Marventano, I., Piancone, F., La Rosa, F., *et al.* (2020) 'IL-33 and its decoy sST2 in patients with Alzheimer's disease and mild cognitive impairment', *Journal of Neuroinflammation*, 17(1), p. 174. doi: 10.1186/s12974-020-01806-4.

Sasaguri, H. *et al.* (2017) 'APP mouse models for Alzheimer's disease preclinical studies', *The EMBO Journal*, 36(17), pp. 2473–2487. doi: 10.15252/embj.201797397.

Scala, F. *et al.* (2019) 'Layer 4 of mouse neocortex differs in cell types and circuit organization between sensory areas', *Nature Communications*, 10(1), p. 4174. doi: 10.1038/s41467-019-12058-z.

Schmitz, J. *et al.* (2005) 'IL-33, an Interleukin-1-like Cytokine that Signals via the IL-1 Receptor-Related Protein ST2 and Induces T Helper Type 2-Associated Cytokines', *Immunity*, 23(5), pp. 479–490. doi: 10.1016/j.immuni.2005.09.015.

Schousboe, A. (2019) 'Metabolic signaling in the brain and the role of astrocytes in control of glutamate and GABA neurotransmission', *Neuroscience Letters*, 689(February 2018), pp. 11–13. doi: 10.1016/j.neulet.2018.01.038.

Schraen- Maschke, S. *et al.* (2008) 'Tau as a biomarker of neurodegenerative diseases', *Biomarkers in Medicine*, 2(4), pp. 363–384. doi: 10.2217/17520363.2.4.363.

Seidel, D. and Thyrian, J. R. (2019) 'Burden of caring for people with dementia – Comparing family caregivers and professional caregivers. A descriptive study', *Journal of Multidisciplinary Healthcare*, 12, pp. 655–663. doi: 10.2147/JMDH.S209106.

Selkoe, D. J. *et al.* (2016) 'The amyloid hypothesis of Alzheimer ' s disease at 25 years', *EMBO Molecular Medicine*, 8(6), pp. 595–608.

Sharpe, R. L. S. *et al.* (2020) 'Gamma entrainment frequency affects mood, memory and cognition: an exploratory pilot study', *Brain Informatics*, 7(1), p. 17. doi: 10.1186/s40708-020-00119-9.

Shen, J. and Kelleher III, R. J. (2006) 'The presenilin hypothesis of Alzheimer's disease: Evidence for a loss-of-function pathogenic mechanism', *PNAS*, 104(2), pp. 403–409. Available at: www.pnas.orgcgidoi10.1073pnas.0608332104.

Shi, M. *et al.* (2022) 'Impact of Anti-amyloid-β Monoclonal Antibodies on the Pathology and Clinical Profile of Alzheimer's Disease: A Focus on Aducanumab and Lecanemab', *Frontiers in Aging Neuroscience*, 14. doi: 10.3389/fnagi.2022.870517.

Shu, R. *et al.* (2015) 'APP intracellular domain acts as a transcriptional regulator of miR-663 suppressing neuronal differentiation', *Cell Death and Disease*, 6(2). doi: 10.1038/cddis.2015.10.

Sil, A. *et al.* (2022) 'Sex Differences in Behavior and Molecular Pathology in the 5XFAD Model', *Journal of Alzheimer's Disease*, 85(2), pp. 755–778. doi: 10.3233/JAD-210523.

Singer, A. C. *et al.* (2018) 'Noninvasive 40-Hz light flicker to recruit microglia and reduce amyloid beta load', *Nature Protocols*, 13(8), pp. 1850–1868. doi: 10.1038/s41596-018-0021-x.

Sobue, A. *et al.* (2021) 'Microglial gene signature reveals loss of homeostatic microglia associated with neurodegeneration of Alzheimer's disease', *Acta Neuropathologica Communications*, 9(1). doi: 10.1186/s40478-020-01099-x.

Sofroniew, M. V. (2015) 'Astrocyte barriers to neurotoxic inflammation', *Nature Reviews Neuroscience*, 16(5), pp. 149–163. doi: doi:10.1038/nrn3898.

Sofroniew, M. V. and Vinters, H. V. (2010) 'Astrocytes: Biology and pathology', *Acta Neuropathologica*, 119(1), pp. 7–35. doi: 10.1007/s00401-009-0619-8.

Söllvander, S. *et al.* (2016) 'Accumulation of amyloid-β by astrocytes result in enlarged endosomes and microvesicle-induced apoptosis of neurons', *Molecular Neurodegeneration*, 11(1), p. 38. doi: 10.1186/s13024-016-0098-z.

Song, Y. *et al.* (2020) 'The Effect of Estrogen Replacement Therapy on Alzheimer's Disease and Parkinson's Disease in Postmenopausal Women: A Meta-Analysis', *Frontiers in Neuroscience*, 14. doi: 10.3389/fnins.2020.00157.

Soula, M. *et al.* (2023) 'Forty-hertz light stimulation does not entrain native gamma oscillations in Alzheimer's disease model mice', *Nature Neuroscience*. doi: 10.1038/s41593-023-01270-2.

Spangenberg, E. E. and Green, K. N. (2017) 'Inflammation in Alzheimer's Disease: Lessons learned from microglial-repletion models', *Brain Behavioural Immunology*, 61, pp. 1–11. doi: 10.1016/j.bbi.2016.07.003.Inflammation.

Squarzoni, P., Thion, M. S. and Garel, S. (2015) 'Neuronal and microglial regulators of cortical wiring: Usual and novel guideposts', *Frontiers in Neuroscience*, 9(JUN). doi: 10.3389/fnins.2015.00248.

Steffen, J. *et al.* (2017) 'Expression of endogenous mouse APP modulates β-amyloid deposition in hAPP-transgenic mice', *Acta Neuropathologica Communications*, 5(1), p. 49. doi: 10.1186/s40478-017-0448-2.

Strang, K. H., Golde, T. E. and Giasson, B. I. (2019) 'MAPT mutations, tauopathy, and mechanisms of neurodegeneration', *Laboratory Investigation*, 99(7), pp. 912–928. doi: 10.1038/s41374-019-0197-x.

De Strooper, B. *et al.* (1999) 'A presenilin-1-dependent γ-secretase-like protease mediates release of Notch intracellular domain', *Nature*, 398(6727), pp. 518–522. doi: 10.1038/19083.

Strooper, B. De, Iwatsubo, T. and Wolfe, M. S. (2012) 'Presenilins and γ-Secretase: Structure, Function and Role in Alzheimer Disease', *Cold Spring Harbour perspectives in medicine*, 2(1), pp. 1–19.

Sundlisæter, E. *et al.* (2012) 'The Alarmin IL-33 Is a Notch Target in Quiescent Endothelial Cells', *The American Journal of Pathology*, 181(3), pp. 1099–1111. doi: 10.1016/j.ajpath.2012.06.003.

Ta, T. T. *et al.* (2019) 'Priming of microglia with IFN-γ slows neuronal gamma oscillations in situ', *Proceedings of the National Academy of Sciences of the United States of America*, 116(10), pp. 4637–4642. doi: 10.1073/pnas.1813562116.

Takahashi, K., Rochford, C. D. P. and Neumann, H. (2005) 'Clearance of apoptotic neurons without inflammation by microglial triggering receptor expressed on myeloid cells-2', *Journal of Experimental Medicine*, 201(4), pp. 647–657. doi: 10.1084/jem.20041611.

Takashima, A. *et al.* (1993) 'tau Protein kinase I is essential for amyloid β-protein-induced neurotoxicity', *Proceedings of the National Academy of Sciences of the United States of America*, 90(16), pp. 7789–7793. doi: 10.1073/pnas.90.16.7789.

Talantova, M. *et al.* (2013) 'Aβ induces astrocytic glutamate release, extrasynaptic NMDA receptor activation, and synaptic loss', *Proceedings of the National Academy of Sciences of the United States of America*, 110(27). doi: 10.1073/pnas.1306832110.

Tan, J. *et al.* (2000) 'CD45 Opposes β-Amyloid Peptide-Induced Microglial Activation via Inhibition of p44/42 Mitogen-Activated Protein Kinase', *The Journal of Neuroscience*, 20(20), pp. 7587–7594. doi: 10.1523/JNEUROSCI.20-20-07587.2000.

Tognatta, R. *et al.* (2020) 'Astrocytes Are Required for Oligodendrocyte Survival and Maintenance of Myelin Compaction and Integrity', *Frontiers in Cellular Neuroscience*, 14. doi: 10.3389/fncel.2020.00074.

Tremere, L. A. *et al.* (2011) 'Organization of Estrogen-Associated Circuits in the Mouse Primary Auditory Cortex', *Journal of Experimental Neuroscience*, 5, p. JEN.S7744. doi: 10.4137/JEN.S7744.

Trepanier, C. H., Jackson, M. F. and MacDonald, J. F. (2012) 'Regulation of NMDA receptors by the tyrosine kinase Fyn', *FEBS Journal*, 279(1), pp. 12–19. doi: 10.1111/j.1742-4658.2011.08391.x.

Turner, P. R. *et al.* (2003) *Roles of amyloid precursor protein and its fragments in regulating neural activity, plasticity and memory*, *Progress in Neurobiology*. doi: 10.1016/S0301-0082(03)00089-3.

U.S. Food and Drug Administration (2023) 'FDA Grants Accelerated Approval for Alzheimer's Disease Treatment ', January.

Vainchtein, I. D. *et al.* (2018) 'Astrocyte-derived Interleukin-33 promotes microglial synapse engulfment and neural circuit development', *Science*, 359(6381), pp. 1269–1273. doi: 10.1126/science.aal3589.Astrocyte-derived.

Varesi, A. *et al.* (2022) 'The Potential Role of Gut Microbiota in Alzheimer's Disease: From Diagnosis to Treatment', *Nutrients*, 14(3), p. 668. doi: 10.3390/nu14030668.

Vasanthakumar, A. *et al.* (2020) 'Sex-specific adipose tissue imprinting of regulatory T cells', *Nature*, 579(7800), pp. 581–585. doi: 10.1038/s41586-020-2040-3.

Vassar, R. *et al.* (1999) 'Secretase Cleavage of Alzheimer's Amyloid Precursor Protein by the Transmembrane Aspartic Protease BACE', *Science*, 286(5440), pp. 735–741. doi: 10.1126/science.286.5440.735.

Verma, M., Vats, A. and Taneja, V. (2015) 'Toxic species in amyloid disorders: Oligomers or mature fibrils', *Annals of Indian Academy of Neurology*. Wolters Kluwer Medknow Publications, pp. 138–145. doi: 10.4103/0972-2327.144284.

Vezzani, A. and Viviani, B. (2015) 'Neuromodulatory properties of inflammatory cytokines and their impact on neuronal excitability', *Neuropharmacology*, 96, pp. 70–82. doi: 10.1016/j.neuropharm.2014.10.027.

van Vugt, M. K. *et al.* (2010) 'Hippocampal Gamma Oscillations Increase with Memory Load', *The Journal of Neuroscience*, 30(7), pp. 2694–2699. doi: 10.1523/JNEUROSCI.0567-09.2010.

Wang, N. *et al.* (2022) 'Opposing effects of apoE2 and apoE4 on microglial activation and lipid metabolism in response to demyelination', *Molecular Neurodegeneration*, 17(1). doi: 10.1186/s13024-022-00577-1.

Wang, Y. *et al.* (2015) 'TREM2 Lipid Sensing Sustains the Microglial Response in an Alzheimer ' s Disease Model Article TREM2 Lipid Sensing Sustains the Microglial Response in an Alzheimer ' s Disease Model', *Cell*, 160(6), pp. 1061–1071. doi: 10.1016/j.cell.2015.01.049.

Ward, L. M. (2003) 'Synchronous neural oscillations and cognitive processes', *Trends in Cognitive Sciences*, 7(12), pp. 553–559. doi: 10.1016/j.tics.2003.10.012.

Waters, A. and Laitner, M. H. (2021) 'Biological sex differences in Alzheimer's preclinical research: A call to action', *Alzheimer's & Dementia: Translational Research & Clinical Interventions*, 7(1). doi: 10.1002/trc2.12111.

Weigand, A. J. *et al.* (2021) 'APOE interacts with tau PET to influence memory independently of amyloid PET in older adults without dementia', *Alzheimer's and Dementia*, 17(1), pp. 61–69. doi: 10.1002/alz.12173.

Wimo, A. *et al.* (2023) 'The worldwide costs of dementia in 2019', *Alzheimer's & Dementia*. doi: 10.1002/alz.12901.

Wisniewski, T. and Sigurdsson, E. M. (2010) 'Murine models of Alzheimer's disease and their use in developing immunotherapies', *Biochimica et Biophysica Acta - Molecular Basis of Disease*, 1802(10), pp. 847–859. doi: 10.1016/j.bbadis.2010.05.004.

Xiong, Z. *et al.* (2014) 'Alzheimer's Disease: Evidence for the Expression of Interleukin-33 and Its Receptor ST2 in the Brain', *Journal of Alzheimer's Disease*, 40(2), pp. 297–308. doi: 10.3233/JAD-132081.

Xu, J. *et al.* (2001) 'Amyloid-β Peptides Are Cytotoxic to Oligodendrocytes', *The Journal of Neuroscience*, 21(1), pp. RC118–RC118. doi: 10.1523/JNEUROSCI.21-01-j0001.2001.

Yang, H. D. *et al.* (2016) 'History of Alzheimer's Disease', *Dementia and Neurocognitive Disorders*, 15(4), p. 115. doi: 10.12779/dnd.2016.15.4.115.

Yang, Y. *et al.* (2017) 'ST2 / IL-33-Dependent Microglial Response Limits Acute Ischemic Brain Injury', *Journal of Neuroscience*, 37(18), pp. 4692–4704. doi: 10.1523/JNEUROSCI.3233-16.2017.

Yao, Y. *et al.* (2020) 'Non-invasive 40-Hz Light Flicker Ameliorates Alzheimer's-Associated Rhythm Disorder via Regulating Central Circadian Clock in Mice', *Frontiers in Physiology*, 11. doi: 10.3389/fphys.2020.00294.

Yeh, F. L. *et al.* (2016) 'TREM2 Binds to Apolipoproteins, Including APOE and CLU/APOJ, and Thereby Facilitates Uptake of Amyloid-Beta by Microglia', *Neuron*, 91(2), pp. 328–340. doi: 10.1016/j.neuron.2016.06.015.

Yokoyama, M. *et al.* (2022) 'Mouse Models of Alzheimer's Disease', *Frontiers in Molecular Neuroscience*, 15. doi: 10.3389/fnmol.2022.912995.

Yue, X. *et al.* (2005) 'Brain estrogen deficiency accelerates Aβ plaque formation in an Alzheimer's disease animal model', *Proceedings of the National Academy of Sciences*, 102(52), pp. 19198–19203. doi: 10.1073/pnas.0505203102.

Zempel, H. *et al.* (2010) 'Aβ oligomers cause localized Ca2+ elevation, missorting of endogenous Tau into dendrites, Tau phosphorylation, and destruction of microtubules and spines', *Journal of Neuroscience*, 30(36), pp. 11938–11950. doi: 10.1523/JNEUROSCI.2357-10.2010.

Zhang, K. *et al.* (2022) 'The Oligodendrocyte Transcription Factor 2 OLIG2 regulates transcriptional repression during myelinogenesis in rodents', *Nature Communications*, 13(1), p. 1423. doi: 10.1038/s41467-022-29068-z.

Zhang, Y. *et al.* (2021) '40 Hz Light Flicker Alters Human Brain Electroencephalography Microstates and Complexity Implicated in Brain Diseases', *Frontiers in Neuroscience*, 15. doi: 10.3389/fnins.2021.777183.

Zhao, J. *et al.* (2007) 'β-Site Amyloid Precursor Protein Cleaving Enzyme 1 Levels Become Elevated in Neurons around Amyloid Plaques: Implications for Alzheimer's Disease Pathogenesis', *The Journal of Neuroscience*, 27(14), pp. 3639–3649. doi: 10.1523/JNEUROSCI.4396-06.2007.

Zharichenko, N. (2020) 'The Role of Pro-Inflammatory and Regulatory Signaling by IL-33 in the Brain and Liver : A Focused Systematic Review of Mouse and Human Data and Risk of Bias Assessment of the Literature', *International Journal of Molecular Sciences*, 21(11), p. 3933.

Zhi, X. *et al.* (2014) 'Alzheimer's Disease: Evidence for the Expression of Interleukin-33 and its Receptor ST2 in the Brain', *Journal of Alzheimer's Disease*, 40(2), pp. 297–308. doi: 10.3233/JAD-132081.Alzheimer.

Zhong, L. *et al.* (2017) 'Soluble TREM2 induces inflammatory responses and enhances microglial survival', *The Journal of experimental medicine*, 214(3), pp. 597–607. doi: 10.1084/jem.20160844.

Zhong, X. *et al.* (2017) 'Association of interleukin-33 gene polymorphisms with susceptibility to late onset Alzheimer’s disease: a meta-analysis', *Neuropsychiatric Disease and Treatment*, Volume 13, pp. 2275–2284. doi: 10.2147/NDT.S138073.

Zhou, C. *et al.* (2020) 'The Effect of Hormone Replacement Therapy on Cognitive Function in Female Patients With Alzheimer's Disease: A Meta-Analysis', *American Journal of Alzheimer's Disease & Other Dementiasr*, 35, p. 153331752093858. doi: 10.1177/1533317520938585.

Zhu, Y. *et al.* (2011) 'CD45 Deficiency Drives Amyloid-β Peptide Oligomers and Neuronal Loss in Alzheimer's Disease Mice', *The Journal of Neuroscience*, 31(4), pp. 1355–1365. doi: 10.1523/JNEUROSCI.3268-10.2011.

Appendix A: Arduino code used to administer 40Hz light flicker via LED circuit.

```
/*
 40 Hz Flicker
 This code generates 40 Hz flicker during which the light turns on for 12.5 ms and
 then off for 12.5 ms.
*/

int RELAY1 = 7;

// the setup routine runs once when you press reset:
void setup() {
  // initialize pins as an output.

  Serial.begin(9600);
  pinMode(RELAY1, OUTPUT);
}

// the loop routine runs over and over again forever:
void loop() {

   digitalWrite(RELAY1,1);         //40 Hz Turns ON Relays 1
   delayMicroseconds(12500);                  // Wait 12.5 milliseconds

   digitalWrite(RELAY1,0);         // Turns Relay Off
   delayMicroseconds(12500);                  // Wait 12.5 milliseconds
}
```

This code was obtained from Singer et.al “Noninvasive 40-Hz light flicker to recruit microglia and reduce amyloid beta load” (2018) Nature Protocols, 13, 1850-1868.